




PROJECT:

## EastMed Pipeline Project






Document Title:	EastMed Greek Section – Environmental and Social Impact Assessment
Document Subtitle	Annex 9 D-Marine sediment dispersion model/ calculations
Project Document No:	PERM-GREE-ESIA-A09_0007_0_Annex9D

	EASTMED PIPELINE PROJECT		 
	EastMed Greek Section – Environmental and Social Impact Assessment		DOCNo: PERM-GREE-ESIA-A09_0007_0_Annex9D
			REV. : 00
			PAGE : 2 OF 178




Document details	
Document title	EastMed Greek Section – Environmental and Social Impact Assessment
Document subtitle	Annex 9 D-Marine sediment dispersion model/ calculations
Company	IGI Poseidon
Author	School of Civil Engineering - National Tech Univ. of Athens
Project	EastMed Pipeline Project
Project Document No.	PERM-GREE-ESIA-A09_0007_0_Annex9D
Date	03/06/2022
Version	00

Document history					
Revision	Author	Reviewed by	Approved by	Date	Status
00	School of Civil Engineering - National Tech Univ. of Athens	ASPROFOS	IGI POSEIDON	03/06/2022	For submission to Authorities




	<p style="text-align: center;"><b>EASTMED PIPELINE PROJECT</b></p> <p style="text-align: center;">EastMed Greek Section – Environmental and Social Impact Assessment</p>	<div style="display: flex; justify-content: space-around; align-items: center;">   </div> <p>DOC No: PERM-GREE-ESIA- A09_0007_0_Annex9D</p> <p>REV. : 00</p> <p>PAGE : 3 OF 178</p>
---	--	---

## Table of Contents

ANNEX 9 D	Marine sediment dispersion model/ calculations .....	13
9 D.1.	Executive Summary .....	14
9 D.2.	Introduction of the Model .....	18
9 D.2.1.	Scope.....	18
9 D.2.2.	Sediment Diffusion Model .....	18
9 D.2.3.	Calculation Scenarios .....	19
9 D.2.4.	Impact Assessment.....	19
9 D.2.5.	Contents of this Report.....	19
9 D.2.6.	Research Team .....	20
9 D.3.	Materials and Methods.....	20
9 D.3.1.	Dredging Categories .....	20
9 D.3.1.1	Introduction .....	20
9 D.3.1.2	Grab Dredgers .....	24
9 D.3.1.3	Cutter Suction Dredgers.....	28
9 D.3.2.	Environmental Impacts of Dredging.....	31
9 D.3.3.	The Plume of Suspended Particulate Matter (SPM).....	33
9 D.3.4.	Sediment Release Rates .....	33
9 D.3.5.	Suspended Sediment Concentrations Measured at Field Dredging Sites .....	35
9 D.3.6.	Summary of Practical Experience on Dredging.....	38
9 D.3.7.	Measures Reducing Suspended Sediment Concentrations during Dredging .....	40
9 D.3.8.	The CORMIX Mathematical Model.....	40
9 D.3.8.1	Development and Application of CORMIX .....	40
9 D.3.8.2	Brief Description of the General Jet Theory and Length Scales.....	41
9 D.3.8.3	Negatively Buoyant Jets in a Moving Ambient .....	45
9 D.3.8.4	Application of CORMIX to Sediment Plumes .....	46
9 D.3.8.5	Discharge (Module 101).....	47
9 D.3.8.6	Near-Field Mixing of a 3D Jet (Module 110).....	48
9 D.3.8.7	Bottom Impingement and Spreading (Module 132) .....	53
9 D.3.8.8	Upstream Spreading (Module 032).....	54
9 D.3.8.9	Bottom Density Current (Module 310) .....	55
9 D.3.8.10	Main Flow Zones.....	61
9 D.3.9.	Required Input Data .....	62
9 D.4.	Calculations at Site LF4 and Discussion.....	63
9 D.4.1.	Input data .....	63

	<b>EASTMED PIPELINE PROJECT</b>		 	
			DOC No: PERM-GREE-ESIA- A09_0007_0_Annex9D	
	EastMed Greek Section – Environmental and Social Impact Assessment		REV. :	00
			PAGE :	4 OF 178

9 D.4.1.1	Dredging characteristics.....	63
9 D.4.1.2	Sediment characteristics.....	66
9 D.4.1.3	Ambient characteristics .....	66
9 D.4.1.4	Site and discharge characteristics .....	67
9 D.4.2.	Flow characteristics for the maximum current velocity.....	71
9 D.4.2.1	Type of flow .....	71
9 D.4.2.2	Plume geometry/trajectory and flow zones .....	72
9 D.4.3.	Sediment characteristics for the maximum current velocity.....	77
9 D.4.3.1	Sediment concentrations in the near field region .....	77
9 D.4.3.2	Sediment concentrations in the bottom layer.....	78
9 D.4.3.3	Suspended sediment concentrations.....	83
9 D.4.4.	Flow and sediment characteristics for the minimum current velocity .....	85
9 D.4.4.1	Type of flow .....	85
9 D.4.4.2	Plume geometry/trajectory and flow zones .....	85
9 D.4.4.3	Sediment concentrations in the near field region .....	88
9 D.4.4.4	Sediment concentrations in the bottom layer.....	90
9 D.4.4.5	Suspended sediment concentrations.....	93
9 D.4.5.	Sensitivity analysis .....	96
9 D.4.5.1	Effect of the current velocity .....	96
9 D.4.5.2	Effect of the composition of solids.....	100
9 D.5.	Calculations at Site LF5 and Discussion.....	102
9 D.5.1.	Input data .....	102
9 D.5.2.	Flow characteristics.....	106
9 D.5.3.	Sediment concentrations.....	109
9 D.5.4.	Suspended sediment concentrations.....	112
9 D.5.5.	Sensitivity analysis .....	115
9 D.5.5.1	Effect of the current velocity .....	116
9 D.5.5.2	Effect of the composition of solids.....	118
9 D.6.	Calculations AT Site LF2 and Discussion.....	120
9 D.6.1.	Input Data .....	120
9 D.6.2.	Flow Characteristics .....	124
9 D.6.3.	Sediment Concentrations .....	127
9 D.6.4.	Suspended Sediment Concentrations .....	129
9 D.6.5.	Sensitivity Analysis.....	132
9 D.6.5.1	Effect of the Current Velocity .....	132
9 D.6.5.2	Effect of the Composition of Solids .....	135

	<p style="text-align: center;"><b>EASTMED PIPELINE PROJECT</b></p> <p style="text-align: center;">EastMed Greek Section – Environmental and Social Impact Assessment</p>	<div style="display: flex; justify-content: space-around; align-items: center;">   </div> <p>DOC No: PERM-GREE-ESIA- A09_0007_0_Annex9D</p> <p>REV. : 00</p> <p>PAGE : 5 OF 178</p>
---	--	---

9 D.7.	Calculations at Site LF3 and Discussion.....	136
9 D.7.1.	Input Data .....	136
9 D.7.2.	Flow Characteristics .....	141
9 D.7.3.	Sediment Concentrations .....	144
9 D.7.4.	Suspended Sediment Concentrations .....	147
9 D.7.5.	Sensitivity Analysis.....	150
9 D.7.5.1	Effect of the Current Velocity .....	150
9 D.7.5.2	Effect of the Composition of Solids .....	152
9 D.8.	Conclusions and Proposals .....	154
9 D.8.1.	Conclusions.....	154
9 D.8.1.1	Flow Behaviour of the Sediment Plume .....	154
9 D.8.1.2	Sediment Concentrations .....	156
9 D.8.1.3	Suspended Sediment Concentrations (SSC).....	156
9 D.8.1.4	Sensitivity Analysis.....	157
9 D.8.2.	Proposed Measures during Dredging.....	158
9 D.9.	References .....	159
Appendix 1	Site Characteristics .....	163
	Site characteristics of LF2 .....	163
	Site characteristics of LF3 .....	165
	Site characteristics of LF4 .....	166
	Site characteristics of LF5 .....	168
Appendix 2	Ambient Physical Properties .....	171
Appendix 3	Ambient Current Velocities.....	174
	Ambient current velocities at site LF2.....	174
	Ambient current velocities at site LF3.....	175
	Ambient current velocities at site LF4.....	176
	Ambient current velocities at site LF5.....	177

## List of Figures

Figure D-1	Sketches of Typical Mechanical Dredgers - (a) Typical Pontoon Mounted Grab Bucket Dredger (Bray et al., 1996).....	21
Figure D-2	Sketches of Typical Mechanical Dredgers - (b) Typical Backhoe Dredger (Bray et al., 1996)	22
Figure D-3	Sketches of Typical Hydraulic Dredgers - (a) Typical Trailing Suction Hopper Dredger (Bray et al., 1996) .....	23




	<b>EASTMED PIPELINE PROJECT</b>		 
	EastMed Greek Section – Environmental and Social Impact Assessment		DOC No: PERM-GREE-ESIA-A09_0007_0_Annex9D
			REV. : 00 PAGE : 6 OF 178

Figure D-4	Sketches of Typical Hydraulic Dredgers -(b) Typical Cutter Suction Dredger (Bray et al., 1996)	24
Figure D-5	Typical (a) Grab Dredger and (b) Grab Bucket (Source: Bray et al, 1996)	25
Figure D-6	Statistical Distribution of Grab Dredgers (Bray et al., 1996)	26
Figure D-7	Grab Dredger: Nominal Output, Pnom, for Various Bucket Sizes and Dredger Characteristics (Bray et al., 1996)	28
Figure D-8	Cutter Suction Dredger	28
Figure D-9	Statistical Distribution of Discharge Pipeline of Cutter Suction Dredgers (Bray et al., 1996)	30
Figure D-10	Characteristics of Cutter Suction Dredgers (Bray et al., 1996)	31
Figure D-11	Schematic Representation of a Jet	42
Figure D-12	Schematic Representation of a Negatively Buoyant Jet (Obtained from Papakostantis et al., 2013)	46
Figure D-13	CORMIX Flow Classification of Negatively Buoyant Discharges in Uniform Layer low: Flow Classes NV and NH (Source: Doneker & Jirka, 2007)	47
Figure D-14	Schematic Diagram of an Inclined Buoyant Jet in Unbounded Stratified Ambient Crossflow (Jirka, 2004)	49
Figure D-15	Schematic Diagram of Impingement Region (Jirka, 2004)	54
Figure D-16	Schematic Diagram Bottom Density Current (Jirka, 2004)	57
Figure D-17	Output of the selected dredger (Bray et al., 1996)	64
Figure D-18	Schematic diagram of trench at LF4	65
Figure D-19	Cumulative volume of excavated material at LF4	65
Figure D-20	Discharge location; see also Appendix 1	69
Figure D-21	Main site and discharge geometrical characteristics of the discharge	71
Figure D-22	CORMIX flow classification of negatively buoyant discharges in uniform layer flow: Flow Classes NV and NH (Source: Doneker & Jirka, 2007)	72
Figure D-23	Trajectory of the axis of the SPM plume in the near field region	74
Figure D-24	Schematic diagram of impingement region (Jirka, 2004)	75
Figure D-25	Variation of 2BH along the bottom layer	76
Figure D-26	Variation of BV along the bottom layer	76
Figure D-27	Variation of the thickness of the bottom layer	77
Figure D-28	Dilution in the near field region	77
Figure D-29	Sediment concentrations (%) in the near field region	78
Figure D-30	Sediment concentrations (mg/L) in the near field region	78
Figure D-31	Dilution in the bottom layer	79
Figure D-32	Sediment concentrations (%) in the bottom layer	80




	<p style="text-align: center;"><b>EASTMED PIPELINE PROJECT</b></p> <p style="text-align: center;">EastMed Greek Section – Environmental and Social Impact Assessment</p>	<div style="display: flex; justify-content: space-around; align-items: center;">   </div> <p>DOC No: PERM-GREE-ESIA- A09_0007_0_Annex9D</p> <p>REV. : 00</p> <p>PAGE : 7 OF 178</p>
---	--	---

Figure D-33	Sediment concentrations (mg/L) in the bottom layer .....	80
Figure D-34	Sediment concentration contours (% of the initial) in the bottom layer .....	81
Figure D-35	Total sediment concentration contours in the bottom layer (a) % of the initial concentration and (b) in mg/L .....	82
Figure D-36	Suspended sediment concentrations (mg/L) from x=0 to x=1200 m .....	83
Figure D-37	Suspended sediment concentrations (mg/L) from x=0 to x=400 m .....	83
Figure D-38	Suspended sediment concentrations (mg/L) .....	84
Figure D-39	Trajectory of the axis of the SPM plume in the near field region .....	86
Figure D-40	Variation of 2BH along the bottom layer .....	87
Figure D-41	Variation of BV along the bottom layer .....	87
Figure D-42	Variation of the thickness of the bottom layer .....	88
Figure D-43	Dilution in the near field region .....	89
Figure D-44	Sediment concentrations (%) in the near field region .....	89
Figure D-45	Sediment concentrations (mg/L) in the near field region .....	90
Figure D-46	Dilution in the bottom layer .....	91
Figure D-47	Sediment concentrations (%) in the bottom layer .....	91
Figure D-48	Sediment concentrations (mg/L) in the bottom layer .....	92
Figure D-49	Sediment concentration contours (% of the initial) in the bottom layer .....	92
Figure D-50	Sediment concentration contours (mg/L) in the bottom layer .....	93
Figure D-51	Suspended sediment concentrations (mg/L) from x=0 to x=1200 m .....	94
Figure D-52	Suspended sediment concentrations (mg/L) from x=0 to x=400 m .....	94
Figure D-53	Suspended sediment concentrations (mg/L) with Google maps background .....	95
Figure D-54	Total suspended sediment concentrations (mg/L) for various current velocities ....	97
Figure D-55	Sediment concentration contours (% of the initial) in the bottom layer for current velocities from 0.50 m/s to 0.90 m/s .....	100
Figure D-56	Output of the dredger (Bray et al., 1996) .....	104
Figure D-57	Schematic diagram of trench at LF5 .....	105
Figure D-58	Discharge location; see also Appendix 1 .....	106
Figure D-59	Trajectory of the axis of the SPM plume in the near field region .....	108
Figure D-60	Variation of the width of the plume (2BH) along the bottom layer .....	109
Figure D-61	Variation of the thickness (BV) along the bottom layer .....	109
Figure D-62	Sediment concentrations (mg/L) in the near field region .....	110
Figure D-63	Sediment concentrations (mg/L) along the bottom layer .....	111
Figure D-64	Total sediment concentration contours in the bottom layer in mg/L for (a) the maximum current velocity and (b) the minimum current velocity (Google Maps background) .....	112






	<p style="text-align: center;"><b>EASTMED PIPELINE PROJECT</b></p> <p style="text-align: center;">EastMed Greek Section – Environmental and Social Impact Assessment</p>	<div style="display: flex; justify-content: space-around; align-items: center;">   </div> <div style="border: 1px solid black; padding: 2px;"> DOC No: PERM-GREE-ESIA- A09_0007_0_Annex9D REV. : 00 PAGE : 8 OF 178 </div>
---	--	---

Figure D-65	Suspended sediment concentrations (mg/L) for (a) the maximum current velocity and (b) the minimum current velocity.....	113
Figure D-66	Suspended sediment concentrations (mg/L) for the maximum current velocity (Google Maps background).....	114
Figure D-67	Suspended sediment concentrations (mg/L) for the minimum current velocity (Google Maps background).....	115
Figure D-68	Total suspended sediment concentrations (mg/L) for various current velocities ..	116
Figure D-69	Sediment concentration contours (% of the initial) in the bottom layer for current velocities 0.50 m/s and 0.90 m/s.....	117
Figure D-70	Output of the Dredger (Bray et al., 1996) .....	122
Figure D-71	Schematic Diagram of Trench at LF2 .....	123
Figure D-72	Discharge Location; See also Appendix 1 .....	124
Figure D-73	Trajectory of the Axis of the SPM Plume in the Near Field Region .....	126
Figure D-74	Variation of the Width of the Plume (2BH) along the Bottom Layer .....	126
Figure D-75	Variation of the Thickness (BV) along the Bottom Layer .....	127
Figure D-76	Sediment Concentrations (mg/L) in the Near Field Region.....	128
Figure D-77	Sediment Concentrations (mg/L) along the Bottom Layer.....	128
Figure D-78	Total Sediment Concentration Contours in the Bottom Layer in mg/L for (a) the Maximum Current Velocity and (b) the Minimum Current Velocity (Google Maps Background)....	129
Figure D-79	Suspended Sediment Concentrations (mg/L) for (a) the Maximum Current Velocity and (b) the Minimum Current Velocity .....	131
Figure D-80	Suspended Sediment Concentrations (mg/L) for the Maximum Current Velocity (Google Maps Background) .....	132
Figure D-81	Total Suspended Sediment Concentrations (mg/L) for Various Current Velocities	133
Figure D-82	Sediment Concentration Contours (% of the Initial) in the Bottom Layer for Current Velocities 0.50 m/s and 0.90 m/s .....	134
Figure D-83	Output of the Dredger (Bray et al., 1996) .....	139
Figure D-84	Schematic Diagram of Trench at LF3 .....	140
Figure D-85	Discharge Location; See also Appendix 1 .....	141
Figure D-86	Trajectory of the Axis of the SPM Plume in the Near Field Region .....	143
Figure D-87	Variation of the Width of the Plume (2BH) along the Bottom Layer .....	143
Figure D-88	Variation of the Thickness (BV) along the Bottom Layer .....	144
Figure D-89	Sediment Concentrations (mg/L) in the Near Field Region.....	145
Figure D-90	Sediment Concentrations (mg/L) along the Bottom Layer.....	145
Figure D-91	Total Sediment Concentration Contours in the Bottom Layer in mg/L for (a) the Maximum Current Velocity and (b) the Minimum Current Velocity (Google Maps Background)....	146






	<p style="text-align: center;"><b>EASTMED PIPELINE PROJECT</b></p> <p style="text-align: center;">EastMed Greek Section – Environmental and Social Impact Assessment</p>	<div style="display: flex; justify-content: space-around; align-items: center;">   </div> <p>DOC No: PERM-GREE-ESIA- A09_0007_0_Annex9D</p> <p>REV. : 00</p> <p>PAGE : 9 OF 178</p>
---	--	---

Figure D-92	Suspended Sediment Concentrations (mg/L) for (a) the Maximum Current Velocity and (b) the Minimum Current Velocity .....	148
Figure D-93	Suspended Sediment Concentrations (mg/L) for the Maximum Current Velocity (Google Maps Background) .....	149
Figure D-94	Total Suspended Sediment Concentrations (mg/L) for Various Current Velocities	151
Figure D-95	Sediment Concentration Contours (% of the Initial) in the Bottom Layer for Current Velocities 0.50 m/s and 0.90 m/s .....	152

### List of Tables

Table D-1	Grab dredger: Modification Factor, fm for Various Soil Types and Bucket Sizes.....	26
Table D-2	Indicative Sediment Release Rates .....	34
Table D-3	Measured Suspended Sediment Concentrations (SSC) at Dredging Sites Using Mechanical Dredgers .....	35
Table D-4	Measured Suspended Sediment Concentrations (SSC) at Dredging Sites Using Mechanical Dredgers .....	37
Table D-5	Dilutions at Distances of 200 m, 500 m and 5000 m from the Source for Various Current Velocities	39
Table D-6	Simple Jet vs. Simple Plume .....	44
Table D-7	Sediment Classes at LF4 .....	66
Table D-8	Initial source concentration of the SPM plume .....	68
Table D-9	Basic geometric characteristics and hydrodynamic for various current velocities.....	96
Table D-10	Examined sediment compositions.....	100
Table D-11	Suspended sediment concentrations (mg/L) for various sediment compositions .....	100
Table D-12	Suspended sediment concentrations (mg/L) for various sediment compositions at x=50 m and x=100 m .....	102
Table D-13	Input data for site LF5 .....	102
Table D-14	Sediment Classes for site LF5.....	103
Table D-15	Flow characteristics for site LF5.....	107
Table D-16	Basic geometric and hydrodynamic characteristics for various current velocities.	116
Table D-17	Examined sediment compositions.....	118
Table D-18	Suspended sediment concentrations (mg/L) for various sediment compositions .....	118
Table D-19	Suspended sediment concentrations (mg/L) at x=50 m and x=100 m .....	120
Table D-20	Input Data for Site LF2.....	120
Table D-21	Sediment Classes for Site LF2 .....	121
Table D-22	Flow Characteristics for Site LF2 .....	125










	EASTMED PIPELINE PROJECT		 	
	EastMed Greek Section – Environmental and Social Impact Assessment		DOC No: PERM-GREE-ESIA-A09_0007_0_Annex9D	
			REV. :	00
			PAGE :	10 OF 178

Table D-23	Basic Geometric and Hydrodynamic Characteristics for Various Current Velocities	133
Table D-24	Examined Sediment Compositions .....	135
Table D-25	Suspended Sediment Concentrations (mg/L) for Various Sediment Compositions	135
Table D-26	Suspended Sediment Concentrations (mg/L) at x=50 m and x=100 m .....	136
Table D-27	Input Data for Site LF3.....	137
Table D-28	Sediment Classes for Site LF3 .....	138
Table D-29	Flow Characteristics for Site LF3.....	142
Table D-30	Basic Geometric and Hydrodynamic Characteristics for Various Current Velocities	150
TableD-31	Examined Sediment Compositions .....	153
Table D-32	Suspended Sediment Concentrations (mg/L) for Various Sediment Compositions	153
Table D-33	Suspended Sediment Concentrations (mg/L) at x=50 m and x=100 m .....	154
Table D-34	Flow Characteristics of the Sediment Plume .....	155
Table D-35	Sediment Concentrations (mg/L) in the Near Field and the Bottom Layer .....	156
Table D-36	Suspended Sediment Concentrations (mg/L) in the Water Column .....	157

	EASTMED PIPELINE PROJECT		 
	EastMed Greek Section – Environmental and Social Impact Assessment		DOC No: PERM-GREE-ESIA-A09_0007_0_Annex9D
			REV. : 00
			PAGE : 11 OF 178

## Abbreviations




Abbreviation	Description
AM	ambient characteristics
CMEMS	Copernicus Marine Environment Monitoring Service
CORMIX	Cornell Mixing Zone Expert System
DR	dredging characteristics
EastMed	Eastern Mediterranean
ECP	EastMed Compression Platform
EGSA	Hellenic Geodetic Reference System
EIA	Environmental Impact Assessment
ESIA	Environmental and Social Impact Assessment
EU	European Union
IFC	International Finance Corporation
mg/L	milligram per liter
MOP	maximum operating pressure
NKUA	National and Kapodistrian University of Athens
SD	site and discharge characteristics
SE	sediment characteristics
SPM	suspended particulate matter
SSC	suspended sediment concentration
ZOFE	Zone of flow establishment

	EASTMED PIPELINE PROJECT		 
	EastMed Greek Section – Environmental and Social Impact Assessment		DOC No: PERM-GREE-ESIA-A09_0007_0_Annex9D
			REV. : 00
			PAGE : 12 OF 178

### External cooperation




This document was drafted with the cooperation of:

- School of Civil Engineering - National Tech Univ. of Athens

	EASTMED PIPELINE PROJECT		 
	EastMed Greek Section – Environmental and Social Impact Assessment		DOC No: PERM-GREE-ESIA-A09_0007_0_Annex9D
			REV. : 00
			PAGE : 13 OF 178

## ANNEX 9 D MARINE SEDIMENT DISPERSION MODEL/

### CALCULATIONS

	EASTMED PIPELINE PROJECT		 
	EastMed Greek Section – Environmental and Social Impact Assessment		DOC No: PERM-GREE-ESIA-A09_0007_0_Annex9D
			REV. : 00
			PAGE : 14 OF 178




## 9 D.1. EXECUTIVE SUMMARY

### 1. Introduction

- 1.1) Dredging construction activities generally fall within two general categories: (I) mechanical dredging (e.g. bucket dredgers, grab dredgers and backhoe dredgers) and (II) hydraulic dredging (e.g. suction dredgers, cutter suction dredgers and trailing suction dredgers).
- 1.2) During dredging operations, sediment particles are removed from the seabed and released into the water column as suspended particulate matter (SPM). The SPM forms a plume that is transported away from the dredging site by water mass circulation following a path that consists of 3 zones: (1) initial mixing, (II) near-field and (III) far-field. The behaviour of the SPM plume depends on the following: (I) dredging characteristics, (II) sediment characteristics, (III) ambient characteristics, and (IV) site and discharge characteristics.
- 1.3) The excessive increase of SPM in coastal waters caused by dredging is considered a pollution event. Increase of SPM is caused due to: (I) the dredging process itself, i.e. the removal of substratum from the seafloor, and (II) the process of disposal.
- 1.4) The most likely effects of dredging are: (I) physical removal of substratum and associated plants and animals from the seabed, (II) burial due to subsequent deposition of material, and (III) enhanced turbidity and sedimentation as a result of dredging and disposal operations. The impact of dredging on marine ecosystems is complex and far from fully understood, despite various research efforts. Changes in suspended sediment concentration (SSC), the parameter used in models to quantify the changes in turbidity, are generally considered the most important.
- 1.5) SSC changes induced by dredging will only result in adverse environmental effects when the turbidity generated is significantly larger than the natural variation of turbidity and sedimentation rates in the area. Such natural variability can sometimes be substantial and may be caused by factors such as storms, wind-induced wave action, river discharges and other local perturbations. Dredging activities often generate no more increased SPM than commercial shipping operations, bottom fishing or severe storms.

### 2. Scope of the present work and the CORMIX model

- 2.1) The scope of the present work is to estimate the impacts caused on the marine environment during the construction phase by applying a sediment diffusion model. The Cornell Mixing Zone Expert System (CORMIX) was selected; CORMIX was developed in

	EASTMED PIPELINE PROJECT		 
	EastMed Greek Section – Environmental and Social Impact Assessment		DOC No: PERM-GREE-ESIA-A09_0007_0_Annex9D
			REV. : 00
			PAGE : 15 OF 178




part through cooperation with the US EPA, the US Army Corps of Engineers, and the US Bureau of Reclamation.

- 2.2) The CORMIX model was applied to estimate the following: (I) concentrations of suspended solids (sediments), (II) trajectory, shape and generally the behaviour of plumes of suspended solids which are created during the construction phase, and (III) the spatial distribution (expansion) of suspended solids that settle using "distribution maps" (in the form of iso-concentration lines / isolines), i.e. lines of equal values of concentrations.

### 3. Input data

- 3.1) The input data refer to the following characteristics: dredging characteristics (DR), sediment characteristics (SE), ambient characteristics (AM) and site and discharge characteristics (SD).
- 3.2) **Dredging data (DR)** include: DR1 type of dredger; DR2 capacity of dredger; DR3 cycle time; DR4 output of dredger. These data were based on information provided by ASPOFOS SA, as well as on the relevant literature and practical experience to represent relatively conservative cases.
- 3.3) **Sediment data (SE)** are: SE1 sediment density and SE2 sediment classes. These data were based on information provided by ASPOFOS SA.
- 3.4) **Ambient data (AM)** are: AM1 ambient temperature; AM2 ambient salinity; AM3 ambient (background) sediment concentration; AM4 ambient density; AM5 flow velocity near the bottom; AM6 flow velocity at the surface. These data were selected based on information provided by ASPOFOS SA; flow velocity data were also provided by the research team of the National and Kapodistrian University of Athens (NKUA) that are based on the Copernicus Marine Environment Monitoring Service (CMEMS). Two basic scenarios were investigated: (I) maximum current velocity and (II) minimum current velocity that is virtually equal to zero. Moreover, a series of calculations were performed using values ranging from 0.5 m/s to 0.9 m/s to examine the effect of current velocity.
- 3.5) **Site and discharge data (SD)** include: SD1 sediment mass released; SD2 sediment plume concentration; SD3 sediment plume density; SD4 sediment plume discharge; SD5 discharge velocity; SD6 sediment plume area; SD7 shore Location; SD8 distance to shoreline; SD9 water depth; SD10 bottom slope; SD11 vertical angle of discharge; SD12 horizontal angle of discharge; SD13 Discharge height above channel bottom; and SD14 water depth at the source of the plume. These data were based on information provided by ASPOFOS SA, as well as on the relevant literature and practical experience; the



	EASTMED PIPELINE PROJECT		 
	EastMed Greek Section – Environmental and Social Impact Assessment		DOC No: PERM-GREE-ESIA-A09_0007_0_Annex9D
			REV. : 00
		PAGE :	16 OF 178




dredging location was initially selected in a conservative way that is to be close to the shore and close to the area of ecological-environmental interest.

#### 4. Calculations and conclusions

**4.1) Scenarios of calculations.** Eight scenarios of calculations were performed for the minimum and maximum current velocities at the 4 sites LF2, LF3, LF4 and LF5 that near the bottom are equal to 0.88 m/s, 0.66 m/s, 0.72 m/s and 0.71 m/s, respectively; moreover, 32 additional scenarios were considered during the sensitivity analysis to investigate the effect of current velocity near the bottom for values ranging from 0.50 to 0.90 m/s and for various compositions of sediments.

**4.2) Flow characteristics. The flow characteristics of the sediment plume are the following:**

- (I) Initially, the flow of the sediment plume is dominated by upward plume momentum (jet-like); the axis of the plume rises to a maximum height, being weakly deflected by the ambient current. The maximum height of the sediment plume is approximately equal to 1.2 m above the seafloor during the maximum current velocity and equal to 2.7 m above the seafloor during the minimum current velocity; the higher height during the minimum current velocity is due to the weaker influence of the ambient currents.
- (II) Then, the plume is strongly affected by gravity and rapidly falls downwards and impinges on the sea bottom; the impingement angle ranges from 20.2° to 32.5° for the maximum current velocity, while it is constant (approximately equal to 57°) for the minimum current velocity. The length of the near field region ranges from 6.7 m to 13.5 m for the maximum current velocity, and it is almost constant (175.0 m) for the minimum current velocity.
- (III) After impingement, the flow laterally spreads across the ambient flow in the downstream direction; its half-width (BH) is steadily increasing and its thickness (BV) is decreasing. At the end of the near field region, BH ranges from 12.4 m to 26.0 m for the maximum current velocity, while for the minimum current velocity it is almost constant and approximately equal to 350.0 m; moreover, BV for the maximum current velocity ranges from 0.9 m to 1.4 m and for the minimum current velocity it is approximately equal to 0.28 m.
- (IV) The dilution factor indicates the magnitude of mixing between the sediment concentration and the ambient water. If an initial concentration of 100 is reduced to 25 at a certain location, the dilution factor is calculated as the initial value divided by the diluted value (100 divided by 25) equal to 4. The mixing rate is relatively small in all scenarios; thus, the dilution factor at 1,200 m downstream

	EASTMED PIPELINE PROJECT		 
	EastMed Greek Section – Environmental and Social Impact Assessment		DOC No: PERM-GREE-ESIA-A09_0007_0_Annex9D
			REV. : 00
			PAGE : 17 OF 178

of the discharge location is also small ranging from 3.3 to 3.9 for the maximum current velocity, while it is constant and equal to 4.7 for the minimum flow velocity. Thus, the worst conditions are those for the maximum current velocity

- (V) The flow characteristics for the minimum current velocity (that is close to zero) are practically the same for all sites.




**4.3) Sediment Concentrations. The main characteristics of the sediment concentrations are the following:**

- (I) The distribution of sediment concentrations for the minimum current velocity is practically the same for all sites.
- (II) At distances shorter than  $x=100$  m from the discharge location, the sediment concentrations for the maximum current velocity range from 106.0 mg/L to 111.8 mg/L; these values are lower than the corresponding values for the minimum current velocity that range from 115.3 mg/L to 173.7 mg/L.
- (III) Far downstream from the discharge location, for example, at a distance equal to  $x=1,200$  m from the discharge location, sediment concentrations for the maximum current velocity range from 63.8 mg/L to 75.0 mg/L; these values are higher than the corresponding value of 53.5 mg/L for the minimum current velocity at all of the sites.

**4.4) Suspended Sediment Concentrations. The main characteristics of the suspended sediment concentrations are the following:**

- (I) At distances shorter than 20 m from the discharge location, the suspended sediment concentrations for the maximum current velocity are lower than the threshold value of 35 mg/L for all sites. For the minimum current velocity, the corresponding concentrations are lower than the threshold value of 35 mg/L with the exception of site LF5 at which the suspended sediment concentration is slightly higher than the threshold value (36.7 mg/L).
- (II) At distances greater than 50 m from the dredging location, suspended sediment concentrations range from 0.8 to 18.2 mg/L for the maximum current velocity, while for the minimum current velocity the corresponding concentrations range from 0.0 mg/L (at sites LF2 and LF3) to 7.6 mg/L.
- (III) It is noted that the duration of the potential impacts lasts as long as dredging takes place and the increased suspended sediment concentrations do not persist in the water column after the dredging procedure.

**4.5) Effect of current velocity.** Sensitivity analysis calculations showed that, when the current velocity increases, the following are observed: (I) the length of the near field region decreases, (II) the initial thickness of the bottom layer increases and the initial half-width

	EASTMED PIPELINE PROJECT		 
	EastMed Greek Section – Environmental and Social Impact Assessment		DOC No: PERM-GREE-ESIA-A09_0007_0_Annex9D
			REV. : 00
			PAGE : 18 OF 178

of the bottom layer decreases, and (III) the suspended solids concentrations in the water column decrease; thus, the decrease of the current velocity results in more favourable conditions.




- 4.6) Effect of the composition of the sediment.** Calculations verified that when the percentages of heavy material, such as chunks, increase, then suspended sediment concentrations and the area covered by relatively high suspended sediment concentrations decreases.
- 4.7) Proposed measures during dredging.** During dredging it is proposed to adopt all available measures to reduce suspended sediment concentrations; some indicative measures are the following:
- (I) Use auger dredgers that employ special equipment to move material towards the suction head and use of pumping by piston action to enable the transportation of high-density material.
  - (II) (II) Use disc-cutter dredgers with a cutter head which rests horizontally and rotates its vertical blades slowly.
  - (III) Use scoop/sweep dredgers with special equipment to scrape the material towards the suction intake.
  - (IV) When using a trailing suction hopper dredger: optimise trailing velocity, suction mouth and suction discharge and reduce or even eliminate overflow.
  - (V) When using a cutter suction dredger: optimise cutter speed, swing velocity and discharge and employ a special cutter-head design.
  - (VI) When using a grab dredger, employ watertight grab/clamshell, use silt screen, limit grab time above water and limit grab dragging on bed.
  - (VII) When using a backhoe dredger, use a special bucket for reducing sediment losses and silt screen (applicable for current velocities less than 0.5 m/s).

## 9 D.2. INTRODUCTION OF THE MODEL

### 9 D.2.1. Scope

The scope of this work is to assess the impact of construction/dredging works on marine sediments. Construction works are expected to cause temporary reversible impacts on the quality of marine sediments and settling of re-suspended sediments. Installation of the pipeline will cause disruption of marine sediments of the seabed resulting in an increase in suspended sediments as well as changes in natural sedimentation.

### 9 D.2.2. Sediment Diffusion Model

	EASTMED PIPELINE PROJECT		 
	EastMed Greek Section – Environmental and Social Impact Assessment		DOC No: PERM-GREE-ESIA-A09_0007_0_Annex9D
			REV. : 00
			PAGE : 19 OF 178

The necessary estimates of the impacts that will be caused to marine sediments during the construction phase will be determined by applying a sediment diffusion model. With the sediment diffusion model, the following calculations/estimates will be carried out:

- Concentrations of suspended solids (sediments);
- Trajectory, the shape and generally behaviour of plumes of suspended solids, which are created during the construction phase; and
- Spatial distribution (expansion) of suspended solids (particles) that settle with "distribution maps" (in the form of iso-concentration lines / isolines), i.e. lines of equal values of suspended solids concentrations, such as e.g. 10 and 100 mg/L.

#### 9 D.2.3. Calculation Scenarios

Calculations have been performed with the sediment diffusion model for 8 scenarios involving 4 investigation areas and 2 flow conditions. The investigation areas that were determined in collaboration with ASPROFOS SA are the following:

- Area LF2 near the landing area in Crete;
- Area LF3 near the landing area in N. Peloponnese; and
- Areas LF4 and LF5 near the intersection of Patraikos Gulf.

The current conditions concerning the maximum and minimum velocity values will be determined with a hydrodynamic model based on the Copernicus Marine Environment Monitoring Service (CMEMS) by EKPA.




#### 9 D.2.4. Impact Assessment

Based on the results of the model, the effects of sediment diffusion on the water column will be assessed.

#### 9 D.2.5. Contents of this Report

This Intermediate Technical Report of Sediment Diffusion contains the calculations that were performed at site L4; it consists of the following chapters:

- Executive summary;

	EASTMED PIPELINE PROJECT		 
	EastMed Greek Section – Environmental and Social Impact Assessment		DOC No: PERM-GREE-ESIA-A09_0007_0_Annex9D
			REV. : 00
			PAGE : 20 OF 178

- Introduction;
- Materials and methods;
- Calculations, results and discussion;
- Conclusions; and
- References.

Appendix 1, Appendix 2 and Appendix 3.

### 9 D.2.6. Research Team

The following scientists participated in this project:

- Prof. Anastasios I. Stamou
- Dr. Aristeidis Bloutsos; and
- Miss Elpida Panagiotatou.

## 9 D.3. MATERIALS AND METHODS




### 9 D.3.1. Dredging Categories

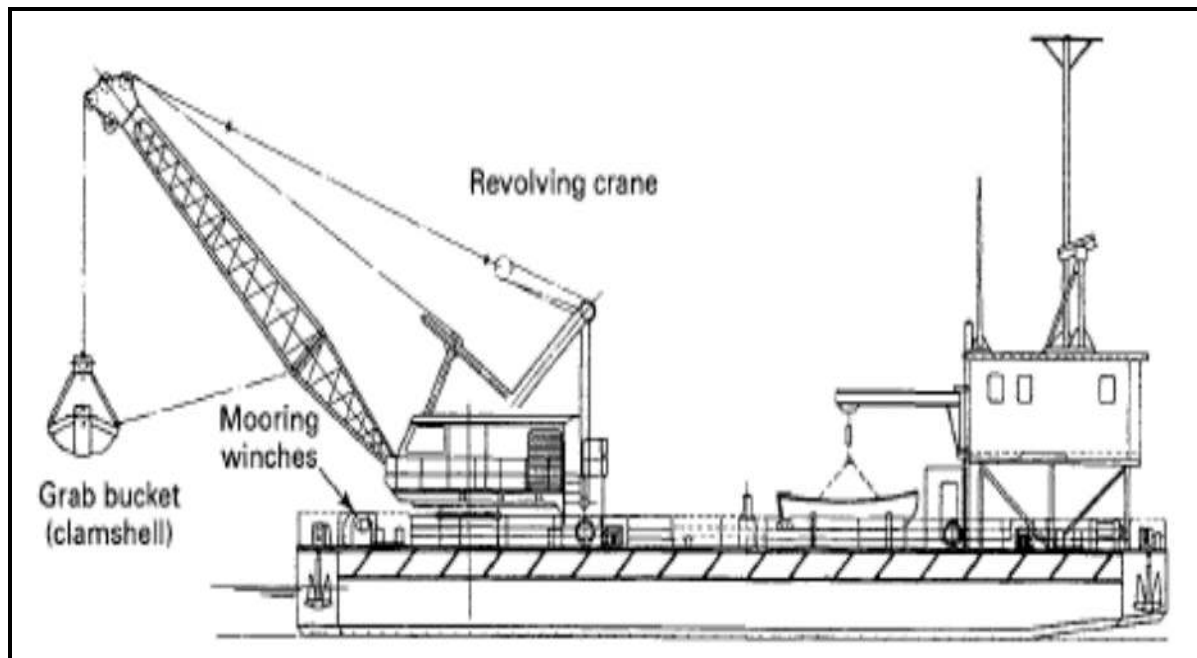
#### 9 D.3.1.1 Introduction

During dredging operations, sediment particles are removed from the seabed and released into the water column as suspended particulate matter (SPM). The excessive increase of SPM in coastal waters caused by dredging is considered a pollution event according to the EU directives of Water Framework (2000/60/EC) and Marine Strategy Framework (2008/56/EC).

Dredging construction activities take many different forms which generally fall within two general categories of mechanical dredging and hydraulic dredging (European Dredging Association, 2018):




- Mechanical dredgers which use a grab or a bucket to loosen the in-situ material on the seabed and raise it to the surface; see Figure D-1 and Figure D-2. These come in different types with the most common types being bucket dredgers, grab dredgers and backhoe dredgers. Indicatively, a grab dredger is described in section 9 D.3.2; and

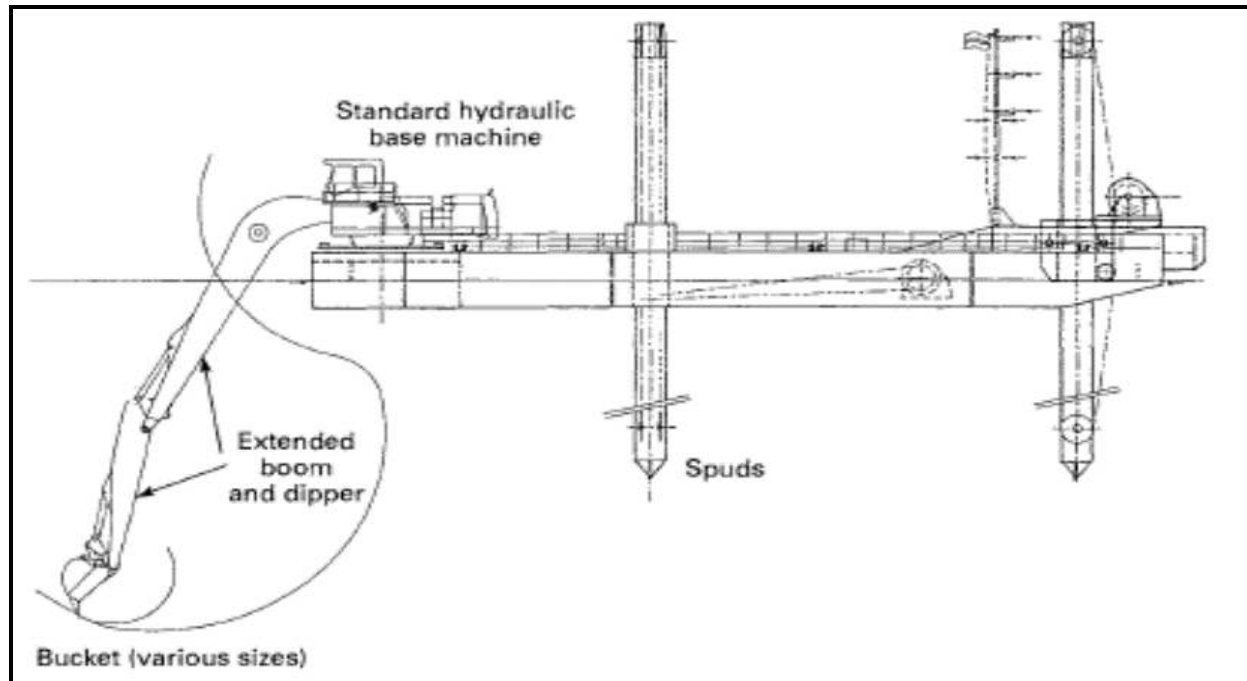
	<p style="text-align: center;"><b>EASTMED PIPELINE PROJECT</b></p> <p style="text-align: center;">EastMed Greek Section – Environmental and Social Impact Assessment</p>	<div style="display: flex; justify-content: space-between; align-items: center;">   </div> <div style="display: flex; justify-content: space-between;"> <div> <p>DOC No: PERM-GREE-ESIA- A09_0007_0_Annex9D</p> <p>REV. : 00</p> <p>PAGE : 21 OF 178</p> </div> </div>
---	--	--



Prepared by School of Civil Engineering - National Tech Univ. of Athens on behalf of ASPROFOS, 2022.

**Figure D-1**      **Sketches of Typical Mechanical Dredgers - (a) Typical Pontoon Mounted Grab Bucket Dredger (Bray et al., 1996)**

	<p style="text-align: center;"><b>EASTMED PIPELINE PROJECT</b></p> <p style="text-align: center;">EastMed Greek Section – Environmental and Social Impact Assessment</p>	<div style="display: flex; justify-content: space-between; align-items: center;">   </div> <div style="border-top: 1px solid black; border-bottom: 1px solid black; padding: 2px;"> DOC No: PERM-GREE-ESIA- A09_0007_0_Annex9D </div> <div style="display: flex; justify-content: space-between; border-bottom: 1px solid black; padding: 2px;"> REV. : 00 </div> <div style="display: flex; justify-content: space-between; padding: 2px;"> PAGE : 22 OF 178 </div>
---	--	--






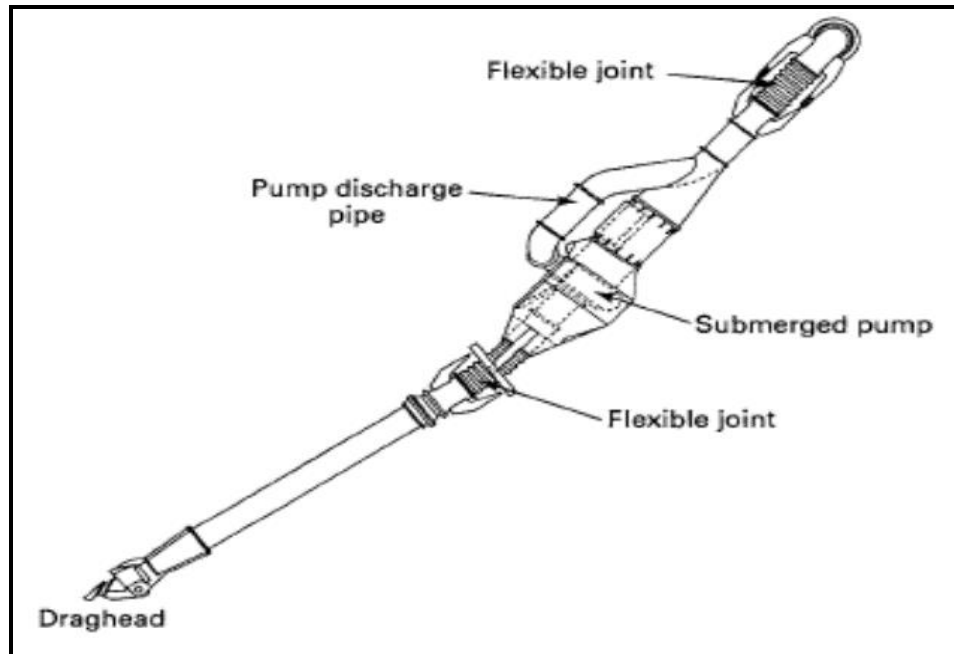
Prepared by School of Civil Engineering - National Tech Univ. of Athens on behalf of ASPROFOS, 2022.

**Figure D-2      Sketches of Typical Mechanical Dredgers - (b) Typical Backhoe Dredger (Bray et al., 1996)**

- Hydraulic dredgers which raise loosened materials from the seabed in suspension through a pipe system connected to a centrifugal pump; hydraulic dredgers include suction dredgers, cutter suction dredgers and trailing suction dredgers. See Figure D-3 and Figure D-4. Indicatively, a cutter suction dredger is described in section 9 D.3.2.






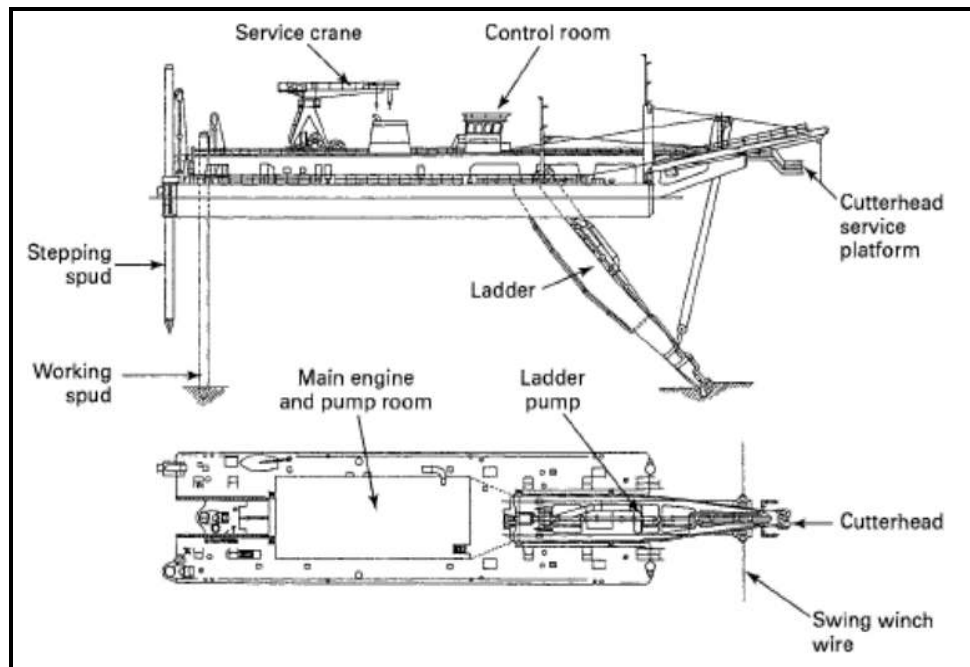
	<p style="text-align: center;"><b>EASTMED PIPELINE PROJECT</b></p> <p style="text-align: center;">EastMed Greek Section – Environmental and Social Impact Assessment</p>	<div style="display: flex; justify-content: space-between; align-items: center;">   </div> <div style="border-top: 1px solid black; padding-top: 5px;"> DOC No: PERM-GREE-ESIA- A09_0007_0_Annex9D </div> <div style="display: flex; justify-content: space-between; border-top: 1px solid black; padding-top: 5px;"> REV. : PAGE : </div> <div style="display: flex; justify-content: space-between; border-top: 1px solid black; padding-top: 5px;"> 00 23 OF 178 </div>
---	--	--



Prepared by School of Civil Engineering - National Tech Univ. of Athens on behalf of ASPROFOS, 2022.

**Figure D-3**      **Sketches of Typical Hydraulic Dredgers - (a) Typical Trailing Suction Hopper Dredger**  
(Bray et al., 1996)

	<p style="text-align: center;"><b>EASTMED PIPELINE PROJECT</b></p> <p style="text-align: center;">EastMed Greek Section – Environmental and Social Impact Assessment</p>	<div style="display: flex; justify-content: space-between; align-items: center;">   </div> <div style="border-top: 1px solid black; border-left: 1px solid black; border-right: 1px solid black; padding: 5px;"> DOC No: PERM-GREE-ESIA- A09_0007_0_Annex9D </div> <div style="border-top: 1px solid black; border-left: 1px solid black; border-right: 1px solid black; padding: 5px;"> REV. : 00 </div> <div style="border-top: 1px solid black; border-left: 1px solid black; border-right: 1px solid black; padding: 5px;"> PAGE : 24 OF 178 </div>
---	--	---






Prepared by School of Civil Engineering - National Tech Univ. of Athens on behalf of ASPROFOS, 2022.

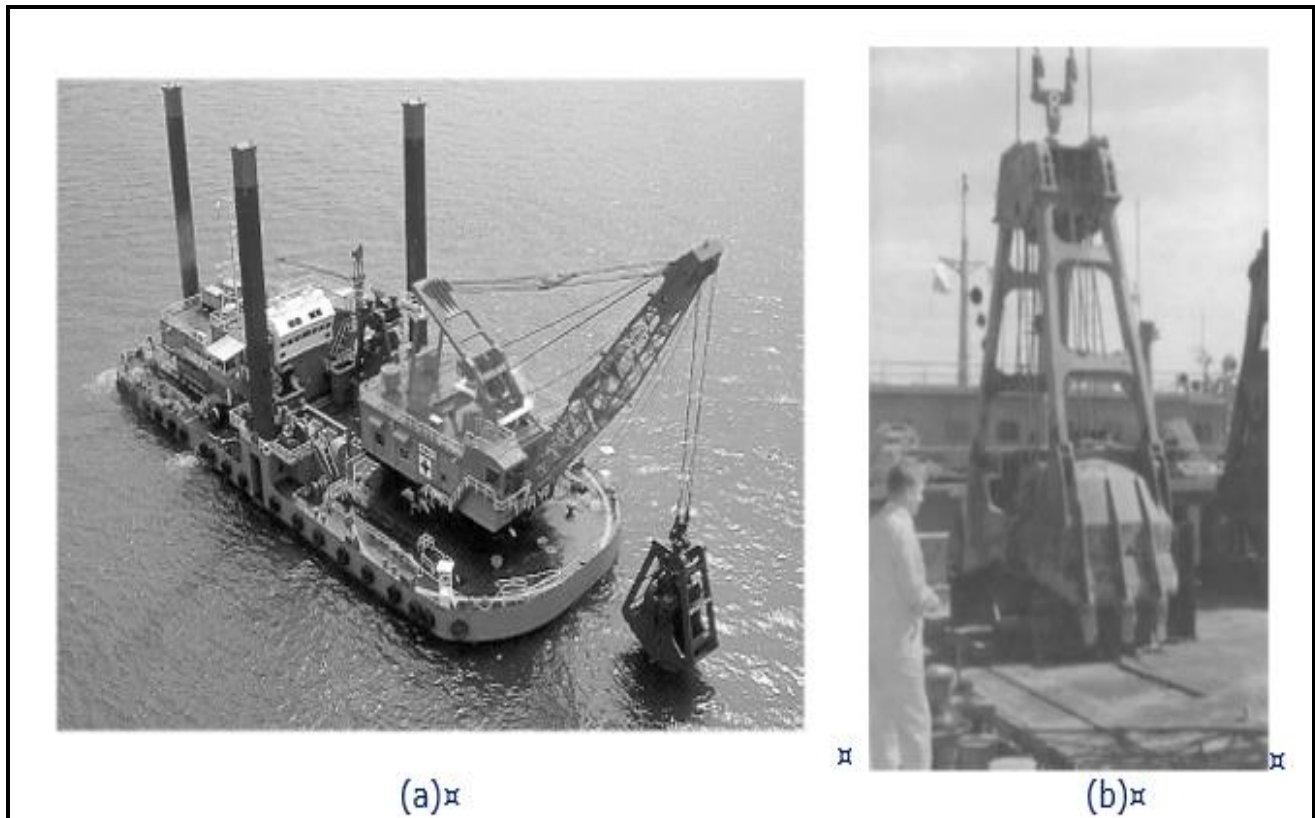
**Figure D-4      Sketches of Typical Hydraulic Dredgers -(b) Typical Cutter Suction Dredger (Bray et al., 1996)**

#### **9 D.3.1.2    Grab Dredgers**

A grab dredger (see Figure D-5) consists of a lattice jib grabbing crane mounted usually on a simple pontoon (grab pontoon dredger) that loads into independent hopper barges. The crane is mounted towards one end of a pontoon which is usually approximately rectangular in plan, but may have a semi-circular or narrowed end projection on which the crane is mounted. The pontoon may be held in position by anchors and winches or may combine the more positive location of spuds during dredging, with winches for pontoon relocation.

The bucket should be carefully selected according to the characteristics of the material to be dredged. When dredging in soft silts, muds and clays, a plain lightweight bucket of the maximum size for which the crane is rated can be used. For stiff clays or very weak rocks a heavy toothed bucket of reduced capacity should be employed. For most applications, a twin jaw configuration will be appropriate, but for special applications, such as the recovery of loose boulders or broken rock, a cactus, or orange peel grab may be more appropriate (Bray et al., 1996).

	<p style="text-align: center;"><b>EASTMED PIPELINE PROJECT</b></p> <p style="text-align: center;">EastMed Greek Section – Environmental and Social Impact Assessment</p>	<div style="display: flex; justify-content: space-between; align-items: center;">   </div> <p>DOC No: PERM-GREE-ESIA- A09_0007_0_Annex9D</p> <p>REV. : 00</p> <p>PAGE : 25 OF 178</p>
---	--	---



Prepared by School of Civil Engineering - National Tech Univ. of Athens on behalf of ASPROFOS, 2022.

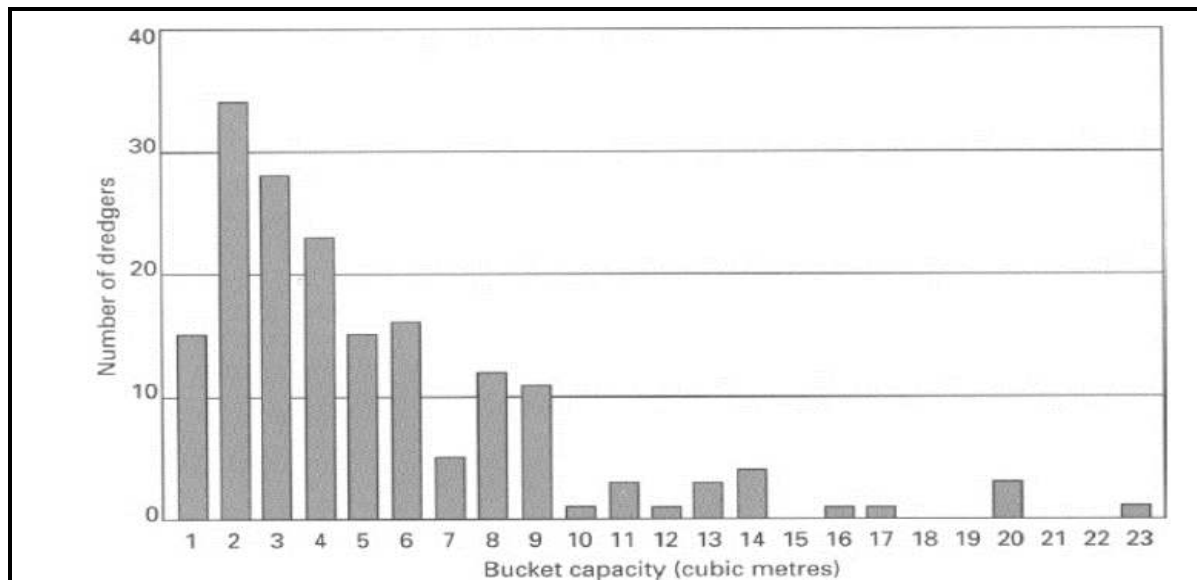
**Figure D-5 Typical (a) Grab Dredger and (b) Grab Bucket (Source: Bray et al, 1996)**

The dredging process is discontinuous and cyclic consisting of the following steps:

- Step 1. Lowering the grab to the bottom;
- Step 2. Closing the grab by pulling the hoisting wire;
- Step 3. Hoisting starts when the bucket is completely closed;
- Step 4. Swinging to the barge or hopper;
- Step 5. Lowering the filled bucket into the barge or hopper; and
- Step 6. Opening the bucket by releasing the closing wire.

Traditionally the cycle time has been assumed to be about 60 seconds. In water depth greater than 10 m the cycle time is greater than 60 seconds.

The grab pontoon dredger is normally rated by its grab bucket capacity (Bray et al., 1996). The capacity of grab buckets range from 0.75 to 200 m<sup>3</sup>, although buckets over 20 m<sup>3</sup> are rare. A statistical distribution of the grab bucket capacity is shown in Figure D-6.



Prepared by School of Civil Engineering - National Tech Univ. of Athens on behalf of ASPROFOS, 2022.

**Figure D-6 Statistical Distribution of Grab Dredgers (Bray et al., 1996)**




Typically, the term “output” is defined as the in situ quantity of material dredged in a given period of time, and it can be qualified as being one of the following:

- Hourly output: average quantity dredged in a working hour;
- Shift output: average quantity dredged during a complete shift;
- Weekly output: average quantity dredged in a complete week; and
- Annual output: total quantity dredged in a calendar year.

The productive unit of the grab depends to the diggability of the soil. The nominal uninterrupted output,  $P_{nom}$ , is the hourly output considering of the basic dredging cycle operation. For a dumb dredger that discharges the dredged material into a hopper alongside,  $P_{nom}$  can be obtained from Figure D-7, where a modification factor of  $f_m = 0.75$  for mud was obtained from Table D-1.

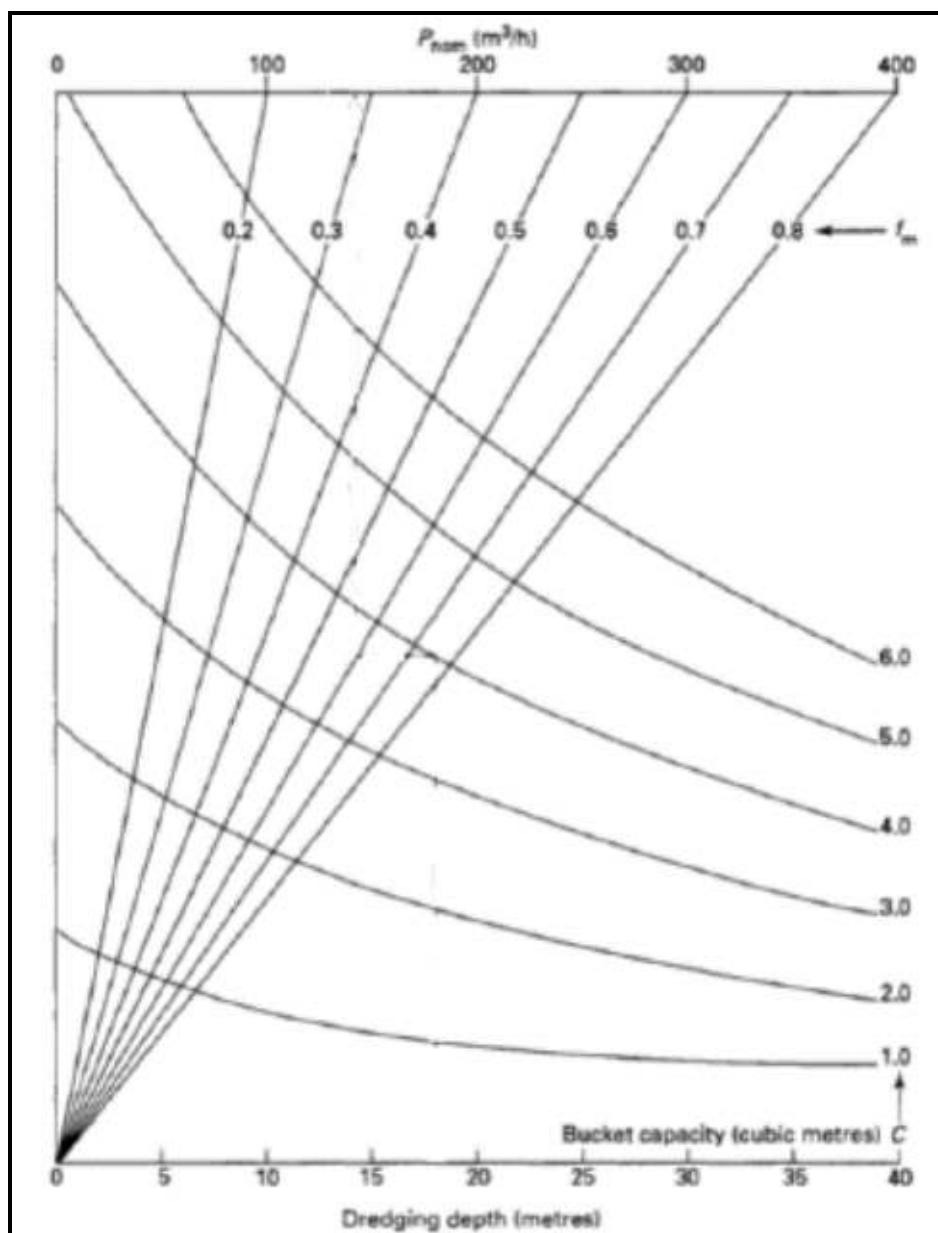
**Table D-1 Grab dredger: Modification Factor,  $f_m$  for Various Soil Types and Bucket Sizes**

Soil type	Modification factor, $f_m$	
	2 m <sup>3</sup> bucket	4 m <sup>3</sup> bucket
Mud	0.75	0.80
Loose sand	0.70	0.75
Compact sand	0.60	0.70
Sand and clay	0.50	0.60




	<p style="text-align: center;"><b>EASTMED PIPELINE PROJECT</b></p> <p style="text-align: center;">EastMed Greek Section – Environmental and Social Impact Assessment</p>	<div style="display: flex; justify-content: space-between; align-items: center;">   </div> <p>DOC No: PERM-GREE-ESIA-A09_0007_0_Annex9D</p> <p>REV. : 00</p> <p>PAGE : 27 OF 178</p>
---	--	--

	Modification factor, $f_m$	
Soil type	2 m <sup>3</sup> bucket	4 m <sup>3</sup> bucket
Stones	0.35	0.45
Broken rock	0.20	0.30

Prepared by School of Civil Engineering - National Tech Univ. of Athens on behalf of ASPROFOS, 2022.



Prepared by School of Civil Engineering - National Tech Univ. of Athens on behalf of ASPROFOS, 2022.

	EASTMED PIPELINE PROJECT		 
	EastMed Greek Section – Environmental and Social Impact Assessment		DOC No: PERM-GREE-ESIA-A09_0007_0_Annex9D
			REV. : 00
		PAGE :	28 OF 178

**Figure D-7 Grab Dredger: Nominal Output,  $P_{nom}$ , for Various Bucket Sizes and Dredger Characteristics (Bray et al., 1996)**

### 9 D.3.1.3 Cutter Suction Dredgers

A cutter suction dredger, shown in Figure D-8, is a stationary dredger which makes use of a cutter head to loosen the material to be dredged. It pumps the dredged material via a pipeline ashore or into barges. While dredging, the cutter head describes arcs and is swung around the spud-pole powered by winches. The cutter suction dredger is comprised of two main components which are: (1) the cutter head and (2) the dredging pump.






Prepared by School of Civil Engineering - National Tech Univ. of Athens on behalf of ASPROFOS, 2022.

**Figure D-8 Cutter Suction Dredger**

The cutter head is mounted at the lower end of the ladder used to support the cutter drive, and the suction pipe and is used to agitate soft materials or to cut harder materials. Two standard forms of the cutter head include (a) the straight arm cutter which has straight blades bolted to a spider and (b) the basket cutter which has spiral blades that are integral with the front hub and back wearing ring. Both the spacing of the blades and the angle of the cutter blade influence the efficiency of the operation (Bray et. al., 1996).



	EASTMED PIPELINE PROJECT		 
	EastMed Greek Section – Environmental and Social Impact Assessment		DOC No: PERM-GREE-ESIA-A09_0007_0_Annex9D
			REV. : 00
			PAGE : 29 OF 178

The dredging pump is located in the body of the dredger and creates a vacuum in the suction pipe that draws the soil up the pipe and through the centrifugal pump. Following that, the soil is discharged by being pumped through a pipeline (Bray et. al., 1996).

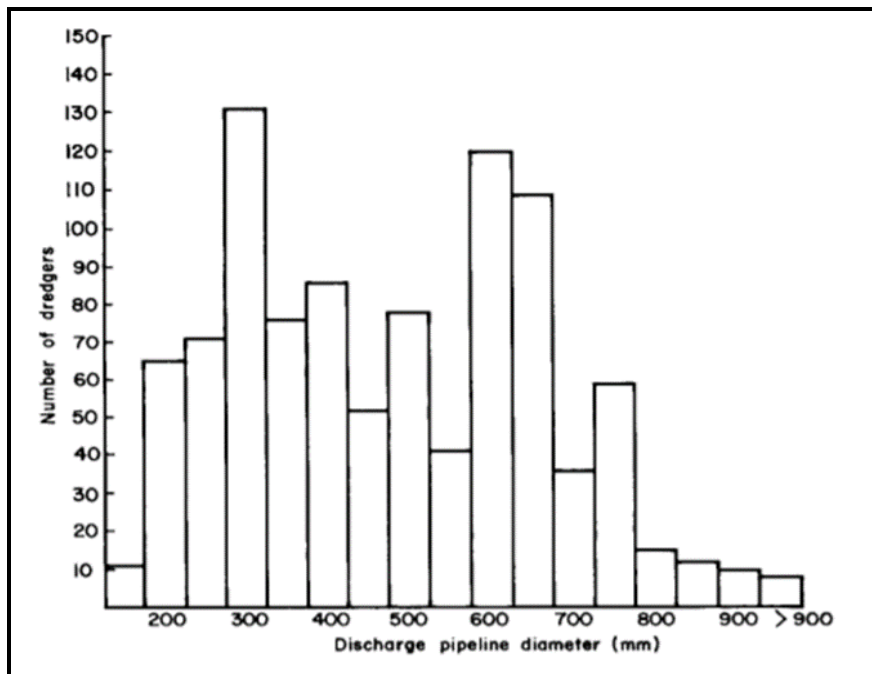
The cutter suction dredger carries out an almost continuous operation. The dredging pump is only stopped when it becomes necessary to move the pipeline, either due to the advance of the dredger or in order to discharge at a new location.

The basic operational cycle is (Bray et. al., 1996):

- Step 1. cut (dredging to a set depth all the material within a reach of the cutter head as it is swung across the spud);
- Step 2. advance on spuds;
- Step 3. cut;
- Step 4. advance on spuds;
- Step 5. repeat steps 1-4 as necessary;
- Step 6. move side wire anchors;
- Step 7. change pipeline position; and
- Step 8. repeat steps 1–8.

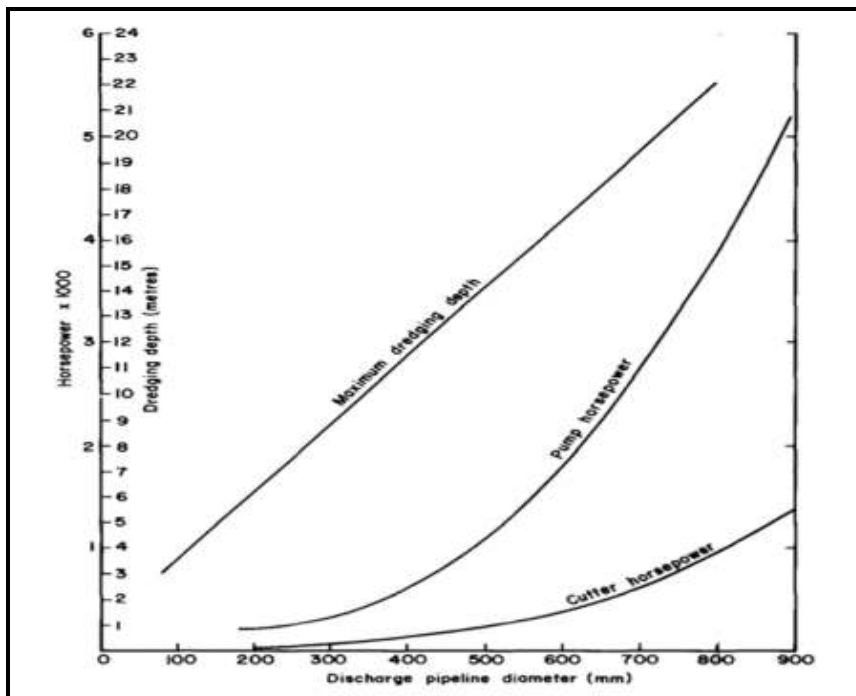
The size of a cutter suction dredger is measured by the diameter of the suction pipe and by the installed machinery power. Pipe diameters are in the range 100 to 1,500 mm. The statistical distribution of cutter suction dredgers and the installed power and maximum dredging depths are shown in Figure D-9 and Figure D-10, respectively (Bray et. al, 1996). A well designed 762 mm dredge with 5,000 to 8,000 hp on the pump and 2,000 hp on the cutter will pump 153 to 1,529 m<sup>3</sup>/h in soft to medium-hard rock through pipeline length up to 4,572 m (Herbich, 1992). A modern, highly automated cutter suction dredger is capable of achieving production rates of around 500,000 m<sup>3</sup>/week under good conditions.





Prepared by School of Civil Engineering - National Tech Univ. of Athens on behalf of ASPROFOS, 2022.

**Figure D-9** Statistical Distribution of Discharge Pipeline of Cutter Suction Dredgers (Bray et al., 1996)



Prepared by School of Civil Engineering - National Tech Univ. of Athens on behalf of ASPROFOS, 2022.

**Figure D-10 Characteristics of Cutter Suction Dredgers (Bray et al., 1996)**

### 9 D.3.2. Environmental Impacts of Dredging




The impact of dredging on marine ecosystems (such as seagrass) is complex and far from fully understood, despite various research efforts. There is an extensive body of experience to learn from, which lies with contractors, in Environmental Impact Assessment (EIA) reports, monitoring data and scientific literature derived from field-based and laboratory studies on potential direct and indirect effects of dredging (Erftemeijer and Lewis, 2006).

The potential effects of dredging are caused due to the following processes:

- the dredging process itself, i.e. the removal of substratum from the seafloor; and
- the process of disposal.

Thus, dredged material may come into suspension:

- during dredging itself as a result of disturbance of the substratum; and
- during transport to the surface, overflow from barges or leakage of pipelines, during transport between dredging and disposal sites, and during disposal of dredged material (Jensen and Mogensen, 2000).

 <b>IGI Poseidon</b>	<b>EASTMED PIPELINE PROJECT</b>	 
	EastMed Greek Section – Environmental and Social Impact Assessment	DOCNo: PERM-GREE-ESIA- A09_0007_0_Annex9D
		REV. : 00 PAGE : 32 OF 178

Generally, the effects of dredging on the physical environment include the following:

- Changes of the bathymetry;
  - Alteration of current velocities and wave conditions (Jensen and Mogensen, 2000) which affect the sedimentary regime and may cause erosion under seagrass beds (MacInnis and Ralph, 2003);
- Temporary decrease in water transparency;
- Increased concentrations of suspended matter; and
- Increased rates of sedimentation.

The most likely direct effects of dredging are:

- Physical removal of substratum and associated plants and animals from the seabed;
- Burial due to subsequent deposition of material (Newell et al., 1998); and
- Enhanced turbidity and sedimentation as a result of dredging and disposal operations.




Turbidity changes induced by dredging will only result in adverse environmental effects when the turbidity generated is significantly larger than the natural variation of turbidity and sedimentation rates in the area (Stern and Stickle, 1978; Orpin et al., 2004). Such natural variability can sometimes be substantial and may be caused by factors such as storms, wind-induced wave action, river discharges and other local perturbations. **Dredging activities often generate no more increased suspended sediments than commercial shipping operations, bottom fishing or severe storms** (Pennekamp et al., 1996).

In many environmental impact studies, attention is paid to the effect of turbidity on seagrass ecosystems that is two-fold:

- Light attenuation by suspended material affects the amount of light available to the seagrass plants and associated epiphytes, microphytobenthos and macroalgae. Depending on the depth at which these organisms occur, high turbidity can cause a significant reduction in light availability leading to sub-lethal effects or death; and
- High levels of suspended material can lead to reduced vitality or death in benthic fauna associated with the seagrass beds through clogging of their feeding mechanisms (cilia and siphons) and smothering, especially in filter-feeding organisms such as mussels, oysters and other bivalves.

To capture both effects of turbidity, critical thresholds for turbidity should therefore ideally be determined in terms of light availability at the bottom (in % of surface irradiance) as well as in concentration of total suspended solids (in mg/L).

Reported tolerance limits of coral reef systems for chronic suspended-sediment concentrations range from <10 mg/L in pristine offshore reef areas to >100 mg/L in marginal near-shore reefs. Some

	EASTMED PIPELINE PROJECT		 
	EastMed Greek Section – Environmental and Social Impact Assessment		DOC No: PERM-GREE-ESIA-A09_0007_0_Annex9D
			REV. : 00
			PAGE : 33 OF 178

individual coral species can tolerate short-term exposure (days) to suspended-sediment concentrations as high as 1,000 mg/L while others show mortality after exposure (weeks) to concentrations as low as 30 mg/L. The guidance value for total suspended solids provided by MARPOL Resolution MEPC.159(55) (IMO, 2006) is 35 mg/L for its maritime effluent discharge standard, as well as by the World Bank and International Finance Corporation (IFC) for marine effluent discharges (World Bank Group, 2015)."

### 9 D.3.3. The Plume of Suspended Particulate Matter (SPM)

SPM forms a plume that is transported away from the dredging site by water mass circulation following a path that consists of **3 zones** (Bridges et al. 2010):

- **Initial mixing:** Dredging activity dominates over natural processes;
- **Near-field:** Dispersion and rapid settling of suspended solids prevail; and
- **Far-field:** SPM gradually diminishes and the advection and settling effects are of the same order of magnitude.




The behaviour of the SPM plume depends on the following parameters:

- **Dredging characteristics**, such as the following:
  - type of dredging equipment and method of operation;
  - capacity and output (production rate) of dredging equipment;
  - thickness of dredge cuts; and
  - skill of the operator.
- **Sediment characteristics**, which include the following:
  - Sediment release rates; and
  - Density, size distribution and settling velocity of sediment particles.
- **Site and discharge characteristics**, including
  - water depth;
  - exposed surface area;
  - prevailing currents and waves; and
  - presence of debris or obstructions.

### 9 D.3.4. Sediment Release Rates

The rates of release are derived (Fissel and Lin, 2018):

- from technical documents on specific marine construction activities; and

	EASTMED PIPELINE PROJECT		 	
	EastMed Greek Section – Environmental and Social Impact Assessment		DOC No: PERM-GREE-ESIA-A09_0007_0_Annex9D	
			REV. :	00
			PAGE :	34 OF 178

- from information provided by the marine construction operators and their equipment suppliers.

The volumes and release rates vary considerably depending on dredging operational parameters; for example for sea disposal:

- from large barges, very high volumes of sediment materials are released, typically 2,000 m<sup>3</sup> with nearly 100% release through the bottom of the barge (a split hull barge used for disposal at sea); and
- for mechanical seabed dredging, the release of sediment mass or volume into the receiving waters is much smaller by 3 to 4 orders of magnitude.

The range in reported rates of release values from mechanical dredges is very large; thus, for each specific dredging operation the sediment release rate needs to be estimated based on:

- type and equipment of dredging;
- physical and geotechnical properties of bottom materials to be excavated; and
- operating conditions.

Indicatively, for mechanical dredging:




- Je et al. (2007) suggest that the rate and mass of sediment re-suspended during standard clamshell bucket dredging varied from 0.16% to 0.88% based on 5 field studies for estuarine and freshwater river environments; and
- Burt et al. (2007) provide a higher range of estimated release rates for a specific dredging operation in a river with normal values being 3.35%, but larger values of 5–6% were reported (Stamou et al., 2009), and even very large transient values of 10% or more were noted.

These above-mentioned values are summarised in Table D-2:

**Table D-2 Indicative Sediment Release Rates**

Release Rate	Reference
0.16 – 0.88% (bucket dredging)	Hayes et al. (2007)
3.35%, 5 - 6%, 10%	Burt et al. (2007)
5%	Stamou et al. (2009)
19.5% (drill cuttings)	Jones et al. (2021)
0.2 – 3% (closed mechanical dredges)	Schroeder and Ziegler (2004)

Prepared by School of Civil Engineering - National Tech Univ. of Athens on behalf of ASPROFOS, 2022.




	<b>EASTMED PIPELINE PROJECT</b>		 	
	EastMed Greek Section – Environmental and Social Impact Assessment		DOC No: PERM-GREE-ESIA-A09_0007_0_Annex9D	
			REV. : PAGE :	00 35 OF 178

### 9 D.3.5. Suspended Sediment Concentrations Measured at Field Dredging Sites

Van Rijn (2019) presented a series of field works at dredging sites with various dredging methods in which suspended sediment concentrations (SSC) were measured during dredging. These field works as well some additional works are summarised in Table D-3 and Table D-4. Cmin and Cmax denote minimum and maximum SSC values, respectively; B, M and S denote near the bottom, mid-depth and surface, respectively; Umin and Umax denote minimum and maximum current velocity, respectively.




**Table D-3 Measured Suspended Sediment Concentrations (SSC) at Dredging Sites Using Mechanical Dredgers**

Researcher	Mechanical Dredging	Region	x	Cmin (mg/L)	Cmax (mg/L)	B/M/S	Umin (m/s)	Umax (m/s)
Hayes et al. (1984)	Closed Clamshell Bucket	USA	6	50	500	B		
Clarke et al. (2007)	Mechanical dredge with an environmental bucket	Arthur Kill Waterway, New Jersey, USA	10	300	300	B	0.3	0.4
Sosnowski (1984)	Grab dredging - barge mounted crane with an open clamshell bucket	New Thames River and Eastern Long Island Sound (USA)	50	100	1000	B	0.5	2.0
Wakeman et al. (1975)	Grab dredging	Oakland Inner Harbour	50	280	280	B		
Clarke et al. (2007)	Mechanical dredge with an environmental bucket	Arthur Kill Waterway, New Jersey, USA	60	100	200	B		
Wakeman et al. (1975)	Grab dredging	Oakland Inner Harbour	100	100	100	B		
Clarke et al. (2007)	Mechanical dredge with an environmental bucket	Arthur Kill Waterway, New Jersey, USA	100		<100	B		

	<p style="text-align: center;"><b>EASTMED PIPELINE PROJECT</b></p> <p style="text-align: center;">EastMed Greek Section – Environmental and Social Impact Assessment</p>	<div style="display: flex; justify-content: space-between; align-items: center;">   </div> <p>DOC No: PERM-GREE-ESIA-A09_0007_0_Annex9D</p> <p>REV. : 00</p> <p>PAGE : 36 OF 178</p>
---	--	--

Researcher	Mechanical Dredging	Region	x	Cmin (mg/L)	Cmax (mg/L)	B/M/S	Umin (m/s)	Umax (m/s)
Sosnowski (1984)	Grab dredging - barge mounted crane with an open clamshell bucket	New Thames River and Eastern Long Island Sound (USA)	300	10	20	B	0.5	2.0
Clarke et al. (2007)	Mechanical dredge with an environmental bucket	Arthur Kill Waterway, New Jersey, USA	350		<20	B		
Wakeman et al. (1975)	Grab dredging	Oakland Inner Harbour	400	40	40	B		
Bernard (1978)	Grab (clamshell)	USA	50-100		<200	B		
Wakeman et al. (1975)	Grab dredging	Oakland Inner Harbour	50	50	50	M		
Wakeman et al. (1975)	Grab dredging	Oakland Inner Harbour	100	60	60	M		
Wakeman et al. (1975)	Grab dredging	Oakland Inner Harbour	50	80	80	S		
Sosnowski (1984)	Grab dredging - barge mounted crane with an open clamshell bucket	New Thames River and Eastern Long Island Sound (USA)	50	10	100	S	0.5	2.0
Wakeman et al. (1975)	Grab dredging	Oakland Inner Harbour	100	40	40	S		
Sosnowski (1984)	Grab dredging - barge mounted crane with an open clamshell bucket	New Thames River and Eastern Long Island Sound (USA)	200	5	5	S	0.5	2.0
Wakeman et al. (1975)	Grab dredging	Oakland Inner Harbour	400	25	25	S		



	<b>EASTMED PIPELINE PROJECT</b>		 	
	EastMed Greek Section – Environmental and Social Impact Assessment		DOC No: PERM-GREE-ESIA-A09_0007_0_Annex9D	
			REV. :	00
			PAGE :	37 OF 178

Prepared by School of Civil Engineering - National Tech Univ. of Athens on behalf of ASPROFOS, 2022.

**Table D-4 Measured Suspended Sediment Concentrations (SSC) at Dredging Sites Using Mechanical Dredgers**

Researcher	Mechanical Dredging	Region	x	Cmin (mg/L)	Cmax (mg/L)	B/M/S	Umin (m/s)	Umax (m/s)
Willoughby and Crabb (1983)	Trailing suction hopper dredger	Moreton Bay, Middle Banks, Australia	3	500	500	B		0.6
Bernard (1978)	Cutter	USA	3	10,000	10,000	B		
Hayes et al. (1984)	Cutterhead	USA	6	100	1,000	B		
Hayes et al. (1984)	Hopper with overflow	USA	30	900	900	B		
Wakeman et al. (1975)	Trailing suction hopper dredging without overflow	Mare Island Strait (San Francisco Bay, USA)	50	230	230	B		
Wakeman et al. (1975)	Cutterhead dredging	Mare Island Strait (San Francisco Bay, USA)	50	70	70	B		
Wakeman et al. (1975)	Trailing suction hopper dredging with overflow	Mare Island Strait (San Francisco Bay, USA)	50	165	870	B		
Wakeman et al. (1975)	Cutterhead dredging	Mare Island Strait (San Francisco Bay, USA)	100	55	55	B		
Stuber (1976)	Agitation dredging	Savannah river channel, USA	100-300	200	400	B		1-1.5
Wakeman et al. (1975)	Cutterhead dredging	Mare Island Strait (San Francisco Bay, USA)	400	50	50	B		




Researcher	Mechanical Dredging	Region	x	Cmin (mg/L)	Cmax (mg/L)	B/M/S	Umin (m/s)	Umax (m/s)
Bernard (1978)	Cutter	USA	500	100	200	B		
Bernard (1978)	Hopper (near drag heads)	USA	1,200	10,000	20,000	B		
Stuber (1976)	Agitation dredging	Savannah river channel, USA	100-300	100	200	M		1-1.5
Willoughby and Crabb (1983)	Trailing suction hopper dredger	Moreton Bay, Middle Banks, Australia	3	50	50	S		
Hayes et al. (1984)	Hopper with overflow	USA	30	350	350	S		
Hayes et al. (1984)	Hopper without overflow	USA	30	50	50	S		
Wakeman et al. (1975)	Trailing suction hopper dredging with overflow	Mare Island Strait (San Francisco Bay, USA)	50	75	350	S		
Wakeman et al. (1975)	Trailing suction hopper dredging without overflow	Mare Island Strait (San Francisco Bay, USA)	50	210	210	S		

Prepared by School of Civil Engineering - National Tech Univ. of Athens on behalf of ASPROFOS, 2022.

### 9 D.3.6. Summary of Practical Experience on Dredging

Van Rijn (2019) summarized the practical experience on suspended sediment concentrations (SSC) during dredging; his main conclusions are as follows:

- Mechanical dredgers cause increases of SSC in the range of 50 to 200 mg/L at about 50 m from the dredge point, but most data are less than 100 mg/L. Generally, the larger the dredger the higher the SSC but, as the size increases, the overall volume of sediment lost as a percentage of the total volume dredged tends to decrease. The mechanical dredgers have relatively high values of re-suspension factor (5-15%) close to the dredging point, but the concentration increase is not

	<p style="text-align: center;"><b>EASTMED PIPELINE PROJECT</b></p> <p style="text-align: center;">EastMed Greek Section – Environmental and Social Impact Assessment</p>	<div style="display: flex; justify-content: space-between; align-items: center;">   </div> <p>DOC No: PERM-GREE-ESIA- A09_0007_0_Annex9D</p> <p>REV. : 00</p> <p>PAGE : 39 OF 178</p>
---	--	---

that high because the sediment is well dispersed throughout the water column and over a wide area at low concentrations before finally settling; and




- Table D-5 shows dilution factors based on measured data and theoretical dispersion studies (Section 9 D.6). In most cases, the SSC decay to the background values within 500 m, except for hopper dredging with overflow.

**Table D-5 Dilutions at Distances of 200 m, 500 m and 5000 m from the Source for Various Current Velocities**

Current velocity (m/s)	At 200 m	At 500 m	At 5,000 m
0.1-0.3	5	10	50
0.3-0.5	5	10	25
0.5-1.0	5	7	15
1.0-1.5	5	7	10

Prepared by School of Civil Engineering - National Tech Univ. of Athens on behalf of ASPROFOS, 2022.

- Cutter suction dredgers produce SSC which are quite high near the cutter-head (1,000-10,000 mg/L), but are quite small away from the cutter. Trailing suction hopper dredgers can inject considerable quantities of fines into the water column when overflowing. SSC close behind the dredger can reach up to 500 mg/L at the water surface and as much as 5,000 mg/L near the bed. If operating without overflow, very little sediment is brought into suspension (generally smaller than about 200 mg/L). The overflow mixture tends to descend towards the bed quite rapidly as a dense plume due to its relatively high density and high rate of delivery;
- Large suction hopper dredgers can produce just as much turbidity (in terms of re-suspension factors) as small backhoe grab dredgers. The values of the re-suspension factor do not depend greatly on production capacity. Results from various field sites show that the SSC (i) are greatest near the bottom, (ii) decrease rapidly with distance from the dredger; decrease is less rapid if currents are relatively swift and (iii) are greatest for very fine sediments;
- The decay times (after cessation of dredging) is about 3 hours at depths of 5 to 10 m, which implies that suspended sediments sink relatively quickly to the bed after cessation of dredging operations in conditions with relatively low currents (< 0.5 m/s). The effective settling velocities of fines/mud are in the range of 0.5 to 2 mm/s (due to flocculation effects);
- The turbidity increase near dredgers in the harbour basins of Rotterdam was found to be of the same order of magnitude as the turbidity increase due to sailing and mooring of vessels (re-suspension due to propeller of vessels with tugs and the return flows between bottom side of vessels and the bed in shallow water). Turbidity increases up to 500 mg/L (background concentration of 20 mg/L) were measured at distances of about 50 to 200 m from a large bulk

	EASTMED PIPELINE PROJECT		 
	EastMed Greek Section – Environmental and Social Impact Assessment		DOC No: PERM-GREE-ESIA-A09_0007_0_Annex9D
			REV. : 00
			PAGE : 40 OF 178

carrier during mooring at the quay wall with assistance of four tugs in one of the harbour basins of Rotterdam. The annual production of turbidity during maintenance dredging in the Botlek harbour basin of Rotterdam is of the same order as the production of turbidity due to the passage and mooring of all vessels in a year in this basin; and

- Turbidity can be greatly reduced by modification of the standard dredging procedures (overflow using special return pipes at bottom side of vessel; closed grab or clamshells; silt curtains or screens around mechanical dredgers); see section 9 D.3.6.

### 9 D.3.7. Measures Reducing Suspended Sediment Concentrations during Dredging




There are various measures that can be applied to reduce the SSC during dredging that are summarised as follows; see Van Rijn (2019) and John et al. (2000):

- Use auger dredgers that employ special equipment to move material towards the suction head and use of pumping by piston action to enable the transportation of high-density material;
- Use disc-cutter dredgers with a cutter head which rests horizontally and rotates its vertical blades slowly;
- Use scoop/sweep dredgers with special equipment to scrape the material towards the suction intake;
- When using a trailing suction hopper dredger: optimise trailing velocity, suction mouth and suction discharge and reduce or even eliminate overflow;
- When using a cutter suction dredger: optimise cutter speed, swing velocity and discharge and employ a special cutter-head design;
- When using a grab dredger, employ watertight grab/clamshell, use silt screen, limit grab time above water and limit grab dragging on bed; and
- When using a backhoe dredger, use a special bucket for reducing sediment losses and silt screen (applicable for current velocities less than 0.5 m/s).

### 9 D.3.8. The CORMIX Mathematical Model

#### 9 D.3.8.1 Development and Application of CORMIX

The CORMIX model was developed in part through cooperation with the US EPA, the US Army Corps of Engineers, and the US Bureau of Reclamation (USEPA, 1999).

	EASTMED PIPELINE PROJECT		 
	EastMed Greek Section – Environmental and Social Impact Assessment		DOC No: PERM-GREE-ESIA-A09_0007_0_Annex9D
			REV. : 00
			PAGE : 41 OF 178

CORMIX (<http://www.cormix.info/>) is used for the analysis, prediction, and design of marine outfall mixing zones resulting from a continuous point discharge of effluents into open coastal waters (Doneker & Jirka, 2007).

CORMIX models the 3 key stages of effluent plume evolution (also, see section 9 D.3.2):

- in the **near field region**, where jet/plume dynamics are dominated by the momentum of the discharge;
- in the **buoyant spreading region**, where buoyancy of the effluent stream is dynamically important; and
- in the **ambient spreading region**, where full vertical mixing has occurred and the effluent plume is controlled by the ambient flow.

Efficient computational algorithms provide simulation results for mixing zone problems with spatial scales of metres to kilometres. Extensive comparison with available field and laboratory data has shown that the CORMIX system predictions on plume concentrations (with associated plume geometries) are reliable for the majority of cases (Jirka, 2004; Doneker et al., 2004).

CORMIX employs an easy-to-use rule-based expert system to screen input data and check for consistency and selects the appropriate hydrodynamic model to simulate the physical mixing processes likely to be present from any complex flow patterns within a given discharge-environment interaction.




The **hydrodynamic flow classification** schemes in the CORMIX system are developed based on dimensional analysis arguments as the detailed methods for modelling the dynamics of effluent discharges in complex physical situations are not available.

CORMIX classifies the flow class of the effluent discharge in the receiving water body based on the relative magnitudes of **length scales**; see section 9 D.3.8.2.

We use these length scales:

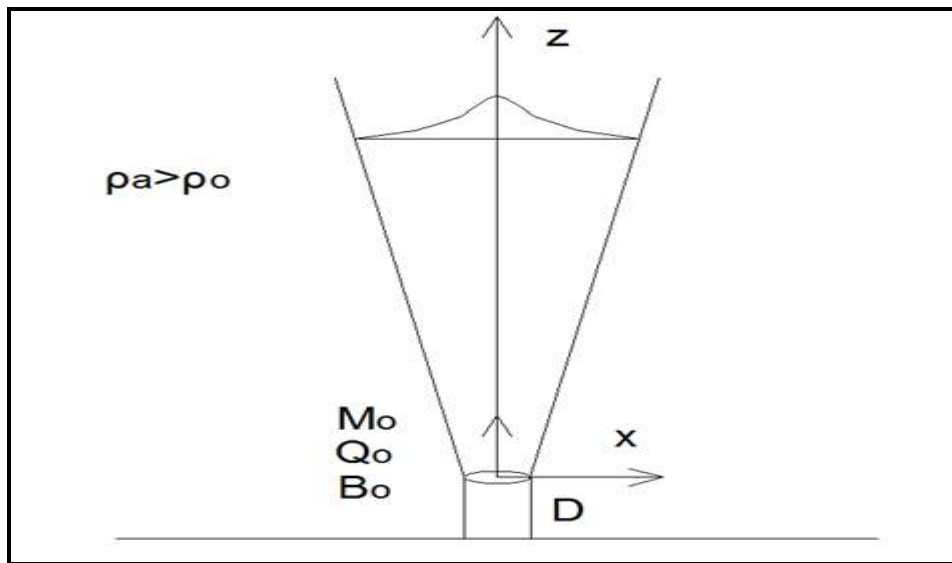
- to measure the influence of each potential mixing process due to momentum flux and buoyancy of the discharge in relation to boundary interactions; and then
- to predict steady-state mixing zone characteristics and plume dynamics, such as free jets, shoreline-attached jets, wall jets, and upstream intruding plumes (Doneker & Jirka, 2007; Jirka, 2004).

#### **9 D.3.8.2 Brief Description of the General Jet Theory and Length Scales**

	<p style="text-align: center;"><b>EASTMED PIPELINE PROJECT</b></p> <p style="text-align: center;">EastMed Greek Section – Environmental and Social Impact Assessment</p>	<div style="display: flex; justify-content: space-between; align-items: center;">   </div> <div style="display: flex; justify-content: space-between;"> <div> DOC No: PERM-GREE-ESIA- A09_0007_0_Annex9D REV. : PAGE : </div> <div> 00 42 OF 178 </div> </div>
---	--	--

Let us assume that a coastal discharge is performed via a single port of diameter  $D$  with an initial velocity ( $U_o$ ), an initial (volume flux or) flow rate ( $Q_o$ ), an initial momentum flux ( $M_o$ ), and an initial density difference ( $\Delta\rho_o = \rho_a - \rho_o$ , where  $\rho_o$  is the initial density of the discharge and  $\rho_a$  is the ambient density), which creates an initial buoyancy flux ( $B_o$ ).

Coastal discharge creates a velocity discontinuity between the discharged fluid and the ambient fluid causing an intense shearing action; this hydrodynamic feature is called “jet” (Jirka et al., 1996).



Prepared by School of Civil Engineering - National Tech Univ. of Athens on behalf of ASPROFOS, 2022.

**Figure D-11 Schematic Representation of a Jet**

We can calculate the initial fluxes using the following equations:

Initial volume flux:

$$Q_o = \frac{\pi D^2}{4} U_o \quad (1)$$




Initial specific momentum flux:

$$M_o = \frac{\pi D^2}{4} U_o^2 = Q_o U_o \quad (2)$$

Initial specific buoyancy flux:

$$B_o = g \frac{\Delta\rho_o}{\rho_a} Q_o = g \frac{\rho_a - \rho_o}{\rho_a} Q_o = g'_o Q_o \quad (3)$$

Where:

	<b>EASTMED PIPELINE PROJECT</b>		 	
	EastMed Greek Section – Environmental and Social Impact Assessment		DOC No: PERM-GREE-ESIA-A09_0007_0_Annex9D REV. : 00 PAGE : 43 OF 178	

$$g'_o = g \frac{\rho_a - \rho_o}{\rho_a} \quad (4)$$

is the effective gravity acceleration.

We characterise a jet as laminar or turbulent based on the Reynolds number ( $Re_o$ ):

$$Re_o = \frac{U_o D}{\nu} \quad (5)$$

Where  $\nu$  is the kinematic viscosity of the discharged effluent; when  $Re_o$  is greater than 2,000 then the jet is turbulent.

It has been found that the above-mentioned initial fluxes govern the dilution of round buoyant turbulent jets provided that  $Re > 4,000$  (Fischer et al., 1979).

There are two extreme cases of jets:

- the simple jet; and
- the simple plume.




The “simple jet” has a density equal to the density of the ambient fluid, i.e.  $\Delta\rho_o = 0$ ; then,  $B_o = 0$  and the behaviour of the flow is dominated by the initial momentum flux ( $M_o$ ). The “simple plume” has a negligible initial velocity and momentum flux, i.e.  $U_o \approx 0$  and  $M_o \approx 0$ , while its density is smaller than the density of the ambient fluid, i.e.  $\Delta\rho_o = \rho_a - \rho_o > 0$ .

There are two basic length scales that affect the behaviour of a jet, which are determined by the following equations:

$$L_M = \frac{M_o^{3/4}}{B_o^{1/2}} = \frac{(Q_o U_o)^{3/4}}{\sqrt{g'_o} Q_o^{1/2}} = \frac{Q_o^{1/4} U_o^{3/4}}{\sqrt{g'_o}} = \frac{\left(\frac{\pi D^2}{4}\right)^{1/4} U_o^{1/4} U_o^{3/4}}{\sqrt{g'_o}} = \left(\frac{\pi}{4}\right)^{1/4} \frac{U_o D^{1/2}}{\sqrt{g'_o}} \quad (6)$$

$$\text{and } L_Q = \frac{Q_o}{M_o^{1/2}} = \frac{\frac{\pi D^2}{4} U_o}{\left(\frac{\pi D^2}{4} U_o^2\right)^{1/2}} = \left(\frac{\pi}{4}\right)^{1/2} D \quad (7)$$

Two of the most important parameters in the study of jets that compare the initial momentum and buoyancy fluxes and length scales (see Fischer et al. (1979) and Chen and Rodi (1980)) are the following:

	<b>EASTMED PIPELINE PROJECT</b>	 	
	EastMed Greek Section – Environmental and Social Impact Assessment	DOC No: PERM-GREE-ESIA-A09_0007_0_Annex9D REV. : 00 PAGE : 44 OF 178	

Initial densimetric Froude number:

$$F_o = \frac{U_o}{\sqrt{g_o' D}} \quad (8)$$

Richardson (plume) number:




$$R_o = \frac{L_Q}{L_M} = \frac{\left(\frac{\pi}{4}\right)^{1/2} D}{\left(\frac{\pi}{4}\right)^{1/4} \frac{U_o D^{1/2}}{\sqrt{g_o'}}} = \left(\frac{\pi}{4}\right)^{1/4} \left(\frac{1}{\frac{U_o}{\sqrt{g_o' D}}}\right) = \left(\frac{\pi}{4}\right)^{1/4} \frac{1}{F_o} \quad (9)$$

In Table D-6 we compare the mentioned length scales and numbers for the cases of simple plume and simple jet for a round and a 2D jet.

**Table D-6 Simple Jet vs. Simple Plume**

Parameter	Round Jet/Plume	2D Jet/Plume	Simple Jet ( $\rho_o - \rho_a = 0$ )	Simple Plume ( $U_o = 0$ )
$g_o'$	$g_o' = g \frac{\rho_a - \rho_o}{\rho_a}$	$g_o' = g \frac{\rho_a - \rho_o}{\rho_a}$	0	Not zero
$Q_o$	$Q_o = \frac{\pi D^2}{4} U_o$	$Q_o = I_d w_d U_o$	Not zero	Not zero
$M_o$	$M_o = Q_o U_o$	$M_o = Q_o U_o$	Not zero	0
$B_o$	$B_o = g_o' Q_o$	$B_o = g_o' Q_o$	0	Not zero
$L_M$	$L_M = \frac{M_o^{3/4}}{B_o^{1/2}} = \left(\frac{\pi}{4}\right)^{1/4} D F_o$	$L_M = \frac{\left(\frac{M_o}{I_d}\right)}{\left(\frac{B_o}{I_d}\right)^{2/3}} = \frac{U_o^{4/3} w_d^{1/3}}{(g_o')^{2/3}}$	Very high	Very low
$L_Q$	$L_Q = \frac{Q_o}{M_o^{1/2}} = \left(\frac{\pi}{4}\right)^{1/2} D$	$L_Q = \frac{\left(\frac{Q_o}{I_d}\right)^2}{\left(\frac{M_o}{I_d}\right)} = w_d$	Not zero	0
$F_o$	$F_o = \frac{U_o}{\sqrt{g_o' D}}$	$F_o = \frac{U_o}{\sqrt{g_o' w_d}}$	Very high	Very low



 <b>IGI Poseidon</b>	<b>EASTMED PIPELINE PROJECT</b>	 
	EastMed Greek Section – Environmental and Social Impact Assessment	DOC No: PERM-GREE-ESIA- A09_0007_0_Annex9D
		REV. : 00
		PAGE : 45 OF 178

Parameter	Round Jet/Plume	2D Jet/Plume	Simple Jet ( $\rho_o - \rho_a = 0$ )	Simple Plume ( $U_o = 0$ )
$R_o = \frac{L_Q}{L_M}$	$R_o = \left(\frac{\pi}{4}\right)^{1/4} \frac{1}{F_o}$	$R_o = \frac{\left(\frac{Q_o}{l_d}\right)^2 \left(\frac{B_o}{l_d}\right)^{2/3}}{\left(\frac{M_o}{l_d}\right)^2} = \frac{1}{F_o^{4/3}}$	0	Very high

Prepared by School of Civil Engineering - National Tech Univ. of Athens on behalf of ASPROFOS, 2022.

#### 9 D.3.8.3 Negatively Buoyant Jets in a Moving Ambient

The introduction in the jet of moving ambient with velocity  $u_a$  results is an **advected jet**. The discharge can be in the same direction as the ambient motion, in the opposite direction, perpendicular to the ambient motion, or at some intermediate angle. These flows are referred to as a jet in a co-flow, jet in a counter-flow, jet in a cross-flow and oblique discharged advected jet, respectively.

In an advected buoyant jet:




- Firstly, the initial momentum flux generally dominates the behaviour close to the source. This type of flow is called a strong jet - weakly advected; the behaviour of the flow is similar to that of the simple jet;
- Secondly, if the buoyancy-generated momentum flux dominates after the strong jet region, the flow behaves like a plume; and
- Then, further away from the source the entrained ambient momentum flux dominates the flow and the type of flow changes; the flow is now said to be strongly advected.

Buoyant jets can be further classified as

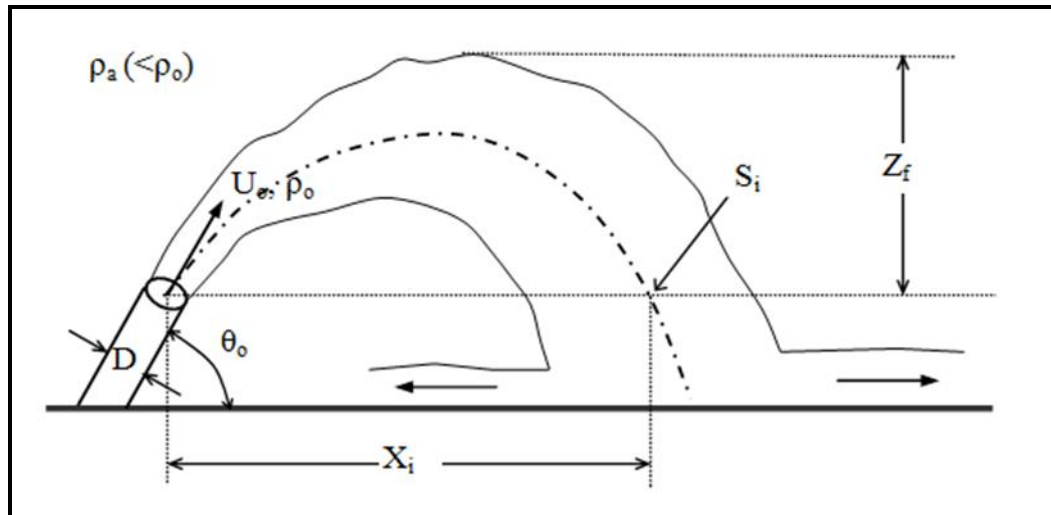
- positively buoyant jets; and
- negatively buoyant jets.

In the positively buoyant jets the vertical component of the initial momentum flux acts in the same direction as the buoyancy force; in these jets the discharge direction can vary from vertical to horizontal, while the remaining initial discharge angles create negatively buoyant jet flows, because the vertical component of the initial momentum flux acts in the opposite direction of the buoyancy force.

**The discharge of sediment into coastal waters creates a negatively buoyant jet.** In Figure D-12 we can see a schematic representation of a negatively buoyant jet with its main geometrical and dilution

	<p style="text-align: center;"><b>EASTMED PIPELINE PROJECT</b></p> <p style="text-align: center;">EastMed Greek Section – Environmental and Social Impact Assessment</p>	<div style="display: flex; justify-content: space-between; align-items: center;">   </div> <p>DOC No: PERM-GREE-ESIA- A09_0007_0_Annex9D</p> <p>REV. : 00</p> <p>PAGE : 46 OF 178</p>
---	--	---

characteristics, such as the maximum rise height ( $Z_f$ ), horizontal distance to impact point ( $X_i$ ) and the dilution at the impact point ( $S_{min}$ ).



Prepared by School of Civil Engineering - National Tech Univ. of Athens on behalf of ASPROFOS, 2022.




**Figure D-12** Schematic Representation of a Negatively Buoyant Jet (Obtained from Papakostantis et al., 2013)

#### 9 D.3.8.4 Application of CORMIX to Sediment Plumes

CORMIX has advanced tools for suspended sediment (dredge sediments option) that extends the capability of CORMIX to simulate the initial mixing and dispersion of dredge sediment discharge, which includes side-casting surface discharge of sediments (Doneker et al., 2004), and the (hydrodynamic module) DHYDRO simulates dense suspended sediment discharges (submerged, surface, and above surface).

The model includes the Stokes effect of particle settling on plume behaviour with emphasis on the resulting plume density current, and accounts for the settling of five particle size classes when using the default dredge sediments option (Doneker & Jirka, 2007; Doneker et al., 2004):

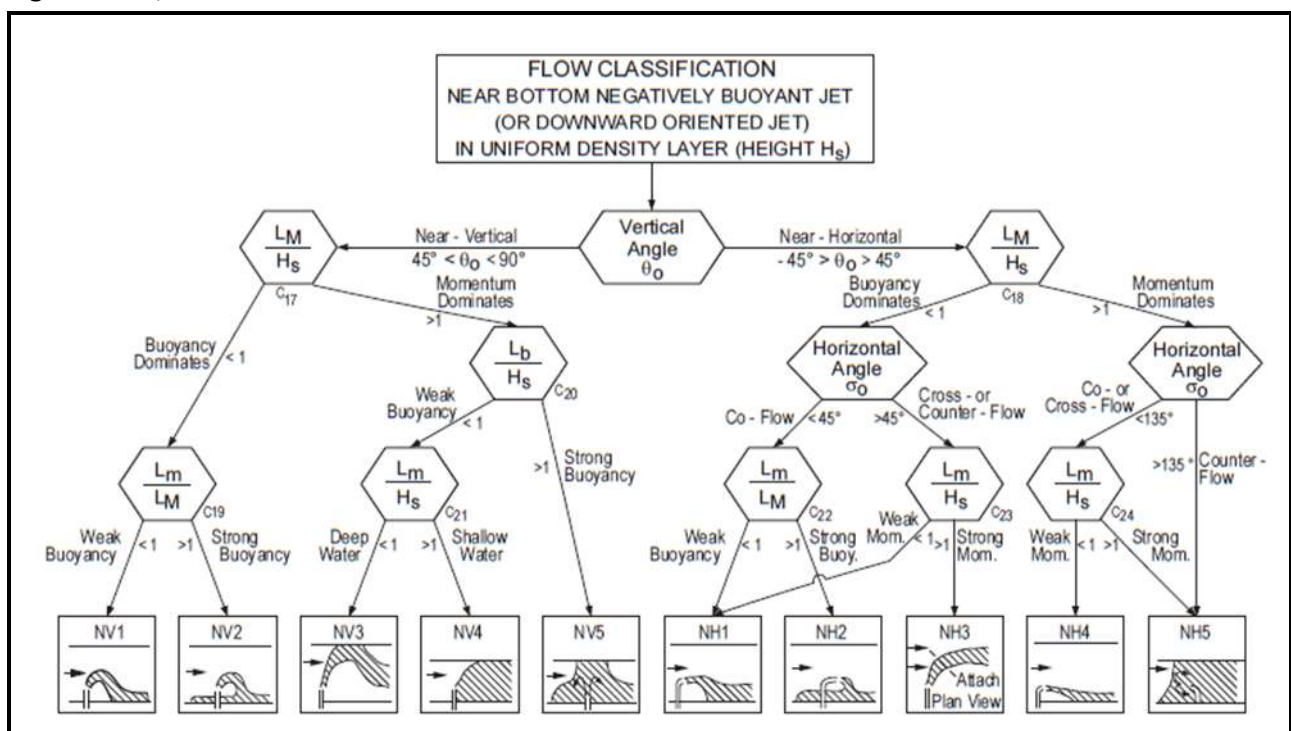
- **Chunks (non-suspended solids and stones)** larger than 2 mm that will separate out immediately from the plume;
- **sand:** suspended particles in the range 0.062 – 2 mm with settling velocity 0.031 m/s;
- **coarse silt:** suspended particles in the range 0.016 – 0.062 mm with settling velocity  $0.42 \times 10^{-3}$  m/s;
- **fine silt:** suspended particles in the range 0.004 – 0.016 mm with settling velocity  $0.26 \times 10^{-4}$  m/s; and

	<p style="text-align: center;"><b>EASTMED PIPELINE PROJECT</b></p> <p style="text-align: center;">EastMed Greek Section – Environmental and Social Impact Assessment</p>	<div style="display: flex; justify-content: space-between; align-items: center;">   </div> <p>DOC No: PERM-GREE-ESIA-A09_0007_0_Annex9D</p> <p>REV. : 00</p> <p>PAGE : 47 OF 178</p>
---	--	--

- **clay**: suspended particles less than 0.004 mm with settling velocity  $0.65 \times 10^{-6}$  m/s.

For the shallow water depth of 3.5 m, the settling time for sand particles is about 2 minutes, for coarse silt about 2.3 hours, for fine silt about 1.6 days, and for clay particle more than 62 days (Purnama et al. 2016).

The CORMIX flow classification of negatively buoyant discharges in uniform layer flow are shown in Figure D-13; the main flow classes are NV and NH.





Prepared by School of Civil Engineering - National Tech Univ. of Athens on behalf of ASPROFOS, 2022.

**Figure D-13 CORMIX Flow Classification of Negatively Buoyant Discharges in Uniform Layer low: Flow Classes NV and NH (Source: Doneker & Jirka, 2007)**

The CORMIX has already been applied in various cases of sediment discharges; see for example Purnama et al. (2015, 2016), Doneker et al. (2004).

### 9 D.3.8.5 Discharge (Module 101)

In this module the flow is converted from a uniform velocity distribution to a Gaussian profile, with equivalent volume flux (note that momentum flux conservation is assured due to the bulk flow parameters used in the analysis). The representative final flow width  $b_f$  for the discharge module is:

	<b>EASTMED PIPELINE PROJECT</b>		
		DOC No: PERM-GREE-ESIA- A09_0007_0_Annex9D REV. : PAGE :	00 48 OF 178

$$b_f = \left( \frac{A_0}{\pi} \right)^{1/2} \quad (10)$$

while  $A_0$  is the port cross sectional area. No dilution is assumed to occur, so that  $S_f = 1.0$  and  $c_f = c_0$ , where  $S_f$  is final dilution and  $c_f$  and  $c_0$  are the final and discharge s concentrations, respectively. The final x- and y- coordinates are 0, but  $z_f = h_0$ .

#### 9 D.3.8.6 Near-Field Mixing of a 3D Jet (Module 110)




A definition diagram for a buoyant jet in unbounded stratified ambient crossflow is given in Figure D-14 in a global Cartesian coordinate system  $x, y, z$  in which  $x$  points down-current and  $z$  upward against gravity  $g$ . The ambient has a stable density distribution  $\rho_a(z)$  that may be given directly, or may depend on one or more state  $\rho = \rho(X_i)$ . Typically,  $X_i$  would be represented by ambient temperature  $T_a$  and salinity  $S_a$  for water bodies. The ambient also has a sheared velocity profile  $u_a(z)$ . The jet efflux with diameter  $d_0$  is located at  $(0, 0, h_0)$ , where  $h_0$  is the height above the  $x$ - $y$  plane. It is oriented with a vertical angle  $\theta_0$  above horizontal and a horizontal angle  $\sigma_0$  defined as the angle between the vertical projection of the jet axis and the  $x$  axis. The buoyant jet has a nominally unsheared (top-hat) efflux velocity  $U_0$ , an efflux density  $\rho_0$  – alternatively given by the discharge state parameters,  $\rho_0 = \rho(X_{i0})$ , and a concentration  $c_0$  representing the tracer or pollutant mass of interest. Thus, the buoyant jet is forced by its initial fluxes of momentum  $M_0$  and of buoyancy  $J_0$  (or  $B_0$ ) (both in kinematic units):

$$M_0 = U_0^2, \quad J_0 = U_0 g'_0 A_0 \quad (11)$$

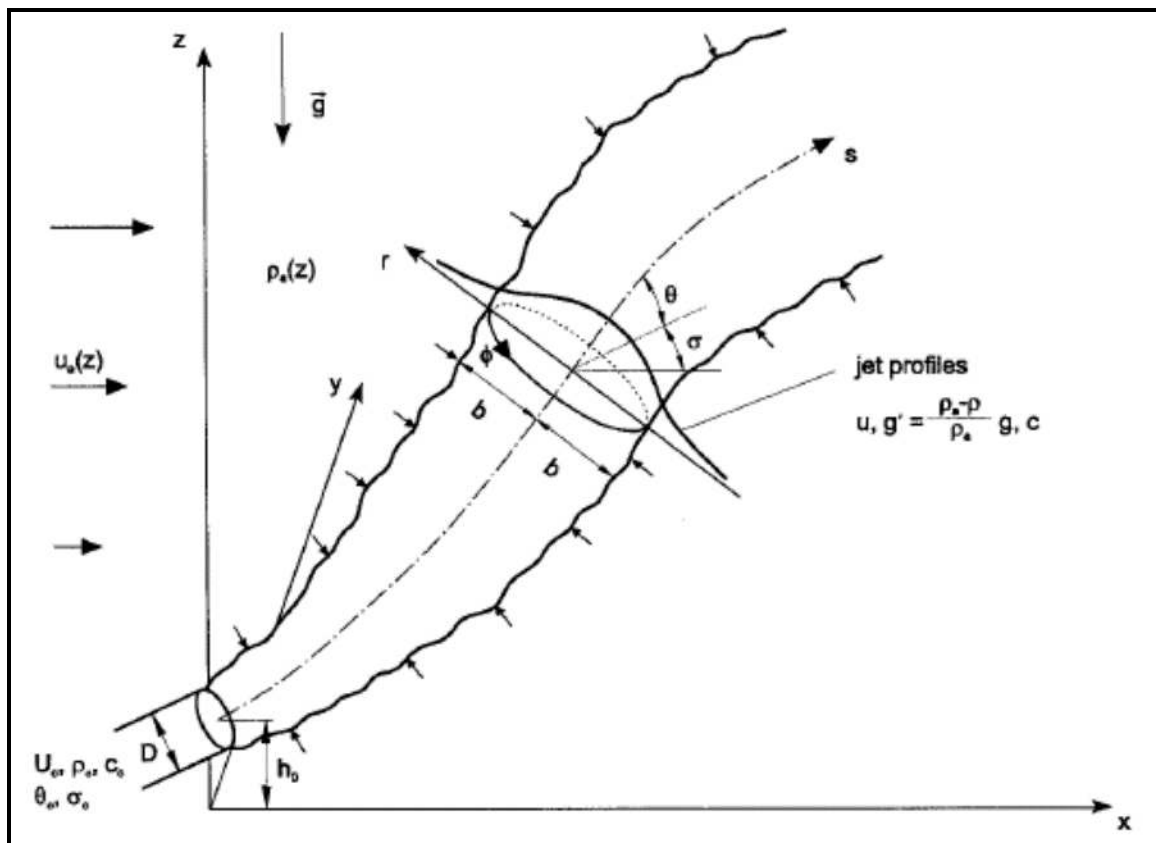
in which  $A_0 = \pi d_0^2 / 4$  is the discharge cross-sectional area and  $g'_0 = [\rho_a(h_0) - \rho_0] g / \rho_{ref}$  the initial buoyant acceleration, where  $\rho_{ref}$  is a constant reference density consistent with the Boussinesq approximation.

The initial mass flux  $Q_{c0} = U_0 c_0 A_0$  is a passive quantity without dynamic influence. The initial discharge (volume flux)  $Q = U_0 A_0$  is a quantity that has limited dynamic influence in the discharge vicinity only, in the so-called **Zone of Flow Establishment (ZOFE)**.

In Figure D-15 the spatial evolution of the buoyant jet along a trajectory  $s$  is shown. A local cylindrical coordinate system with axial distance  $s$ , radial distance  $r$  and azimuthal angle  $\phi$  is defined along the trajectory, and inclined with the local horizontal angle  $\theta$  and horizontal angle  $\sigma$ .

	<p style="text-align: center;"><b>EASTMED PIPELINE PROJECT</b></p> <p style="text-align: center;">EastMed Greek Section – Environmental and Social Impact Assessment</p>	<div style="display: flex; justify-content: space-between; align-items: center;">   </div> <div style="display: flex; justify-content: space-between;"> <div> <p>DOC No: PERM-GREE-ESIA- A09_0007_0_Annex9D</p> <p>REV. : 00</p> <p>PAGE : 49 OF 178</p> </div> </div>
---	--	--




We need to specify **boundary conditions** at the jet efflux, i.e. at the excavation trench (note: in CORMIX these are called initial conditions). The actual jet discharge conditions occur at some location  $(0, 0, h_0)$  where nominally unsheared efflux conditions occur, or in practice, the jet exit velocity profile may contain peripheral boundary layers characteristic of a nozzle flow or of a longer preceding pipe flow section. These conditions are described by the initial values of the flux variables  $M_0$ ,  $J_0$  and  $Q_{c0}$  and the initial angles  $\theta_0$  and  $\sigma_0$ . Two non-dimensional measures, a cross-flow parameter  $R = U_0 / u_a$  and a densimetric Froude number  $F_0 = U_0 / \sqrt{g'_0 d_0}$  characterise the crossflow and buoyancy interaction of the discharge, respectively.



Prepared by School of Civil Engineering - National Tech Univ. of Athens on behalf of ASPROFOS, 2022.

**Figure D-14 Schematic Diagram of an Inclined Buoyant Jet in Unbounded Stratified Ambient Crossflow (Jirka, 2004)**

The objective of any jet analysis is the determination of the **jet trajectory**  $x(s)$ ,  $y(s)$ ,  $z(s)$ , the geometrical factors  $\theta(s)$ ,  $\sigma(s)$ , along with the distributions  $f(r, \phi)$  for the local axial velocity  $u$ , density  $\rho$  (or alternatively, state parameters  $X_i$ ) and concentration  $c$ . In the case of the **jet integral method**, the distribution functions  $f(r, \phi)$  are specified a priori and cease to be the object of analysis. This

	<p style="text-align: center;"><b>EASTMED PIPELINE PROJECT</b></p> <p style="text-align: center;">EastMed Greek Section – Environmental and Social Impact Assessment</p>	<div style="display: flex; justify-content: space-between; align-items: center;">   </div> <p>DOC No: PERM-GREE-ESIA- A09_0007_0_Annex9D</p> <p>REV. : 00</p> <p>PAGE : 50 OF 178</p>
---	--	---

approach is obviously inspired by the tenets of self-similarity for simple free turbulence motions (e.g., jets, wakes), but can only be approximate for the general buoyant jet that is not in equilibrium, but rather in transition among five possible states of self-similarity, as is shown below. With this restriction, we derive the following distribution functions based on Gaussian profiles:

$$u = u_c e^{-r^2/b^2} + u_a \cos \theta \cos \sigma \quad (12)$$

$$g' = g'_c e^{-r^2/(\lambda b)^2} \quad (13)$$

$$X_i = X_{ic} e^{-r^2/(\lambda b)^2} + X_{ia}(z) \quad (14)$$

$$c = c_c e^{-r^2/(\lambda b)^2} \quad (15)$$

in which  $u_c$  is the excess axial velocity,  $g'_c = [\rho_\alpha(z) - \rho_c] g / \rho_{ref}$ ,  $\rho_c$  is the density,  $X_{ic}$  the excess value of the state parameters, and  $c_c$  the concentration, all on the centreline.  $b$  is a measure of the jet width where the excess velocity is  $e^{-1} = 37\%$  of the centreline value  $u_c$ ,  $\lambda > 1$  is a dispersion ratio as the observed width of the scalar distribution is larger than for the velocity (turbulent Schmidt number).

Through cross-sectional integration the following bulk variables for total volume flux  $Q$ , axial momentum flux  $M$ , buoyancy flux  $J$ , flux of excess state parameter  $Q_{xi}$  and tracer mass flux  $Q_c$ , respectively, are obtained:

$$Q = 2\pi \int_0^{R_j} u r dr = \pi b^2 (u_c + 2u_a \cos \theta \cos \sigma) \quad (16)$$



$$M = 2\pi \int_0^{R_j} u^2 r dr = \frac{1}{2} \pi b^2 (u_c + 2u_a \cos \theta \cos \sigma)^2 \quad (17)$$

$$J = 2\pi \int_0^{R_j} u g' r dr = \pi b^2 \left( u_c \frac{\lambda^2}{1 + \lambda^2} + \lambda^2 u_a \cos \theta \cos \sigma \right) g'_c \quad (18)$$

$$Q_{xi} = 2\pi \int_0^{R_j} u (X_i - X_{ia}) r dr = \pi b^2 \left( u_c \frac{\lambda^2}{1 + \lambda^2} + \lambda^2 u_a \cos \theta \cos \sigma \right) X_{ic} \quad (19)$$

$$Q_c = 2\pi \int_0^{R_j} u c r dr = \pi b^2 \left( u_c \frac{\lambda^2}{1 + \lambda^2} + \lambda^2 u_a \cos \theta \cos \sigma \right) c_c \quad (20)$$

When evaluating the individual terms in these flux quantities the integration limit  $R_j$  is usually taken as  $R_j \rightarrow \infty$  as the definite integrals over the jet profiles, yield bounded values. There are two exceptions in the crossflow contributions (second terms under the parenthesis) for  $Q$  and  $M$ , respectively, in which  $R_j = \sqrt{2}b$ .

	<b>EASTMED PIPELINE PROJECT</b>		
		DOC No: PERM-GREE-ESIA- A09_0007_0_Annex9D REV. : PAGE :	00 51 OF 178

The aforementioned equations are formulated for a jet element of length  $ds$  centred on the trajectory. We make the following assumptions:

- pressure deviations from hydrostatic within the jet are neglected consistent with the boundary layer nature of the flow,
- acceleration effects due to jet curvature are neglected, and
- turbulent momentum and scalar fluxes are neglected relative to the mean fluxes of momentum and scalars.

The conservation principles for volume (continuity), momentum components in the global directions  $x$ ,  $y$  and  $z$ , state parameters, and scalar mass lead to the following equations:

$$\frac{dQ}{ds} = E \quad (21)$$

$$\frac{d}{ds}(M \cos \theta \cos \sigma) = Eu_a + F_D \sqrt{1 - \cos^2 \theta \cos^2 \sigma} \quad (22)$$

$$\frac{d}{ds}(M \cos \theta \sin \sigma) = -F_D \frac{\cos^2 \theta \sin \sigma \cos \sigma}{\sqrt{1 - \cos^2 \theta \cos^2 \sigma}} \quad (23)$$

$$\frac{d}{ds}(M \sin \theta) = \pi \lambda^2 b^2 g'_c - F_D \frac{\sin \theta \cos \theta \cos \sigma}{\sqrt{1 - \cos^2 \theta \cos^2 \sigma}} \quad (24)$$

$$\frac{dQ_{xi}}{ds} = -Q \frac{dX_{ia}}{dz} \sin \theta \quad (25)$$

$$\frac{dQ_c}{ds} = 0 \quad (26)$$

Furthermore, the geometry of the trajectory is defined by:




$$\frac{dx}{ds} = \cos \theta \cos \sigma, \quad \frac{dy}{ds} = \cos \theta \sin \sigma, \quad \frac{dz}{ds} = \sin \theta \quad (27)$$

and the centreline density  $\rho_c$  is given by the equation of state:

$$\rho_c = \rho_c(X_{ic}) \quad (28)$$

The terms  $E$  and  $F_D$  in the equations above represent the entrainment rate and an ambient drag force acting on the jet element. The specification of these turbulent processes constitutes the “**turbulence closure problem**” in the integral formulation. The force term  $Eu_a$  is the entrainment of ambient momentum into the jet and the term  $\pi \lambda^2 b^2 g'_c$  is the buoyancy force.



	<b>EASTMED PIPELINE PROJECT</b>	 	
	EastMed Greek Section – Environmental and Social Impact Assessment	DOC No: PERM-GREE-ESIA-A09_0007_0_Annex9D REV. : 00 PAGE : 52 OF 178	

The **entrainment rate**  $E$  is specified as the additive contributions of the different streamwise and azimuthal shear mechanisms that lead to entrainment of ambient:

$$E = 2\pi b u_c \left( a_1 + a_2 \frac{\sin \theta}{F_l^2} + a_3 \frac{u_a \cos \theta \cos \sigma}{u_c + u_a} \right) + 2\pi b u_a \sqrt{1 - \cos^2 \theta \cos^2 \sigma} a_4 |\cos \theta \cos \sigma| \quad (29)$$

where  $F_l = u_c / \sqrt{g' b}$  is the local densimetric Froude number and depends on the vertical angle  $\theta$ .

CorJet uses the following values for the constants  $a_1$ ,  $a_2$ ,  $a_3$  and  $a_4$ : 0.055, 0.6, 0.055, and 0.5, respectively.

The jet drag  $F_D$  is parameterized as a quadratic law force mechanism:

$$F_D = c_D 2\sqrt{2}b \frac{u_a^2 (1 - \cos^2 \theta \cos^2 \sigma)}{2} \quad (29)$$

in which  $u_a \sqrt{1 - \cos^2 \theta \cos^2 \sigma}$  is the transverse velocity component,  $2\sqrt{2}b$  the jet diameter, and  $c_D = 1.3$  the drag coefficient in obvious analogy to the flow around a cylindrical solid body for which boundary layer separation leads to a pressure reduction in the lee of the body and a turbulent wake that is distinguished by a momentum deficit flux and a vorticity field consisting of unsteady counter-rotating vortices.




According to Jirka (2004), the transition from that more or less uniform efflux section to a fully established jet flow that can be characterised by the approximately self-similar distribution functions takes place in the **initial zone of flow establishment (ZOF)**. The ZOF is a transition region that lacks self-similarity as the initial unsheared profiles undergo changes in form of peripherally growing axisymmetric mixing layers until the final jet profiles are reached. This transition is quite complex, in particular for ambient crossflow on the one hand, and reasonably rapid, up to a distance of about (5 to 10)  $d_0$  on the other. Given the overall jet region of interest, an empirical formulation based on experimental observations is therefore most appropriate for the ZOF.

Subscript e denotes conditions at the end of the ZOF. The ZOF length  $L_e$  is found from a linear spread of the shear layer to be about 6.2  $d_0$  based on velocity profiles or about 5.0  $d_0$  based on scalar profiles, due to the typical dispersion ratio,  $\lambda > 1$  (typical value  $\lambda = 1.20$ ). This basic result is extended to general conditions using the empirical approach of Schatzmann (1978) for **crossflow effects** and the model formulation of Lee and Jirka (1981) for **buoyancy effects**.

Supplementary discharge angles are defined as:

$$\gamma_0 = \sin^{-1} \left( \sqrt{1 - \cos^2 \theta_0 \sin^2 \sigma_0} \right) \quad (30)$$



	<p style="text-align: center;"><b>EASTMED PIPELINE PROJECT</b></p> <p style="text-align: center;">EastMed Greek Section – Environmental and Social Impact Assessment</p>	<div style="display: flex; justify-content: space-around; align-items: center;">   </div> <p>DOC No: PERM-GREE-ESIA- A09_0007_0_Annex9D</p> <p>REV. : 00</p> <p>PAGE : 53 OF 178</p>
---	--	--

$$\delta_0 = \tan^{-1}(\tan \theta_0 / \sin \sigma_0) \quad (31)$$

in which  $\gamma_0$  is the transverse discharge angle relative to the ambient current direction and  $\delta_0$  its projection onto the x-y plane. The modified ZOFE length  $L_e$  and its final transverse angle  $\gamma_e$  are:

$$L_e = 5.0 d_0 (1 - 3.22 \sin \gamma_0 / R) (1 - e^{-2.0 F_0 / F_{lp}}) \quad (32)$$

$$\gamma_e = \tan^{-1} \left( \frac{\sin \gamma_0}{\cos \gamma_0 - (\sqrt{2} - 1) / R} \right) \quad (33)$$

in which  $F_{lp} = u_c / \sqrt{g'_c b}$  ( $b$  is the lateral width at plume cross section where  $u = e^{-1} u_c$ ) is the asymptotic value of the local densimetric Froude number of a pure plume. Hence the initial conditions for the solution of the jet equation system can be stated, for the geometry:

$$\theta_e = \sin^{-1}(\sin \gamma_e \sin \delta_0) \quad (34)$$

$$\sigma_e = \tan^{-1}(\sin \gamma_e \cos \delta_0 / \cos \gamma_e) \quad (35)$$

$$x_e = L_e \cos \theta_{ave} \cos \sigma_{ave} \quad (36)$$




$$y_e = L_e \cos \theta_{ave} \sin \sigma_{ave} \quad (37)$$

$$z_e = h_0 + L_e \sin \sigma_{ave} \quad (38)$$

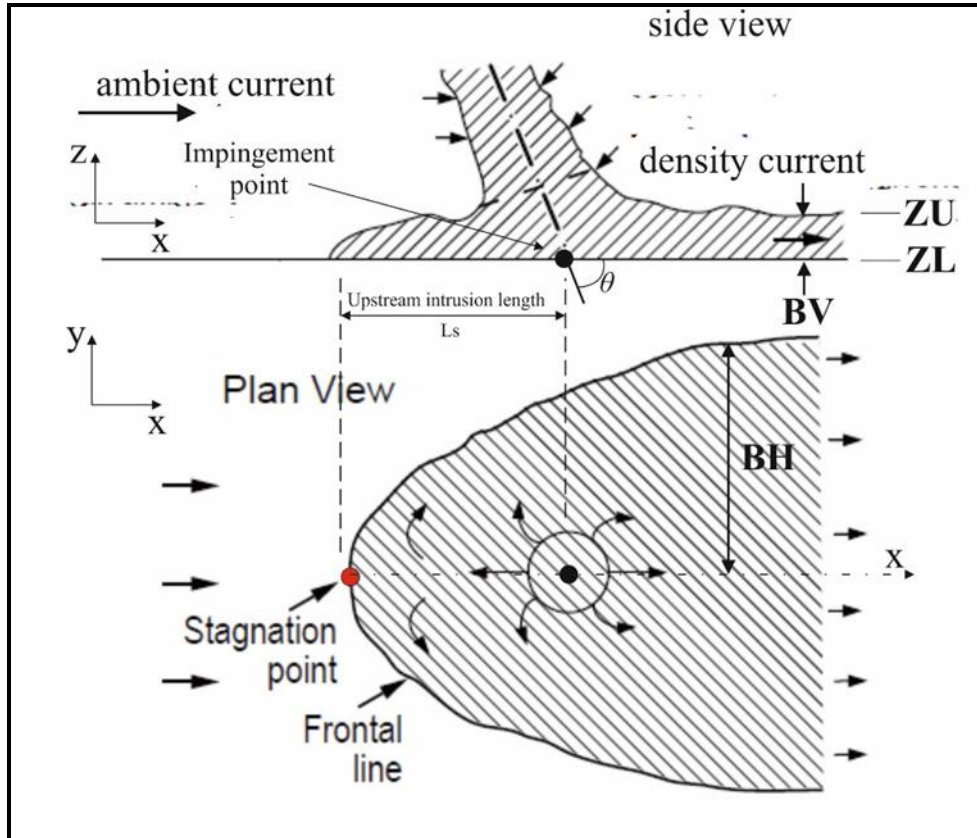
in which  $\theta_{ave} = (\theta_0 + \theta_e) / 2$  and  $\sigma_{ave} = (\sigma_0 + \sigma_e) / 2$ , and for the fluxes  $Q_e = \sqrt{2} Q_0$ ,  $M_e = M_0$ ,  $Q_{Xie} = Q_{Xi0}$  or  $(J_e = J_0)$ ,  $Q_{ce} = Q_{c0}$ , respectively, where  $Q_{xi}$  is the flux of excess state parameter and  $Q_c$  is the tracer's mass flux.

#### 9 D.3.8.7 Bottom Impingement and Spreading (Module 132)

In this surface approach condition, the weakly bent flow impinges on the bottom at a near-vertical angle  $\theta$ , as shown in Figure D-15, where  $\theta_i > 45^\circ$ . After impingement the flow spreads more or less radially along the water surface as a **density current**. In particular, the flow spreads some distance upstream against the ambient flow, and laterally across the ambient flow. This spreading is dominated by the strong buoyancy of the discharge.

	<p style="text-align: center;"><b>EASTMED PIPELINE PROJECT</b></p> <p style="text-align: center;">EastMed Greek Section – Environmental and Social Impact Assessment</p>	<div style="display: flex; justify-content: space-between; align-items: center;">   </div> <div style="display: flex; justify-content: space-between;"> <div> DOC No: PERM-GREE-ESIA- A09_0007_0_Annex9D REV. : 00 PAGE : 54 OF 178 </div> </div>
---	--	---

The lateral spreading of the flow in the surface impingement region is driven by both the flow momentum and buoyancy force. Of interest is the upstream intrusion length  $L_s$ , dilution  $S$ , horizontal width  $B_h$ , and vertical depth  $B_v$  of the density current at surface impingement.



Prepared by School of Civil Engineering - National Tech Univ. of Athens on behalf of ASPROFOS, 2022.




Figure D-15 Schematic Diagram of Impingement Region (Jirka, 2004)

#### 9 D.3.8.8 Upstream Spreading (Module 032)

After impingement the flow spreads more or less radially along the water surface as a density current. In particular, the flow spreads some distance upstream against the ambient flow and laterally across the ambient flow. This spreading is dominated by the strong buoyancy of the discharge. The dilution is expressed as:

$$S_f = S_i S_{SB32} \left[ \frac{L_b}{H_s (1 - \cos \theta_i \cos \sigma_i)} \right]^{1/3} \quad (39)$$

where  $S_{SB32}$  is a dilution constant. The upstream intrusion length  $L_s$  is given by

	<b>EASTMED PIPELINE PROJECT</b>		 	
	EastMed Greek Section – Environmental and Social Impact Assessment		DOC No: PERM-GREE-ESIA-A09_0007_0_Annex9D REV. : 00 PAGE : 55 OF 178	

$$L_s = AL_{32A} \left( \frac{1 - \cos \theta_i \cos \sigma_i}{L_b / H_s} \right)^{2/3} \text{ for } \frac{L_b}{H_s} \leq 165(1 - \cos \theta_i \cos \sigma_i), \text{ and} \quad (40)$$

$$L_s = AL_{32B} L_b \text{ for } \frac{L_b}{H_s} > 165(1 - \cos \theta_i \cos \sigma_i) \quad (41)$$

where  $AL_{32A}$  and  $AL_{32B}$  are constants. The typical vertical thickness within the upstream stagnation region is

$$h_s = CD_{32} S_f L_m \frac{L_Q}{L_b} \quad (42)$$

where  $CD_{32}$  is a constant. The dimensions of the effluent are:

$$b_{hf} = BH_{32} L_s \quad (43)$$

$$b_{vf} = \frac{S_f L_m L_Q}{2b_{hf}} \quad (44)$$

$$\text{The final flow coordinates are: } x_f = x_i + 0.5b_{vf}, \quad y_f = y_i, \text{ and } x_f = x_i. \quad (45)$$




The values of aforementioned constants  $S_{SB32}$ ,  $AL_{32A}$ ,  $AL_{32B}$ ,  $CD_{32}$ ,  $BH_{32}$ , are listed below:

$S_{SB32} = 1.4$ ,  $AL_{32A} = 11.4$ ,  $AL_{32B} = 0.38$ ,  $CD_{32} = 1.0$ , and  $BH_{32} = 2.6$ .

#### 9 D.3.8.9 Bottom Density Current (Module 310)

CORMIX module MOD310 predicts density current behaviour on the inclined seabed using an **integral model approach** that is described below.

The governing integral equations of a steady-state sediment depositing density current on an inclined plane are summarised below (Nash et. al., 1995). The approach includes stepwise-continuous ambient density stratification, crossflow velocity, and bottom inclination. Flow on a sloping bottom with bottom detachment or a surface plunge point is calculated, and sediment accretion rates are reported. This formulation is developed from the mechanics of the buoyant spreading process (Akar and Jirka 1994, 1995). The definition diagram for a density current with particle settling on an incline plane in crossflow appears at the bottom in Figure D-16. The following flux definitions along the sediment density current trajectory assume a top-hat profile distribution for velocity, suspended sediment concentration, and buoyancy:

	<b>EASTMED PIPELINE PROJECT</b>	 	
	EastMed Greek Section – Environmental and Social Impact Assessment	DOC No: PERM-GREE-ESIA-A09_0007_0_Annex9D	
		REV. :	00
		PAGE :	56 OF 178

Volume flux:

$$Q = 2b_v b_h (u_c + u_a \cos \theta \cos \sigma) \quad (46)$$

Momentum flux:

$$Q = 2b_v b_h (u_c + u_a \cos \theta \cos \sigma)^2 \quad (47)$$

Buoyancy flux:

$$J = Qg', \quad g' = g(\rho_\alpha - \rho)\rho_\alpha \quad (48)$$

Clearwater volume flux:

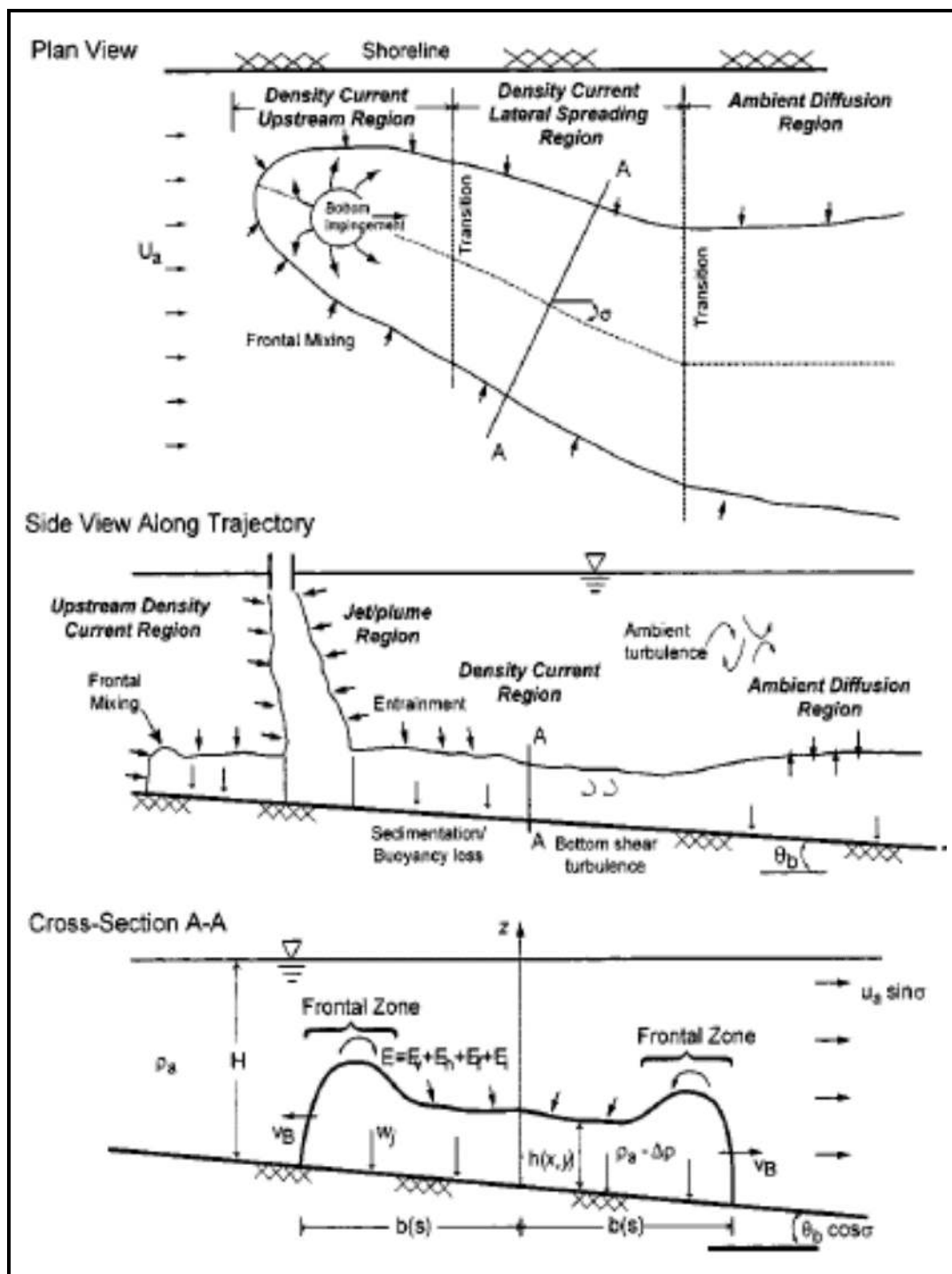
$$Q_{cw} = Q - Q_p / \rho_s \quad (49)$$

Sediment mass flux for particle size class  $j$ :

$$[Q_p]_j = 2b_v b_h (u_c + u_a \cos \theta \cos \sigma) P_j \quad (50)$$




from which the total sediment concentration is given by:

$$P = \sum_1^n P_j \quad (51)$$



Prepared by School of Civil Engineering - National Tech Univ. of Athens on behalf of ASPROFOS, 2022.

Figure D-16 Schematic Diagram Bottom Density Current (Jirka, 2004)

	<p style="text-align: center;"><b>EASTMED PIPELINE PROJECT</b></p> <p style="text-align: center;">EastMed Greek Section – Environmental and Social Impact Assessment</p>	<div style="display: flex; justify-content: space-between; align-items: center;">   </div> <p>DOC No: PERM-GREE-ESIA- A09_0007_0_Annex9D</p> <p>REV. : 00</p> <p>PAGE : 58 OF 178</p>
---	--	---

The change of these flux quantities along the trajectory  $s$  is given by the following conservation equations that are obtained by cross-sectional integration of the following 10 governing turbulent Reynolds equations:

1. Volume flux conservation accounting for turbulent entrainment:

$$\frac{dQ}{ds} = E \quad (52)$$

2. X-momentum flux conservation that is parallel to ambient flow, which accounts for entrainment drag, frontal drag, bottom friction, and buoyant pressure force:

$$\frac{d}{ds}(M \cos \theta \cos \sigma) = F_e + F_D \sqrt{1 - \cos^2 \theta \cos^2 \sigma} - F_\tau \cos \theta \cos \sigma - \frac{d}{ds}(F_p \cos \sigma) \quad (53)$$

3. y-momentum flux conservation (perpendicular to ambient flow) accounting for frontal drag, bottom friction, buoyant body force, and buoyant pressure force:

$$\frac{d}{ds}(M \cos \theta \sin \sigma) = -F_D \frac{\cos^2 \theta \sin \sigma \cos \sigma}{\sqrt{1 - \cos^2 \theta \cos^2 \sigma}} - F_\tau \sin \sigma \sqrt{1 - \cos^2 \theta \cos^2 \sigma} + F_b - \frac{d}{ds}(F_p \sin \sigma) \quad (54)$$

4. Lateral spreading under the influence of buoyancy force against the retarding effects of frontal drag and interfacial friction (Akar and Jirka 1994, 1995):

$$\frac{db_h}{ds} = \sqrt{\frac{-3g'b_v^2}{3C_D b_v (u_c + u_a \cos \theta \cos \sigma)^2 + 2f_i b_h (u_c + u_a \cos \theta \cos \sigma)^2}}, C_D = 1 \quad (55)$$

5. Clearwater buoyancy flux conservation:

$$\frac{d(Q_{cw} \Delta \rho_{cw})}{ds} = Q_{cw} \frac{d\rho_a}{dx} \sqrt{1 - \cos^2 \theta \cos^2 \sigma}, \Delta \rho_{cw} = \rho_a(z) - \rho_{cw} \quad (56)$$

6. Tracer flux conservation:

$$\frac{dQ_c}{ds} = 0 \quad (57)$$

7. Sediment mass flux conservation accounting for particle settling:

$$\frac{d[Q_p]_j}{ds} = -2b_h P_j w_j \text{ for particle sizes } j = 1, 2, 3, 4 \quad (58)$$




8. Longitudinal (x) position:

$$\frac{dx}{ds} = \cos \theta \cos \sigma \quad (59)$$

9. Lateral (y) position:

$$\frac{dy}{ds} = \cos \theta \sin \sigma \quad (60)$$

10. Vertical (z) position:

	EASTMED PIPELINE PROJECT		 	
	EastMed Greek Section – Environmental and Social Impact Assessment		DOC No: PERM-GREE-ESIA-A09_0007_0_Annex9D	
			REV. :	00
			PAGE :	59 OF 178

$$\frac{dz}{ds} = \sin \theta \quad (61)$$

where:

s = distance along plume trajectory;

E = entrainment;

$\theta$  = angle between plume centreline and horizontal plane;

$\sigma$  = angle between plan projection of plume centreline on the horizontal plane and the ambient current direction;  $F_e$  = entrainment force per unit length;

$F_D$  = drag force per unit length;

$F_p$  = pressure force;

$F_\tau$  = bottom shear stress per unit length;

$F_b$  = body force per unit length;

$b_h$  = plume horizontal half-width;

$b_v$  = plume vertical thickness;

$C_D$  = drag coefficient (=1.0);

$u_a$  = ambient velocity;

$u_c$  = plume centreline velocity;

$f_i$  = bottom Darcy friction factor;

$\rho_{cw}$  = clearwater density;

$\rho_a(z)$  = ambient density at level z;

$Q_p$  = mass flux of sediment particles;

$P_j$  = mass density of particle size class j;




$w_j$  = settling velocity for particle size j;

x = coordinate in downstream direction;

z = vertical coordinate; and

y = lateral coordinate.

The following supporting relations apply to the above equations:

	<b>EASTMED PIPELINE PROJECT</b>		 	
	EastMed Greek Section – Environmental and Social Impact Assessment		DOC No: PERM-GREE-ESIA-A09_0007_0_Annex9D	
			REV. :	00
			PAGE :	60 OF 178

Stokes settling for a particle distribution with lower size  $a_j$  and upper size  $b_j$ :

$$w_j = \frac{(b_j^3 - a_j^3)}{b_j - a_j} \frac{2}{27} \frac{\Delta \rho g}{\mu} \quad (62)$$

Hindered settling (optional):

$$\bar{w} = w_j \left( 1 - \frac{Q_p}{Q_{\rho sed}} \right)^{4.7} \quad (63)$$

Density of sediment/water mixture:

$$\rho = \rho_{cw} + P \left( 1 - \frac{\rho_{cw}}{\rho_{sed}} \right) \quad (64)$$

The density current is subject to several types of entrainment mechanisms. The following entrainment definitions are adapted from surface or interface spreading density currents (Akar and Jirka 1994, 1995):

Total entrainment:

$$E = E_v + E_h + E_f + E_i \quad (65)$$

Vertical entrainment from forward plume motion:

$$E_v = \frac{2a_v b_h u_c}{R_i^2}, \quad R_i = \frac{(\rho - \rho_a) g b_v}{\rho_a u_c^2}, \quad a_v = 0.057 \quad (66)$$

Horizontal entrainment from forward plume motion:

$$E_h = 2a_h b_v u_c, \quad a_h = 0.057 \quad (67)$$

Frontal entrainment from perpendicular advancement of plume edge:




$$E_f = \beta b_v \left[ (u_a \cos \sigma + u_c) \frac{db_h}{ds} + u_a \sin \sigma \right], \quad \beta = 0.15 - 0.25 \quad (68)$$

Interfacial entrainment due to turbulence induced by bottom and interfacial shear:

$$E_i = 2b_h a_i \left\{ \left[ \frac{f_b}{8} (u_c + u_a \cos \theta \cos \sigma)^2 \right]^{3/2} + \left[ \frac{f_i}{8} u_a^2 (1 - \cos^2 \theta \cos^2 \sigma) \right]^{3/2} \right\}^{1/3}, \quad a_i = 0.234 \quad (69)$$

Finally, a number of internal force definitions describe the plume dynamics:



	<b>EASTMED PIPELINE PROJECT</b>		 	
	EastMed Greek Section – Environmental and Social Impact Assessment		DOC No: PERM-GREE-ESIA-A09_0007_0_Annex9D	
			REV. : PAGE :	00 61 OF 178

Buoyant body force/unit length:

$$F_b = 2g' \sin \theta b_v b_h \quad (70)$$

Bottom shear stress/unit length:

$$F_\tau = \frac{f_b}{4} b_h u_c (u_c + u_a \cos \theta \cos \sigma) \quad (71)$$

Buoyant pressure force:

$$F_p = b_v^2 b_h g' \cos \theta \quad (72)$$

Drag force/unit length along plume density current front:

$$F_D = C_D b_v u_a^2 (1 - \cos^2 \theta \cos^2 \sigma) \quad (73)$$




Entrainment force/unit length due to transfer of ambient momentum:

$$F_e = E u_a \quad (74)$$

#### 9 D.3.8.10 Main Flow Zones

Based on Doneker et al. (2004) the following 4 flow zones (FZ1, FZ2, FZ3 and FZ4) of the SPM plume are defined.

- **FZ1. Weakly deflected jet in crossflow.** Initially, the flow is dominated by the upward plume momentum (jet-like) and is weakly deflected by the ambient current. It rises to a maximum height, less than the layer depth, which is controlled by the opposing action of the negative buoyancy;
- **FZ2. Weakly deflected plume in crossflow.** After the maximum height of rise, the negative discharge buoyancy becomes the dominating factor (plume-like flow). The strongly deflected plume is rapidly falling toward the bottom;
- **FZ3. Bottom boundary impingement/upstream spreading.** The weakly bent jet/plume impinges on the bottom boundary at a near-vertical angle. After impingement, the flow spreads more or less radially along the bottom. In particular, the flow spreads some distance upstream against the ambient flow and laterally across the ambient flow. This spreading is dominated by the strong buoyancy of the discharge; and

	EASTMED PIPELINE PROJECT		 	
	EastMed Greek Section – Environmental and Social Impact Assessment		DOC No: PERM-GREE-ESIA-A09_0007_0_Annex9D	
			REV. :	00
			PAGE :	62 OF 178

- **FZ4. Buoyant spreading at bottom boundary.** The plume spreads laterally along the bottom, while it is being advected by the ambient current. The plume thickness may decrease during this phase. The mixing rate is relatively small. The plume may interact with a nearby bank or shoreline.

### 9 D.3.9. Required Input Data

#### DR. Dredging characteristics

- DR1. Type;
- DR2. Capacity;
- DR3. Cycle time; and
- DR4. Output.

#### SE. Sediment characteristics




- SE1. Sediment density; and
- SE2. Sediment classes.

#### AM. Ambient characteristics

- AM1. Ambient temperature;
- AM2. Ambient salinity;
- AM3. Ambient (background) sediment concentration;
- AM4. Ambient density;
- AM5. Flow velocity near the bottom; and
- AM6. Flow velocity at the surface.

#### SD. Site and discharge characteristics

- SD1. Sediment mass released;
- SD2. Sediment plume concentration;
- SD3. Sediment plume density;
- SD4. Sediment plume discharge;
- SD5. Discharge velocity;
- SD6. Sediment plume area;
- SD7. Shore location;
- SD8. Distance to shoreline;
- SD9. Water depth;
- SD10. Bottom slope;
- SD11. Vertical angle;
- SD12. Horizontal angle;
- SD13. Discharge height above channel bottom; and
- SD14. Water depth at the source of the plume.

	EASTMED PIPELINE PROJECT		 
	EastMed Greek Section – Environmental and Social Impact Assessment		DOC No: PERM-GREE-ESIA-A09_0007_0_Annex9D
			REV. : 00
			PAGE : 63 OF 178

## 9 D.4. CALCULATIONS AT SITE LF4 AND DISCUSSION

### 9 D.4.1. Input data

CORMIX calculations were performed for a bottom current velocity equal to 0.7 m/s that is the maximum velocity for RP=100 years; see Table III-1 (Appendix 3). These calculations are presented in sections 9 D.4.2 and 9 D.4.2.1. CORMIX calculations were also performed for the minimum current velocity that practically is close to zero; these calculations are described in the section 9 D.4.3.

#### 9 D.4.1.1 Dredging characteristics

Dredging is performed via a grab dredger with the following characteristics:

**DR1. Type.**

- Bucket.

**DR2. Capacity.**

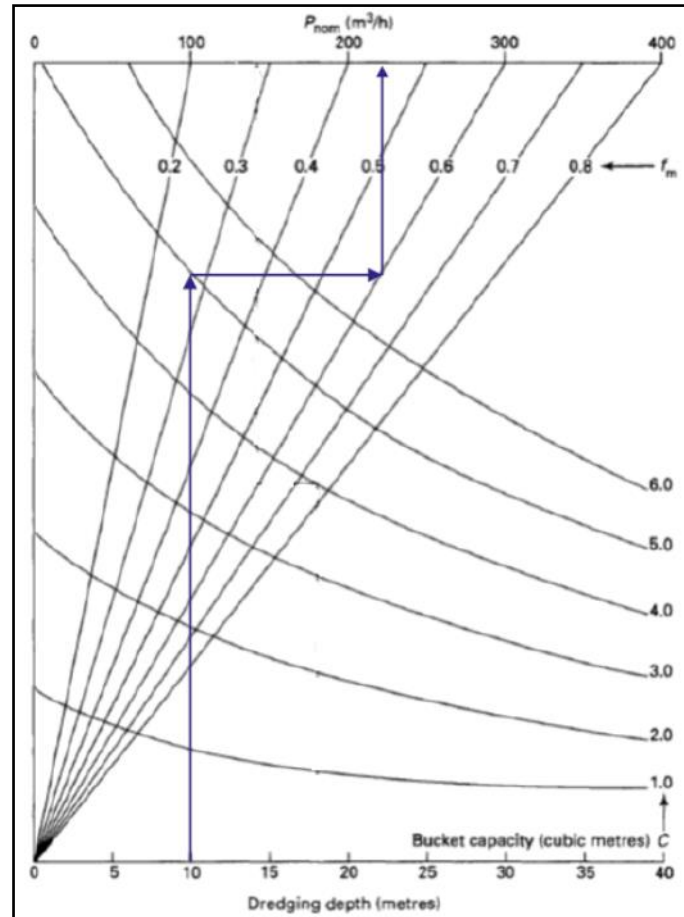
- The capacity of the dredger is assumed equal to 5 m<sup>3</sup>.

**DR3. Cycle time.**

- Traditionally the cycle time has been assumed to be about 60 seconds. In water depths greater than 10 m the cycle time is greater than 60 seconds.

**DR4. Output.**

- The output of the dredger of capacity  $C = 5 \text{ m}^3$ , at a dredging depth equal to  $H_A = 10.0 \text{ m}$ ; see Section 9 D.4.1-9 D.5, using a modification factor  $f_m = 0.6$  according to the digability of the soil and the grab capacity (Bray et al. 1996) is calculated using Figure D-17 equal to 220 m<sup>3</sup>/h.



Prepared by School of Civil Engineering - National Tech Univ. of Athens on behalf of ASPROFOS, 2022.

**Figure D-17 Output of the selected dredger (Bray et al., 1996)**




The dry solids density of the dredged material is equal to  $1800 \text{ kg/m}^3$  and the dry bulk density is equal to  $0.8 \times 1800 = 1440 \text{ kg/m}^3$ .

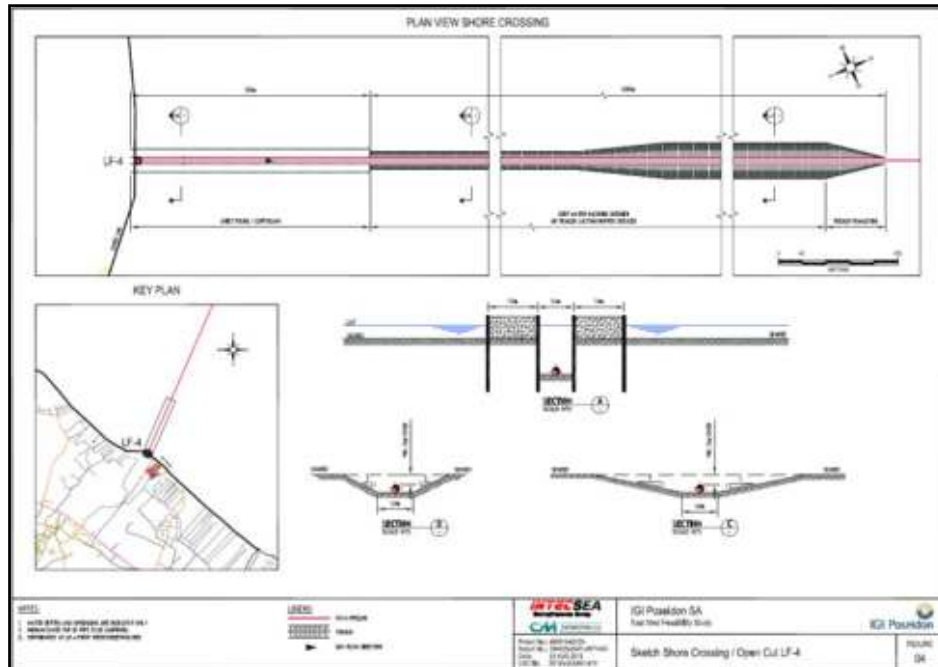
Based on Table D-2, the sediment release rate was taken equal to 4.0 % and the corresponding re-suspension factor (dry solids) is calculated equal to  $0.8 \times 4.0 = 3.2\%$  ( $\text{m}^3 \text{ dry solids re-suspended} / \text{m}^3 \text{ dredged material}$ ).

Based on Figure D-18 and Figure D-18 Schematic diagram of trench at LF4

, the total excavation volume is calculated equal to  $163000 \text{ m}^3$  and the number of total required hours of dredging is equal to 741 h.

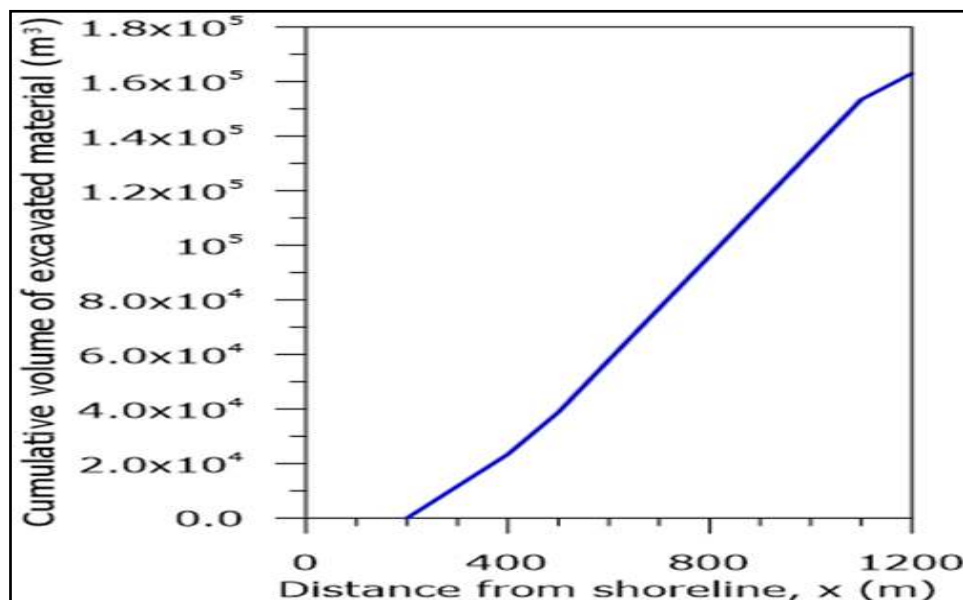
The mass of dredged material is calculated equal to  $220 \times 1440 = 316800 \text{ kg/h}$  and the mass of re-suspended solids equal to  $4\% \times 316800 = 12672 \text{ kg/h}$ .

	<p align="center"><b>EASTMED PIPELINE PROJECT</b></p> <p align="center">EastMed Greek Section – Environmental and Social Impact Assessment</p>	<div>   </div> <p>DOC No: PERM-GREE-ESIA-A09_0007_0_Annex9D</p> <p>REV. : 00</p> <p>PAGE : 65 OF 178</p>
---	--	--






Prepared by School of Civil Engineering - National Tech Univ. of Athens on behalf of ASPROFOS, 2022.

**Figure D-18 Schematic diagram of trench at LF4**



Prepared by School of Civil Engineering - National Tech Univ. of Athens on behalf of ASPROFOS, 2022.

**Figure D-19 Cumulative volume of excavated material at LF4**

 <b>IGI Poseidon</b>	<b>EASTMED PIPELINE PROJECT</b>		 
	EastMed Greek Section – Environmental and Social Impact Assessment		DOCNo: PERM-GREE-ESIA- A09_0007_0_Annex9D
			REV. : 00
			PAGE : 66 OF 178

#### 9 D.4.1.2 Sediment characteristics

The characteristics of the sediment are the following:

##### SE1. Sediment density.

The density of sediments is equal to the density of the dredged material, i.e. 1800 kg/m<sup>3</sup>.

##### SE2. Sediment classes.

According to Table D-7, the following 3 sediment categories are specified: sand (70 %), coarse silt (20 %) and fine silt (10 %). The fine-grained/cohesive sediment content (clay and silt) in the dredge material is 30 %. In Table D-7, the settling velocities of the sediment classes are also shown. Moreover, a series of calculations were performed to investigate the effect of sediment compositions by increasing the percentage of fine silt from 10% to 40 %; see section 9 D.4.5.2 The sediment mass released is calculated equal to 12672 kg/h; see Table D-7.

**Table D-7 Sediment Classes at LF4**

Class	Material	%	Settling Velocity (m/s)	Concentration (mg/L)	Sediment mass release (kg/s)
1	Chunks	0	0.000	0	0.00
2	Sand	70	0.031	175	2.47
3	Coarse Silt	20	0.00042	50	0.70
4	Fine Silt	10	0.000026	25	0.35
5	Clay	0	0.00000065	0	0.00
Total	-	100	-	250	3.52

Prepared by School of Civil Engineering - National Tech Univ. of Athens on behalf of ASPROFOS, 2022.

#### 9 D.4.1.3 Ambient characteristics

The ambient characteristics are the following:




##### AM1. Ambient temperature.

- Based on the data of Appendix 2 the ambient temperature is equal to 25.08°C.

##### AM2. Ambient salinity.

- Based on the data of Appendix 2 the ambient salinity is equal to 38.64 psu.

##### AM3. Ambient (background) sediment concentration.

	EASTMED PIPELINE PROJECT		 
	EastMed Greek Section – Environmental and Social Impact Assessment		DOC No: PERM-GREE-ESIA-A09_0007_0_Annex9D
			REV. : 00
		PAGE :	67 OF 178

- The ambient background sediment concentration is assumed equal to 0.0. Thus, all calculated concentrations are excess concentrations.

#### AM4. Ambient density.

- Based on the data of Appendix 2 the ambient salinity is equal to 1026.07 kg/m<sup>3</sup>.

#### AM5. Flow (current) velocity near the bottom.

- Calculations were performed for the maximum current velocity near the bottom that is equal to 0.70 m/s (see Appendix 3) and for the minimum current velocity that is nearly zero. Moreover, sensitivity analysis calculations were performed for velocities ranging from 0.50 m/s to 0.90 m/s to examine the effect of current velocity; see section 9 D.4.5.1.

#### AM6. Flow velocity at the surface.

- The flow velocity near the surface was taken equal to 0.70 m/s; its effect is expected not to be significant.

### 9 D.4.1.4 Site and discharge characteristics

The SPM plume that originates from the excavation trench during dredging is issued near-vertically from an area that is estimated equal to 3.75 m x 3.75 m (14.09 m<sup>2</sup>). The initial velocity that is imposed by the movement of the grab is assumed equal to 1 m/s (see SD5, below); this movement affects the inclination angle of the plume that is assumed to be nearly vertical (SD11,  $\theta_0 = 75^\circ$ ).

The plume starts at a short distance from the seabed (SD13, 1.0 m); the slope of the seabed is approximately equal to 1.75 %.




The main characteristics of the SPM plume are the following:

#### SD1. Rate of sediment mass release.

- It is calculated equal to  $12672/3600 = 3.52$  kg/s; this value corresponds to a depth average source strength equal to  $1.7 \times 10^5$  mg/(m s).
- This value is within the range of values used by other researchers in modeling studies; for example 4.0 kg/s (Shao et al., 2015) and 1.89 kg/s and  $1.7 \times 10^5$  mg/(m s) (Je et al., 2007).

#### SD2. Sediment plume concentration.

- Based on existing field studies (see section 9 D.3.5) near the excavation region the concentration for the plume ranges from 100 mg/L to 300 mg/L. In Table D-8 the indicative initial source concentration used in numerical studies is shown. Combining these values, it was assumed that the initial concentration of the plume is equal to 250 mg/L. As shown in Table D-7, it consists of sand (175 mg/L, 70 %), coarse silt (50 mg/L, 20 %) and fine silt (25 mg/L, 10 %).

	<b>EASTMED PIPELINE PROJECT</b>		 	
	EastMed Greek Section – Environmental and Social Impact Assessment		DOC No: PERM-GREE-ESIA-A09_0007_0_Annex9D	
			REV. : PAGE :	00 68 OF 178

**Table D-8 Initial source concentration of the SPM plume**

Initial concentration (mg/L)	Reference
230	Je & Hayes (2004)
100 – 300	Kuo & Hayes (1991)
282	Je et al. (2007)
250	Stamou et al. (2009)

Prepared by School of Civil Engineering - National Tech Univ. of Athens on behalf of ASPROFOS, 2022.

**SD3. Sediment plume density.**

- The density of the sediment plume is calculated equal to  $1133.5 \text{ kg/m}^3$ .

**SD4. Sediment plume discharge.**

- The discharge of the sediment plume is calculated equal to  $12672/0.250 = 50716 \text{ m}^3/\text{h}$  or  $50716/3600 = 14.09 \text{ m}^3/\text{s}$ .

**SD5. Discharge velocity.**

- The discharge velocity is assumed equal to  $1.0 \text{ m/s}$ .

**SD6. Sediment plume area.**

- The area of the sediment plume is calculated equal to  $14.09/1.00 = 14.09 \text{ m}^2$ .

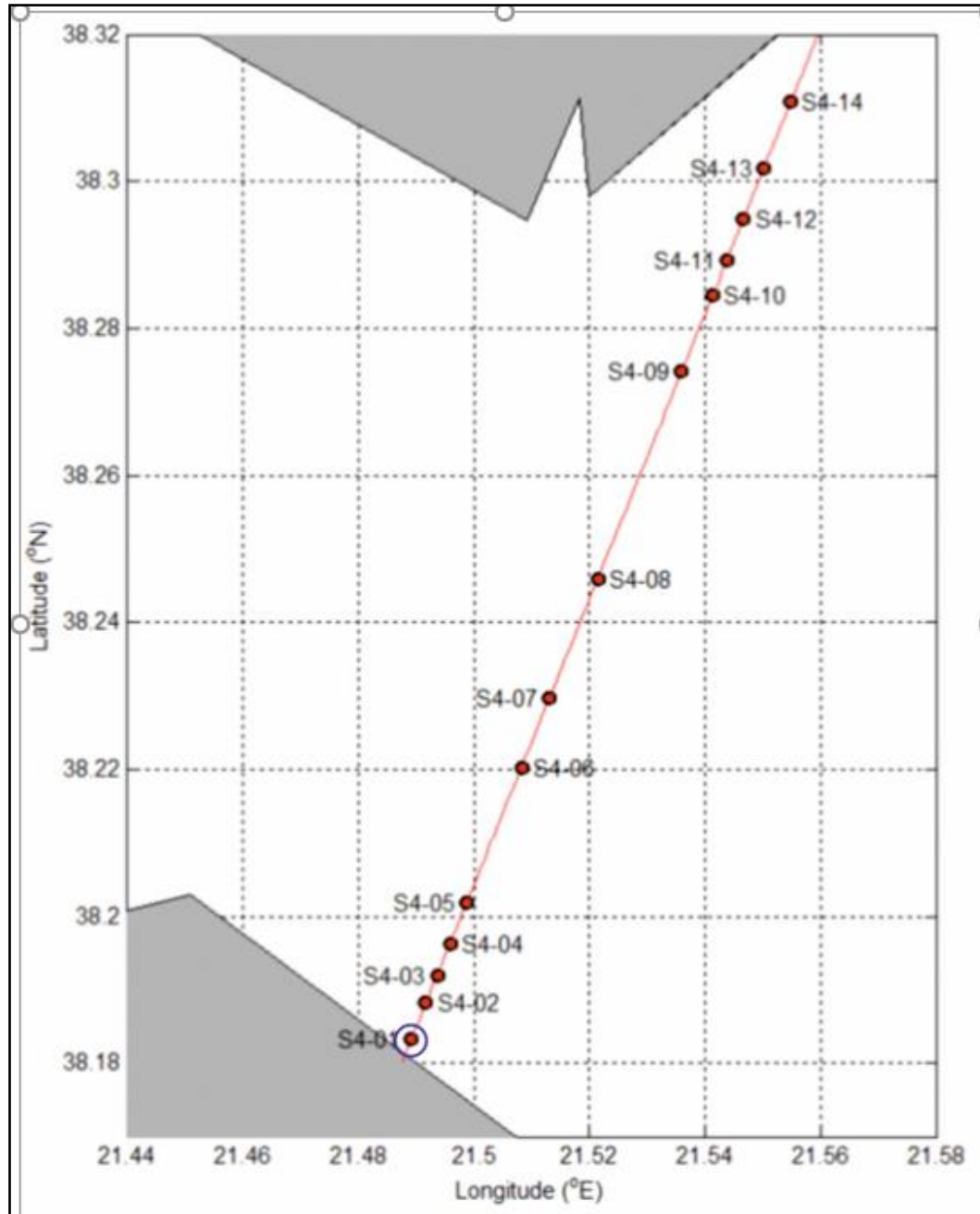
**SD7. Shore Location.**

- The shore location is on the left; see Table D-8

**SD8. Distance to shoreline.**

- The most conservative source location was considered that is S4-01, as shown in Figure D-20; the distance of the dredging location to the shore line (variable DISTB) is equal to 360 m; see Figure D-21.








Prepared by School of Civil Engineering - National Tech Univ. of Athens on behalf of ASPROFOS, 2022.

**Figure D-20 Discharge location; see also Appendix 1**

**SD9. Water depth at the discharge location.**

- The water depth at the dredging location is equal to  $H_A=10.0$  m; see Figure D-20. It is noted however that the calculations showed that for water depths at the dredging location greater

	<p style="text-align: center;"><b>EASTMED PIPELINE PROJECT</b></p> <p style="text-align: center;">EastMed Greek Section – Environmental and Social Impact Assessment</p>	<div style="display: flex; justify-content: space-between; align-items: center;">   </div> <p>DOC No: PERM-GREE-ESIA- A09_0007_0_Annex9D</p> <p>REV. : 00</p> <p>PAGE : 70 OF 178</p>
---	--	---

than approximately 10.0 m the characteristics of the SPM plume are not affected significantly by the water depth.

**SD10. Bottom Slope.**

- The bottom slope is measured equal to approximately 1.75 %; based on the data of Appendix 1

**SD11. Vertical Angle.**

- The vertical angle is equal to  $\theta=75^\circ$ ; see Figure D-21

**SD12. Horizontal Angle.**

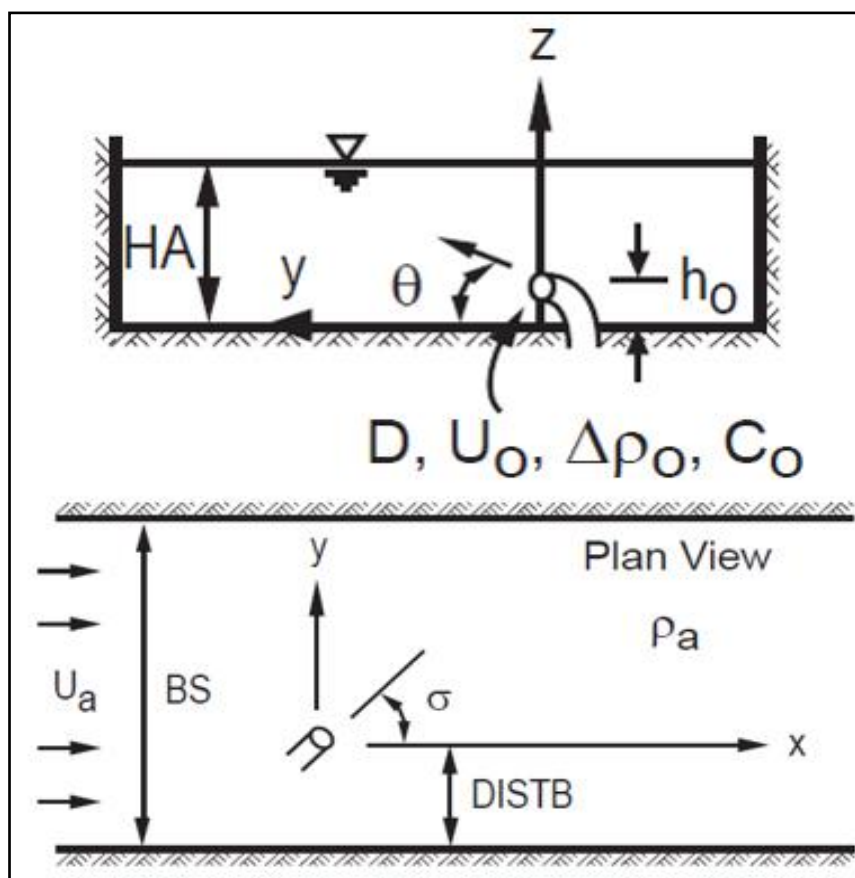
- The horizontal angle is equal to  $\sigma=0^\circ$ ; see Figure D-21

**SD13. Discharge height above channel bottom.**

- The discharge height above channel bottom is equal to  $h_0=1.0$  m; see Figure D-21

**SD14. Water depth at the source of the plume.**

- The water depth at the source of the plume is calculated equal to  $= 10.0 - 1.0 = 9.0$  m.



Prepared by School of Civil Engineering - National Tech Univ. of Athens on behalf of ASPROFOS, 2022.




	EASTMED PIPELINE PROJECT		 
	EastMed Greek Section – Environmental and Social Impact Assessment		DOC No: PERM-GREE-ESIA-A09_0007_0_Annex9D
			REV. : 00
		PAGE :	71 OF 178

Figure D-21 Main site and discharge geometrical characteristics of the discharge

## 9 D.4.2. Flow characteristics for the maximum current velocity

### 9 D.4.2.1 Type of flow

The discharge/environment length scales are calculated as follows:

The “jet to plume transition scale” that defines where flow properties change from jet-like motion to plume-like motions.

$$L_M = \frac{M_0^{3/4}}{J_0^{1/2}} = 1.91 \text{ m}$$

The “discharge length scale” that relates the volume flux ( $Q_0$ ) to the momentum flux ( $M_0$ ).

$$L_Q = \frac{Q_0}{M_0^{1/2}} = 3.75 \text{ m}$$

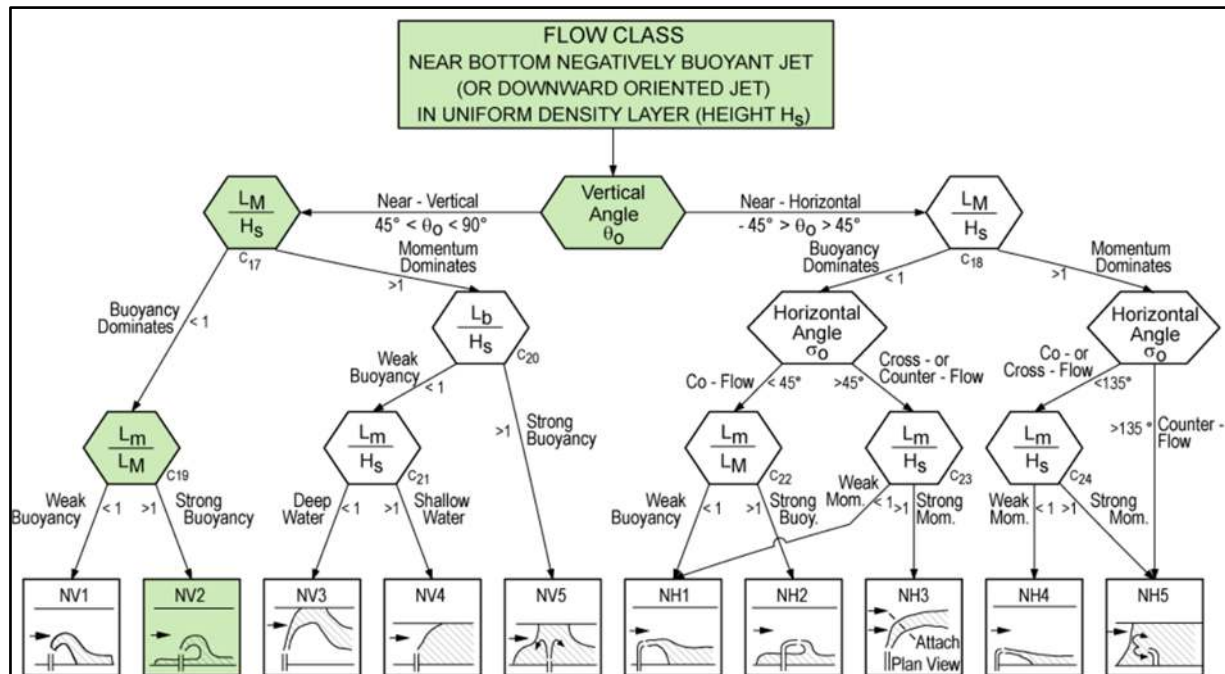
The “jet/cross-flow scale” that defines the distance of the transverse jet penetration beyond which the jet is strongly deflected (advected) by the cross flow.

$$L_m = \frac{M_0^{1/2}}{u_a} = 5.36 \text{ m}$$

The “plume/cross-flow length scale” that defines the vertically upward or downward distance beyond which a plume becomes strongly advected by the cross-flow.

$$L_b = \frac{J_0^{1/2}}{u_a^3} = 42.18 \text{ m}$$

The SPM plume discharges at a depth  $H_s = 9.0 \text{ m}$  below the sea surface with an initial inclination angle that is near vertical ( $45^\circ < \theta_0 = 75^\circ < 90^\circ$ ) and negatively buoyant ( $g'_0 = -1.027 \text{ m/s}^2$ ). Thus, the SPM plume is classified as “**near-vertical class**” (NV) (Jirka & Doneker, 1991); see Figure D-22. Moreover, the discharge configuration is hydrodynamically “stable”, that is the discharge strength (measured by its momentum flux) is weak in relation to the layer depth and the stabilizing effect of the negative discharge buoyancy (measured by its buoyancy flux).



Prepared by School of Civil Engineering - National Tech Univ. of Athens on behalf of ASPROFOS, 2022.

**Figure D-22 CORMIX flow classification of negatively buoyant discharges in uniform layer flow: Flow Classes NV and NH (Source: Doneker & Jirka, 2007)**




Firstly, the ratio  $L_m/H_s$  is calculated to check whether momentum or buoyancy dominates the flow with respect to the ambient-layer depth  $H_s$ . The ratio  $L_m/H_s$  is calculated equal to  $0.09 < 1$ . Thus, the plume **will be dominated by buoyancy** after a short distance and therefore it will quickly fall back towards the bottom (Jirka & Doneker, 1991); see Figure D-22

Secondly, the ratio  $L_m/L_M$  is calculated to check whether the effect of buoyancy is strong or weak. The ratio  $L_m/L_M$  is calculated equal to  $2.81 > 1$  and thus **the flow has strong buoyancy** (Jirka & Doneker, 1991) and the **SPM plume is classified as the flow class NV2** in CORMIX system (Jirka & Doneker, 1991); see Figure D-22

#### 9 D.4.2.2 Plume geometry/trajectory and flow zones

Figure D-23 shows the trajectory of the axis of the SPM plume in the initial mixing and near field regions that include the first 3 flow zones: FZ1, FZ2 and FZ3.

**FZ1. Weakly deflected jet in cross-flow.**

	EASTMED PIPELINE PROJECT		 
	EastMed Greek Section – Environmental and Social Impact Assessment		DOC No: PERM-GREE-ESIA-A09_0007_0_Annex9D
			REV. : 00
			PAGE : 73 OF 178

Initially, the flow is dominated by the upward plume momentum (jet-like); the axis of the SPM plume rises to a maximum height that is equal to  $z_{\max}=1.2$  m (elevation,  $z = -8.8$  m). The effect of the ambient current is weak (since  $z_{\max}/L_b=0.03<1$ ), i.e. the jet is weakly deflected by the ambient current.

#### **FZ2. Weakly deflected plume in cross-flow.**

Then, the SPM plume is strongly affected by gravity and rapidly falls towards the bottom; after a very short time the SPM plume impinges on the sea bottom (boundary) at  $z = -10.0$  m (below the point of discharge) with an angle that is equal to  $\Theta=29.91^\circ$ ; see Figure D-23 and Figure D-24.

#### **FZ3. Bottom impingement/upstream spreading.**




After impingement, the flow spreads more or less radially along the bottom, at an upstream intrusion length,  $L_s = 15.62$  m (see Figure D-24) against the ambient flow, and also laterally spreads across the ambient flow. Its half-width ( $B_H$ ) is steadily increasing from 17.43 m (at impingement) to 22.35 m at  $x = 11.63$  m (end of near field region), downstream. The thickness ( $B_V$ ) in the intrusion region is 1.00 m (at impingement) and at the downstream end of this region is 0.94 m.

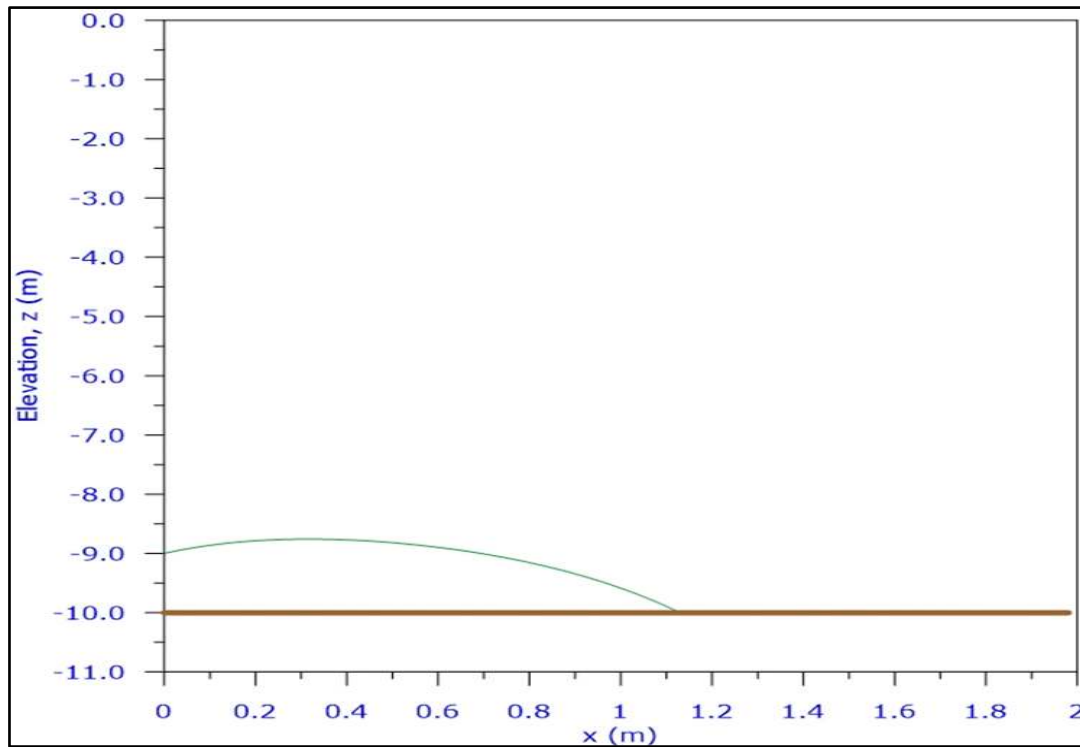
#### **FZ4. Buoyant spreading at bottom layer.**

The bottom layer is formed where the plume spreads laterally (in the y-direction) along the bottom, while it is being advected by the ambient current.

In this zone, the plume thickness ( $B_V$ ) decreases; at  $x=11.63$  m the initial thickness is equal to 0.94 m; at  $x=1200$  m downstream, it is reduced to 0.16 m. The half-width ( $B_H$ ) of the bottom layer increases from 22.35 m at  $x=11.63$  m to 180.02 m at  $x=1200$  m downstream. The plume does not interact with the shoreline.

The mixing rate is relatively small; thus, the dilution is also small ranging from 2.1 to 3.4.

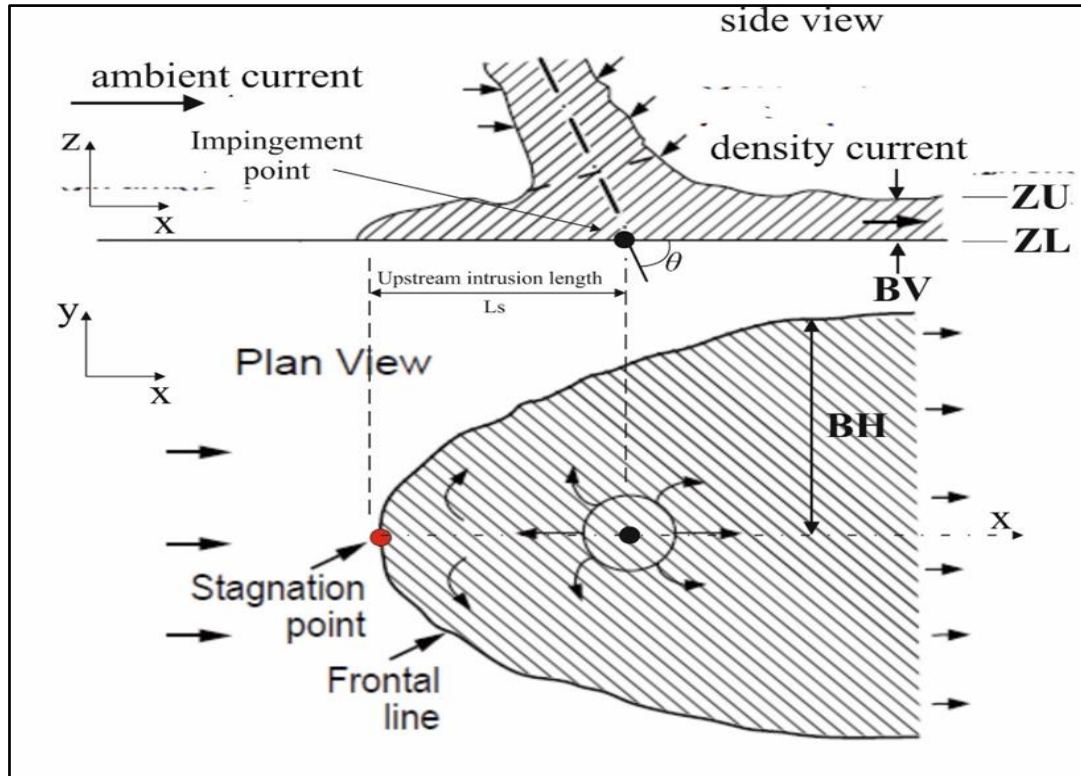
	<p><b>EASTMED PIPELINE PROJECT</b></p> <p>EastMed Greek Section – Environmental and Social Impact Assessment</p>	<div>   </div> <p>DOC No: PERM-GREE-ESIA-A09_0007_0_Annex9D</p> <p>REV. : 00</p> <p>PAGE : 74 OF 178</p>
---	--	--



Prepared by School of Civil Engineering - National Tech Univ. of Athens on behalf of ASPROFOS, 2022.

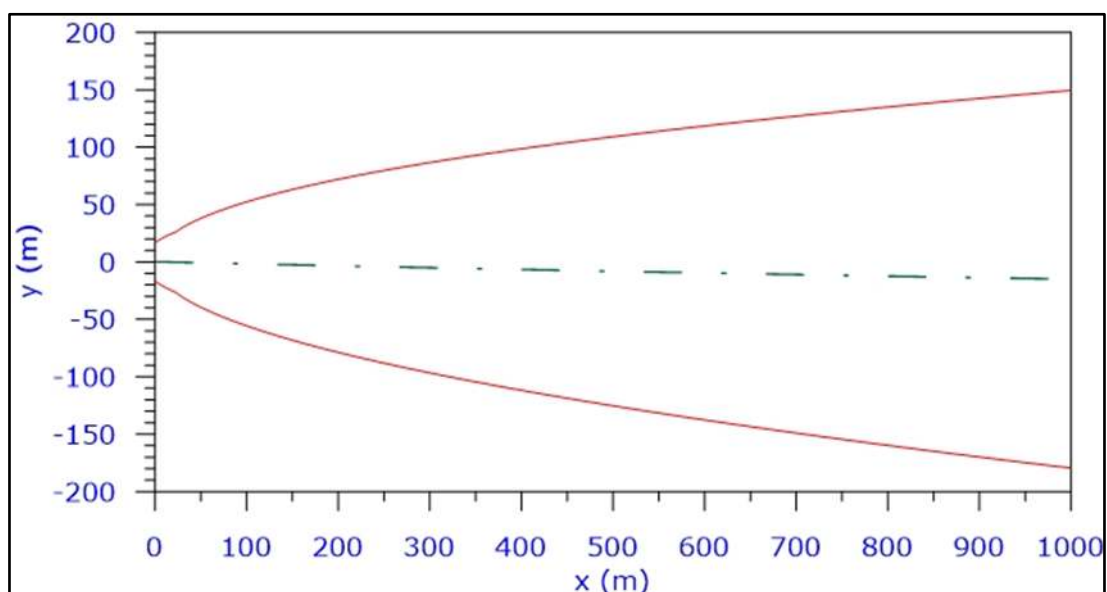
**Figure D-23** Trajectory of the axis of the SPM plume in the near field region





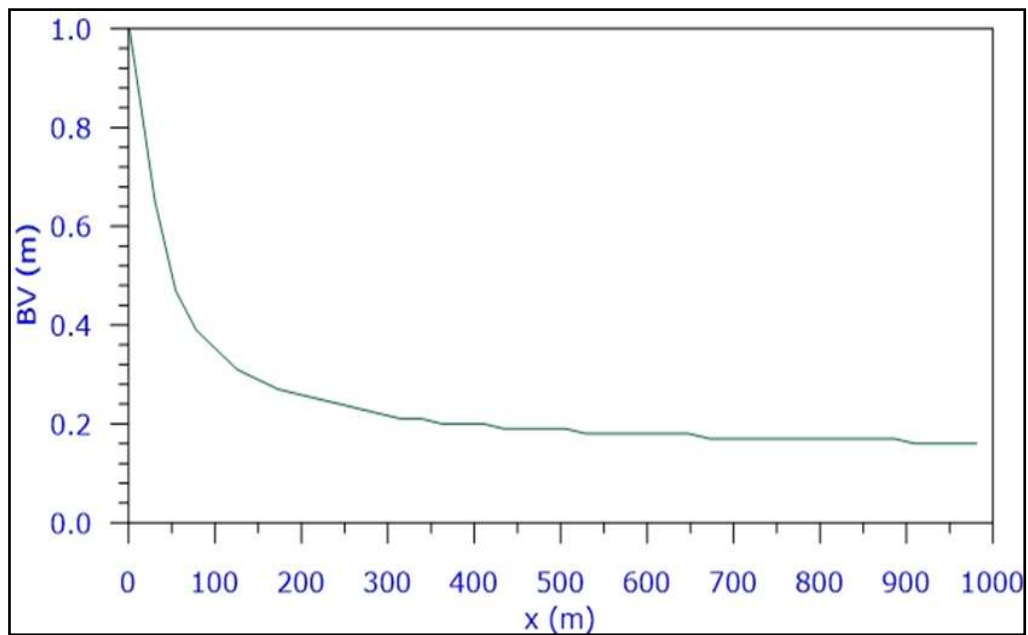
Prepared by School of Civil Engineering - National Tech Univ. of Athens on behalf of ASPROFOS, 2022.

Figure D-24 Schematic diagram of impingement region (Jirka, 2004)



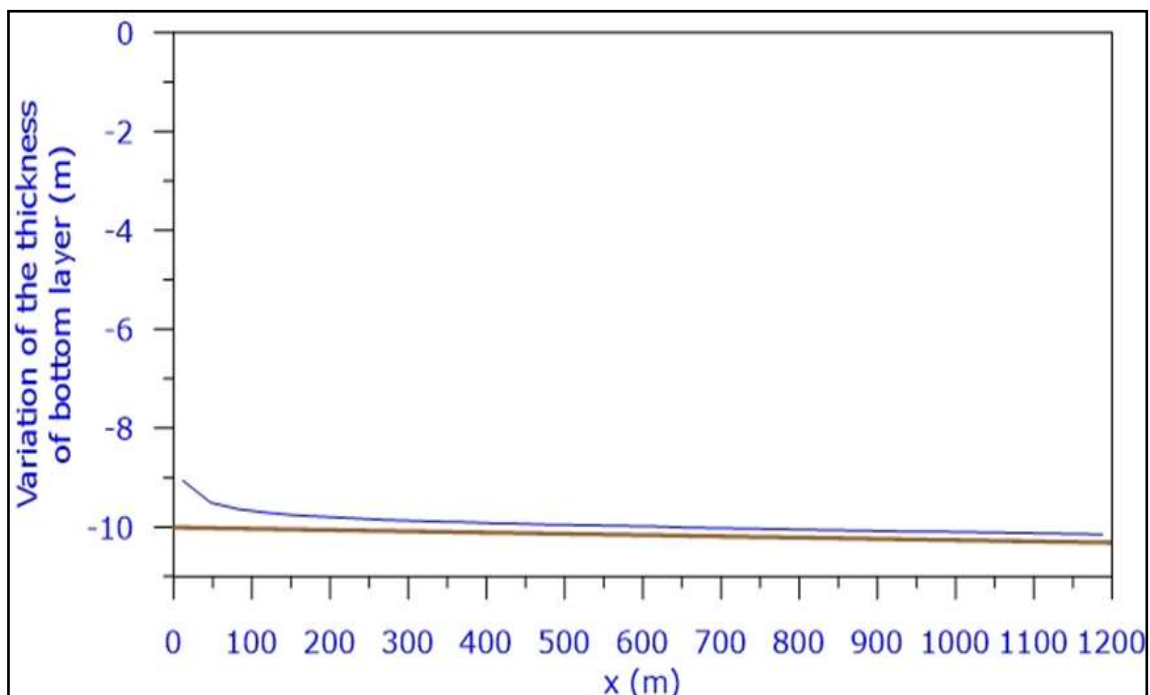
Prepared by School of Civil Engineering - National Tech Univ. of Athens on behalf of ASPROFOS, 2022.

Figure D-25 Variation of 2BH along the bottom layer






Prepared by School of Civil Engineering - National Tech Univ. of Athens on behalf of ASPROFOS, 2022.

Figure D-26 Variation of BV along the bottom layer





	<p style="text-align: center;"><b>EASTMED PIPELINE PROJECT</b></p> <p style="text-align: center;">EastMed Greek Section – Environmental and Social Impact Assessment</p>	<div style="display: flex; justify-content: space-between; align-items: center;">   </div> <div style="border-top: 1px solid black; padding-top: 5px;"> DOC No: PERM-GREE-ESIA- A09_0007_0_Annex9D </div> <div style="display: flex; justify-content: space-between; border-top: 1px solid black; padding-top: 5px;"> REV. : 00 </div> <div style="display: flex; justify-content: space-between; border-top: 1px solid black; padding-top: 5px;"> PAGE : 77 OF 178 </div>
---	--	--

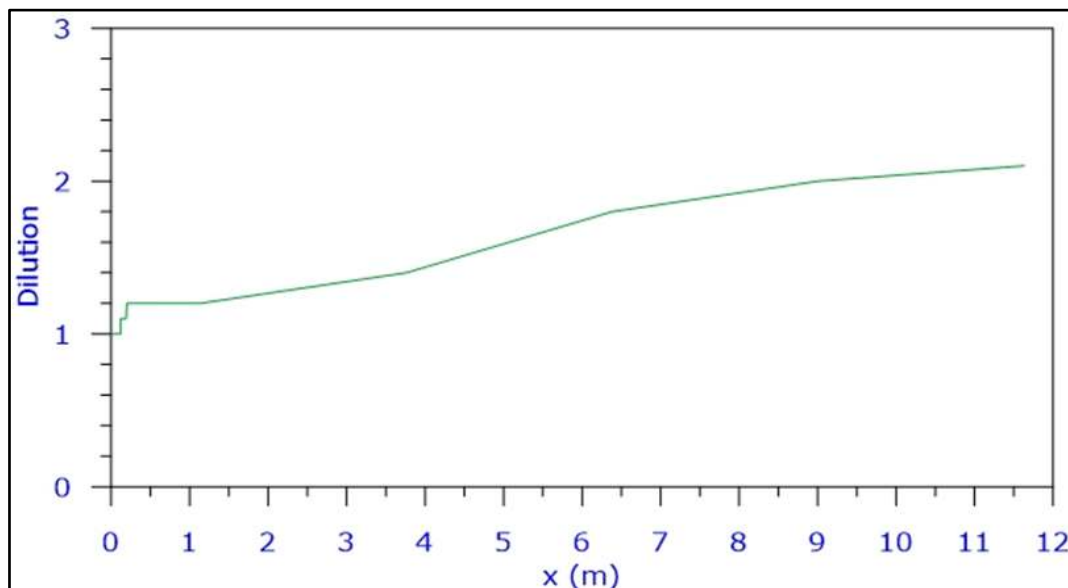
Prepared by School of Civil Engineering - National Tech Univ. of Athens on behalf of ASPROFOS, 2022.

Figure D-27 Variation of the thickness of the bottom layer

### 9 D.4.3. Sediment characteristics for the maximum current velocity

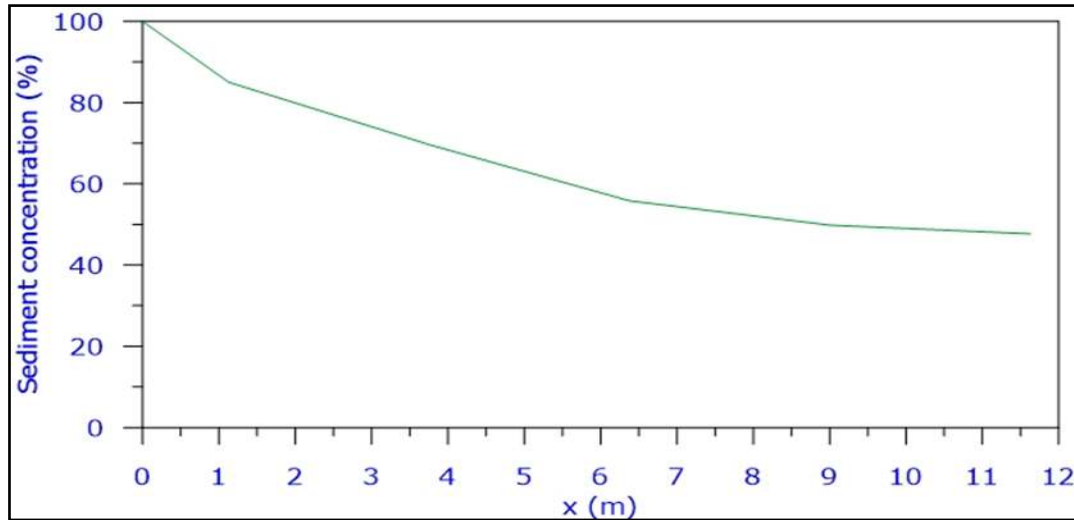
#### 9 D.4.3.1 Sediment concentrations in the near field region

Figure D-28 depicts the variation of dilution of the SPM in the near field region. In Figure D-29 and Figure D-30 the variation of the sediment concentration in the near field region as percentage of the initial concentration (%) and actual concentrations (mg/L) are shown, respectively. At the end of the near field region (at  $x=11.63$  m), the dilution is equal to 2.1, which corresponds to a reduction of the initial concentration equal to 47.6 % and to a sediment concentration that is equal to 119 mg/L.



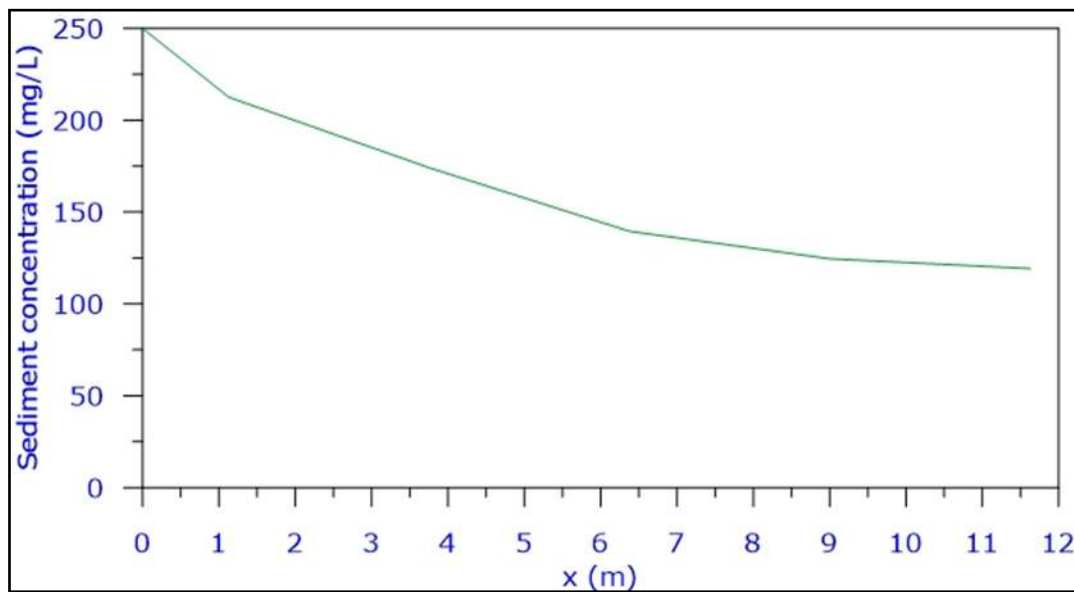
Prepared by School of Civil Engineering - National Tech Univ. of Athens on behalf of ASPROFOS, 2022.

Figure D-28 Dilution in the near field region



Prepared by School of Civil Engineering - National Tech Univ. of Athens on behalf of ASPROFOS, 2022.

**Figure D-29 Sediment concentrations (%) in the near field region**



Prepared by School of Civil Engineering - National Tech Univ. of Athens on behalf of ASPROFOS, 2022.

**Figure D-30 Sediment concentrations (mg/L) in the near field region**

#### **9 D.4.3.2 Sediment concentrations in the bottom layer**




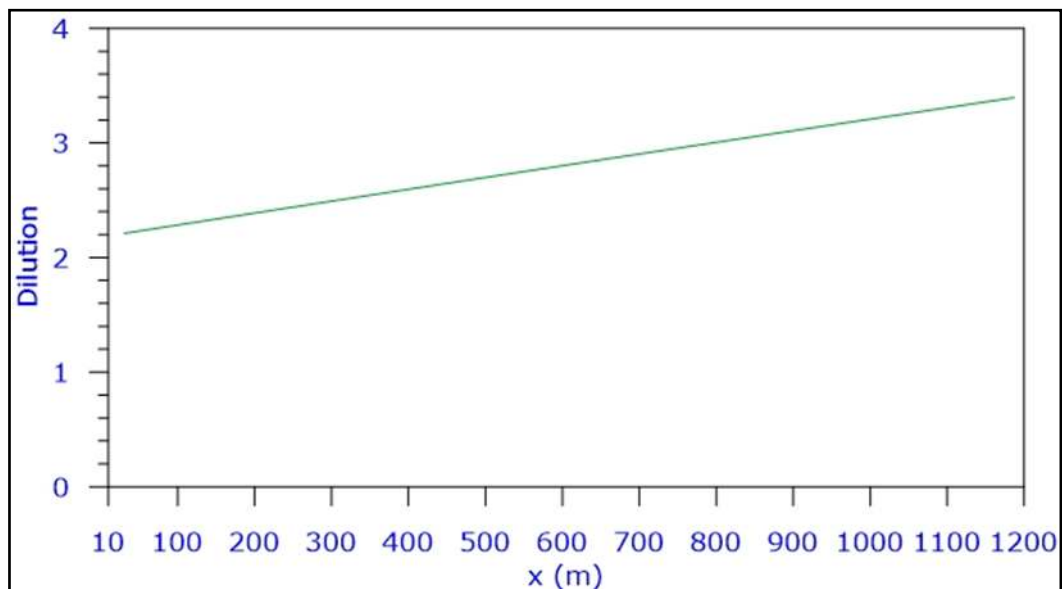
	<p style="text-align: center;"><b>EASTMED PIPELINE PROJECT</b></p> <p style="text-align: center;">EastMed Greek Section – Environmental and Social Impact Assessment</p>	<div style="display: flex; justify-content: space-between; align-items: center;">   </div> <div style="font-size: small;"> DOC No: PERM-GREE-ESIA- A09_0007_0_Annex9D  REV. : 00  PAGE : 79 OF 178 </div>
---	--	---




Figure D-31, Figure D-32 and Figure D-33 show the dilution, sediment concentrations (as percentages of the initial concentration, %) and actual concentrations (mg/L) in the bottom layer, respectively. The (total) concentration contours of the simulated SPM plume are shown in Figure D-34 (percentages) and 3.3-8.0 (mg/L).

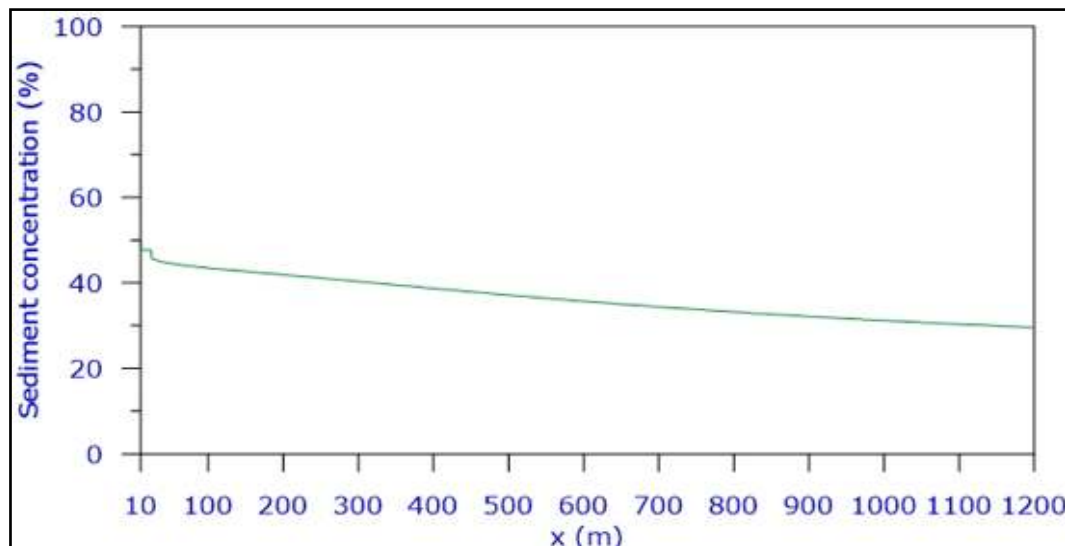
The total concentration in the bottom layer is steadily reducing (after loss of suspended particles by settling) from 119.0 mg/L at the beginning of the bottom layer, to 111.5 mg/L at 50 m downstream, to 108.8 mg/L at 100 m and to 74.0 mg/L at 1200 m, downstream.



Prepared by School of Civil Engineering - National Tech Univ. of Athens on behalf of ASPROFOS, 2022.

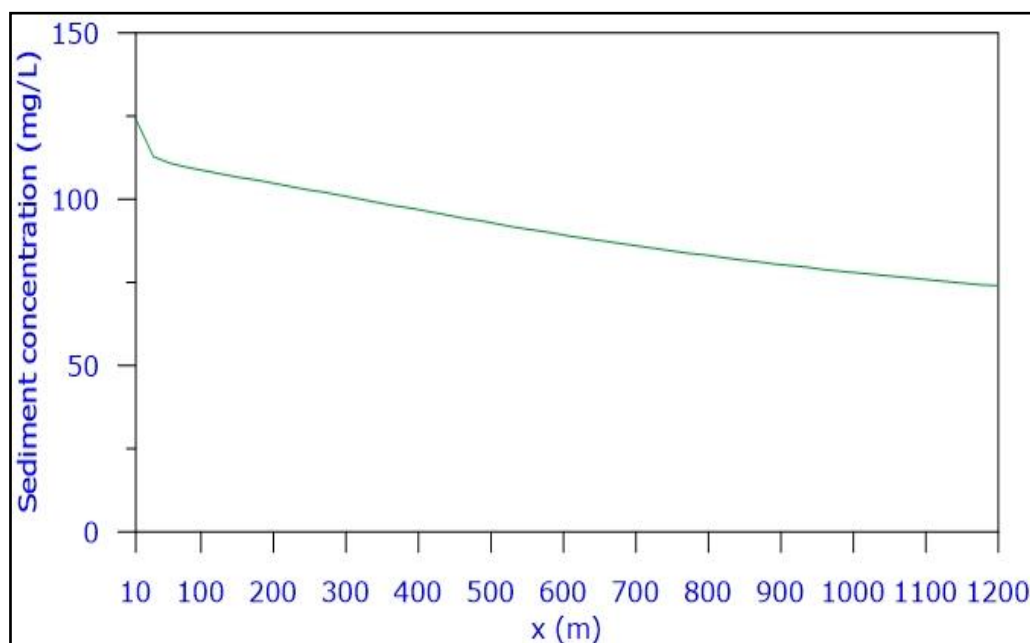
**Figure D-31 Dilution in the bottom layer**

	<p align="center"><b>EASTMED PIPELINE PROJECT</b></p> <p align="center">EastMed Greek Section – Environmental and Social Impact Assessment</p>	<div>   </div> <p>DOC No: PERM-GREE-ESIA- A09_0007_0_Annex9D</p> <p>REV. : 00</p> <p>PAGE : 80 OF 178</p>
---	--	---






Prepared by School of Civil Engineering - National Tech Univ. of Athens on behalf of ASPROFOS, 2022.

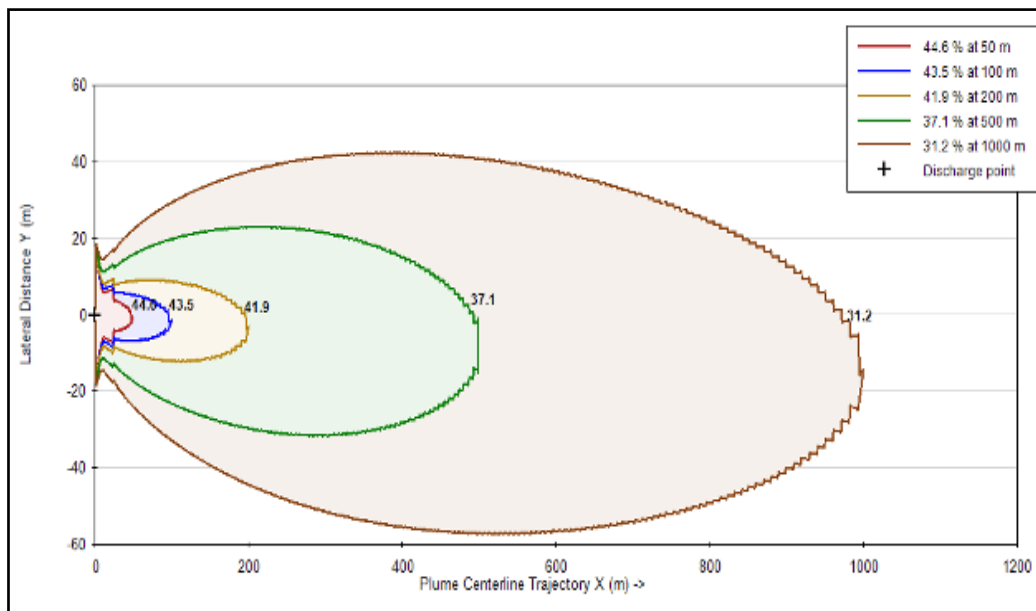
**Figure D-32** Sediment concentrations (%) in the bottom layer



Prepared by School of Civil Engineering - National Tech Univ. of Athens on behalf of ASPROFOS, 2022.

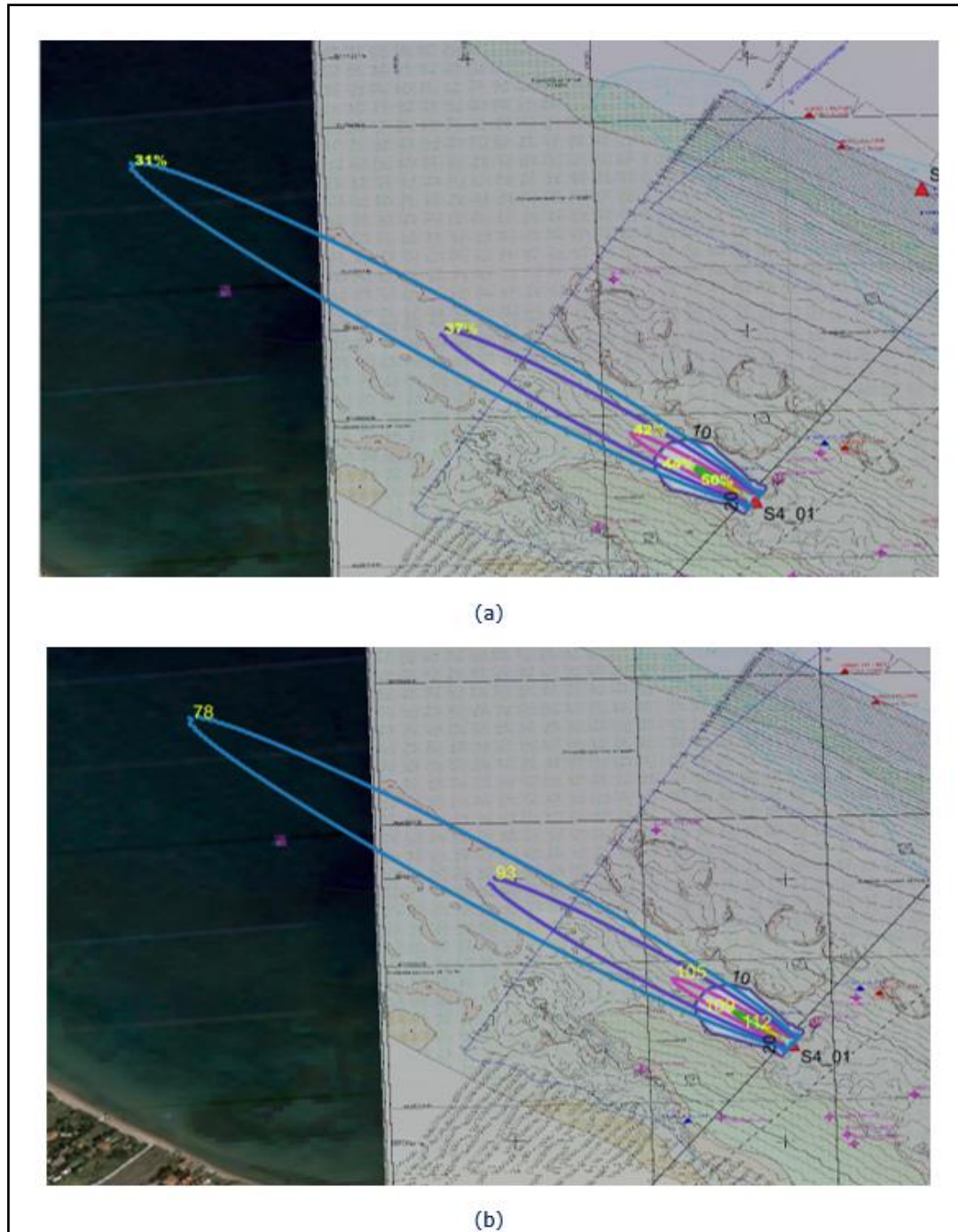
**Figure D-33** Sediment concentrations (mg/L) in the bottom layer

	<p style="text-align: center;"><b>EASTMED PIPELINE PROJECT</b></p> <p style="text-align: center;">EastMed Greek Section – Environmental and Social Impact Assessment</p>	<div style="display: flex; justify-content: space-between; align-items: center;">   </div> <p>DOC No: PERM-GREE-ESIA- A09_0007_0_Annex9D</p> <p>REV. : 00</p> <p>PAGE : 81 OF 178</p>
---	--	---



Prepared by School of Civil Engineering - National Tech Univ. of Athens on behalf of ASPROFOS, 2022.




**Figure D-34** Sediment concentration contours (% of the initial) in the bottom layer



Prepared by School of Civil Engineering - National Tech Univ. of Athens on behalf of ASPROFOS, 2022.

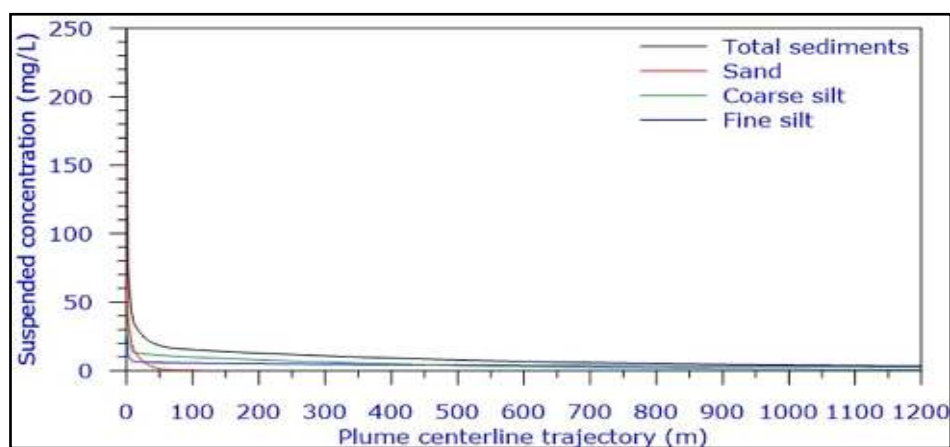
**Figure D-35** Total sediment concentration contours in the bottom layer (a) % of the initial concentration and (b) in mg/L



	<p style="text-align: center;"><b>EASTMED PIPELINE PROJECT</b></p> <p style="text-align: center;">EastMed Greek Section – Environmental and Social Impact Assessment</p>	<div style="display: flex; justify-content: space-between; align-items: center;">   </div> <div style="border-top: 1px solid black; padding-top: 5px;"> DOC No: PERM-GREE-ESIA- A09_0007_0_Annex9D </div> <div style="border-top: 1px solid black; padding-top: 5px;"> REV. : 00 </div> <div style="border-top: 1px solid black; padding-top: 5px;"> PAGE : 83 OF 178 </div>
---	--	--

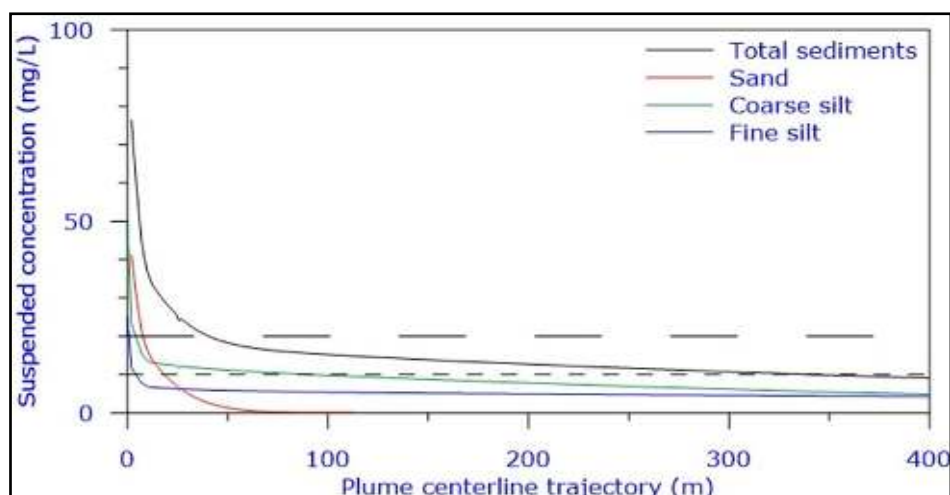
#### 9 D.4.3.3 *Suspended sediment concentrations*

Figure D-36 and Figure D-37 and Figure D-38 show the suspended sediment concentrations, SSC (mg/L) in the water column. The suspended sediment concentrations decrease continuously downstream; at 1.1 m SSC = 77.3 mg/L, at 9.0 m SSC = 41.3 mg/L, at 11.63 m (end of near field) SSC = 34.9 mg/L, at 27.2 m SSC = 24.1 mg/L, at 117.5 m SSC = 14.7 mg/L and at x= 955.2 m SSC is practically equal to zero.



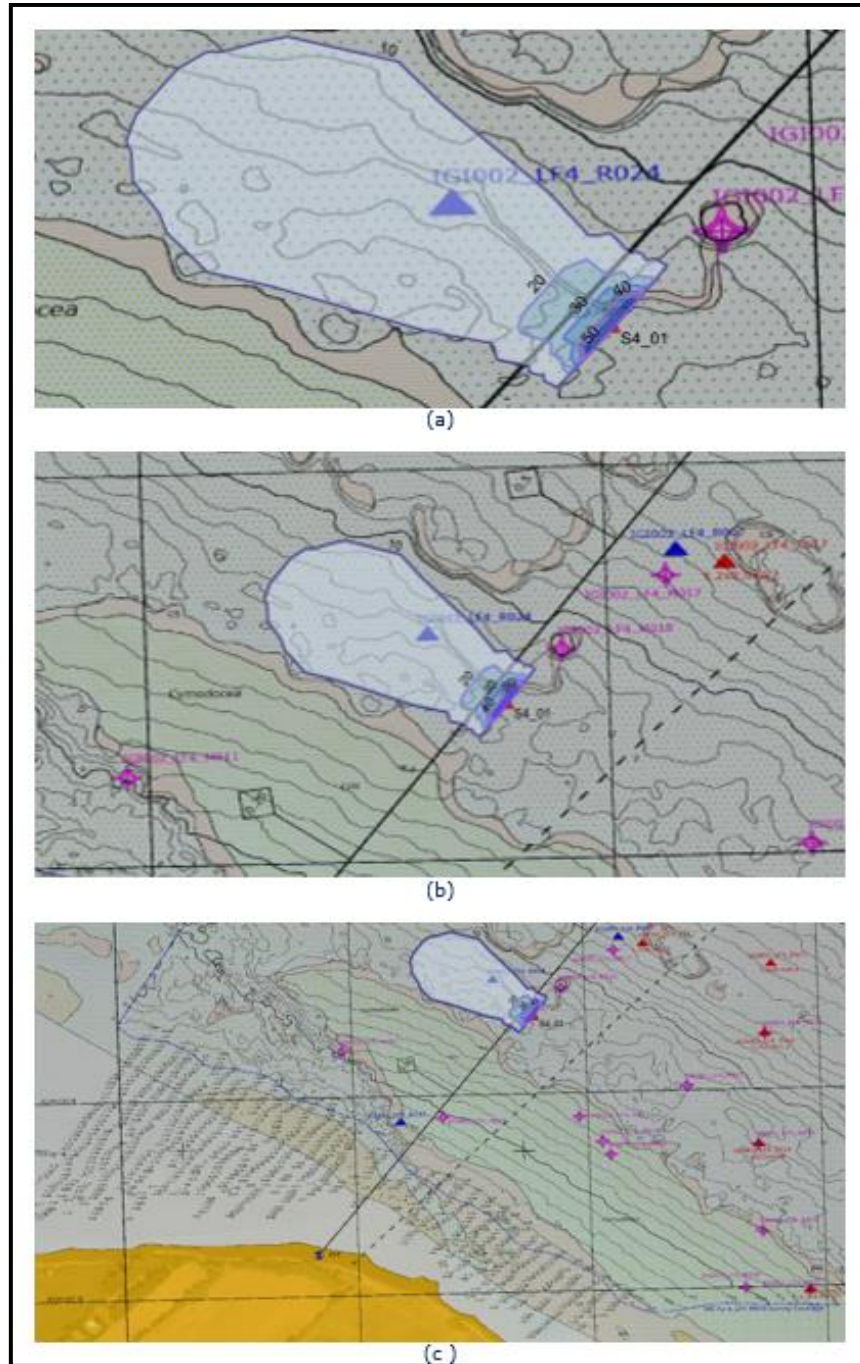
Prepared by School of Civil Engineering - National Tech Univ. of Athens on behalf of ASPROFOS, 2022.

Figure D-36 Suspended sediment concentrations (mg/L) from x=0 to x=1200 m



Prepared by School of Civil Engineering - National Tech Univ. of Athens on behalf of ASPROFOS, 2022.




Figure D-37 Suspended sediment concentrations (mg/L) from x=0 to x=400 m



Prepared by School of Civil Engineering - National Tech Univ. of Athens on behalf of ASPROFOS, 2022.

**Figure D-38**    **Suspended sediment concentrations (mg/L)**



	EASTMED PIPELINE PROJECT		 
	EastMed Greek Section – Environmental and Social Impact Assessment		DOC No: PERM-GREE-ESIA-A09_0007_0_Annex9D
			REV. : 00
			PAGE : 85 OF 178

#### 9 D.4.4. Flow and sediment characteristics for the minimum current velocity

##### 9 D.4.4.1 Type of flow

The discharge/environment length scales are calculated as follows:

$$L_M = \frac{M_0^{3/4}}{J_0^{1/2}} = 1.91 \text{ m}$$

$$L_Q = \frac{Q_0}{M_0^{1/2}} = 3.75 \text{ m}$$




$$L_m = \frac{M_0^{1/2}}{u_a} \rightarrow \text{very large value}$$

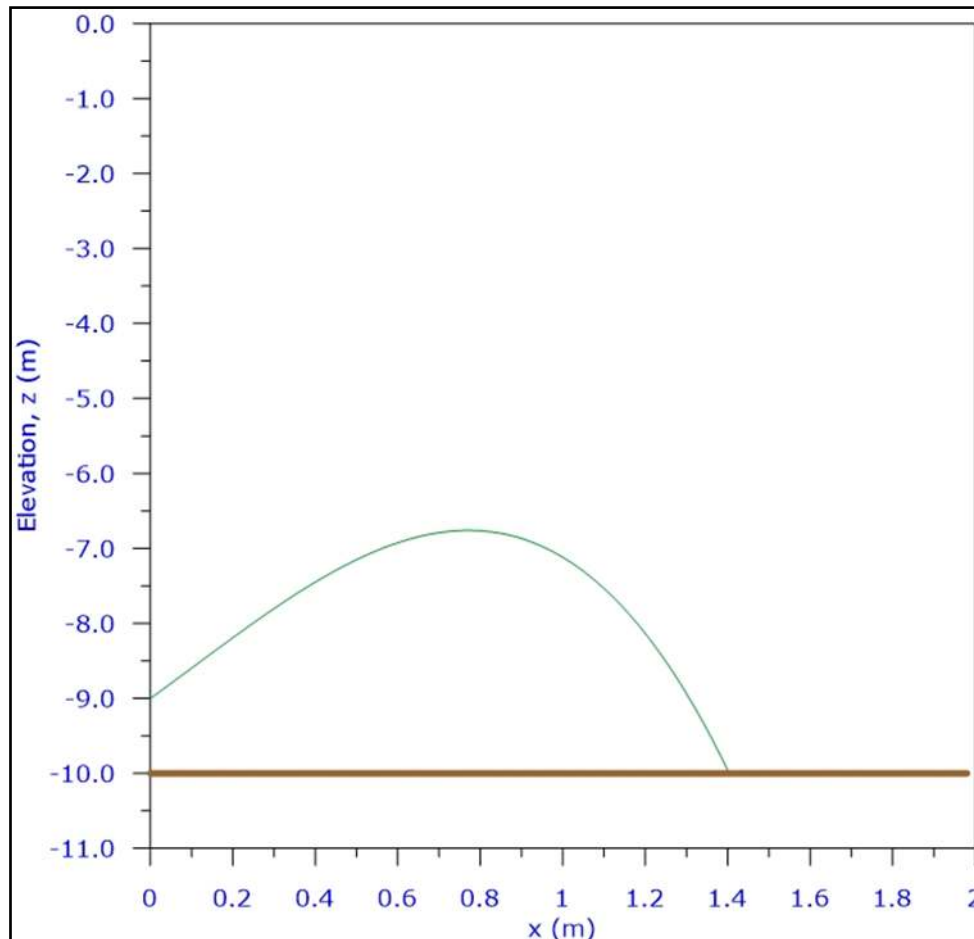
$$L_b = \frac{J_0^{1/2}}{u_a^3} \rightarrow \text{very large value}$$

As in the case of the maximum current velocity, the SPM plume is classified as NV2.

##### 9 D.4.4.2 Plume geometry/trajectory and flow zones

Figure D-39 shows the trajectory of the axis of the SPM plume in the initial mixing and near field regions. The behavior of the SPM plume is very similar to the case of maximum current velocity.

	<p style="text-align: center;"><b>EASTMED PIPELINE PROJECT</b></p> <p style="text-align: center;">EastMed Greek Section – Environmental and Social Impact Assessment</p>	<div style="display: flex; justify-content: space-between; align-items: center;">   </div> <div style="border-top: 1px solid black; padding-top: 5px;"> DOC No: PERM-GREE-ESIA- A09_0007_0_Annex9D </div> <div style="display: flex; justify-content: space-between; border-top: 1px solid black; padding-top: 5px;"> REV. : 00 </div> <div style="display: flex; justify-content: space-between; border-top: 1px solid black; padding-top: 5px;"> PAGE : 86 OF 178 </div>
---	--	--

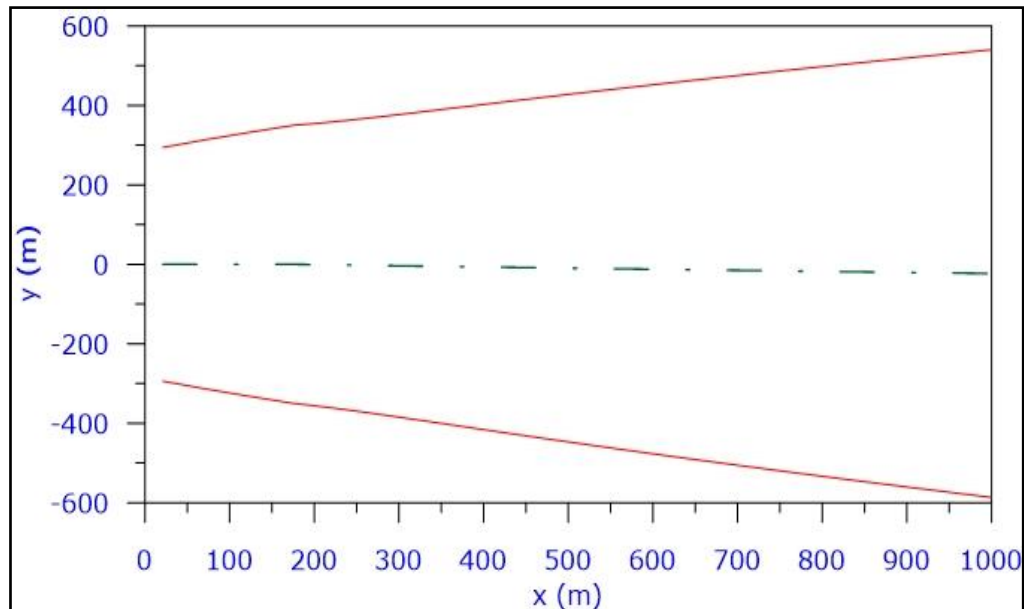


Prepared by School of Civil Engineering - National Tech Univ. of Athens on behalf of ASPROFOS, 2022.

**Figure D-39 Trajectory of the axis of the SPM plume in the near field region**

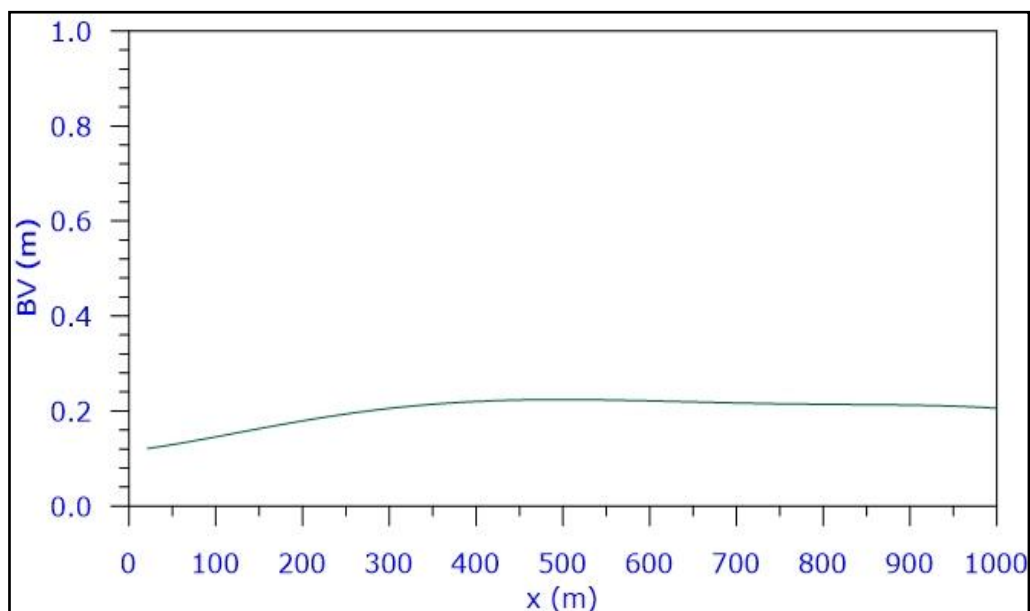
Initially, the flow is dominated by the upward plume momentum (jet-like); the axis of the SPM plume rises to a maximum height of 3.3 m, being weakly deflected by the ambient current. Then, the SPM plume is strongly affected by gravity and rapidly falls towards the bottom and impinges on the bottom.

Figure D-40, Figure D-41 and Figure D-42 depict that after impingement, the flow spreads more or less radially along the bottom; downstream, its half-width is steadily increasing from 294.29 m (at impingement) to 350.25 m at 175.64 m (end of near field region) and to 608.43 m at  $x=1200$  m, while its thickness at impingement is 0.12 m and at  $x=1200$  m downstream it is equal to 0.21 m.






Prepared by School of Civil Engineering - National Tech Univ. of Athens on behalf of ASPROFOS, 2022.

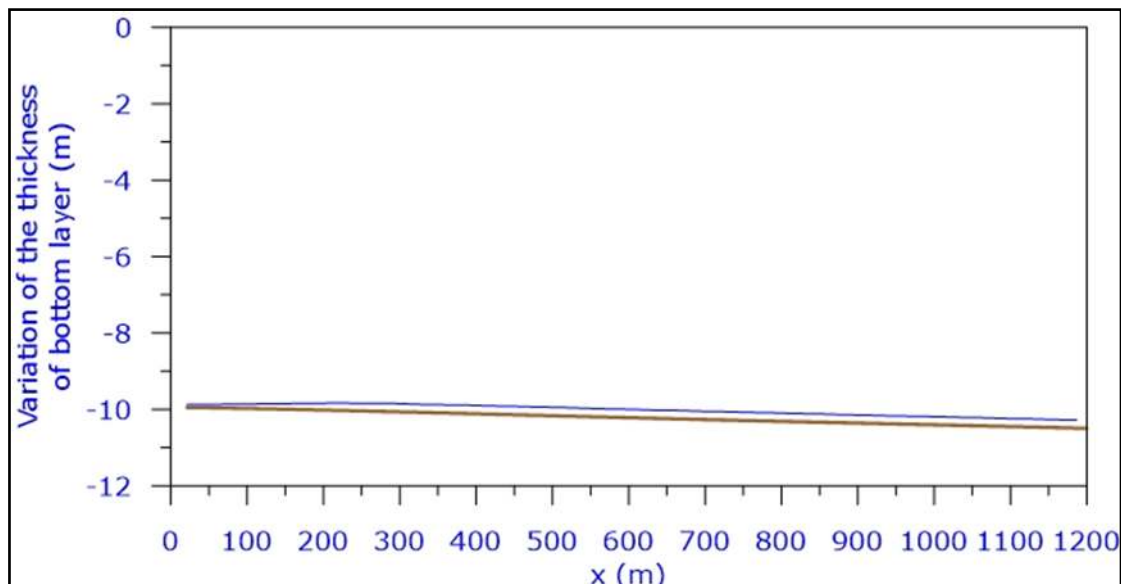
**Figure D-40** Variation of 2BH along the bottom layer



Prepared by School of Civil Engineering - National Tech Univ. of Athens on behalf of ASPROFOS, 2022.

**Figure D-41** Variation of BV along the bottom layer

	<p style="text-align: center;"><b>EASTMED PIPELINE PROJECT</b></p> <p style="text-align: center;">EastMed Greek Section – Environmental and Social Impact Assessment</p>	<div style="display: flex; justify-content: space-between; align-items: center;">   </div> <div style="border: 1px solid black; padding: 2px;"> DOC No: PERM-GREE-ESIA- A09_0007_0_Annex9D REV. : 00 PAGE : 88 OF 178 </div>
---	--	--

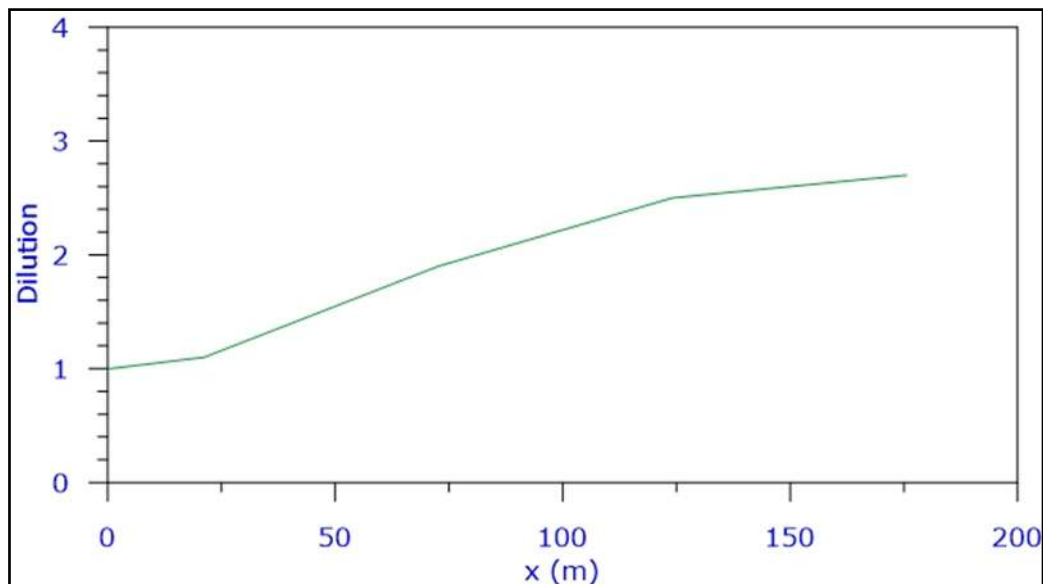


Prepared by School of Civil Engineering - National Tech Univ. of Athens on behalf of ASPROFOS, 2022.

**Figure D-42** Variation of the thickness of the bottom layer

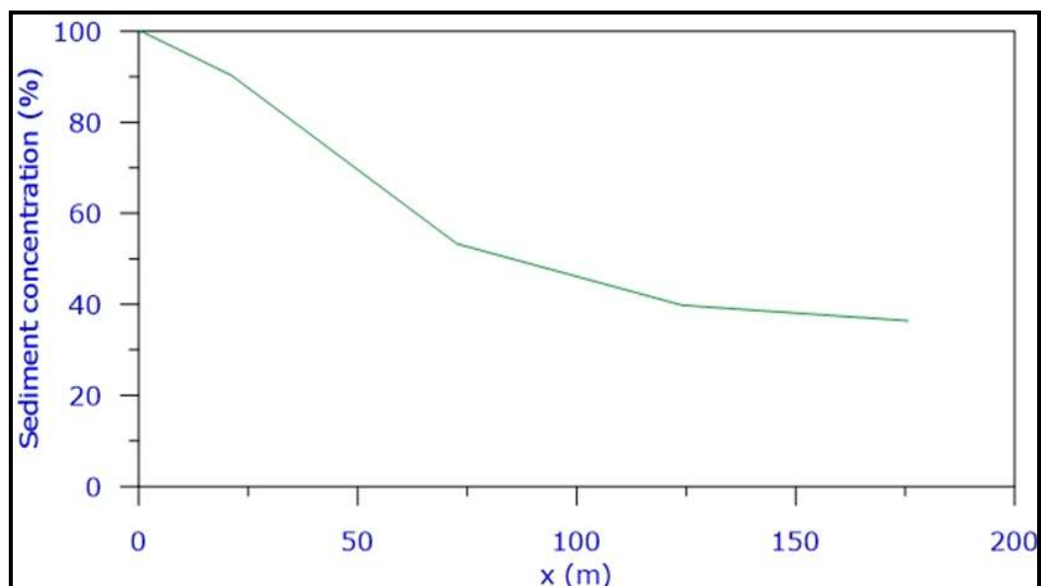
#### **9 D.4.4.3 Sediment concentrations in the near field region**

Figure D-43 depicts the variation of dilution of the SPM in the near field region. In Figure D-44 and Figure D-45 the variation of the sediment concentration in the near field region as percentage of the initial concentration (%) and actual concentrations (mg/L) are shown, respectively. At the end of the near field region (at  $x=175.64$  m), the dilution is equal to 2.7, which corresponds to a reduction of the initial concentration equal to 36.4 % and to a sediment concentration that is equal to 91.0 mg/L.






Prepared by School of Civil Engineering - National Tech Univ. of Athens on behalf of ASPROFOS, 2022.

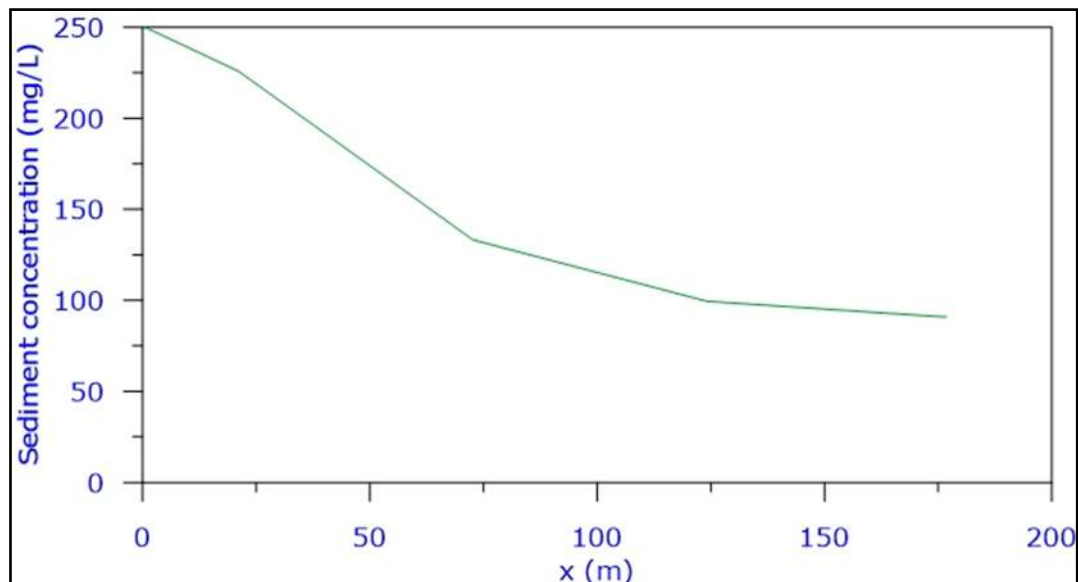
**Figure D-43 Dilution in the near field region**



Prepared by School of Civil Engineering - National Tech Univ. of Athens on behalf of ASPROFOS, 2022.

**Figure D-44 Sediment concentrations (%) in the near field region**

	<p align="center"><b>EASTMED PIPELINE PROJECT</b></p> <p align="center">EastMed Greek Section – Environmental and Social Impact Assessment</p>	<div>   </div> <p>DOC No: PERM-GREE-ESIA- A09_0007_0_Annex9D</p> <p>REV. : 00</p> <p>PAGE : 90 OF 178</p>
---	--	---






Prepared by School of Civil Engineering - National Tech Univ. of Athens on behalf of ASPROFOS, 2022.

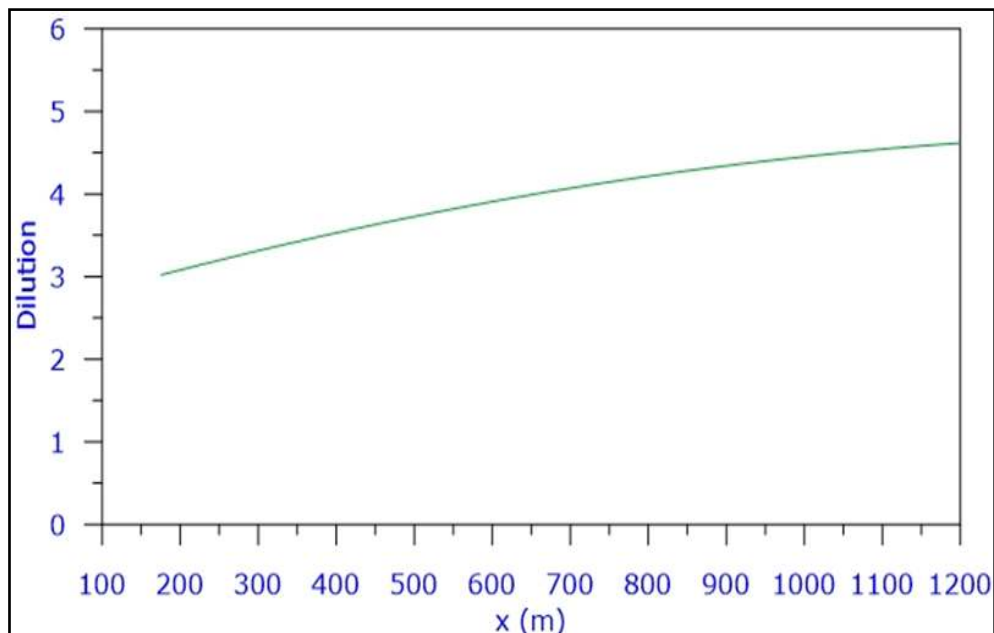
**Figure D-45 Sediment concentrations (mg/L) in the near field region**

#### **9 D.4.4.4 Sediment concentrations in the bottom layer**

Figure D-46, Figure D-47 and Figure D-48 show the dilution, sediment concentrations (as percentages of the initial concentration, %) and actual concentrations (mg/L) in the bottom layer, respectively. The (total) concentration contours of the simulated SPM plume are shown in Figure D-49 (percentages) and Figure D-50.

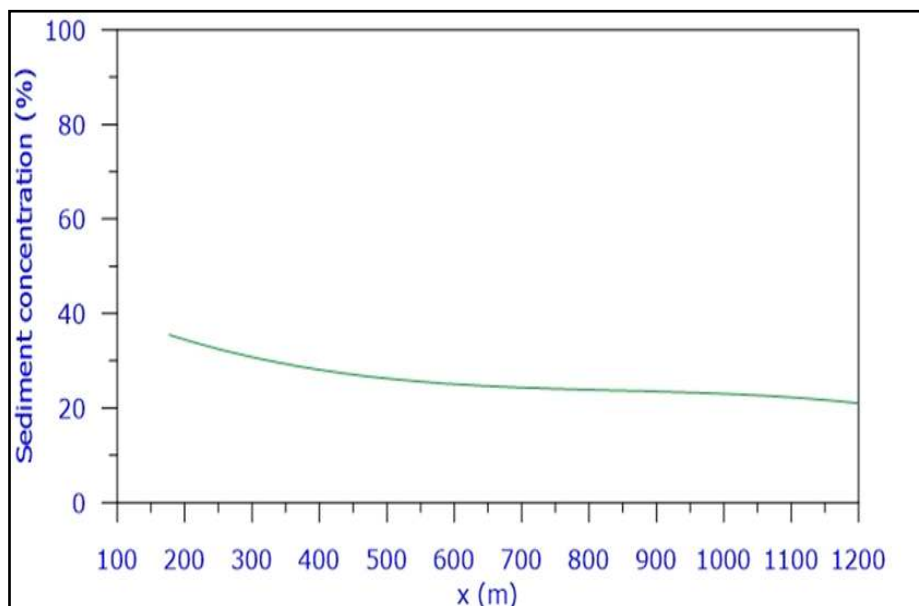
The total concentration in the bottom layer is steadily reducing (after loss of suspended particles by settling) from 91.0 mg/L at the beginning of the bottom layer, to 69.8 mg/L at 400 m downstream, to 64.0 mg/L at 600 m and to 53.50 mg/L at 1,200 m downstream.

	<p align="center"><b>EASTMED PIPELINE PROJECT</b></p> <p align="center">EastMed Greek Section – Environmental and Social Impact Assessment</p>	<div>   </div> <p>DOC No: PERM-GREE-ESIA- A09_0007_0_Annex9D</p> <p>REV. : 00</p> <p>PAGE : 91 OF 178</p>
---	--	---



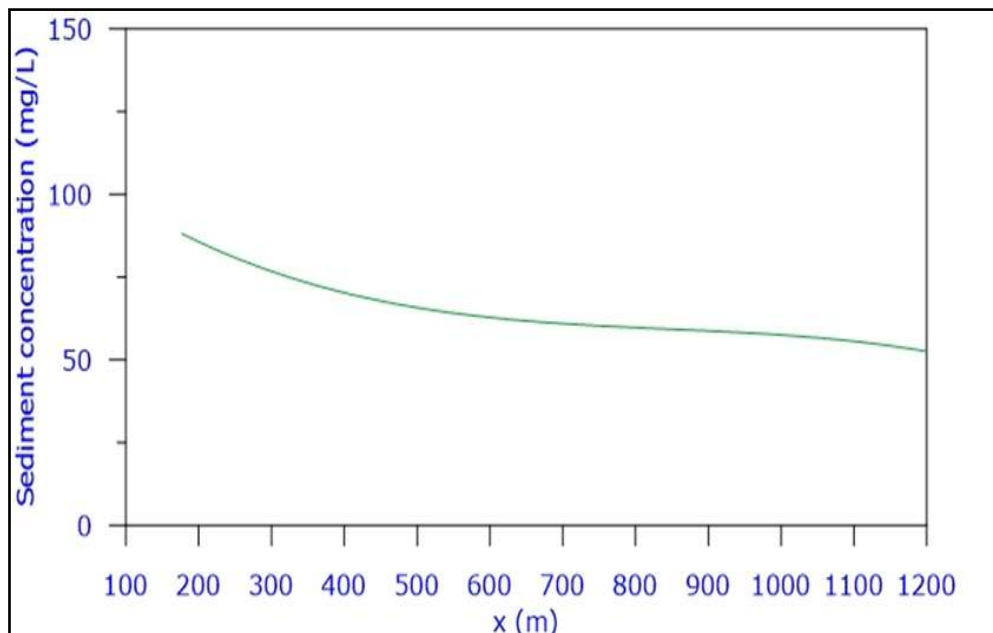
Prepared by School of Civil Engineering - National Tech Univ. of Athens on behalf of ASPROFOS, 2022.

**Figure D-46 Dilution in the bottom layer**



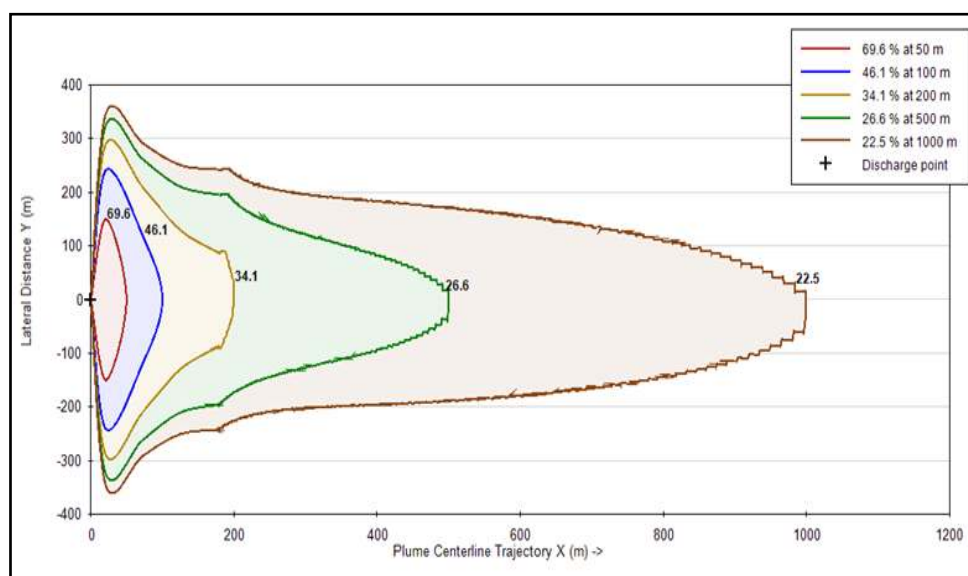
Prepared by School of Civil Engineering - National Tech Univ. of Athens on behalf of ASPROFOS, 2022.

**Figure D-47 Sediment concentrations (%) in the bottom layer**



Prepared by School of Civil Engineering - National Tech Univ. of Athens on behalf of ASPROFOS, 2022.




**Figure D-48** Sediment concentrations (mg/L) in the bottom layer



Prepared by School of Civil Engineering - National Tech Univ. of Athens on behalf of ASPROFOS, 2022.

**Figure D-49** Sediment concentration contours (% of the initial) in the bottom layer



	<p style="text-align: center;"><b>EASTMED PIPELINE PROJECT</b></p> <p style="text-align: center;">EastMed Greek Section – Environmental and Social Impact Assessment</p>	<div style="display: flex; justify-content: space-between; align-items: center;">   </div> <div style="display: flex; justify-content: space-between;"> <div> DOC No: PERM-GREE-ESIA- A09_0007_0_Annex9D REV. : PAGE : </div> <div> 00 93 OF 178 </div> </div>
---	--	--



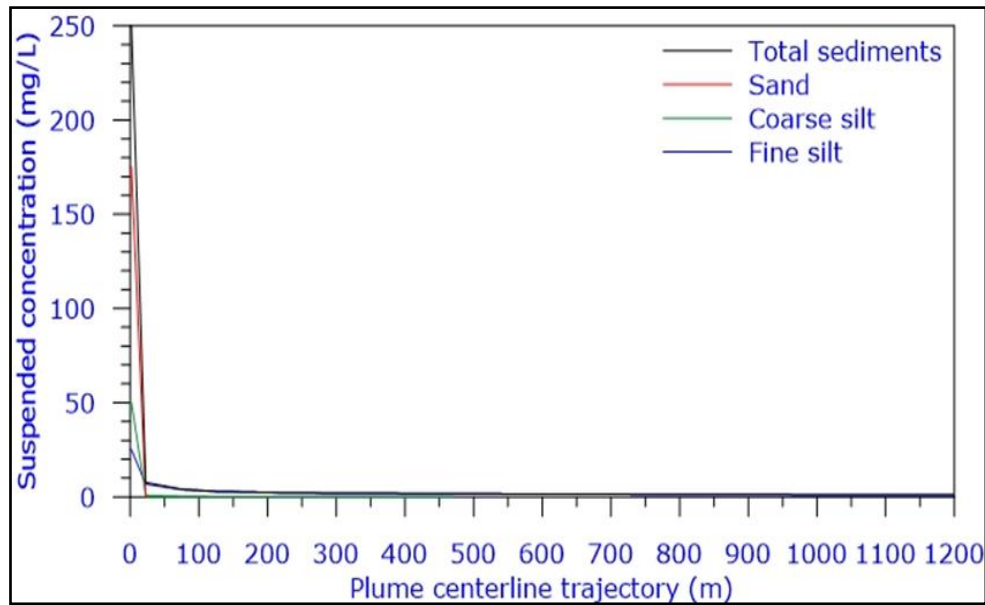
Prepared by School of Civil Engineering - National Tech Univ. of Athens on behalf of ASPROFOS, 2022.

**Figure D-50 Sediment concentration contours (mg/L) in the bottom layer**

#### **9 D.4.4.5 Suspended sediment concentrations**

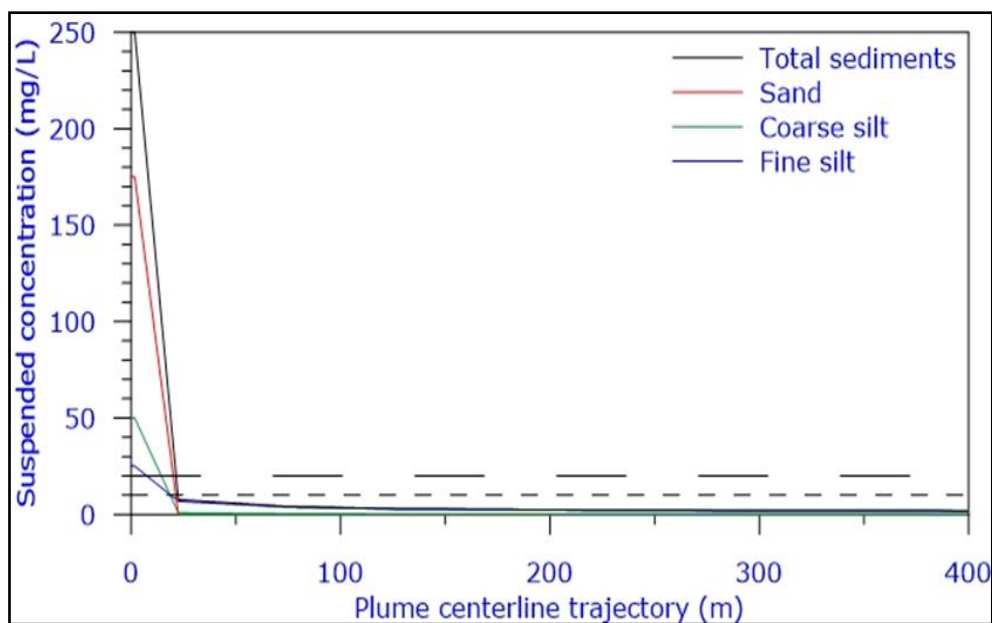
Figure D-51 and Figure D-52 and Figure D-53 show the suspended sediment concentrations (mg/L) in the water column.

The suspended sediment concentrations (SSC) decrease continuously downstream; at 21.2 m SSC = 8.45 mg/L, at 72.7 m SSC = 7.0 mg/L, at 175.64 m (end of near field) SSC = 2.8 mg/L, at 357.1 m SSC = 1.8 mg/L and at 555.7 m SSC = 1.5 mg/L; at x= 901.0 m SSC is practically equal to zero.






Prepared by School of Civil Engineering - National Tech Univ. of Athens on behalf of ASPROFOS, 2022.

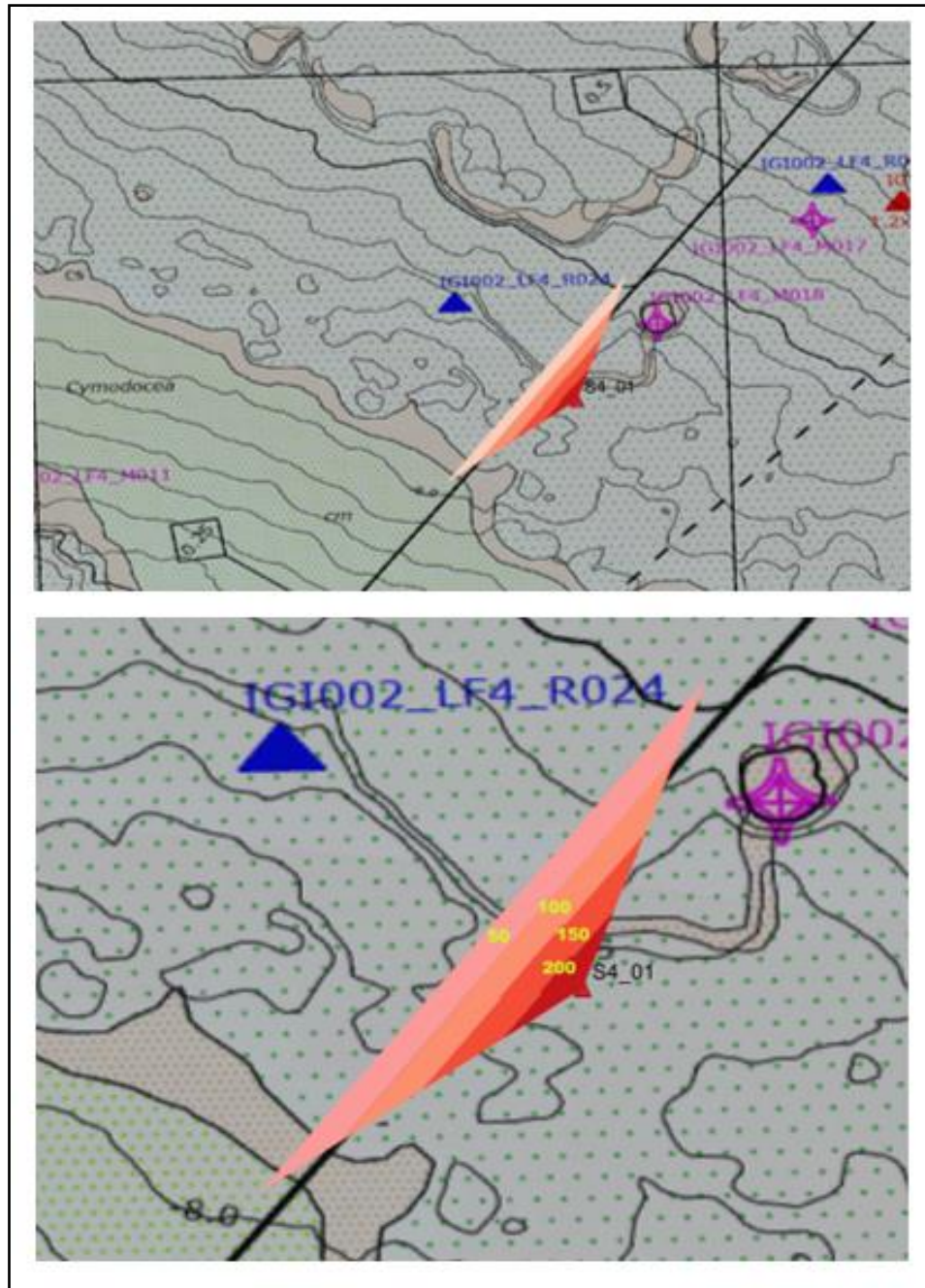
Figure D-51 Suspended sediment concentrations (mg/L) from x=0 to x=1200 m



Prepared by School of Civil Engineering - National Tech Univ. of Athens on behalf of ASPROFOS, 2022.

Figure D-52 Suspended sediment concentrations (mg/L) from x=0 to x=400 m




	<p style="text-align: center;"><b>EASTMED PIPELINE PROJECT</b></p> <p style="text-align: center;">EastMed Greek Section – Environmental and Social Impact Assessment</p>	<div style="display: flex; justify-content: space-between; align-items: center;">   </div> <div style="display: flex; justify-content: space-between;"> <div> DOC No: PERM-GREE-ESIA- A09_0007_0_Annex9D REV. : PAGE : </div> <div> 00 95 OF 178 </div> </div>
---	--	--



Prepared by School of Civil Engineering - National Tech Univ. of Athens on behalf of ASPROFOS, 2022.

**Figure D-53**    **Suspended sediment concentrations (mg/L) with Google maps background**



	EASTMED PIPELINE PROJECT		 	
	EastMed Greek Section – Environmental and Social Impact Assessment		DOC No: PERM-GREE-ESIA-A09_0007_0_Annex9D	
			REV. :	00
			PAGE :	96 OF 178

## 9 D.4.5. Sensitivity analysis

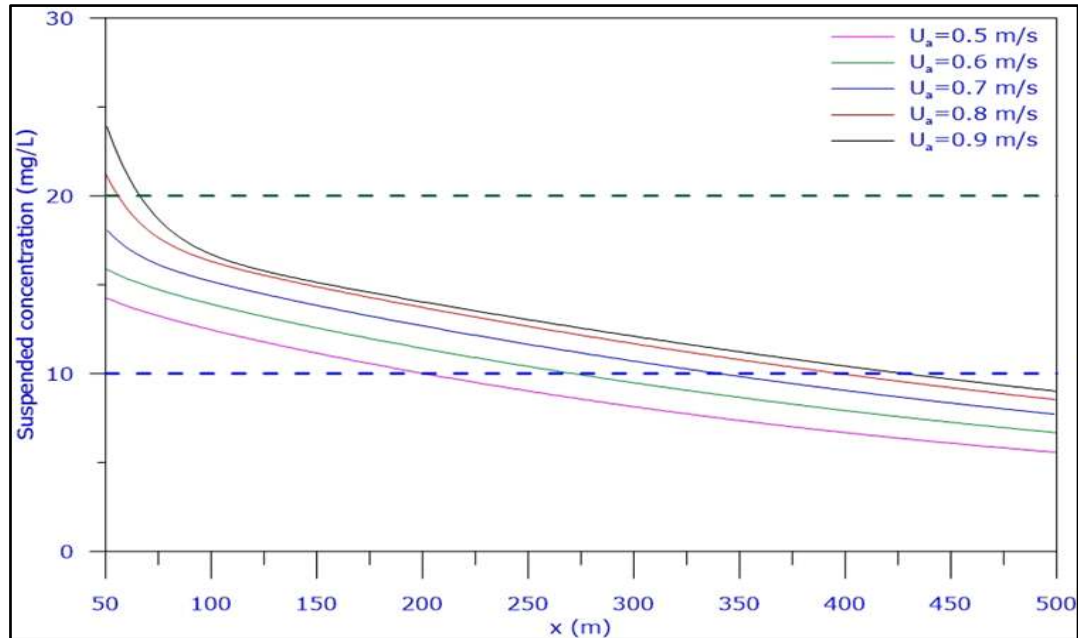
### 9 D.4.5.1 Effect of the current velocity

Calculations have been performed to investigate the effect of current velocity with values that ranged from 0.50 to 0.90 m/s. Table turbidity summarizes the effect of current velocity on the main geometric and hydrodynamic characteristics of the flow. At Figure D-54 the suspended sediment concentrations (mg/L) distributions for various current velocities are presented. In Figure D-55 sediment concentration contours (% of the initial) in the bottom layer are shown for current velocities from 0.50 m/s to 0.90 m/s.

**Table D-9 Basic geometric characteristics and hydrodynamic for various current velocities**

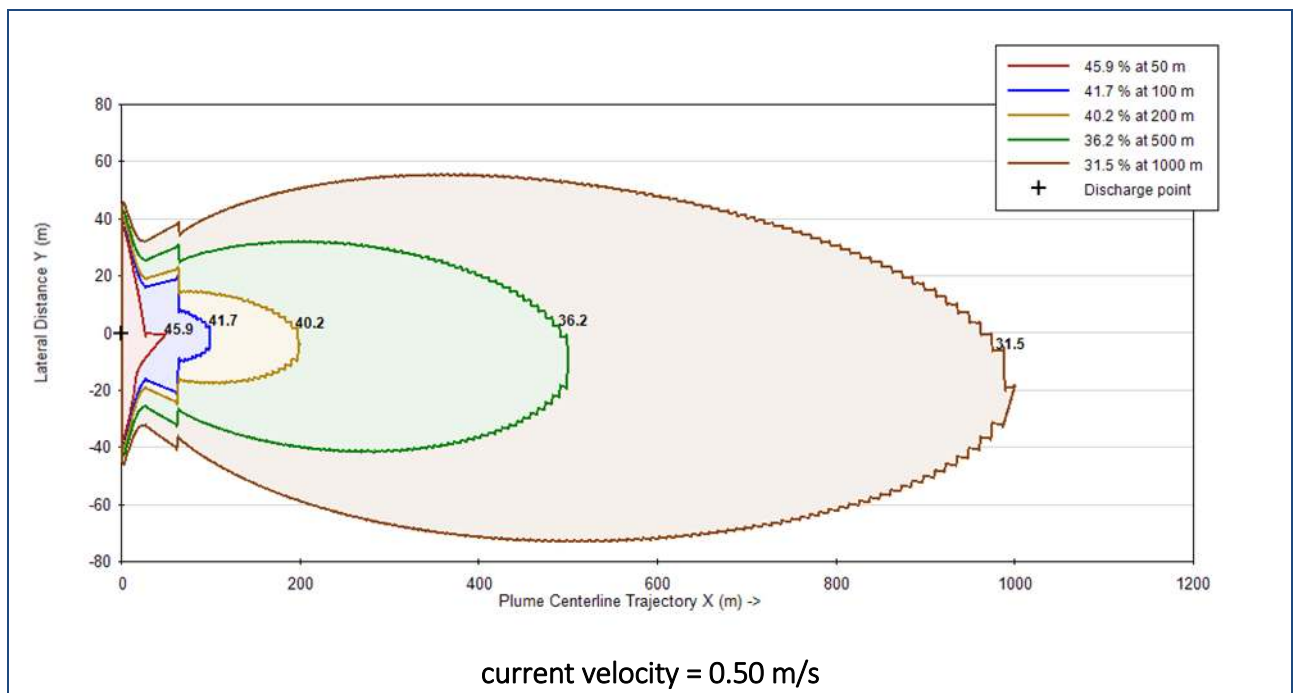
Current velocity (m/s)	Length of the near field (m)	BV (m)			BH (m)		
		At the end of near field	At x=400 m	At x=1000 m	At the end of near field	At x=400 m	At x=1000 m
0.50	26.61	0.59	0.20	0.16	52.36	151.41	231.38
0.60	17.13	0.75	0.20	0.16	33.37	127.00	195.57
0.70	11.63	0.94	0.20	0.16	22.35	105.23	164.53
0.80	8.34	1.16	0.21	0.17	15.73	88.77	141.52
0.90	6.40	1.43	0.22	0.19	11.83	78.92	127.31

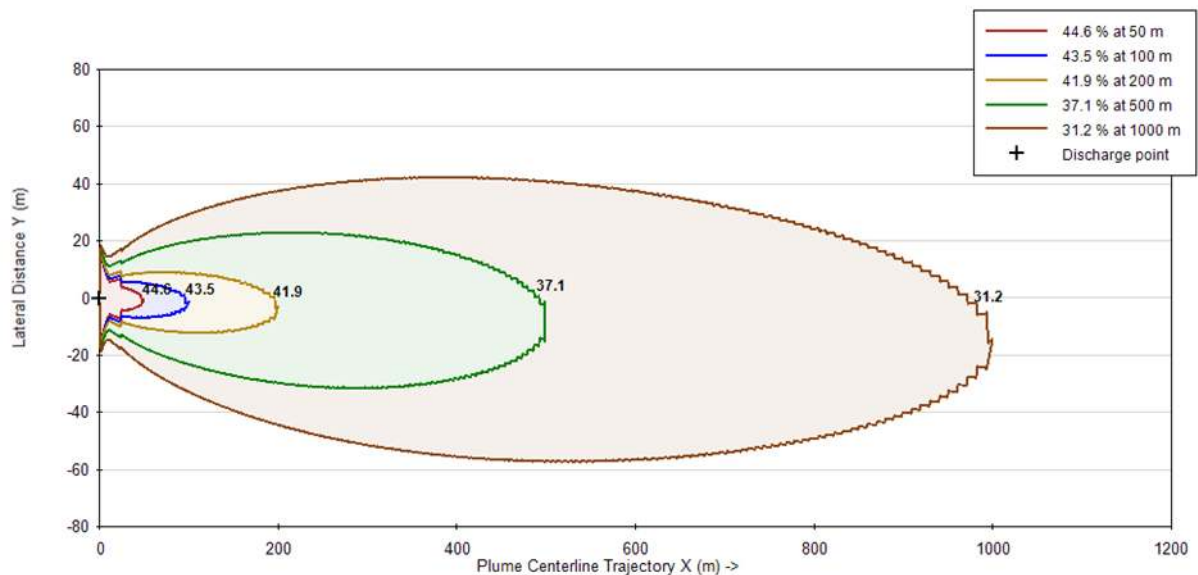
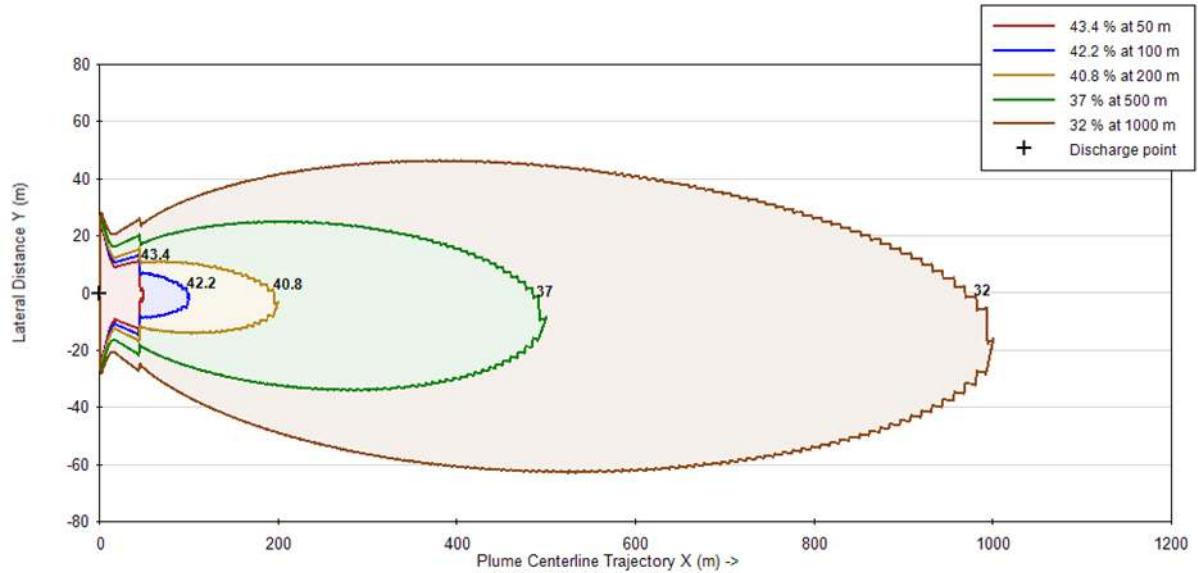
Prepared by School of Civil Engineering - National Tech Univ. of Athens on behalf of ASPROFOS, 2022.

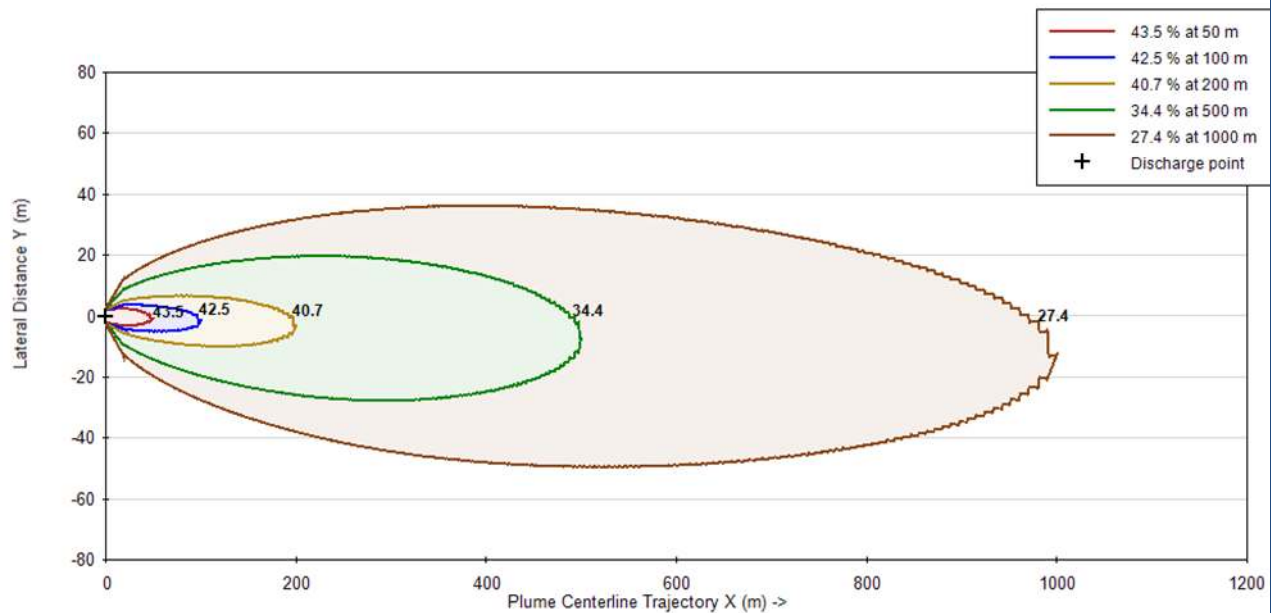
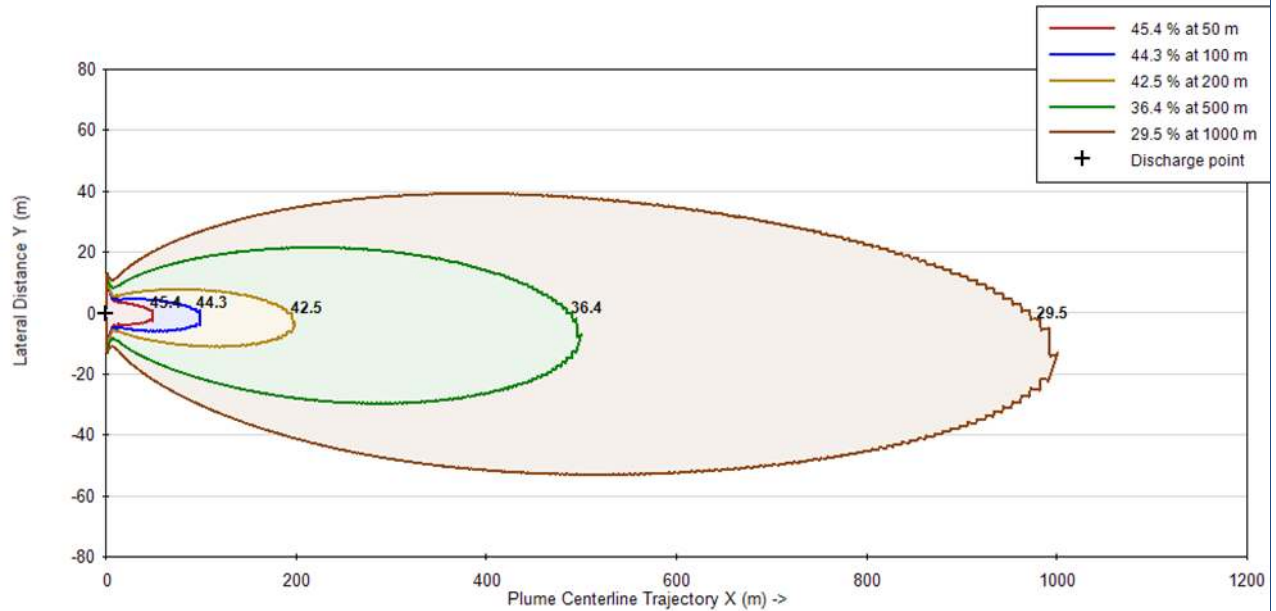


Prepared by School of Civil Engineering - National Tech Univ. of Athens on behalf of ASPROFOS, 2022.




**Figure D-54** Total suspended sediment concentrations (mg/L) for various current velocities







Prepared by School of Civil Engineering - National Tech Univ. of Athens on behalf of ASPROFOS, 2022.

 <b>IGI Poseidon</b>	<b>EASTMED PIPELINE PROJECT</b>	 
	EastMed Greek Section – Environmental and Social Impact Assessment	DOCNo: PERM-GREE-ESIA- A09_0007_0_Annex9D
		REV. : 00 PAGE : 100 OF 178

**Figure D-55 Sediment concentration contours (% of the initial) in the bottom layer for current velocities from 0.50 m/s to 0.90 m/s**

From Table D-9, Figure D-54 and Figure D-55 and the calculations, when the current velocity increases from 0.50 m/s to 0.90 m/s, the following are observed:

- The length of the near field region decreases from 26.62 m to 6.40 m.
- The thickness of the bottom layer (BV) at the end of the near field increases from 0.59 m to 1.43 m; far from the dredging location, it approaches values that range from 0.16 m to 0.19 m.
- The half-width of the bottom layer (BH) at the end of the near field decreases from 52.36 m to 11.83 m; far from the dredging location, it approaches values that range from 231.38 m to 127.31 m.
- The suspended solids concentrations in the water column decrease; thus, the decrease of the current velocity results in more favourable conditions.

#### 9 D.4.5.2 Effect of the composition of solids

Calculations have been performed to investigate the effect of sediment compositions by increasing the percentage of fine silt from 10% to 40 %, as shown in Table D-10. The calculated suspended sediment concentrations (mg/L) are shown in Table D-11.

**Table D-10 Examined sediment compositions**

Class	Material	C1	C2	C3	C4
1	Chunks	-	-	-	-
2	Sand	70 %	60 %	50 %	40 %
3	Coarse Silt	20 %	20 %	20 %	20 %
4	Fine Silt	10 %	20 %	30 %	40 %
5	Clay	-	-	-	-
Total	-	100 %	100 %	100 %	100 %

Prepared by School of Civil Engineering - National Tech Univ. of Athens on behalf of ASPROFOS, 2022.




**Table D-11 Suspended sediment concentrations (mg/L) for various sediment compositions**

x(m)	C1	C2	C3	C4
1.1	77.3	83.3	89.2	95.2
3.8	71.5	78.1	84.6	91.2



x(m)	C1	C2	C3	C4
6.4	54.8	60.7	66.6	72.5
9.0	41.3	46.4	51.5	56.7
11.6	34.9	39.7	44.6	49.4
12.9	32.4	37.1	41.9	46.6
14.1	31.5	36.3	41.1	45.9
15.3	30.7	35.5	40.4	45.3
16.5	29.8	34.8	39.8	44.7
27.2	24.1	29.5	34.8	40.2
28.4	23.6	29.0	34.4	39.8
39.1	20.2	25.8	31.4	37.0
40.2	19.9	25.5	31.1	36.7
117.5	14.7	20.0	25.2	30.5
118.7	14.7	19.9	25.2	30.5
130.6	14.3	19.5	24.8	30.0
131.7	14.3	19.5	24.7	29.9
293.3	10.8	15.4	20.0	24.6
294.5	10.8	15.4	20.0	24.5
295.7	10.8	15.4	19.9	24.5
342.0	10.0	14.4	18.8	23.3
343.2	10.0	14.4	18.8	23.2
344.4	9.9	14.4	18.8	23.2
485.8	7.9	11.9	15.9	20.0
636.7	6.3	10.0	13.6	17.3
637.9	6.3	9.9	13.6	17.3
955.2	4.2	7.3	10.4	13.5
956.4	0.0	0.0	0.0	0.0

Prepared by School of Civil Engineering - National Tech Univ. of Athens on behalf of ASPROFOS, 2022.

	<b>EASTMED PIPELINE PROJECT</b>		 	
	EastMed Greek Section – Environmental and Social Impact Assessment		DOC No: PERM-GREE-ESIA-A09_0007_0_Annex9D	
			REV. :	00
			PAGE :	102 OF 178

**Table D-12**      **Suspended sediment concentrations (mg/L) for various sediment compositions at x=50 m and x=100 m**

x(m)	C1	C2	C3	C4
50.0	18.2	23.7	29.5	35.2
100.0	16.7	20.6	26.0	31.4

Prepared by School of Civil Engineering - National Tech Univ. of Athens on behalf of ASPROFOS, 2022.

Table D-12 the calculations show that when the percentage of fine silt increase from 10% to 40 %, then:

- The increases concentration increases at x=50.0 m from 18.2 mg/L to 35.2 mg/L and at x=100.0 m increase from 16.7 mg/L to 31.4 mg/L.
- The area covered by relatively high suspended sediment concentrations increases.




## **9 D.5.      CALCULATIONS AT SITE LF5 AND DISCUSSION**

### **9 D.5.1.    Input data**

The input data and the sediment classes for site LF5 are shown in Table D-13 and Table D-14, respectively. In Figure D-56, Figure D-57 and Figure D-58 the output of the dredger, the schematic diagram of the trench and the discharge location are shown, respectively.

**Table D-13      Input data for site LF5**

	Characteristic	Value	Units
DR1	Type	Bucket	-
DR2	Capacity	5.0	m <sup>3</sup>
DR3	Cycle time	60	s
DR4	Output	220	m <sup>3</sup> /h
	Dry solids density of the dredged material	1800	kg/m <sup>3</sup>
	Dry bulk density	1440	kg/m <sup>3</sup>
	Sediment release rate	4.0	%
	Re-suspension factor	3.2	%
	Total excavation volume	240000	m <sup>3</sup>
	Total required hours of dredging	1091	h




	<p style="text-align: center;"><b>EASTMED PIPELINE PROJECT</b></p> <p style="text-align: center;">EastMed Greek Section – Environmental and Social Impact Assessment</p>	<div style="display: flex; justify-content: space-between; align-items: center;">   </div> <p>DOC No: PERM-GREE-ESIA-A09_0007_0_Annex9D</p> <p>REV. : 00</p> <p>PAGE : 103 OF 178</p>
---	--	---

	Characteristic	Value	Units
	Mass of dredged material	316800 kg/h	kg/h
	Mass of re-suspended solids	12672	kg/h
SE1	Sediment density	1800	kg/m <sup>3</sup>
SE2	Sediment classes	See Table D-14	
AM1	Ambient temperature	25.23	°C
AM2	Ambient salinity	38.64	psu
AM3	Ambient sediment concentration	0.0	mg/L
AM4	Ambient density	1026.11	kg/m <sup>3</sup>
AM5	Flow velocity near the bottom	0.71	m/s
AM6	Flow velocity at the surface	1.10	m/s
SD1	Rate of sediment mass release	3.52	kg/s
SD2	Sediment plume concentration	250	mg/L
SD2	Sediment plume density	1133.5	kg/m <sup>3</sup>
SD4	Sediment plume discharge	14.09	m <sup>3</sup> /s
SD5	Discharge velocity	1.0	m/s
SD6	Sediment plume area	14.09	m <sup>2</sup>
SD7	Shore Location	Left	
SD8	Distance to shoreline	1000	m
SD9	Water depth at the discharge location	6.25	m
SD10	Bottom Slope	0.625	%
SD11	Vertical Angle	75	°
SD12	Horizontal Angle	0	°
SD13	Discharge height above channel bottom	1.0	m
SD14	Water depth at the source of the plume	5.25	m

Prepared by School of Civil Engineering - National Tech Univ. of Athens on behalf of ASPROFOS, 2022.

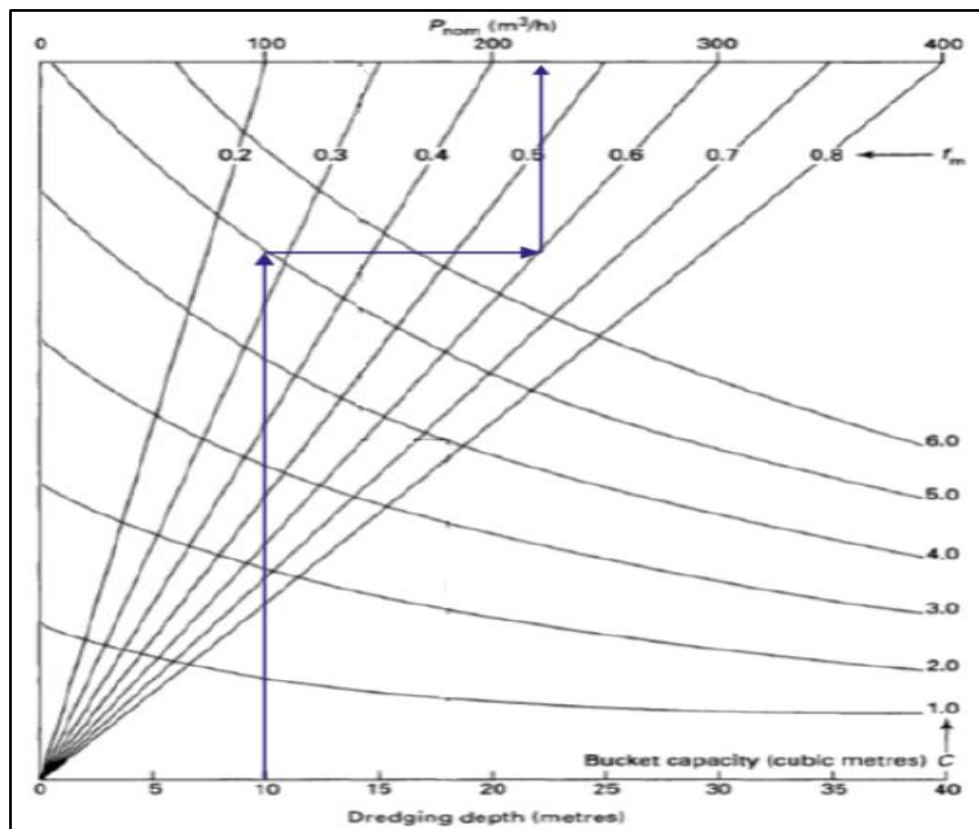
**Table D-14 Sediment Classes for site LF5**

Class	Material	%	Settling Velocity (m/s)	Concentration (mg/L)	Sediment mass release (kg/s)
1	Chunks	0	Instantaneous*	-	0.00
2	Sand	80	0.031	200	2.81

	<b>EASTMED PIPELINE PROJECT</b>		 	
	EastMed Greek Section – Environmental and Social Impact Assessment		DOC No: PERM-GREE-ESIA-A09_0007_0_Annex9D	
			REV. :	00
			PAGE :	104 OF 178




Class	Material	%	Settling Velocity (m/s)	Concentration (mg/L)	Sediment mass release (kg/s)
3	Coarse Silt	10	0.00042	25	0.35
4	Fine Silt	5	0.000026	12.5	0.18
5	Clay	5	0.00000065	12.5	0.18
Total	-	100	-	250.0	3.52

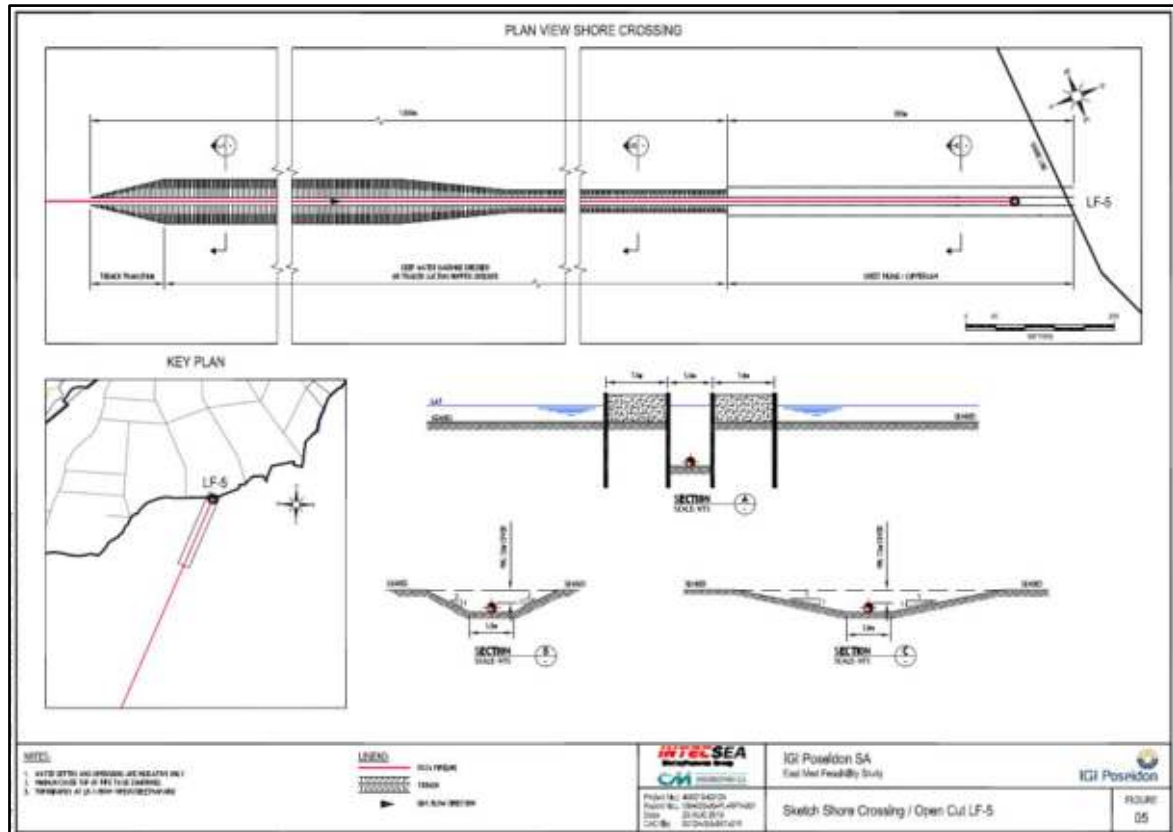
Prepared by School of Civil Engineering - National Tech Univ. of Athens on behalf of ASPROFOS, 2022.



Prepared by School of Civil Engineering - National Tech Univ. of Athens on behalf of ASPROFOS, 2022.

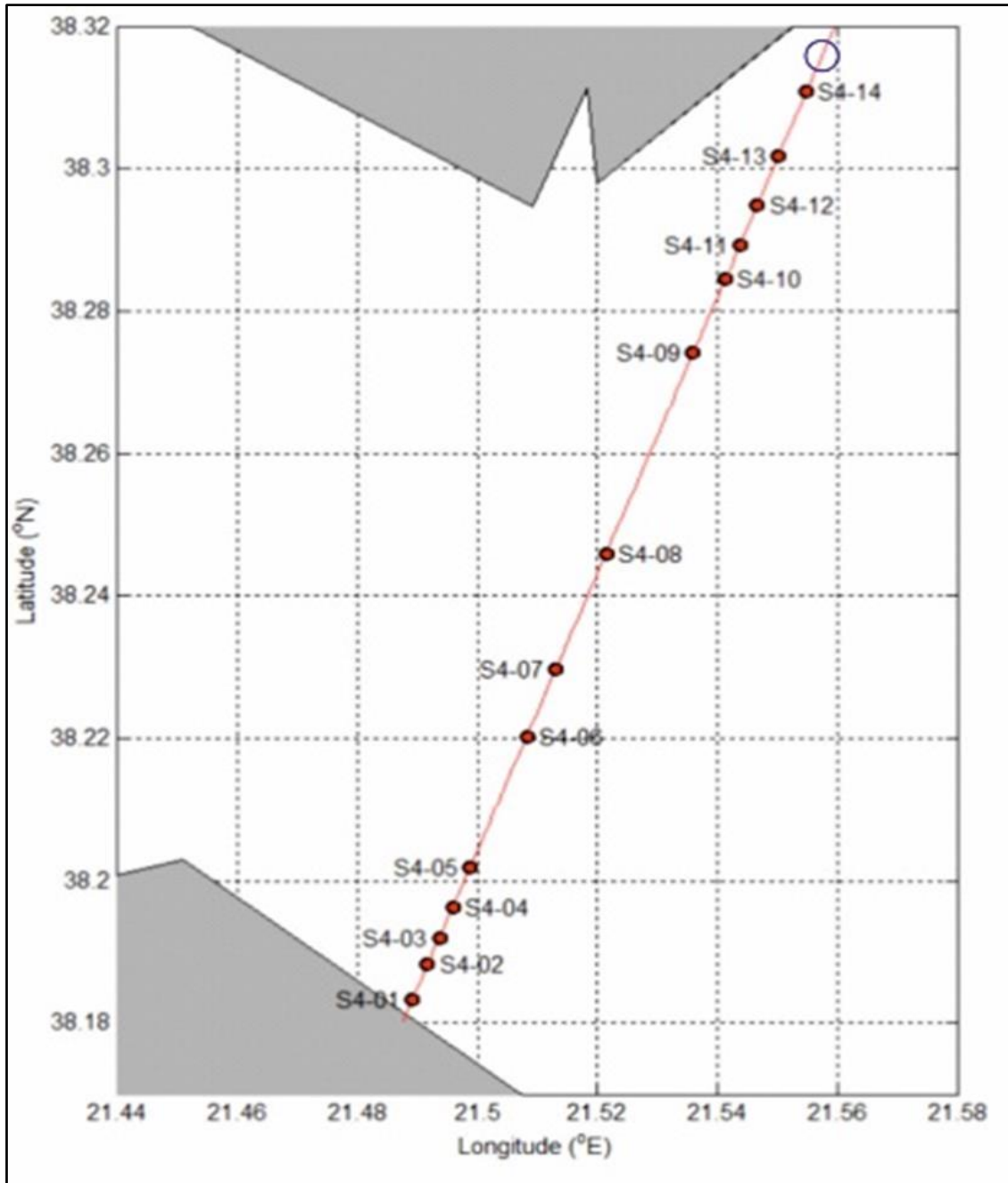
Figure D-56 Output of the dredger (Bray et al., 1996)

	<p><b>EASTMED PIPELINE PROJECT</b></p> <p>EastMed Greek Section – Environmental and Social Impact Assessment</p>	<div>   </div> <p>DOC No: PERM-GREE-ESIA-A09_0007_0_Annex9D</p> <p>REV. : 00</p> <p>PAGE : 105 OF 178</p>
---	--	---



Prepared by School of Civil Engineering - National Tech Univ. of Athens on behalf of ASPROFOS, 2022.

Figure D-57 Schematic diagram of trench at LF5



Prepared by School of Civil Engineering - National Tech Univ. of Athens on behalf of ASPROFOS, 2022.

Figure D-58 Discharge location; see also Appendix 1

## 9 D.5.2. Flow characteristics




	<b>EASTMED PIPELINE PROJECT</b>		 	
			DOC No: PERM-GREE-ESIA-A09_0007_0_Annex9D	
	EastMed Greek Section – Environmental and Social Impact Assessment		REV. :	00
			PAGE :	107 OF 178

Figure D-59 shows the trajectory of the axis of the SPM plume in the near field region that include the first 3 flow zones: FZ1, FZ2 and FZ3. In Figure D-60 and Figure D-61 the variation of width (2BH) and the thickness (BV) of the plume along the bottom layer are shown, respectively.

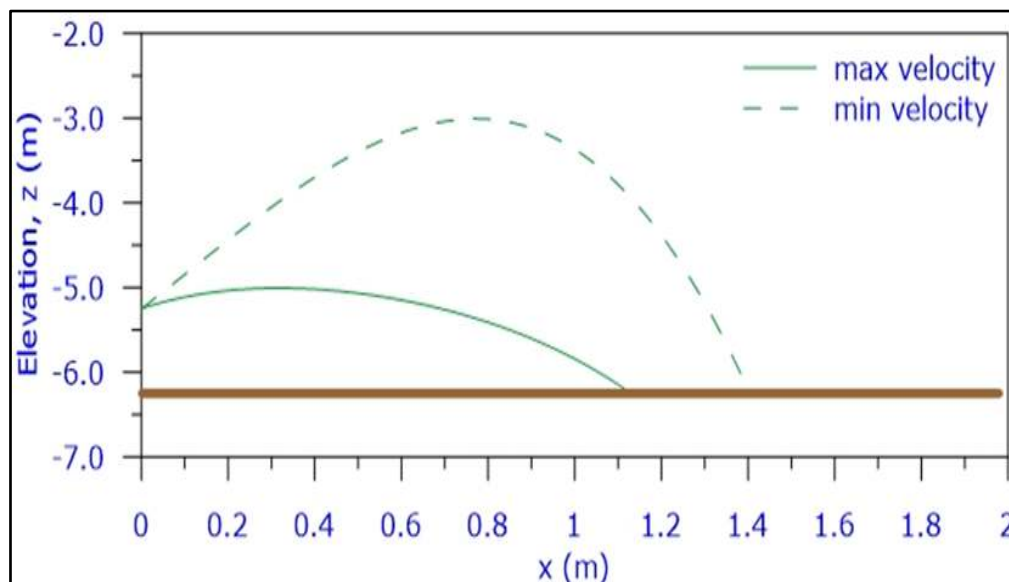
Initially, the flow is dominated by the upward plume momentum (jet-like); the axis of the SPM plume rises to a maximum height ( $z_{max}$ ), being weakly deflected by the ambient current ( $z_{max}/L_b \ll 1$ ). Then, the SPM plume is strongly affected by gravity and rapidly falls downwards and impinges on the sea bottom ( $z$ ), with an angle that is equal to  $\Theta$ . After impingement, the flow spreads more or less radially along the bottom, at an upstream intrusion length ( $L_s$ ) against the ambient flow, and also laterally spreads across the ambient flow. Its half-width (BH) is steadily increasing along the near field region, downstream. The thickness (BV) is steadily decreasing along the near field region, downstream. The mixing rate is relatively small; thus, the dilution range is also small. Table D-15 summarizes the above-mentioned flow characteristics. As already being observed in the site LF4, dilution increases with decreasing current velocity.

**Table D-15 Flow characteristics for site LF5**

Characteristics	Maximum flow velocity	Minimum flow velocity
$L_M = \frac{M_0^{3/4}}{J_0^{1/2}}$	1.91 m	1.91 m
$L_Q = \frac{Q_0}{M_0^{1/2}}$	3.75 m	3.75 m
$L_m = \frac{M_0^{1/2}}{u_a}$	5.29 m	Very large value
$L_b = \frac{J_0^{1/2}}{u_a^3}$	40.44 m	Very large value
SPM plume classification	Near-vertical class (NV)	Near-vertical class (NV)
Discharge configuration	Hydrodynamically stable	Hydrodynamically stable
$L_M/H_s$	$0.31 < 1$ Buoyancy dominated	$0.31 < 1$ Buoyancy dominated
$L_m/L_M$ Classification	$2.77 > 1$ Strong buoyancy – NV2	Strong buoyancy – NV2
FZ1- Maximum height ( $z_{max}$ )	1.24 m	3.27 m
FZ1 - Effect of ambient current ( $z_{max}/L_b$ )	Weak ( $0.03 \ll 1$ )	Very small value
FZ2	Weakly deflected plume in cross-flow	Weakly deflected plume in cross-flow

Characteristics	Maximum flow velocity	Minimum flow velocity
FZ2 - Impingement at sea bottom (z/angle $\Theta$ )	-6.25 m/29.68°	-6.25 m /57.88°
FZ3 - Upstream intrusion length, $L_s$	15.01 m	-
FZ3 – End of near field region	11.23 m	175.71 m
FZ3 - BH at impingement	16.79 m	294.41 m
FZ3 - BH at the end of near field	21.54 m	350.39 m
FZ4 - BH at x=1200 m	177.13 m	608.29 m
FZ3 – BV at impingement	1.03 m	0.12 m
FZ3 – BV at the end of near field	0.96 m	0.28 m
FZ4 – BV at x=1200 m	0.16 m	0.21 m
Interaction with shoreline	No	No
Dilution at the end of near field	2.1	2.7
Dilution at x=1200 m	3.4	4.7

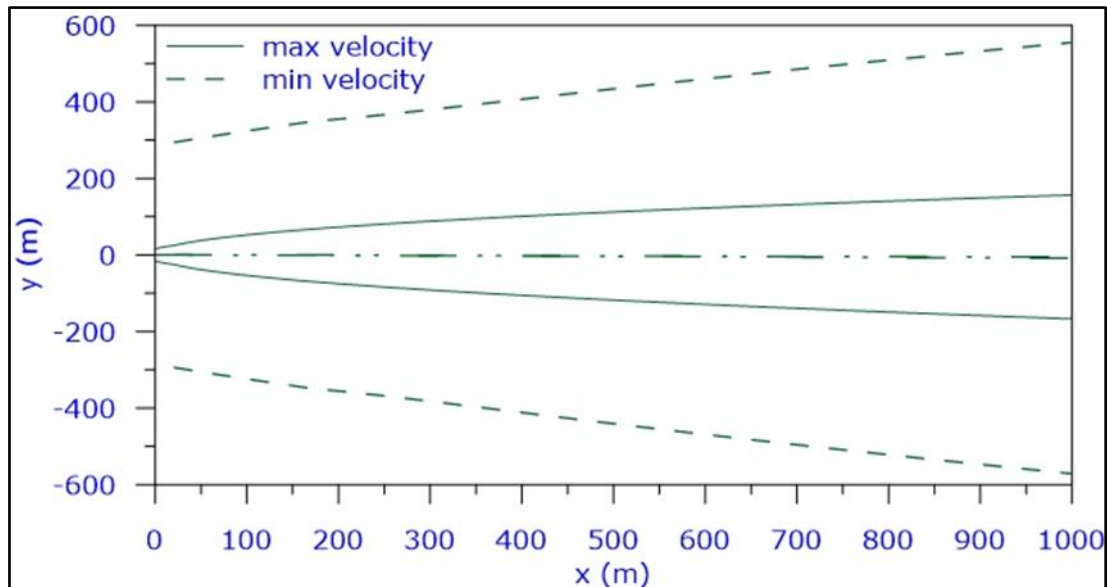
Prepared by School of Civil Engineering - National Tech Univ. of Athens on behalf of ASPROFOS, 2022.



Prepared by School of Civil Engineering - National Tech Univ. of Athens on behalf of ASPROFOS, 2022.

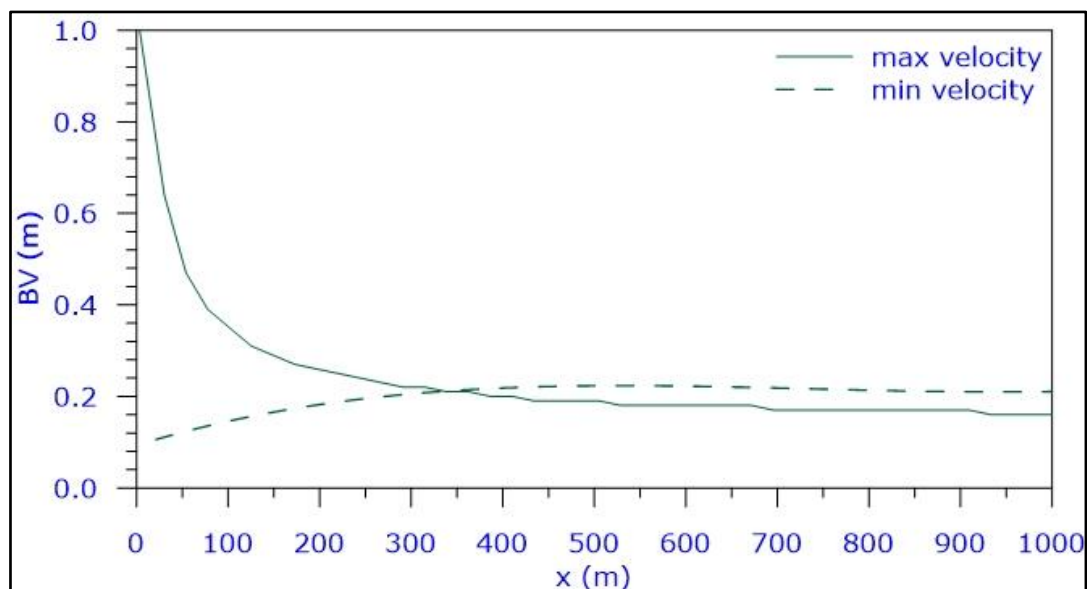
**Figure D-59** Trajectory of the axis of the SPM plume in the near field region





Prepared by School of Civil Engineering - National Tech Univ. of Athens on behalf of ASPROFOS, 2022.

Figure D-60 Variation of the width of the plume (2BH) along the bottom layer



Prepared by School of Civil Engineering - National Tech Univ. of Athens on behalf of ASPROFOS, 2022.

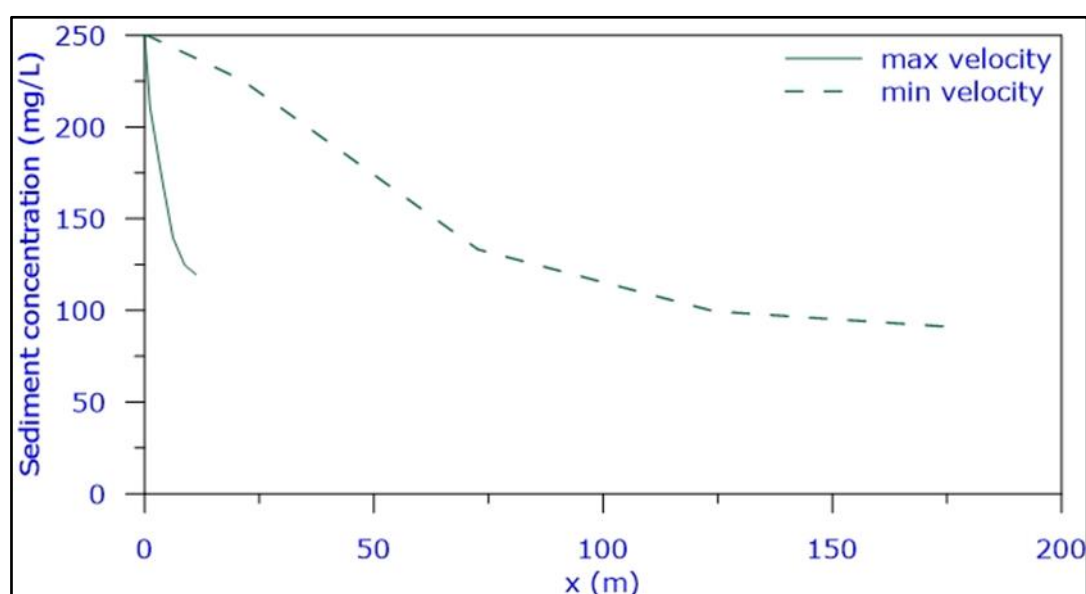
Figure D-61 Variation of the thickness (BV) along the bottom layer

### 9 D.5.3. Sediment concentrations

Figure D-62 and Figure D-63 show the variation of sediment concentrations (mg/L) in the near field region and along the bottom layer, respectively. In Figure D-64 the total sediment concentration contours in the bottom layer are shown for the maximum and minimum current velocity.

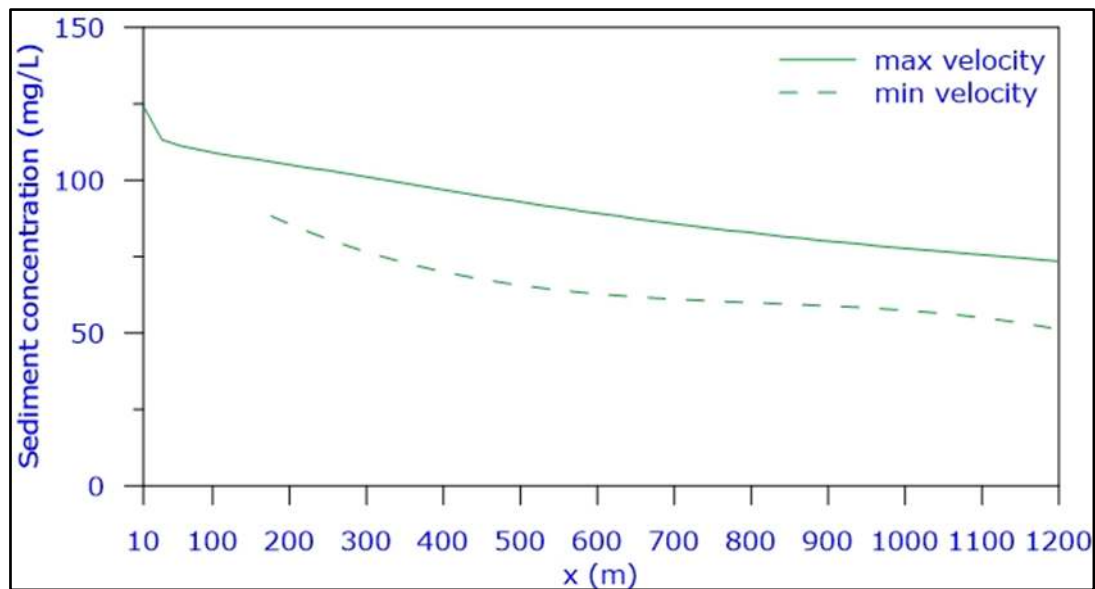
Figure D-62 and Figure D-63 depict that the total sediment concentration in the bottom layer is steadily decreasing; this decrease is more pronounced for the minimum flow velocity than for the maximum current velocity. More analytically:

- For the maximum current velocity: sediment concentration decreases from 119.5 mg/L (47.8 %) at the beginning of the bottom layer, to 111.8 mg/L (44.7 %) at 50 m downstream, to 109.0 mg/L (43.6 %) at 100 m and to 73.5 mg/L (29.4 %) at 1200 m, downstream.
- For the minimum current velocity: sediment concentration decreases from 91.0 mg/L (36.4 %) at the beginning of the bottom layer, to 69.8 mg/L (27.9 %) at 400 m downstream, to 64.0 mg/L (25.6 %) at 600 m and to 53.5 mg/L (21.4 %) at 1200 m downstream.






Prepared by School of Civil Engineering - National Tech Univ. of Athens on behalf of ASPROFOS, 2022.

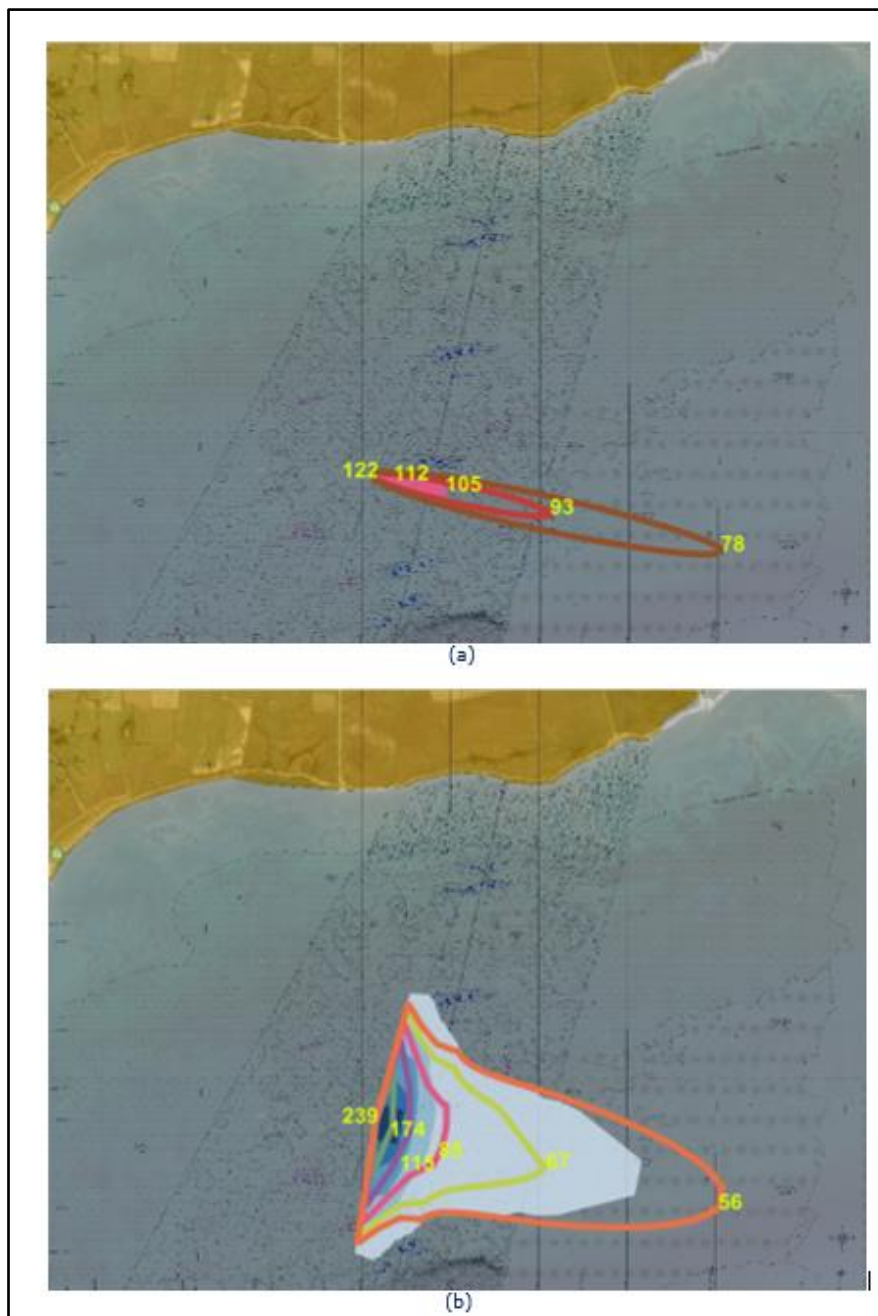
**Figure D-62 Sediment concentrations (mg/L) in the near field region**



Prepared by School of Civil Engineering - National Tech Univ. of Athens on behalf of ASPROFOS, 2022.

**Figure D-63** Sediment concentrations (mg/L) along the bottom layer

	<p style="text-align: center;"><b>EASTMED PIPELINE PROJECT</b></p> <p style="text-align: center;">EastMed Greek Section – Environmental and Social Impact Assessment</p>	<div style="display: flex; justify-content: space-between; align-items: center;">   </div> <div style="font-size: small;"> DOC No: PERM-GREE-ESIA- A09_0007_0_Annex9D REV. : 00 PAGE : 112 OF 178 </div>
---	--	--



Prepared by School of Civil Engineering - National Tech Univ. of Athens on behalf of ASPROFOS, 2022.

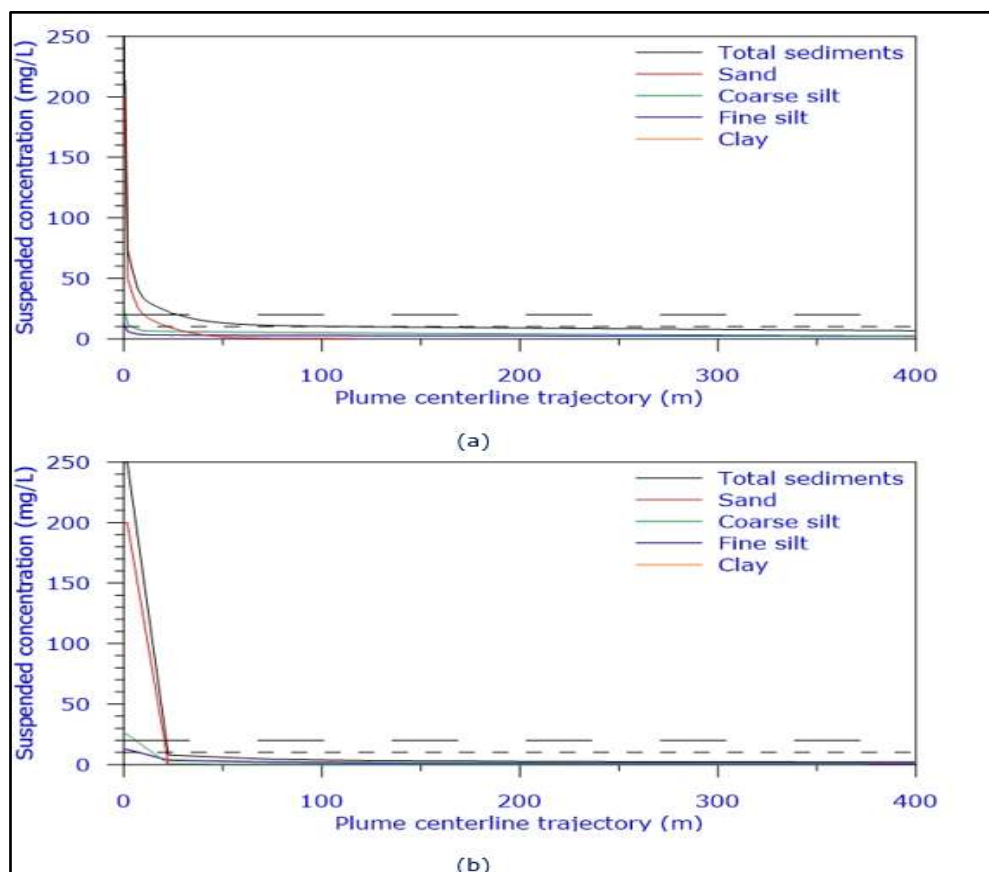
**Figure D-64** Total sediment concentration contours in the bottom layer in mg/L for (a) the maximum current velocity and (b) the minimum current velocity (Google Maps background)

#### 9 D.5.4. Suspended sediment concentrations

Figure D-65 shows the variation of suspended sediment concentration, SSC (mg/L) in the water column, while in Figure D-67 the SSC concentration contours in the water column are shown.

Figure D-65 and Figure D-66 depict that SSC values in the water column are steadily decreasing; this decrease is more pronounced for the minimum flow velocity than for the maximum current velocity. More analytically:




- For the maximum current velocity: at 1.1 m SSC = 74.0 mg/L (29.6 %), at 9.0 m SSC = 38.3 mg/L (15.3 %), at 11.23 m (end of near field) SSC = 31.9 mg/L (12.8 %), at 26.8 m SSC = 19.8 mg/L (7.9 %), at 117.1 m SSC = 10.1 mg/L (4.0 %) and at x= 954.9 m SSC is practically equal to zero.
- For the minimum current velocity: at 21.2 m SSC = 22.7 mg/L (9.1 %), at 72.7 m SSC = 4.6 mg/L (1.8 %), at 175.71 m (end of near field) SSC = 2.9 mg/L (1.1 %), at 357.0 m SSC = 2.2 mg/L (0.9 %) and at 555.7 m SSC = 1.9 mg/L (0.8 %); at x= 990.7 m SSC is practically equal to zero.

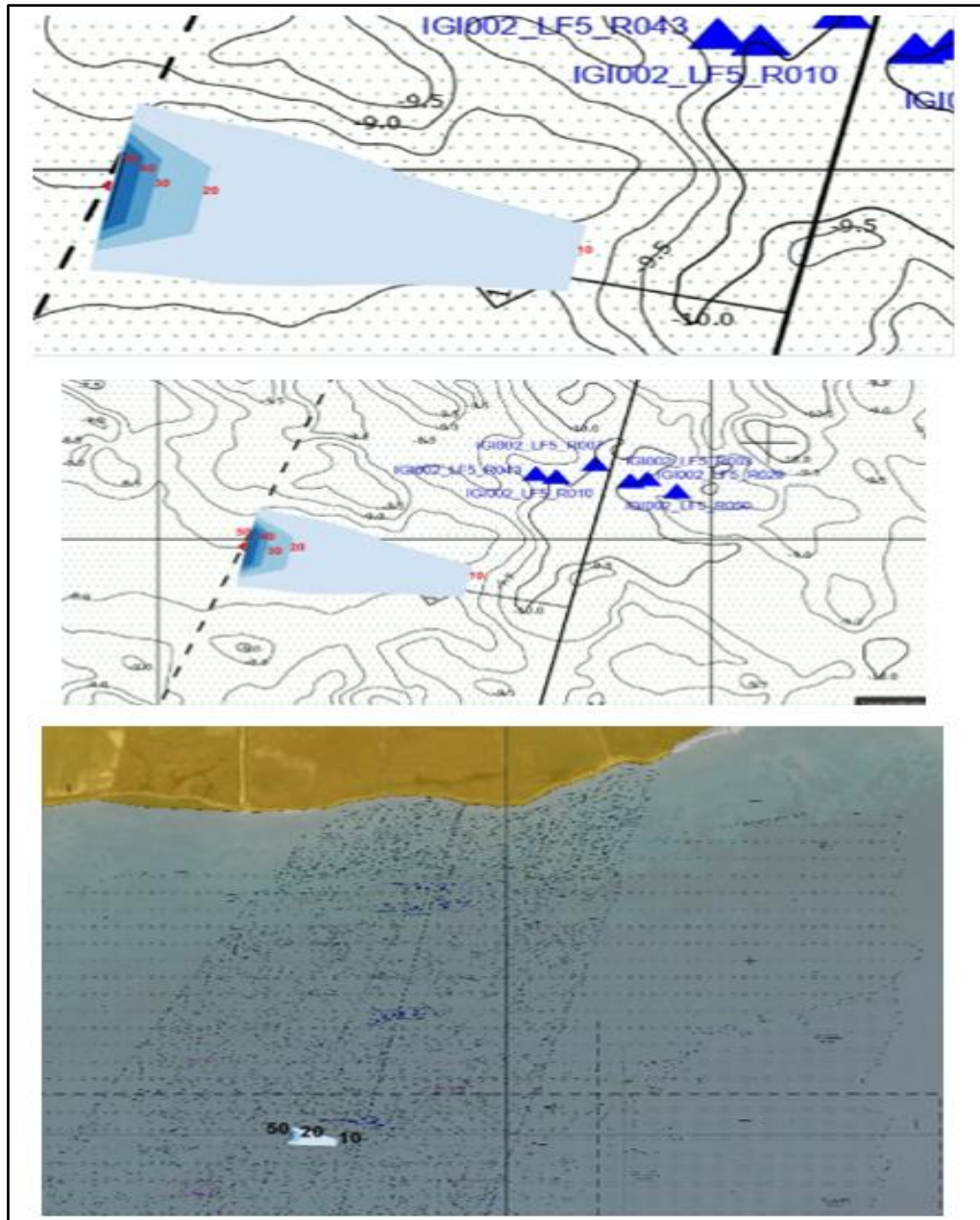


Prepared by School of Civil Engineering - National Tech Univ. of Athens on behalf of ASPROFOS, 2022.

**Figure D-65**    **Suspended sediment concentrations (mg/L) for (a) the maximum current velocity and (b) the minimum current velocity**






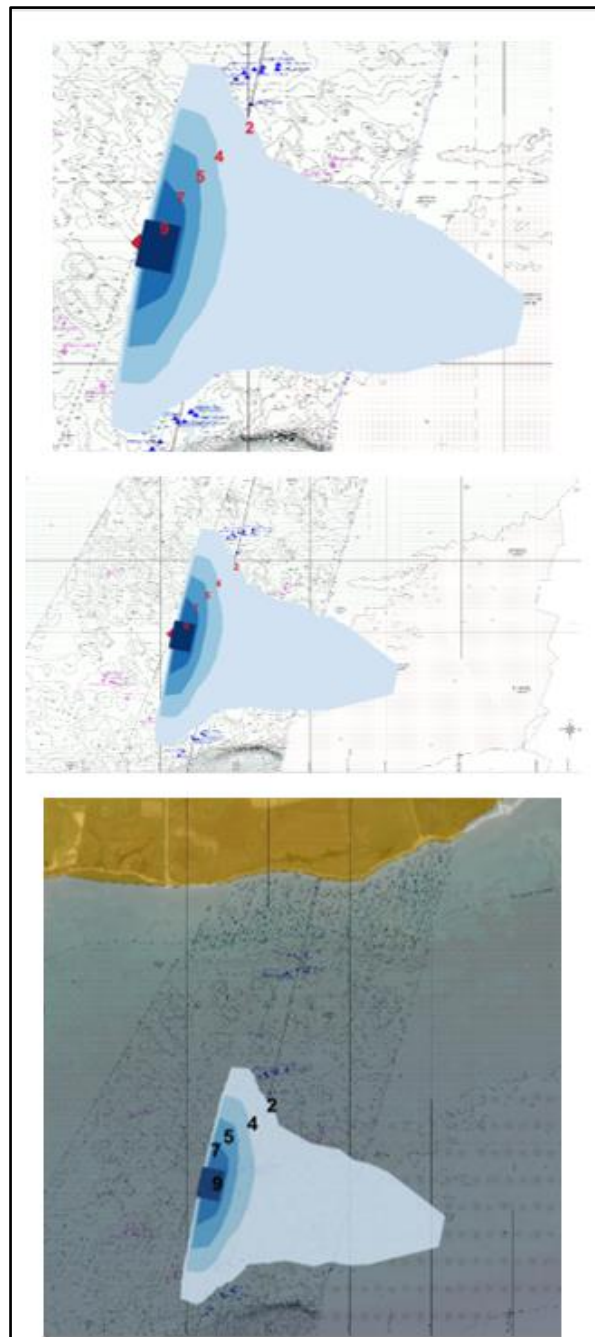
	<p style="text-align: center;"><b>EASTMED PIPELINE PROJECT</b></p> <p style="text-align: center;">EastMed Greek Section – Environmental and Social Impact Assessment</p>	<div style="display: flex; justify-content: space-between; align-items: center;">   </div> <div style="display: flex; justify-content: space-between;"> <div> <p>DOC No: PERM-GREE-ESIA- A09_0007_0_Annex9D</p> <p>REV. : 00</p> <p>PAGE : 114 OF 178</p> </div> </div>
---	--	---



Prepared by School of Civil Engineering - National Tech Univ. of Athens on behalf of ASPROFOS, 2022.

**Figure D-66**    Suspended sediment concentrations (mg/L) for the maximum current velocity (Google Maps background)

	<p style="text-align: center;"><b>EASTMED PIPELINE PROJECT</b></p> <p style="text-align: center;">EastMed Greek Section – Environmental and Social Impact Assessment</p>	<div style="display: flex; justify-content: space-between; align-items: center;">   </div> <div style="border-top: 1px solid black; border-bottom: 1px solid black; padding: 2px;"> DOC No: PERM-GREE-ESIA-A09_0007_0_Annex9D </div> <div style="display: flex; justify-content: space-between; border-bottom: 1px solid black; padding: 2px;"> <div>REV. :</div> <div>00</div> </div> <div style="display: flex; justify-content: space-between; padding: 2px;"> <div>PAGE :</div> <div>115 OF 178</div> </div>
---	--	---



Prepared by School of Civil Engineering - National Tech Univ. of Athens on behalf of ASPROFOS, 2022.

**Figure D-67**    Suspended sediment concentrations (mg/L) for the minimum current velocity (Google Maps background)

### 9 D.5.5.    Sensitivity analysis



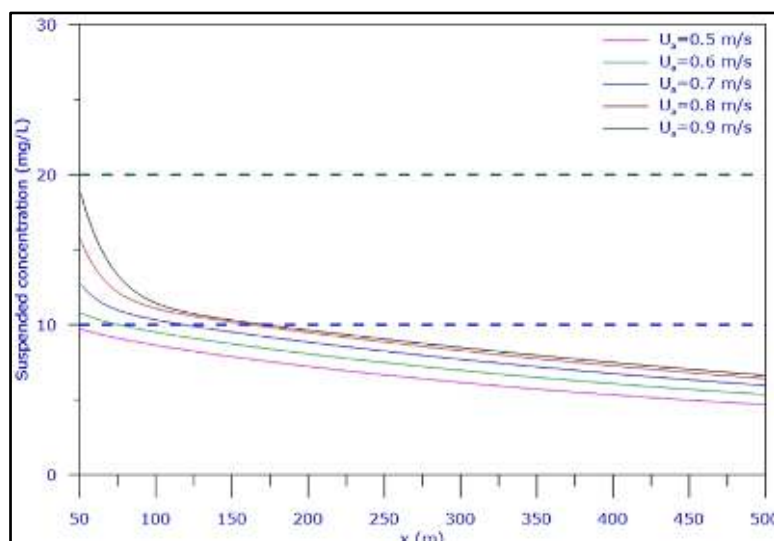
### 9 D.5.5.1 Effect of the current velocity

Calculations have been performed to investigate the effect of current velocity for values ranging from 0.50 to 0.90 m/s. Table D-16 summarizes the effect of current velocity on the main geometric and hydrodynamic characteristics of the flow. At Figure D-68 the suspended sediment concentrations (mg/L) distributions for various current velocities are presented. In Figure D-69 sediment concentration contours (% of the initial) in the bottom layer are shown for current velocities 0.50 m/s and 0.90 m/s.

**Table D-16 Basic geometric and hydrodynamic characteristics for various current velocities**

Current velocity (m/s)	Length of the near field (m)	BV (m)			BH (m)		
		At the end of near field	At x=400 m	At x=1000 m	At the end of near field	At x=400 m	At x=1000 m
0.50	26.62	0.59	0.20	0.16	52.39	151.46	231.33
0.60	17.14	0.75	0.20	0.15	33.39	127.00	195.46
0.70	11.64	0.94	0.20	0.16	22.36	105.21	164.51
0.80	8.35	1.16	0.21	0.17	15.74	88.76	141.43
0.90	6.40	1.43	0.22	0.19	11.84	78.89	127.28

Prepared by School of Civil Engineering - National Tech Univ. of Athens on behalf of ASPROFOS, 2022.

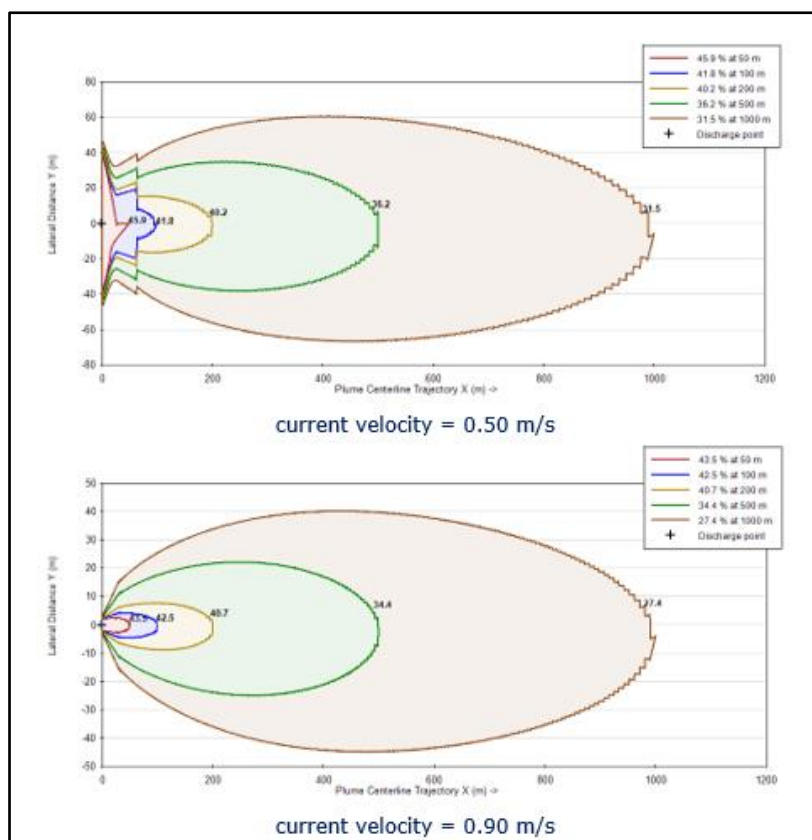


Prepared by School of Civil Engineering - National Tech Univ. of Athens on behalf of ASPROFOS, 2022.

**Figure D-68 Total suspended sediment concentrations (mg/L) for various current velocities**

From Table D-16, Figure D-68 and Figure D-69 and the calculations, when the current velocity increases from 0.50 m/s to 0.90 m/s, the following are observed:

- The length of the near field region decreases from 26.62 m to 6.40 m.
- The thickness of the bottom layer (BV) at the end of the near field increases from 0.59 m to 1.43 m; far from the dredging location, it approaches values that range from 0.16 m to 0.19 m.
- The half-width of the bottom layer (BH) at the end of the near field decreases from 52.39 m to 11.84 m; far from the dredging location, it approaches values that range from 231.33 m to 127.28 m.
- The suspended solids concentrations in the water column decrease; thus, the decrease of the current velocity results in more favorable conditions.



Prepared by School of Civil Engineering - National Tech Univ. of Athens on behalf of ASPROFOS, 2022.

**Figure D-69** Sediment concentration contours (% of the initial) in the bottom layer for current velocities 0.50 m/s and 0.90 m/s

### 9 D.5.5.2 Effect of the composition of solids

Calculations have been performed to investigate the effect of sediment composition on SSC concentration by increasing the percentage of fine silt from 5% to 20 %, as shown in Table D-17. The calculated suspended sediment concentrations (mg/L) are shown in Table D-18.

From Table D-18 and Table D-19 and the calculations, when the percentage of fine silt increases from 5 % to 20 %, then:

- The suspended sediment concentration increases at x=50.0 m from 13.1 mg/L to 21.6 mg/L and at x=100.0 m from 10.4 mg/L to 18.5 mg/L.
- The area covered by relatively high suspended sediment concentrations increases




**Table D-17 Examined sediment compositions**

Class	Material	C1	C2	C3	C4
1	Chunks	-	-	-	-
2	Sand	80 %	75 %	70 %	65 %
3	Coarse Silt	10 %	10 %	10 %	10 %
4	Fine Silt	5 %	10 %	15 %	20 %
5	Clay	5 %	5 %	5 %	5 %
Total	-	100 %	100 %	100 %	100 %

Prepared by School of Civil Engineering - National Tech Univ. of Athens on behalf of ASPROFOS, 2022.




**Table D-18 Suspended sediment concentrations (mg/L) for various sediment compositions**

x(m)	C1	C2	C3	C4
1.1	74.0	76.8	79.7	82.5
3.7	67.6	70.8	73.9	77.1
6.2	51.4	54.2	57.0	59.9
8.7	38.3	40.8	43.3	45.7
11.2	31.9	34.3	36.6	39.0
12.5	29.4	31.7	34.0	36.3
13.7	28.4	30.7	33.1	35.4
14.9	27.4	29.8	32.2	34.6
22.0	22.5	25.0	27.6	30.2
23.2	21.7	24.3	26.9	29.5

	<b>EASTMED PIPELINE PROJECT</b>		 	
			DOC No: PERM-GREE-ESIA-A09_0007_0_Annex9D	
	EastMed Greek Section – Environmental and Social Impact Assessment		REV. :	00
			PAGE :	119 OF 178

x(m)	C1	C2	C3	C4
24.4	21.1	23.7	26.3	28.9
25.5	20.4	23.1	25.7	28.3
26.8	19.8	22.4	25.1	27.8
28.0	19.2	21.9	24.6	27.3
29.1	18.7	21.4	24.1	26.8
30.3	18.2	20.9	23.6	26.3
50.5	13.0	15.8	18.6	21.5
60.0	12.0	14.8	17.6	20.4
76.7	11.0	13.8	16.6	19.4
125.4	10.0	12.6	15.2	17.9
126.6	9.9	12.6	15.2	17.8
273.9	8.0	10.4	12.7	15.0
275.1	8.0	10.4	12.7	15.0
276.3	8.0	10.4	12.7	15.0
278.7	8.0	10.3	12.6	15.0
279.9	8.0	10.3	12.6	15.0
281.1	8.0	10.3	12.6	14.9
282.3	8.0	10.3	12.6	14.9
383.3	7.0	9.1	11.3	13.4
508.1	6.0	8.0	9.9	11.9
675.6	5.0	6.8	8.6	10.4
931.1	4.0	5.5	7.1	8.7
953.7	3.9	5.4	7.0	8.6
954.9	0.0	0.0	0.0	0.0

Prepared by School of Civil Engineering - National Tech Univ. of Athens on behalf of ASPROFOS, 2022.

	<b>EASTMED PIPELINE PROJECT</b>		 	
	EastMed Greek Section – Environmental and Social Impact Assessment		DOC No: PERM-GREE-ESIA-A09_0007_0_Annex9D	
			REV. :	00
			PAGE :	120 OF 178

**Table D-19**      **Suspended sediment concentrations (mg/L) at x=50 m and x=100 m**

x(m)	C1	C2	C3	C4
50.0	13.1	15.9	18.7	21.6
100.0	10.4	13.1	15.8	18.5

Prepared by School of Civil Engineering - National Tech Univ. of Athens on behalf of ASPROFOS, 2022.




## 9 D.6.      **CALCULATIONS AT SITE LF2 AND DISCUSSION**

### 9 D.6.1.      **Input Data**

The input data and the sediment classes for site LF5 are shown in Table D-20 and Table D-21, respectively. In Figure D-70, Figure D-71 and Figure D-72 the output of the dredger (Bray et al., 1996), the schematic diagram of the trench and the discharge location are shown, respectively.

**Table D-20**      **Input Data for Site LF2**

	Characteristic	Value	Units
DR1	Type	Bucket	-
DR2	Capacity	5	m <sup>3</sup>
DR3	Cycle time	60	s
DR4	Output	220	m <sup>3</sup> /h
	Dry solids density of the dredged material	1,800	kg/m <sup>3</sup>
	Dry bulk density	1440	kg/m <sup>3</sup>
	Sediment release rate	4.0	%
	Re-suspension factor	3.2	%
	Total excavation volume	50,000	m <sup>3</sup>
	Total required hours of dredging	227	h
	Mass of dredged material	316,800 kg/h	kg/h
	Mass of re-suspended solids	12,672	kg/h
SE1	Sediment density	1,800	kg/m <sup>3</sup>
SE2	Sediment classes	See Table D-21	
AM1	Ambient temperature	25.72	°C
AM2	Ambient salinity	39.21	psu
AM3	Ambient sediment concentration	0.0	mg/L
AM4	Ambient density	1,026.30	kg/m <sup>3</sup>

	<p style="text-align: center;"><b>EASTMED PIPELINE PROJECT</b></p> <p style="text-align: center;">EastMed Greek Section – Environmental and Social Impact Assessment</p>	<div style="display: flex; justify-content: space-between; align-items: center;">   </div> <p>DOC No: PERM-GREE-ESIA-A09_0007_0_Annex9D</p> <p>REV. : 00</p> <p>PAGE : 121 OF 178</p>
---	--	--

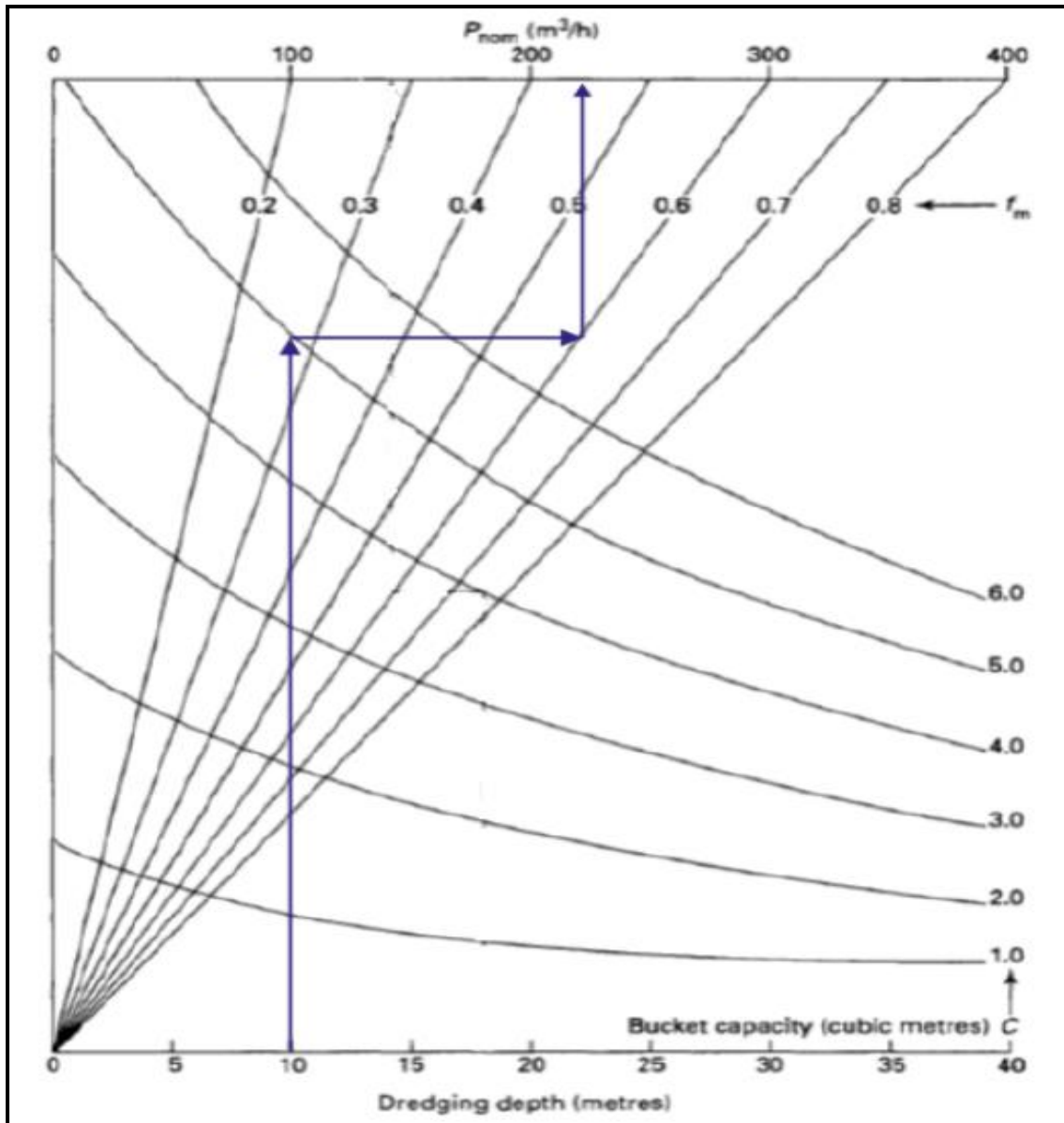
	Characteristic	Value	Units
AM5	Flow velocity near the bottom	0.88	m/s
AM6	Flow velocity at the surface	1.35	m/s
SD1	Rate of sediment mass release	3.52	kg/s
SD2	Sediment plume concentration	250	mg/L
SD2	Sediment plume density	1,133.47	kg/m <sup>3</sup>
SD4	Sediment plume discharge	14.09	m <sup>3</sup> /s
SD5	Discharge velocity	1.0	m/s
SD6	Sediment plume area	14.09	m <sup>2</sup>
SD7	Shore Location	Left	
SD8	Distance to shoreline	160	m
SD9	Water depth at the discharge location	10.0	m
SD10	Bottom Slope	9.72	%
SD11	Vertical Angle	75	°
SD12	Horizontal Angle	0	°
SD13	Discharge height above channel bottom	1.0	m
SD14	Water depth at the source of the plume	9.0	m

Prepared by School of Civil Engineering - National Tech Univ. of Athens on behalf of ASPROFOS, 2022.

**Table D-21 Sediment Classes for Site LF2**

Class	Material	%	Settling Velocity (m/s)	Concentration (mg/L)	Sediment Mass Release (kg/s)
1	Chunks	85	Instantaneous*	-	0.00
2	Sand	15	0.031	200	2.81
3	Coarse Silt	0	0.00042	25	0.35
4	Fine Silt	0	0.000026	12.5	0.18
5	Clay	0	0.00000065	12.5	0.18
Total	-	100	-	250.0	3.52

Prepared by School of Civil Engineering - National Tech Univ. of Athens on behalf of ASPROFOS, 2022.

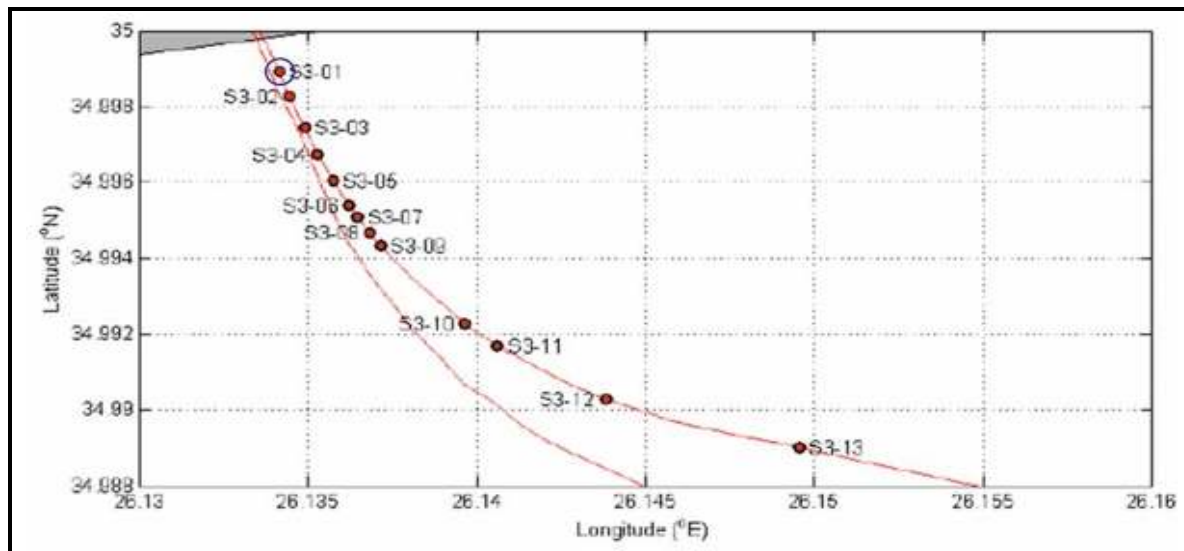


Prepared by School of Civil Engineering - National Tech Univ. of Athens on behalf of ASPROFOS, 2022.

Figure D-70 Output of the Dredger (Bray et al., 1996)










Prepared by School of Civil Engineering - National Tech Univ. of Athens on behalf of ASPROFOS, 2022.

**Figure D-72 Discharge Location; See also Appendix 1**

### 9 D.6.2. Flow Characteristics

Figure D-73 shows the trajectory of the axis of the SPM plume in the near field region that includes the first 3 flow zones: FZ1, FZ2 and FZ3. In Figure D-74 and Figure D-75 the variation of width ( $2BH$ ) and the thickness ( $BV$ ) of the plume along the bottom layer are shown, respectively.




Initially, the flow is dominated by the upward plume momentum (jet-like); the axis of the SPM plume rises to a maximum height ( $z_{max}$ ), being weakly deflected by the ambient current ( $z_{max}/L_b \ll 1$ ). Then, the SPM plume is strongly affected by gravity and rapidly falls downwards and impinges on the sea bottom ( $z$ ), with an angle that is equal to  $\Theta$ . After impingement, the flow spreads more or less radially along the bottom at an upstream intrusion length ( $L_s$ ) against the ambient flow, and laterally spreads across the ambient flow. Its half-width ( $BH$ ) is steadily increasing along the near field region downstream. The thickness ( $BV$ ) is steadily decreasing along the near field region downstream. The mixing rate is relatively small; thus, the dilution range is also small. Table D-22 summarises the above-mentioned flow characteristics. As already observed at sites LF4 and LF5, dilution increases with decreasing current velocity.

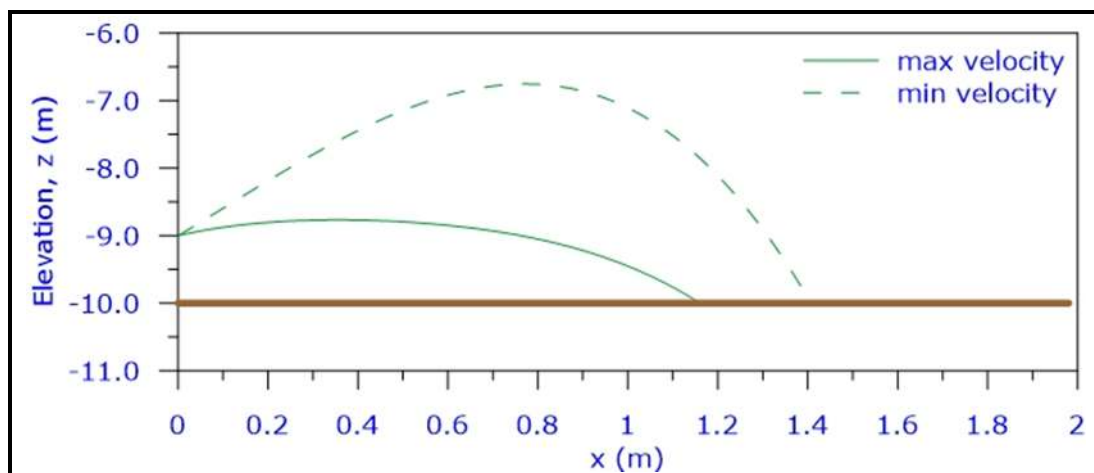
	<p style="text-align: center;"><b>EASTMED PIPELINE PROJECT</b></p> <p style="text-align: center;">EastMed Greek Section – Environmental and Social Impact Assessment</p>	<div style="display: flex; justify-content: space-around; align-items: center;">   </div> <p>DOC No: PERM-GREE-ESIA- A09_0007_0_Annex9D</p> <p>REV. : 00</p> <p>PAGE : 125 OF 178</p>

**Table D-22 Flow Characteristics for Site LF2**

Characteristics	Maximum Flow Velocity	Minimum Flow Velocity
$L_M = \frac{M_0^{3/4}}{J_0^{1/2}}$	1.91 m	1.91 m
$L_Q = \frac{Q_0}{M_0^{1/2}}$	3.75 m	3.75 m
$L_m = \frac{M_0^{1/2}}{u_a}$	4.27 m	Very large value
$L_b = \frac{J_0^{1/2}}{u_a^3}$	21.17 m	Very large value
SPM plume classification	Near-vertical class (NV)	Near-vertical class (NV)
Discharge configuration	Hydrodynamically stable	Hydrodynamically stable
$L_M/H_s$	$0.19 < 1$ Buoyancy dominated	$0.19 < 1$ Buoyancy dominated
$L_m/L_M$ Classification	$2.97 > 1$ Strong buoyancy – NV2	Strong buoyancy – NV2
FZ1- Maximum height ( $z_{max}$ )	1.23 m	3.27 m
FZ1 - Effect of ambient current ( $z_{max}/L_b$ )	Weak ( $0.06 \ll 1$ )	Very small value
FZ2	Weakly deflected plume in cross-flow	Weakly deflected plume in cross-flow
FZ2 - Impingement at sea bottom ( $z/\text{angle } \Theta$ )	-10.0 m/20.18°	-10.0 m/57.92°
FZ3 - Upstream intrusion length, $L_s$	7.90 m	-
FZ3 – End of near field region	6.69 m	174.87 m
FZ3 - BH at impingement	9.68 m	292.99 m
FZ3 - BH at the end of near field	12.41 m	348.70 m
FZ4 - BH at x=1200 m	143.24 m	611.97 m
FZ3 – BV at impingement	1.38 m	0.12 m
FZ3 – BV at the end of near field	1.38 m	0.28 m
FZ4 – BV at x=1200 m	0.18 m	0.21 m
Interaction with shoreline	No	Yes
Dilution at the end of near field	2.1	2.7
Dilution at x=1200 m	3.9	4.7

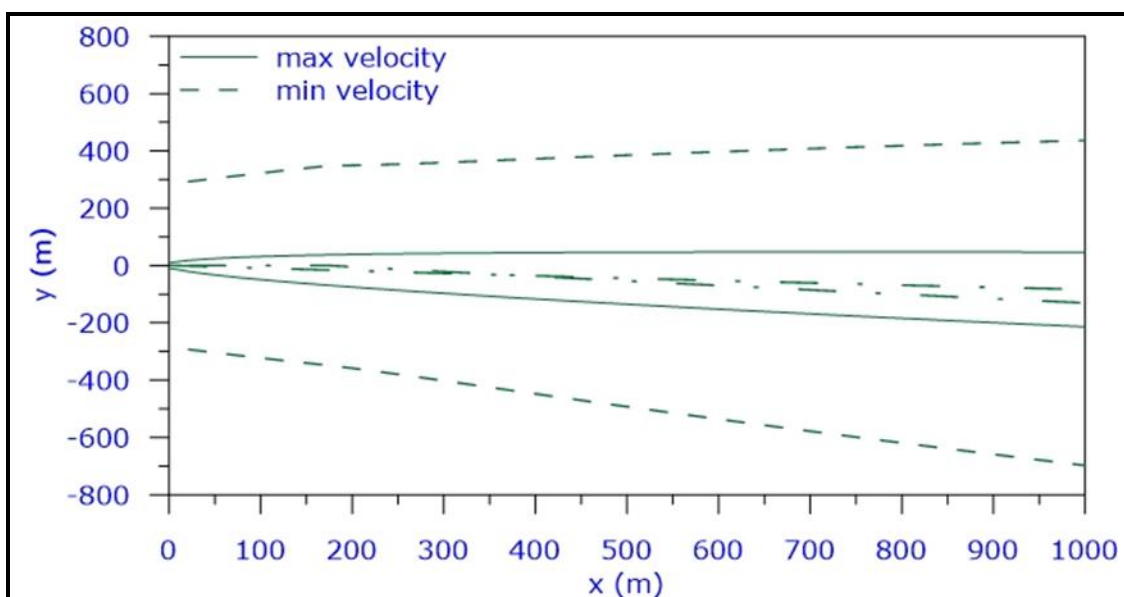
Prepared by School of Civil Engineering - National Tech Univ. of Athens on behalf of ASPROFOS, 2022.

	<p style="text-align: center;"><b>EASTMED PIPELINE PROJECT</b></p> <p style="text-align: center;">EastMed Greek Section – Environmental and Social Impact Assessment</p>	<div style="display: flex; justify-content: space-between; align-items: center;">   </div> <div style="font-size: small;"> DOC No: PERM-GREE-ESIA- A09_0007_0_Annex9D  REV. : 00  PAGE : 126 OF 178 </div>
---	--	--



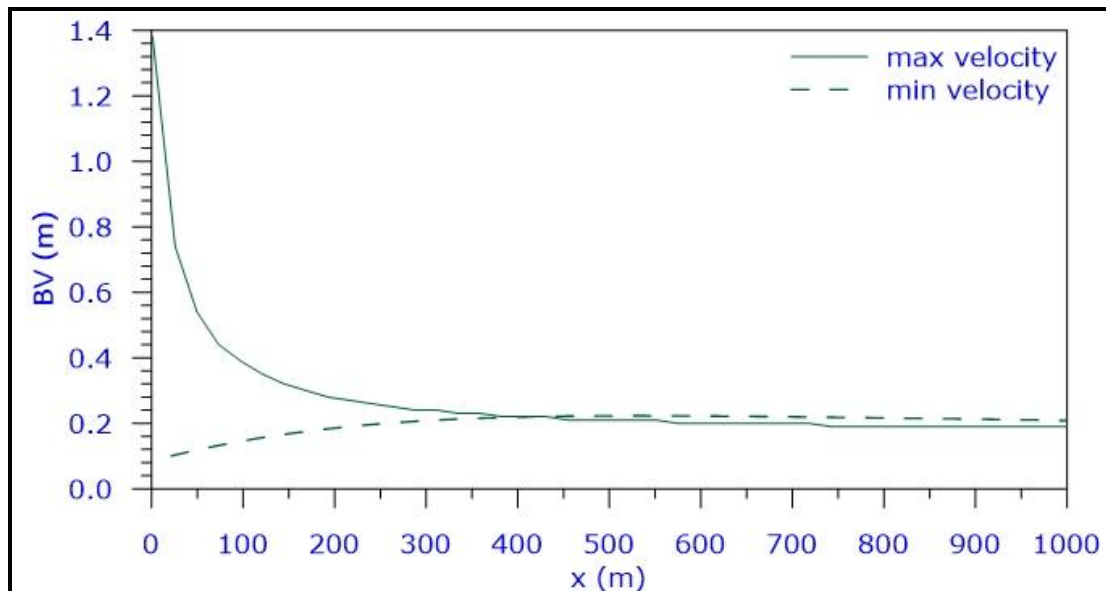
Prepared by School of Civil Engineering - National Tech Univ. of Athens on behalf of ASPROFOS, 2022.

**Figure D-73** Trajectory of the Axis of the SPM Plume in the Near Field Region



Prepared by School of Civil Engineering - National Tech Univ. of Athens on behalf of ASPROFOS, 2022.

**Figure D-74** Variation of the Width of the Plume (2BH) along the Bottom Layer



Prepared by School of Civil Engineering - National Tech Univ. of Athens on behalf of ASPROFOS, 2022.




**Figure D-75** Variation of the Thickness (BV) along the Bottom Layer

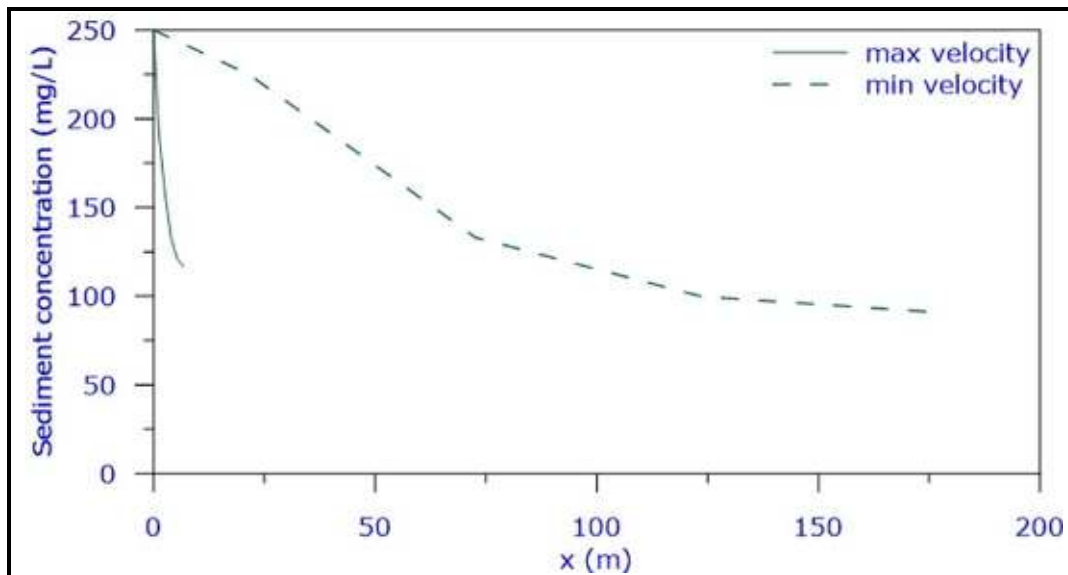
### 9 D.6.3. Sediment Concentrations

Figure D-76 and Figure D-77 show the variation of sediment concentrations (mg/L) in the near field region and along the bottom layer, respectively. In Figure D-78 the total sediment concentration contours in the bottom layer are shown for the maximum and minimum current velocity.

Figure D-76 and Figure D-77 depict that the total sediment concentration in the bottom layer is steadily decreasing; this decrease is more pronounced for the minimum flow velocity than for the maximum current velocity. More analytically:

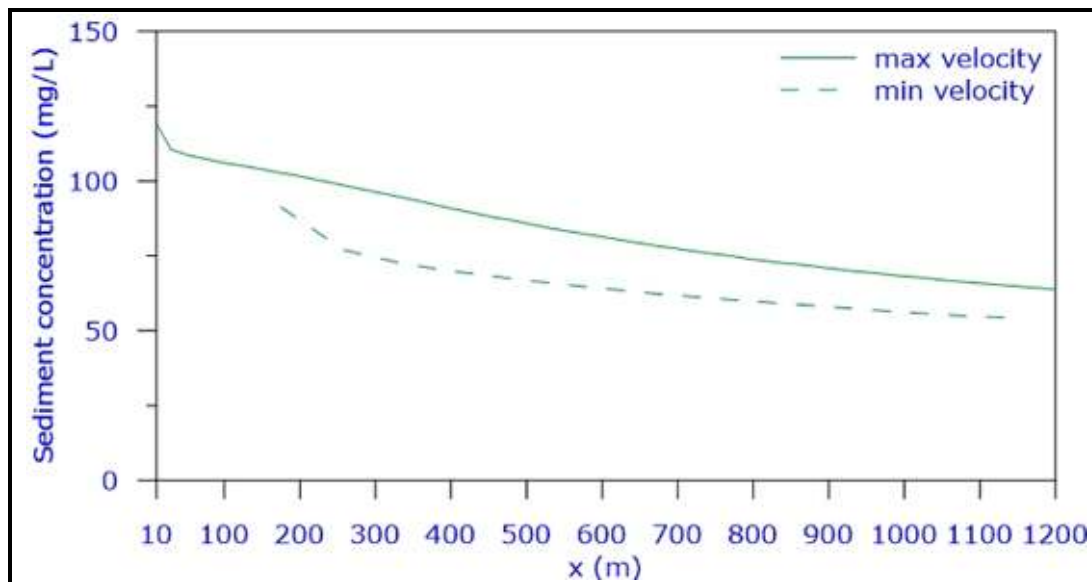
- For maximum current velocity: sediment concentration decreases from 116.8 mg/L (46.7 %) at the beginning of the bottom layer to 108.8 mg/L (43.5 %) at 50 m downstream, to 106.0 mg/L (42.4 %) at 100 m and to 63.8 mg/L (25.5 %) at 1200 m, downstream; and
- For minimum current velocity: sediment concentration decreases from 91.3 mg/L (36.5 %) at the beginning of the bottom layer to 69.8 mg/L (27.9 %) at 400 m downstream, to 64.0 mg/L (25.6 %) at 600 m and to 53.3 mg/L (21.3 %) at 1200 m downstream.

	<p align="center"><b>EASTMED PIPELINE PROJECT</b></p> <p align="center">EastMed Greek Section – Environmental and Social Impact Assessment</p>	<div>   </div> <p>DOC No: PERM-GREE-ESIA- A09_0007_0_Annex9D</p> <p>REV. : 00</p> <p>PAGE : 128 OF 178</p>
---	--	--



Prepared by School of Civil Engineering - National Tech Univ. of Athens on behalf of ASPROFOS, 2022.

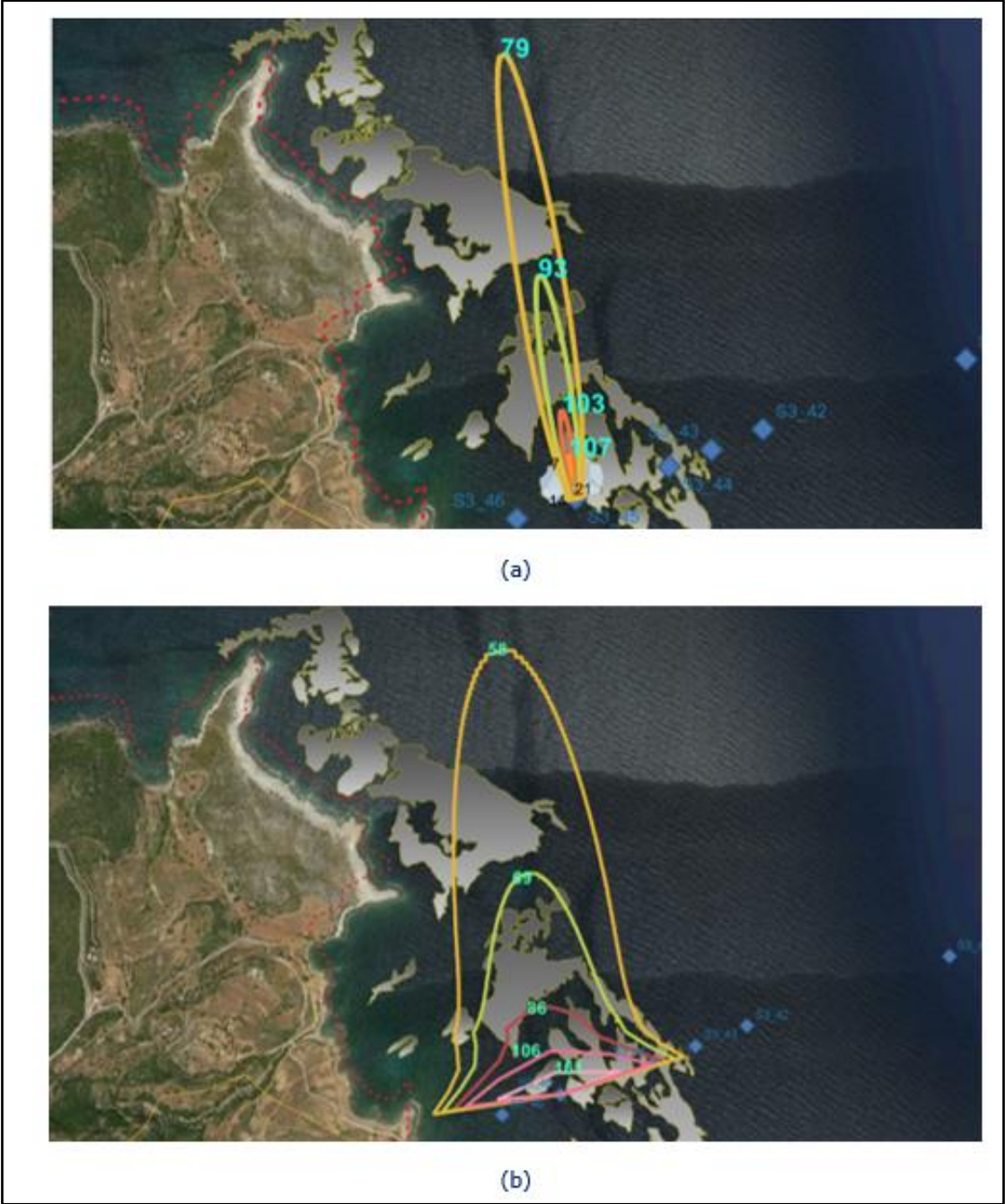
**Figure D-76 Sediment Concentrations (mg/L) in the Near Field Region**



Prepared by School of Civil Engineering - National Tech Univ. of Athens on behalf of ASPROFOS, 2022.

**Figure D-77 Sediment Concentrations (mg/L) along the Bottom Layer**





Prepared by School of Civil Engineering - National Tech Univ. of Athens on behalf of ASPROFOS,2022Figure D-78  
Total Sediment Concentration Contours in the Bottom Layer in mg/L for (a) the Maximum Current Velocity and (b) the Minimum Current Velocity (Google Maps Background)

9 D.6.4.    **Suspended Sediment Concentrations**









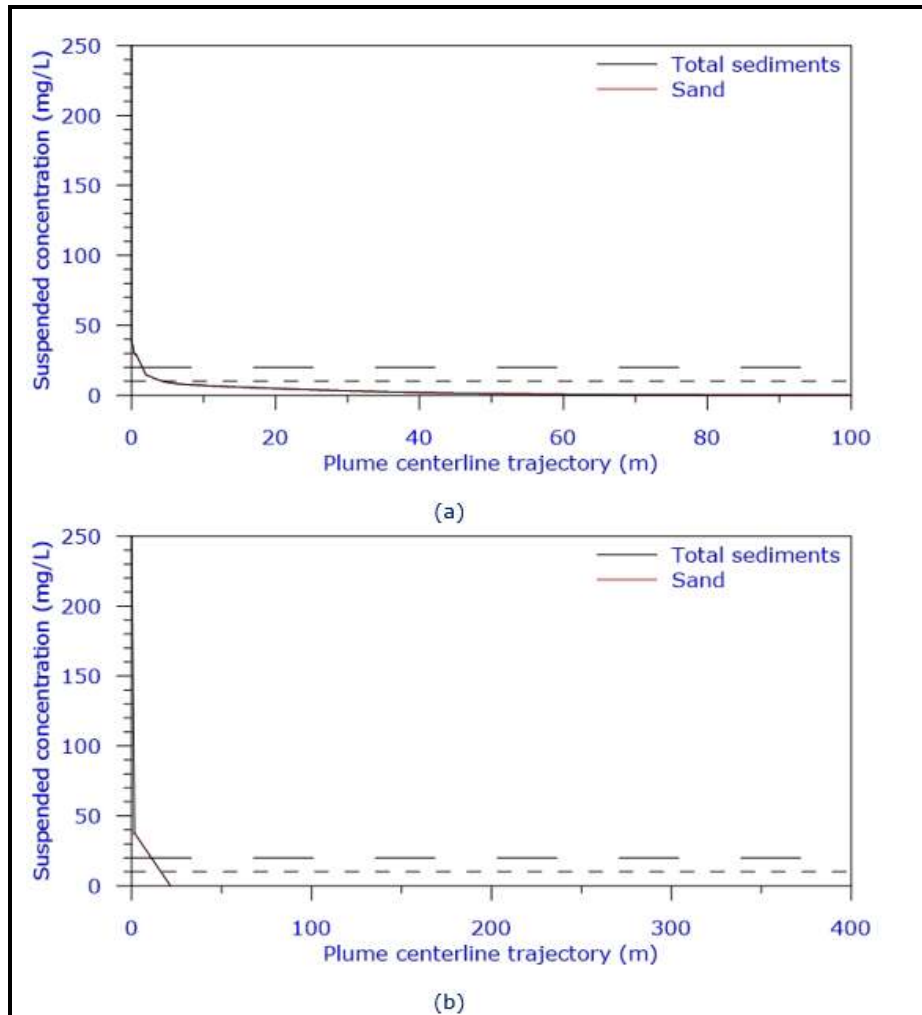
	EASTMED PIPELINE PROJECT		 
	EastMed Greek Section – Environmental and Social Impact Assessment		DOC No: PERM-GREE-ESIA-A09_0007_0_Annex9D
			REV. : 00
			PAGE : 130 OF 178

Figure D-79 shows the variation of suspended sediment concentration SSC (mg/L) in the water column, while in Figure D-80 the SSC concentration contours in the water column are shown for the maximum current velocity.

Figure D-79 and Figure D-80 depict that SSC values in the water column are steadily decreasing; this decrease is more pronounced for the minimum flow velocity than for the maximum current velocity. More analytically:




- For the maximum current velocity: at 1.1 m SSC = 15.2 mg/L (6,1 %), at 3.9 m SSC = 11.3 mg/L (2.8 %), at 6.69 m (end of near field) SSC = 8.0 mg/L (3.2 %), at 27.0 m SSC = 3.5 mg/L (1.4 %), at 41.31 m SSC = 1.8 mg/L (0.7 %) and at x= 108.6 m SSC is practically equal to zero; and
- For the minimum current velocity: at 21.3 m SSC is practically equal to zero.

	<p style="text-align: center;"><b>EASTMED PIPELINE PROJECT</b></p> <p style="text-align: center;">EastMed Greek Section – Environmental and Social Impact Assessment</p>	<div style="display: flex; justify-content: space-between; align-items: center;">   </div> <div style="font-size: small;"> DOC No: PERM-GREE-ESIA- A09_0007_0_Annex9D REV. : 00 PAGE : 131 OF 178 </div>
---	--	--



Prepared by School of Civil Engineering - National Tech Univ. of Athens on behalf of ASPROFOS, 2022.

**Figure D-79**      **Suspended Sediment Concentrations (mg/L) for (a) the Maximum Current Velocity and (b) the Minimum Current Velocity**

	<p style="text-align: center;"><b>EASTMED PIPELINE PROJECT</b></p> <p style="text-align: center;">EastMed Greek Section – Environmental and Social Impact Assessment</p>	<div style="display: flex; justify-content: space-between; align-items: center;">   </div> <div style="border-top: 1px solid black; border-bottom: 1px solid black; padding: 2px;"> DOC No: PERM-GREE-ESIA-A09_0007_0_Annex9D </div> <div style="display: flex; justify-content: space-between; border-bottom: 1px solid black; padding: 2px;"> REV. : 00 </div> <div style="display: flex; justify-content: space-between; padding: 2px;"> PAGE : 132 OF 178 </div>
---	--	--



Prepared by School of Civil Engineering - National Tech Univ. of Athens on behalf of ASPROFOS, 2022.

**Figure D-80**    **Suspended Sediment Concentrations (mg/L) for the Maximum Current Velocity (Google Maps Background)**

## 9 D.6.5.    **Sensitivity Analysis**

### 9 D.6.5.1    ***Effect of the Current Velocity***

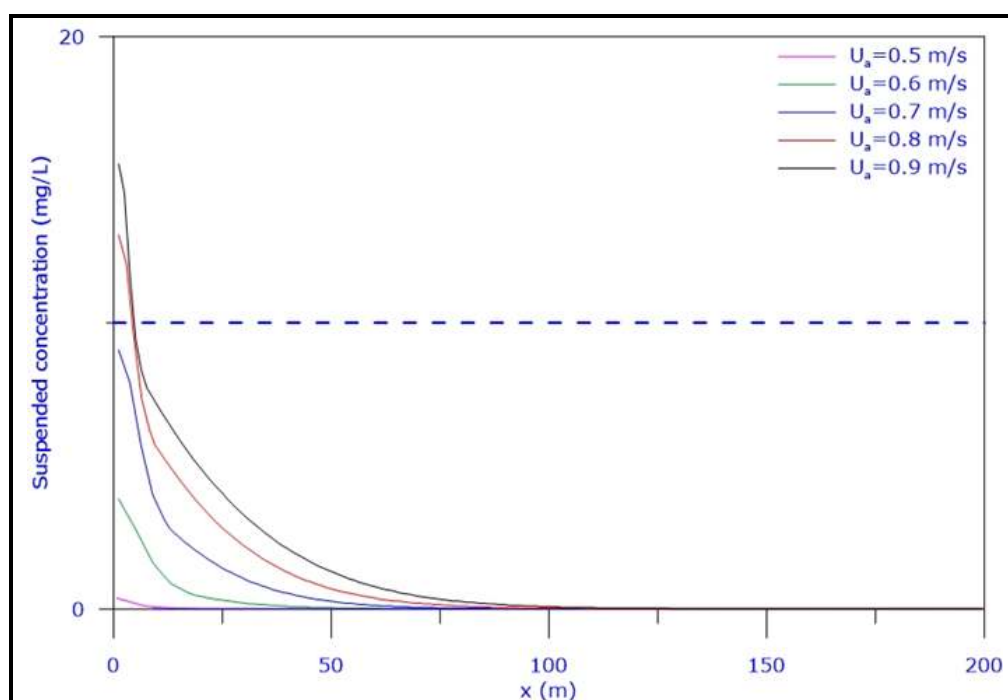
Calculations have been performed to investigate the effect of current velocity for values ranging from 0.50 to 0.90 m/s. Table D-23 summarises the effect of current velocity on the main geometric and hydrodynamic characteristics of the flow. The suspended sediment concentration (mg/L) distributions for various current velocities are presented in Figure D-81. Sediment concentration

contours (% of the initial) in the bottom layer are shown for current velocities 0.50 m/s and 0.90 m/s in Figure D-82.

**Table D-23 Basic Geometric and Hydrodynamic Characteristics for Various Current Velocities**

Current Velocity (m/s)	Length of Near Field (m)	BV (m)			BH (m)		
		At the End of Near Field	At x=400 m	At x=1000 m	At the End of Near Field	At x=400 m	At x=1000 m
0.50	26.44	0.59	0.20	0.16	52.01	151.85	232.21
0.60	16.99	0.76	0.20	0.16	33.08	126.98	195.80
0.70	11.55	0.95	0.20	0.16	22.18	105.25	164.80
0.80	8.26	1.17	0.21	0.18	15.57	88.75	141.63
0.90	6.36	1.44	0.22	0.19	11.76	79.03	127.56

Prepared by School of Civil Engineering - National Tech Univ. of Athens on behalf of ASPROFOS, 2022.

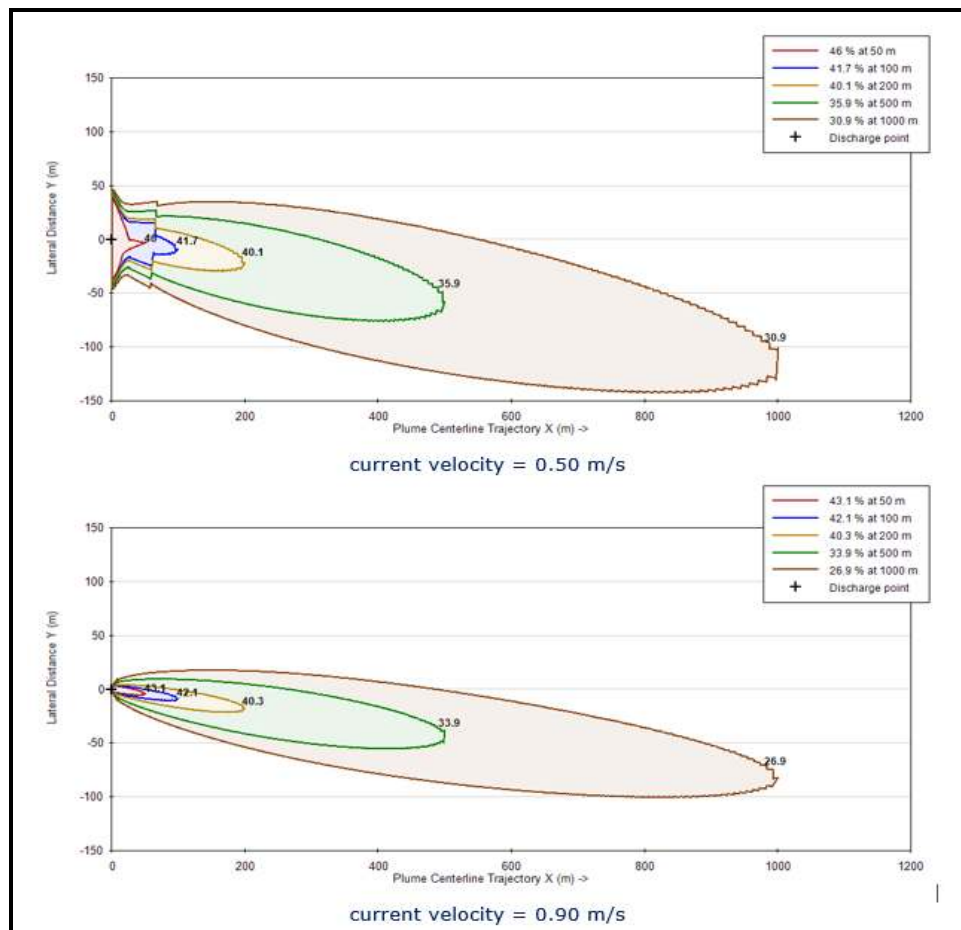


Prepared by School of Civil Engineering - National Tech Univ. of Athens on behalf of ASPROFOS, 2022.

**Figure D-81 Total Suspended Sediment Concentrations (mg/L) for Various Current Velocities**

From Table D-23, Figure D-81 and Figure D-82 and the calculations, when the current velocity increases from 0.50 m/s to 0.90 m/s, the following are observed:

- The length of the near field region decreases from 26.44 m to 6.36 m;
- The thickness of the bottom layer (BV) at the end of the near field increases from 0.59 m to 1.44 m; far from the dredging location, it approaches values that range from 0.16 m to 0.19 m;
- The half-width of the bottom layer (BH) at the end of the near field decreases from 52.01 m to 11.76 m; far from the dredging location, it approaches values that range from 232.21 m to 127.56 m; and
- The suspended solids concentrations in the water column decrease; thus, the decrease of the current velocity results in more favourable conditions.



Prepared by School of Civil Engineering - National Tech Univ. of Athens on behalf of ASPROFOS, 2022.

**Figure D-82 Sediment Concentration Contours (% of the Initial) in the Bottom Layer for Current Velocities 0.50 m/s and 0.90 m/s**

### 9 D.6.5.2 Effect of the Composition of Solids

Calculations have been performed to investigate the effect of sediment compositions by increasing the percentage of sand from 15% to 30 %, as shown in Table D-24. The calculated suspended sediment concentrations (mg/L) are shown in Table D-25.

From Table D-25 and Table D-26 the calculations show that, when the percentage of sand increases from 15% to 30 %, then:

- The suspended sediment concentration increases at x=50.0 m from 1.2 mg/L to 2.4 mg/L and at x=100.0 m from 0.05 mg/L to 0.13 mg/L; and
- The area covered by relatively high suspended sediment concentrations increases.

**Table D-24 Examined Sediment Compositions**

Class	Material	C1	C2	C3	C4
1	Chunks	85 %	80 %	75 %	70 %
2	Sand	15 %	20 %	25 %	30 %
3	Coarse Silt	-	-	-	-
4	Fine Silt	-	-	-	-
5	Clay	-	-	-	-
Total	-	100 %	100 %	100 %	100 %

Prepared by School of Civil Engineering - National Tech Univ. of Athens on behalf of ASPROFOS, 2022.

**Table D-25 Suspended Sediment Concentrations (mg/L) for Various Sediment Compositions**

x(m)	C1	C2	C3	C4
1.2	15.2	20.2	25.2	30.3
3.9	11.3	15.0	18.8	22.5
5.3	9.1	12.1	15.1	18.2
6.7	8.0	10.7	13.3	16.0
7.9	7.4	9.9	12.3	14.8
12.7`	6.2	8.3	10.4	12.4
13.9	6.0	7.9	9.9	11.9
16.3	5.4	7.2	9.0	10.8
24.6	3.9	5.2	6.5	7.7



x(m)	C1	C2	C3	C4
27.0	3.5	4.7	5.8	7.0
35.3	2.4	3.2	4.0	4.8
40.1	1.9	2.6	3.2	3.9
46.1	1.4	1.9	2.4	2.9
52.0	1.1	1.4	1.8	2.1
54.4	0.9	1.3	1.6	1.9
59.2	0.7	1.0	1.2	1.5
60.4	0.7	0.9	1.1	1.4
63.9	0.6	0.8	0.9	1.1
67.5	0.5	0.6	0.8	0.9
80.6	0.2	0.3	0.4	0.4
90.2	0.1	0.2	0.2	0.2
108.1	0.0	0.1	0.1	0.1
111.7	0.0	0.0	0.1	0.1
115.2	0.0	0.0	0.0	0.1
117.6	0.0	0.0	0.0	0.0

Prepared by School of Civil Engineering - National Tech Univ. of Athens on behalf of ASPROFOS, 2022.

**Table D-26**      **Suspended Sediment Concentrations (mg/L) at x=50 m and x=100 m**




x(m)	C1	C2	C3	C4
50.0	1.2	1.6	2.0	2.4
100.0	0.1	0.1	0.1	0.1

Prepared by School of Civil Engineering - National Tech Univ. of Athens on behalf of ASPROFOS, 2022.

## 9 D.7.      **CALCULATIONS AT SITE LF3 AND DISCUSSION**

### 9 D.7.1.      **Input Data**






	<b>EASTMED PIPELINE PROJECT</b>		 
			DOC No: PERM-GREE-ESIA-A09_0007_0_Annex9D
	EastMed Greek Section – Environmental and Social Impact Assessment		REV. : 00
			PAGE : 137 OF 178

The input data and sediment classes for site LF3 are shown in Table D-27 and Table D-28, respectively. In Figure D-83, Figure D-84 and Figure D-85 output of the dredger (Bray et al., 1996), the schematic diagram of the trench and discharge location are shown, respectively.

**Table D-27 Input Data for Site LF3**

	Characteristic	Value	Units
DR1	Type	Bucket	-
DR2	Capacity	5	m <sup>3</sup>
DR3	Cycle time	60	s
DR4	Output	220	m <sup>3</sup> /h
	Dry solids density of the dredged material	1,800	kg/m <sup>3</sup>
	Dry bulk density	1,440	kg/m <sup>3</sup>
	Sediment release rate	4.0	%
	Re-suspension factor	3.2	%
	Total excavation volume	50,000	m <sup>3</sup>
	Total required hours of dredging	227	h
	Mass of dredged material	316,800	kg/h
	Mass of re-suspended solids	12,672	kg/h
SE1	Sediment density	1800	kg/m <sup>3</sup>
SE2	Sediment classes	See Table D-28	
AM1	Ambient temperature	24.83	°C
AM2	Ambient salinity	38.65	psu
AM3	Ambient sediment concentration	0.0	mg/L
AM4	Ambient density	1,026.16	kg/m <sup>3</sup>
AM5	Flow velocity near the bottom	0.66	m/s
AM6	Flow velocity at the surface	0.95	m/s
SD1	Rate of sediment mass release	3.52	kg/s
SD2	Sediment plume concentration	250	mg/L
SD2	Sediment plume density	1,133.47	kg/m <sup>3</sup>
SD4	Sediment plume discharge	14.09	m <sup>3</sup> /s
SD5	Discharge velocity	1.0	m/s
SD6	Sediment plume area	14.09	m <sup>2</sup>
SD7	Shore Location	Left	
SD8	Distance to shoreline	360	m

	<b>EASTMED PIPELINE PROJECT</b>		 
	EastMed Greek Section – Environmental and Social Impact Assessment		DOC No: PERM-GREE-ESIA-A09_0007_0_Annex9D
			REV. : 00
			PAGE : 138 OF 178

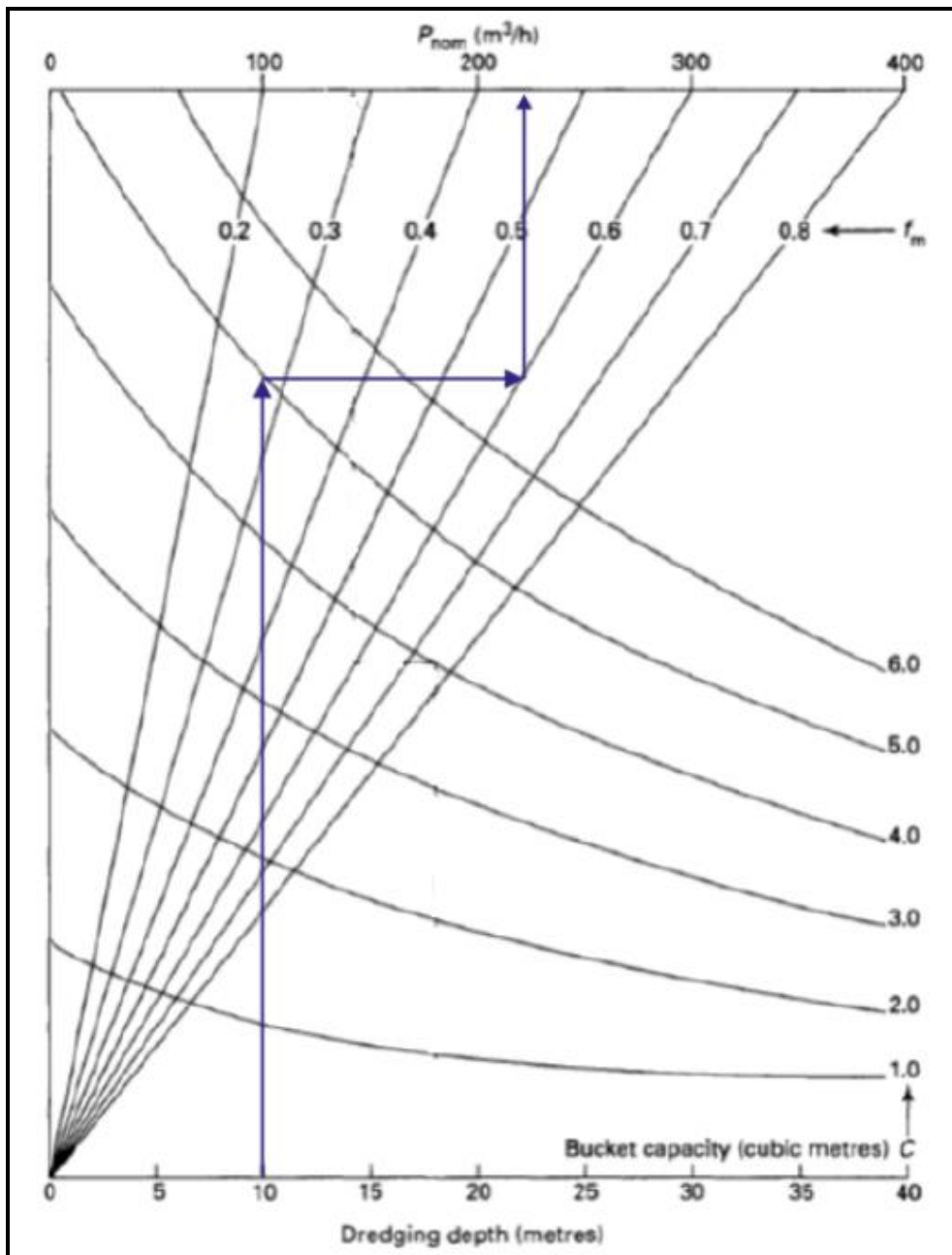
	Characteristic	Value	Units
SD9	Water depth at the discharge location	20.3	m
SD10	Bottom Slope	6.62	%
SD11	Vertical Angle	75	°
SD12	Horizontal Angle	0	°
SD13	Discharge height above channel bottom	1.0	m
SD14	Water depth at the source of the plume	19.3	m

Prepared by School of Civil Engineering - National Tech Univ. of Athens on behalf of ASPROFOS, 2022.

**Table D-28 Sediment Classes for Site LF3**

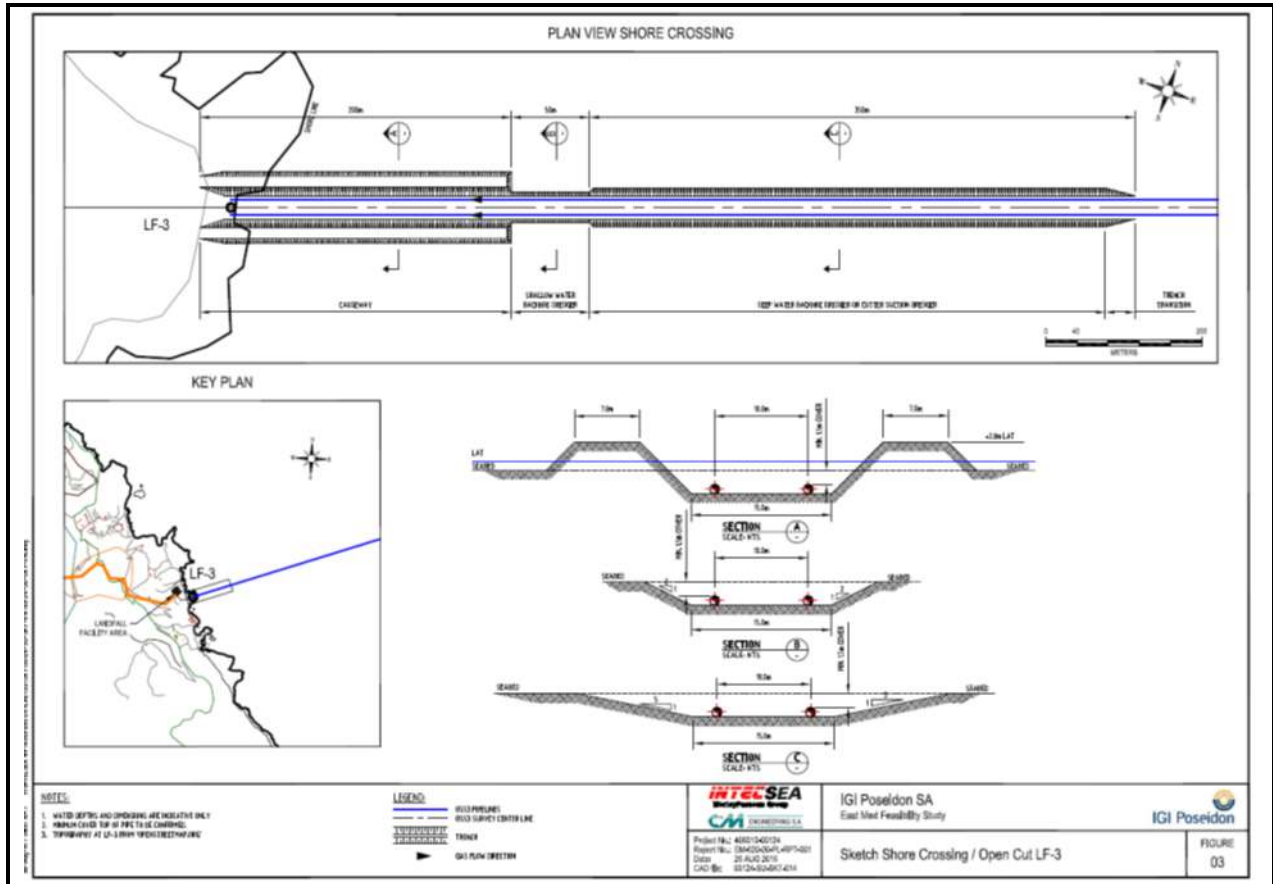
Class	Material	%	Settling Velocity (m/s)	Concentration (mg/L)	Sediment Mass Release (kg/s)
1	Chunks	20	Instantaneous*	50	0.70
2	Sand	80	0.031	200	2.82
3	Coarse Silt	0	0.00042	0	0.00
4	Fine Silt	0	0.000026	0	0.00
5	Clay	0	0.00000065	0	0.00
Total	-	100	-	250	3.52

Prepared by School of Civil Engineering - National Tech Univ. of Athens on behalf of ASPROFOS, 2022.



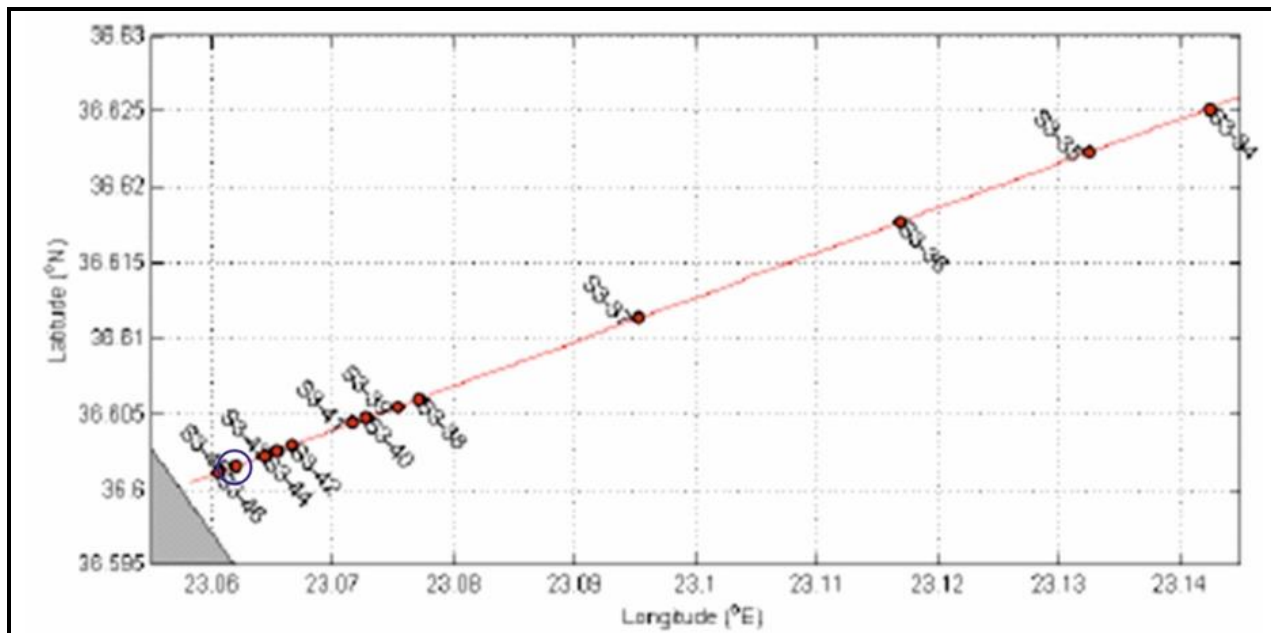
Prepared by School of Civil Engineering - National Tech Univ. of Athens on behalf of ASPROFOS, 2022.

Figure D-83 Output of the Dredger (Bray et al., 1996)



Prepared by School of Civil Engineering - National Tech Univ. of Athens on behalf of ASPROFOS, 2022.

**Figure D-84 Schematic Diagram of Trench at LF3**






Prepared by School of Civil Engineering - National Tech Univ. of Athens on behalf of ASPROFOS, 2022.

**Figure D-85 Discharge Location; See also Appendix 1**

### 9 D.7.2. Flow Characteristics

Figure D-86 shows the trajectory of the axis of the SPM plume in the near field region that includes the first 3 flow zones: FZ1, FZ2 and FZ3. In Figure D-87 and Figure D-88 the variation of width ( $2BH$ ) and the thickness ( $BV$ ) of the plume along the bottom layer are shown, respectively.

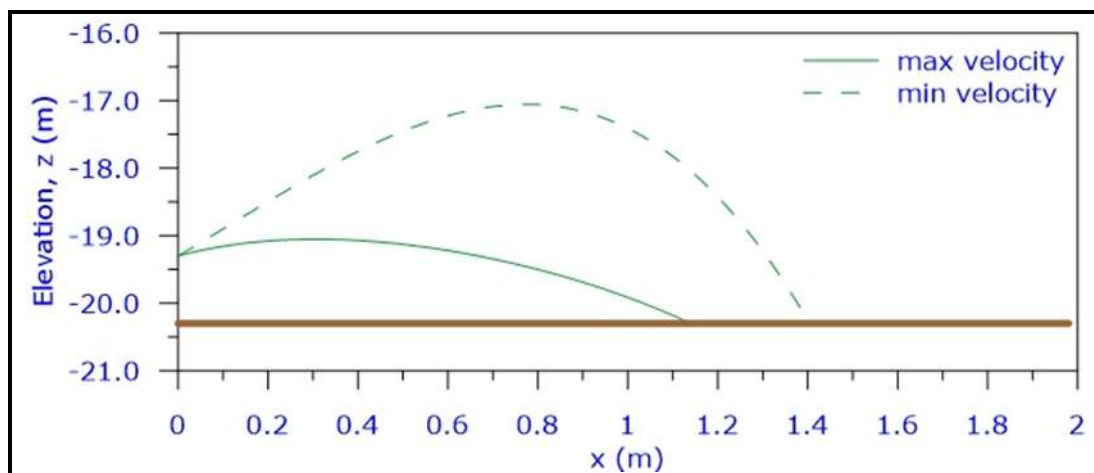
Initially, the flow is dominated by the upward plume momentum (jet-like); the axis of the SPM plume rises to a maximum height ( $z_{max}$ ), being weakly deflected by the ambient current ( $z_{max}/L_b \ll 1$ ). Then, the SPM plume is strongly affected by gravity and rapidly falls downwards and impinges on the sea bottom ( $z$ ), with an angle that is equal to  $\Theta$ . After impingement, the flow spreads more or less radially along the bottom, at an upstream intrusion length ( $L_s$ ) against the ambient flow, and spreads laterally across the ambient flow. Its half-width ( $BH$ ) is steadily increasing along the near field region, downstream. The thickness ( $BV$ ) is steadily decreasing along the near field region, downstream. The mixing rate is relatively small; thus, the dilution range is also small. Table D-29 summarises the above-mentioned flow characteristics. As already observed at sites LF4, LF5 and LF2, dilution increases with decreasing current velocity.

	<p style="text-align: center;"><b>EASTMED PIPELINE PROJECT</b></p> <p style="text-align: center;">EastMed Greek Section – Environmental and Social Impact Assessment</p>	<div style="display: flex; justify-content: space-around; align-items: center;">   </div> <p>DOC No: PERM-GREE-ESIA- A09_0007_0_Annex9D</p> <p>REV. : 00</p> <p>PAGE : 142 OF 178</p>
---	--	---

**Table D-29      Flow Characteristics for Site LF3**

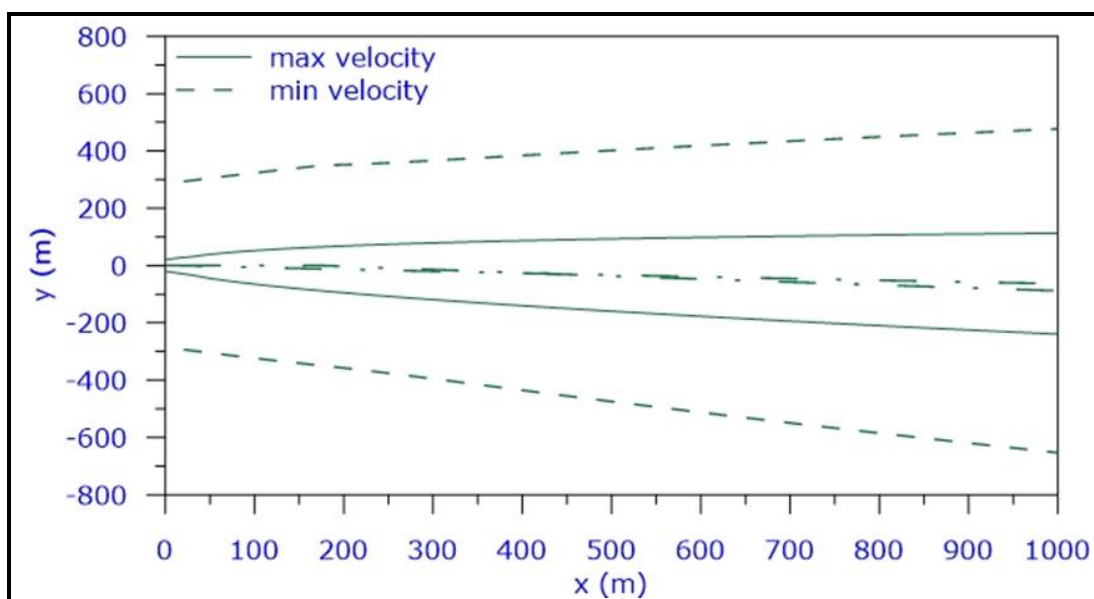
Characteristics	Maximum Flow Velocity	Minimum Flow Velocity
$L_M = \frac{M_0^{3/4}}{J_0^{1/2}}$	1.91 m	1.91 m
$L_Q = \frac{Q_0}{M_0^{1/2}}$	3.75 m	3.75 m
$L_m = \frac{M_0^{1/2}}{u_a}$	5.69 m	Very large value
$L_b = \frac{J_0^{1/2}}{u_a^3}$	50.26 m	Very large value
SPM plume classification	Near-vertical class (NV)	Near-vertical class (NV)
Discharge configuration	Hydrodynamically stable	Hydrodynamically stable
$L_M/H_s$	$0.09 < 1$ Buoyancy dominated	$0.09 < 1$ Buoyancy dominated
$L_m/L_M$ Classification	$2.97 > 1$ Strong buoyancy – NV2	Strong buoyancy – NV2
FZ1- Maximum height ( $z_{max}$ )	1.25 m	3.27 m
FZ1 - Effect of ambient current ( $z_{max}/L_b$ )	Weak ( $0.02 \ll 1$ )	Very small value
FZ2	Weakly deflected plume in cross-flow	Weakly deflected plume in cross-flow
FZ2 - Impingement at sea bottom ( $z/\text{angle } \Theta$ )	-20.3 m/32.49°	-20.3/57.76°
FZ3 - Upstream intrusion length, $L_s$	18.42 m	-
FZ3 – End of near field region	13.46 m	175.29 m
FZ3 - BH at impingement	20.27 m	293.69 m
FZ3 - BH at the end of near field	26.00 m	349.53 m
FZ4 - BH at x=1200 m	192.50 m	609.92 m
FZ3 – BV at impingement	0.90 m	0.12 m
FZ3 – BV at the end of near field	0.87 m	0.28 m
FZ4 – BV at x=1200 m	0.15 m	0.21 m
Interaction with shoreline	No	Yes
Dilution at the end of near field	2.1	2.7
Dilution at x=1200 m	3.3	4.7

Prepared by School of Civil Engineering - National Tech Univ. of Athens on behalf of ASPROFOS, 2022.



Prepared by School of Civil Engineering - National Tech Univ. of Athens on behalf of ASPROFOS, 2022.

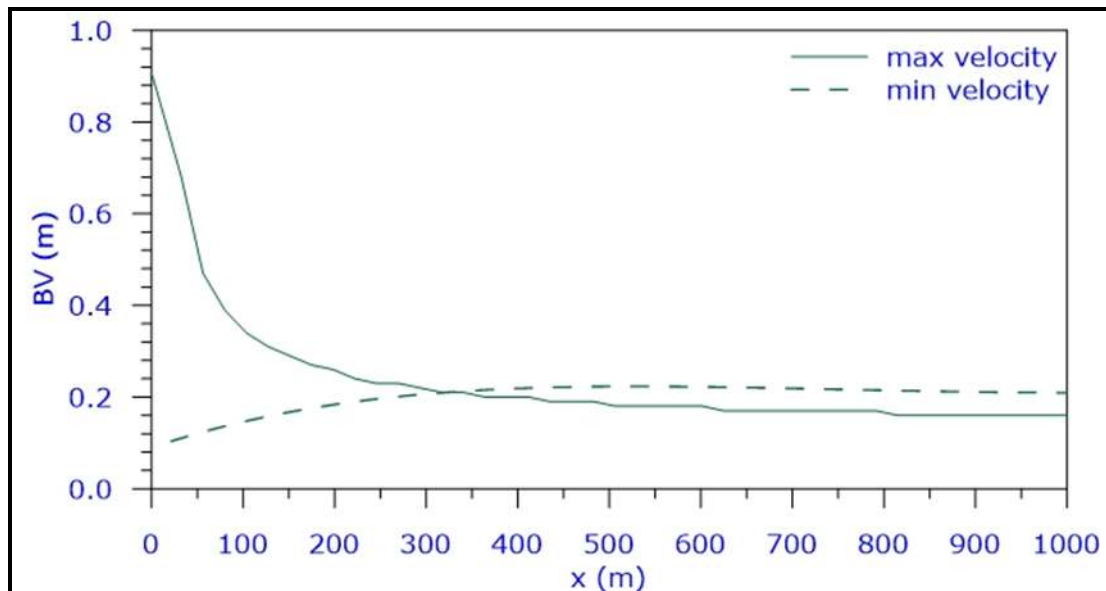
**Figure D-86** Trajectory of the Axis of the SPM Plume in the Near Field Region



Prepared by School of Civil Engineering - National Tech Univ. of Athens on behalf of ASPROFOS, 2022.

**Figure D-87** Variation of the Width of the Plume (2BH) along the Bottom Layer





Prepared by School of Civil Engineering - National Tech Univ. of Athens on behalf of ASPROFOS, 2022.




**Figure D-88** Variation of the Thickness (BV) along the Bottom Layer

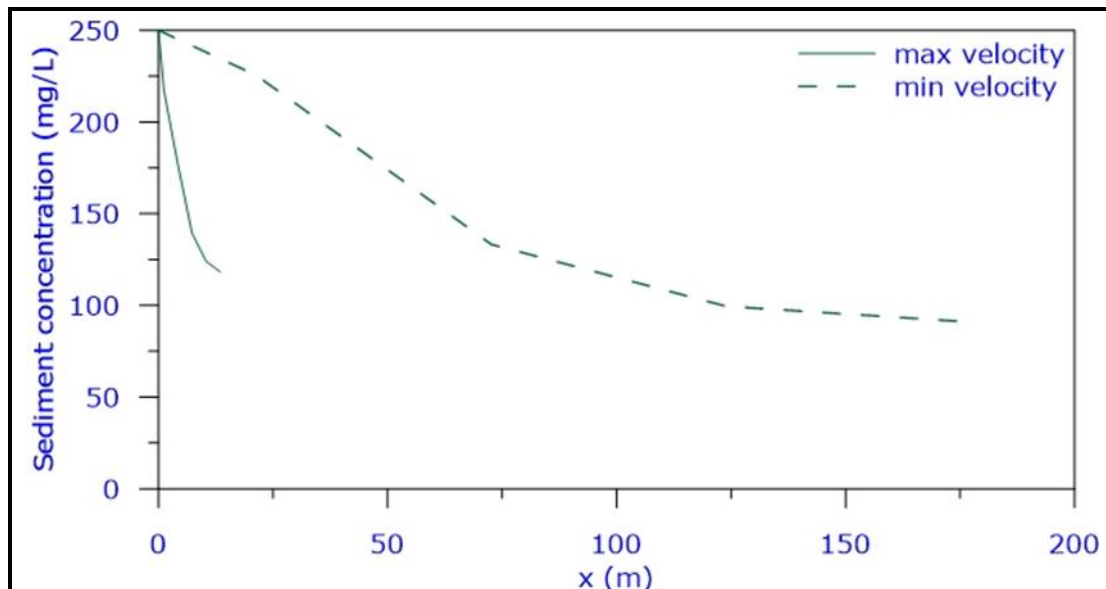
### 9 D.7.3. Sediment Concentrations

Figure D-89 and Figure D-90 show the variation of sediment concentrations (mg/L) in the near field region and along the bottom layer, respectively. In Figure D-91 the total sediment concentration contours in the bottom layer are shown for the maximum and minimum current velocity.

Figure D-89 and Figure D-90 depict that the total sediment concentration in the bottom layer is steadily decreasing; this decrease is more pronounced for the minimum flow velocity than for the maximum current velocity. More analytically:

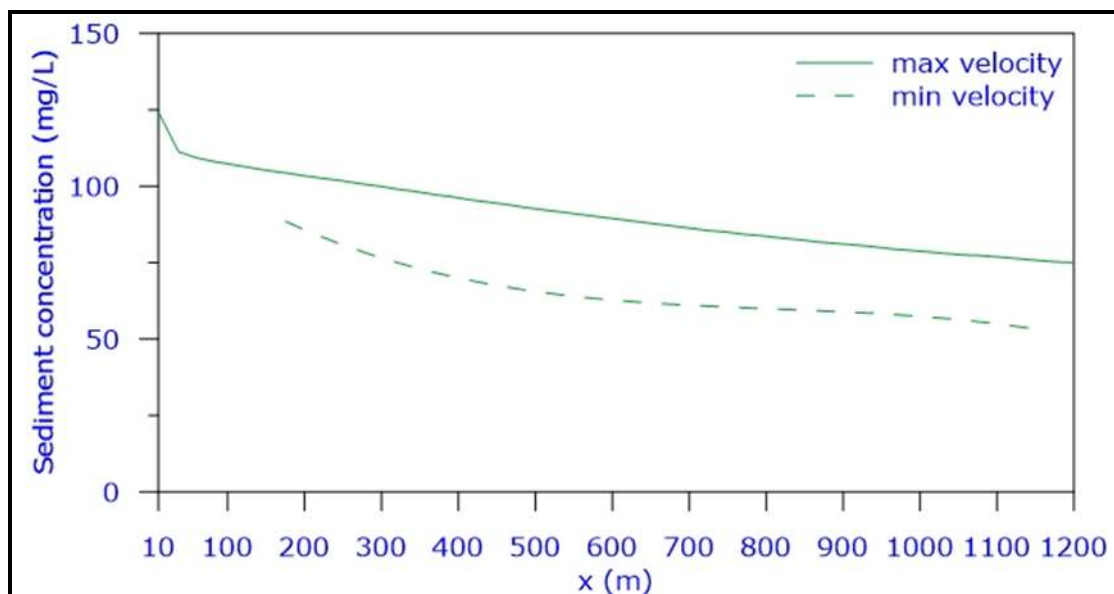
- For the maximum current velocity: sediment concentrations decrease from 118.3 mg/L (47.3 %) at the beginning of the bottom layer, to 110.0 mg/L (44.0 %) at 50 m downstream, to 107.3 mg/L (42.9 %) at 100 m and to 75.0 mg/L (30.0 %) at 1200 m, downstream; and
- For the minimum current velocity: sediment concentrations decrease from 91.3 mg/L (36.5 %) at the beginning of the bottom layer, to 69.8 mg/L (27.9 %) at 400 m downstream, to 64.0 mg/L (25.6 %) at 600 m and to 53.50 mg/L (21.4 %) at 1200 m, downstream.

	<p align="center"><b>EASTMED PIPELINE PROJECT</b></p> <p align="center">EastMed Greek Section – Environmental and Social Impact Assessment</p>	<div>   </div> <p>DOC No: PERM-GREE-ESIA- A09_0007_0_Annex9D</p> <p>REV. : 00</p> <p>PAGE : 145 OF 178</p>
---	--	--



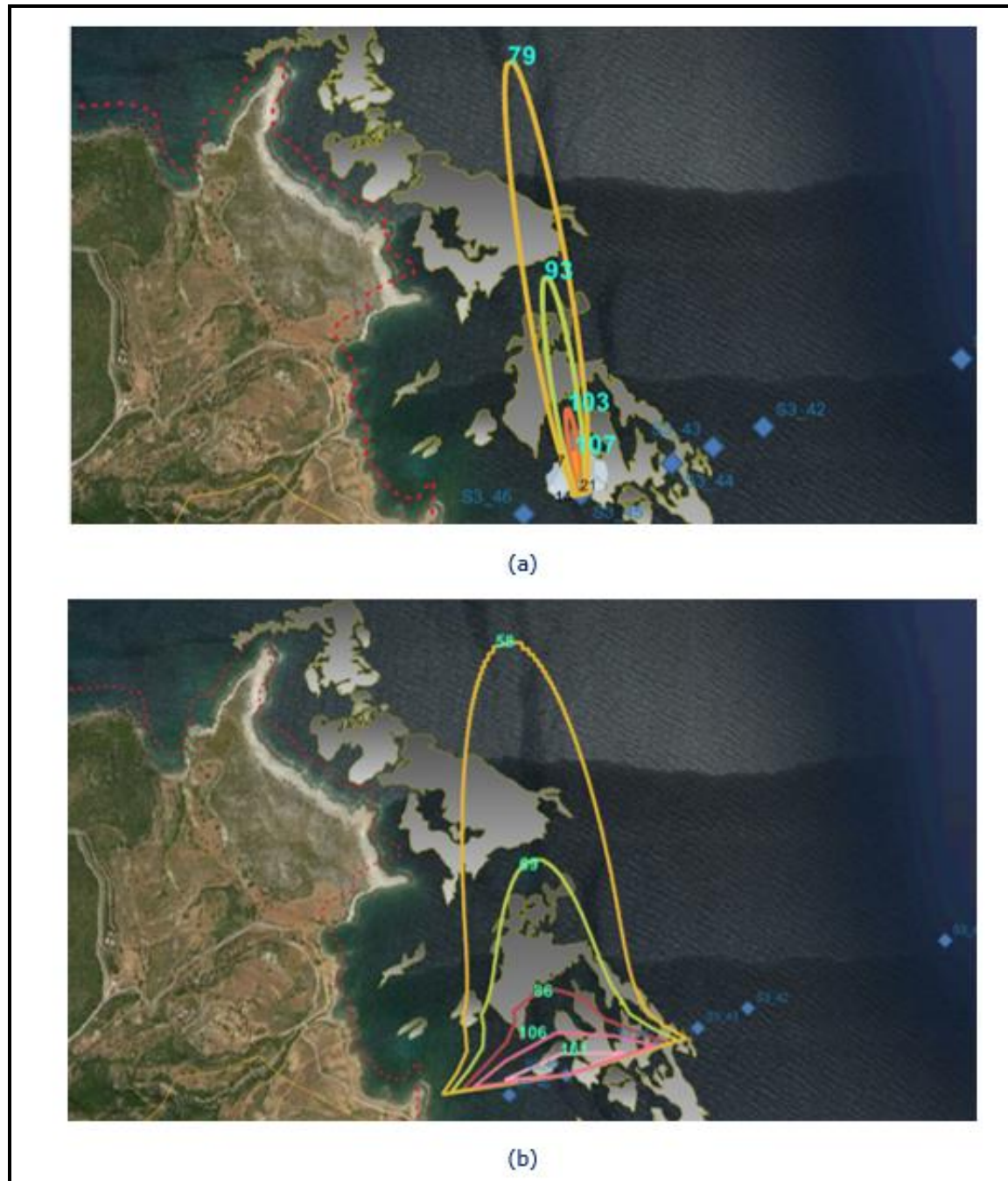
Prepared by School of Civil Engineering - National Tech Univ. of Athens on behalf of ASPROFOS, 2022.

**Figure D-89 Sediment Concentrations (mg/L) in the Near Field Region**






Prepared by School of Civil Engineering - National Tech Univ. of Athens on behalf of ASPROFOS, 2022.

**Figure D-90 Sediment Concentrations (mg/L) along the Bottom Layer**



Prepared by School of Civil Engineering - National Tech Univ. of Athens on behalf of ASPROFOS, 2022.

**Figure D-91** Total Sediment Concentration Contours in the Bottom Layer in mg/L for (a) the Maximum Current Velocity and (b) the Minimum Current Velocity (Google Maps Background)




	EASTMED PIPELINE PROJECT		 	
	EastMed Greek Section – Environmental and Social Impact Assessment		DOC No: PERM-GREE-ESIA-A09_0007_0_Annex9D	
			REV. :	00
			PAGE :	147 OF 178

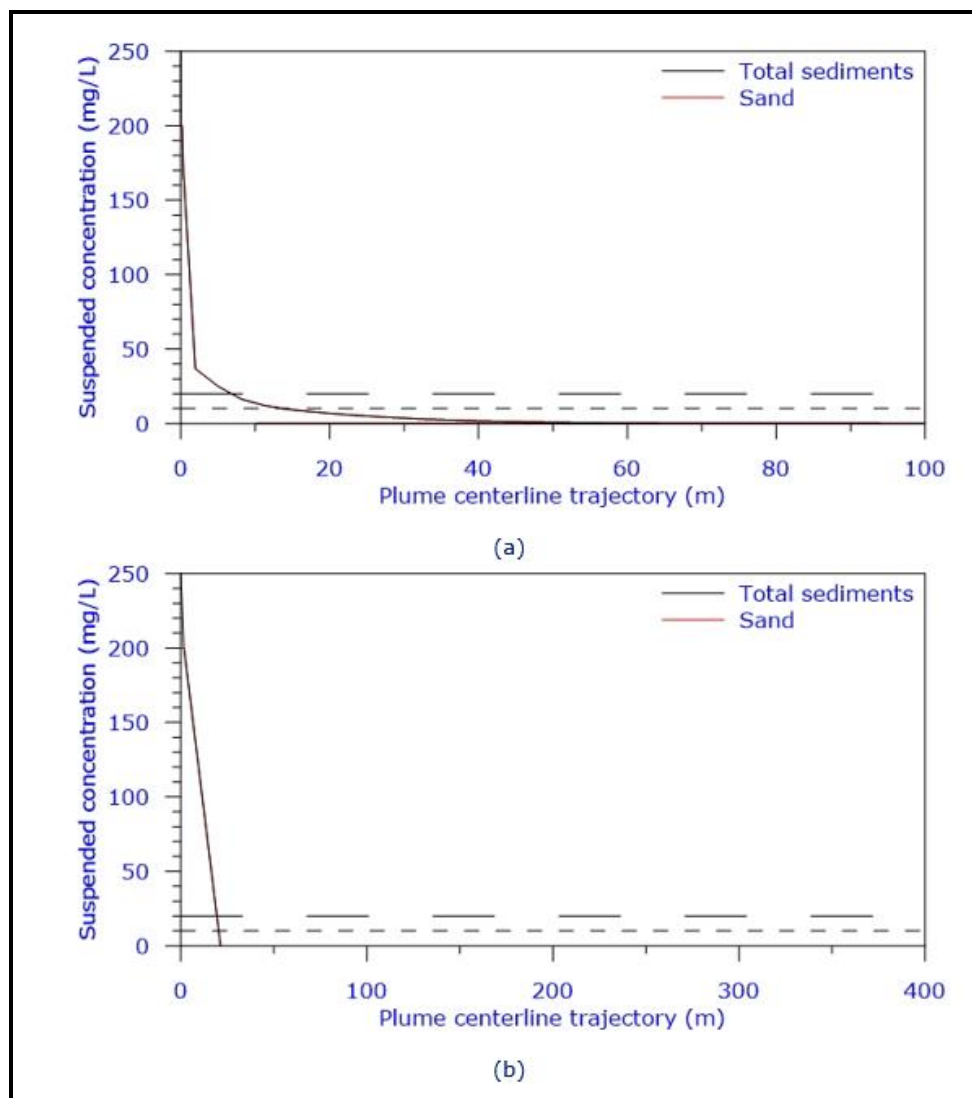
#### 9 D.7.4. Suspended Sediment Concentrations

Figure D-92 shows the variation of suspended sediment concentration, SSC (mg/L) in the water column, while in Figure D-93 the SSC concentration contours in the water column are shown for the maximum current velocity.

Figure D-92 and Figure D-93 depict that SSC values in the water column are steadily decreasing; this decrease is more pronounced for the minimum flow velocity than for the maximum current velocity. More analytically:

- For the maximum current velocity: at 1.1 m SSC = 37.1 mg/L (14.8 %), at 7.3 m SSC = 20.8 mg/L (8.3 %), at 13.46 m (end of near field) SSC = 10.1 mg/L (4.0 %), at 28.9 m SSC = 3.7 mg/L (1.5 %), at 47.9 m SSC = 0.9 mg/L (0.4 %) and at x= 84.6 m SSC is practically equal to zero; and
- For the minimum current velocity: at 21.3 m SSC is practically equal to zero.

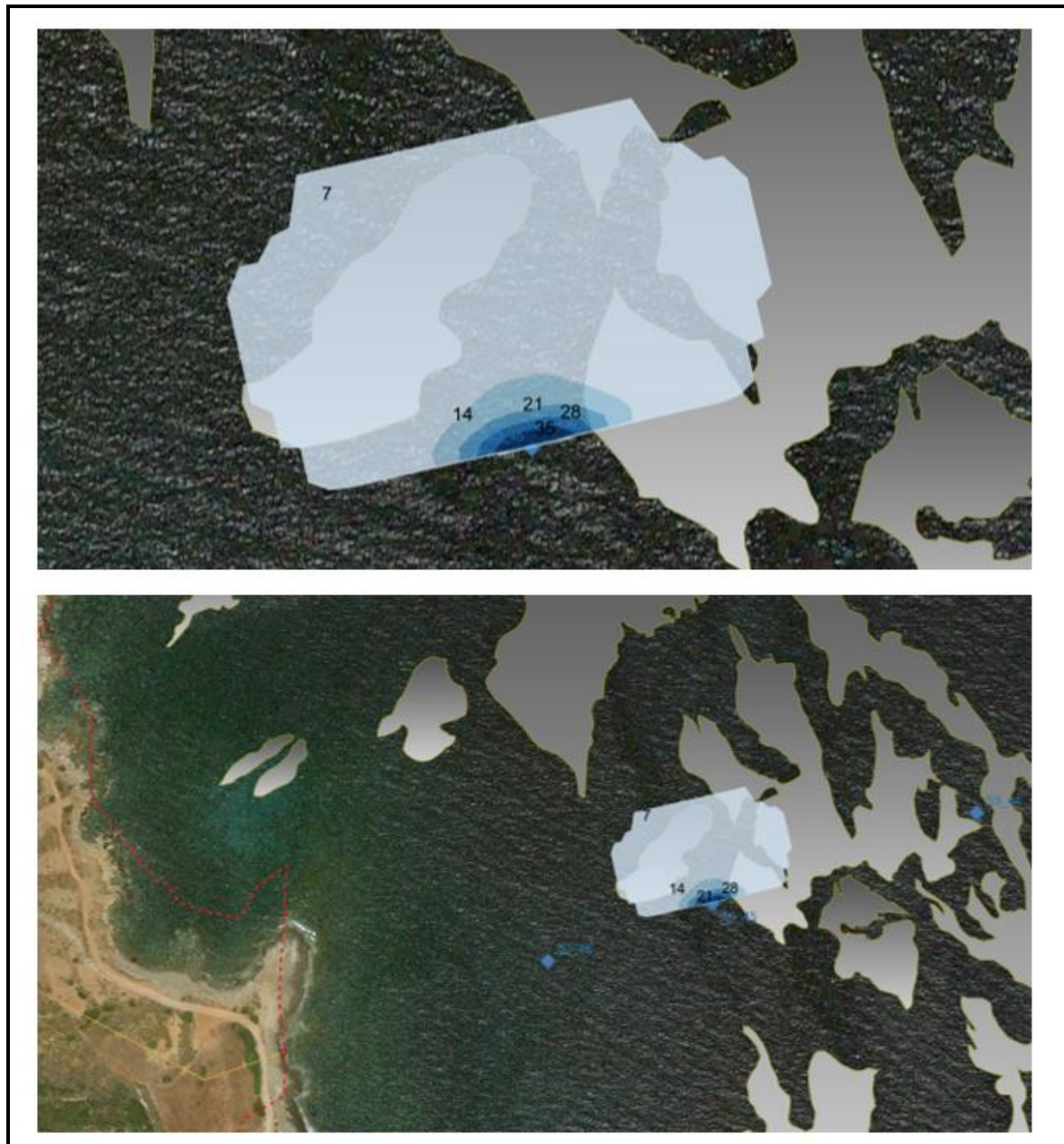
	<p style="text-align: center;"><b>EASTMED PIPELINE PROJECT</b></p> <p style="text-align: center;">EastMed Greek Section – Environmental and Social Impact Assessment</p>	<div style="display: flex; justify-content: space-between; align-items: center;">   </div> <div style="font-size: small;"> DOC No: PERM-GREE-ESIA- A09_0007_0_Annex9D  REV. : 00  PAGE : 148 OF 178 </div>
---	--	--



Prepared by School of Civil Engineering - National Tech Univ. of Athens on behalf of ASPROFOS, 2022.




**Figure D-92**    **Suspended Sediment Concentrations (mg/L) for (a) the Maximum Current Velocity and (b) the Minimum Current Velocity**





Prepared by School of Civil Engineering - National Tech Univ. of Athens on behalf of ASPROFOS, 2022.

**Figure D-93**     **Suspended Sediment Concentrations (mg/L) for the Maximum Current Velocity (Google Maps Background)**

	EASTMED PIPELINE PROJECT		 	
	EastMed Greek Section – Environmental and Social Impact Assessment		DOC No: PERM-GREE-ESIA-A09_0007_0_Annex9D	
			REV. :	00
			PAGE :	150 OF 178

## 9 D.7.5. Sensitivity Analysis

### 9 D.7.5.1 Effect of the Current Velocity

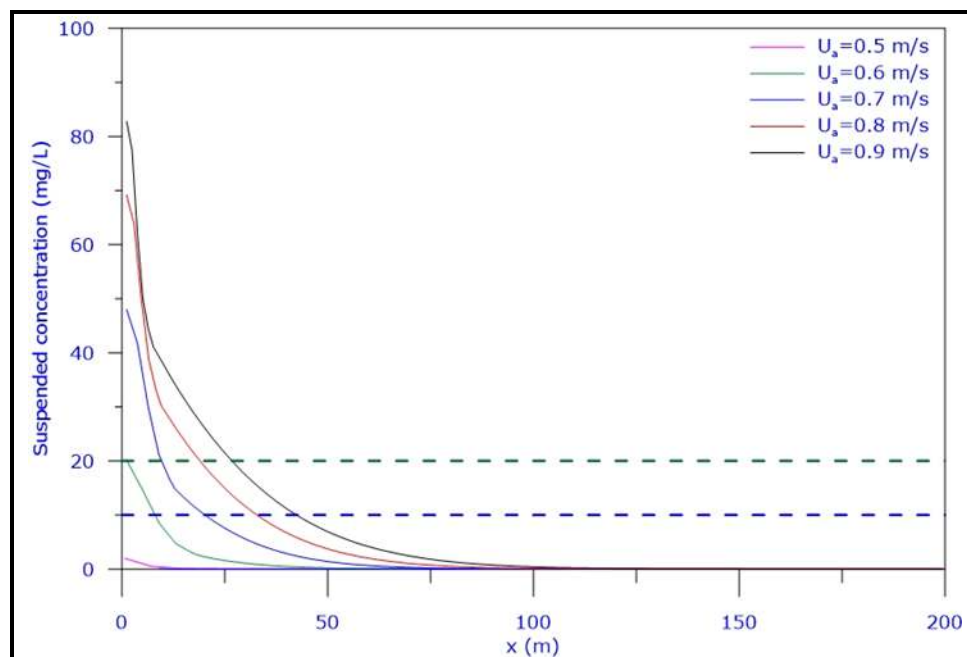
Calculations have been performed to investigate the effect of current velocity for values ranging from 0.50 to 0.90 m/s. Table D-30 summarises the effect of current velocity on the main geometric and hydrodynamic characteristics of the flow. At Figure D-94 the suspended sediment concentrations (mg/L) distributions for various current velocities are presented. In Figure D-95 sediment concentration contours (% of the initial) in the bottom layer are shown for current velocities 0.50 m/s and 0.90 m/s, respectively.

**Table D-30 Basic Geometric and Hydrodynamic Characteristics for Various Current Velocities**

Current Velocity (m/s)	Length of the Near Field (m)	BV (m)			BH (m)		
		At the End of Near Field	At x=400 m	At x=1,000 m	At the End of Near Field	At x=400 m	At x=1000 m
0.50	26.53	0.59	0.20	0.16	52.20	151.79	231.70
0.60	17.05	0.75	0.20	0.15	25.90	126.82	195.59
0.70	11.60	0.95	0.20	0.16	22.27	105.31	164.70
0.80	8.32	1.16	0.21	0.18	15.69	88.91	141.64
0.90	6.38	1.43	0.22	0.19	11.80	79.04	127.47

Prepared by School of Civil Engineering - National Tech Univ. of Athens on behalf of ASPROFOS, 2022.



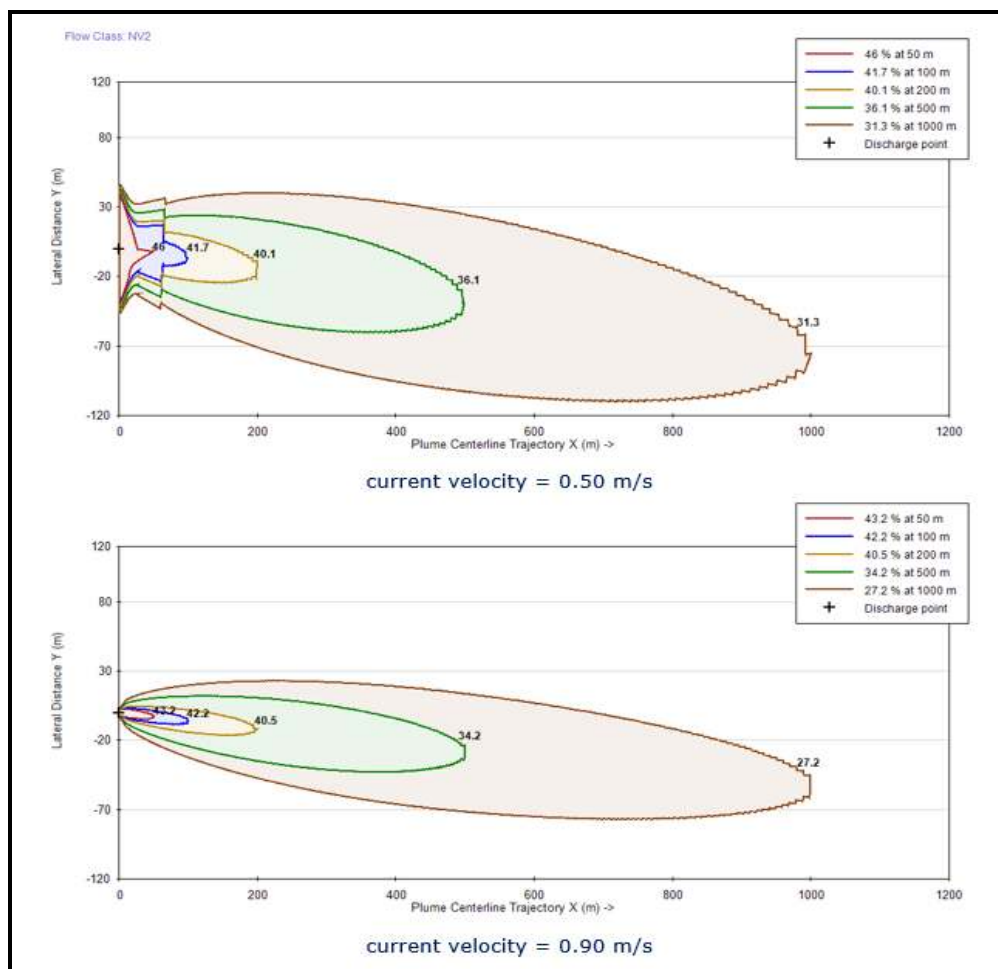


Prepared by School of Civil Engineering - National Tech Univ. of Athens on behalf of ASPROFOS, 2022.

**Figure D-94 Total Suspended Sediment Concentrations (mg/L) for Various Current Velocities**

From Table D-30, Figure D-94 and Figure D-95 and the calculations, when the current velocity increases from 0.50 m/s to 0.90 m/s, the following are observed:

- The length of the near field region decreases from 26.53 m to 6.38 m;
- The thickness of the bottom layer (BV) at the end of the near field increases from 0.59 m to 1.43 m; far from the dredging location, it approaches values that range from 0.16 m to 0.19 m;
- The half-width of the bottom layer (BH) at the end of the near field decreases from 52.20 m to 11.80 m; far from the dredging location, it approaches values that range from 231.70 m to 127.47 m; and
- The suspended solids concentrations in the water column decrease; thus, the decrease of current velocity results in more favourable conditions.



Prepared by School of Civil Engineering - National Tech Univ. of Athens on behalf of ASPROFOS, 2022.

**Figure D-95 Sediment Concentration Contours (% of the Initial) in the Bottom Layer for Current Velocities 0.50 m/s and 0.90 m/s**

#### 9 D.7.5.2 Effect of the Composition of Solids

Calculations have been performed to investigate the effect of sediment compositions by increasing the percentage of chunks from 20 % to 50 %, as shown in TableD-31. The calculated suspended sediment concentrations (mg/L) are shown in Table D-32.

In Table D-32 and Table D-33 the calculations show that when the percentage of chunks increases from 20 % to 50 %, then:

- The concentration at x=50.0 m decreases from 0.8 mg/L to 0.5 mg/L;
- The concentration at x=100.0 m is 0 mg/L in all cases; and

- The area covered by relatively high suspended sediment concentrations decrease.




**TableD-31 Examined Sediment Compositions**

Class	Material	C1	C2	C3	C4
1	Chunks	20 %	30 %	40 %	50 %
2	Sand	80 %	70 %	60 %	50 %
3	Coarse Silt	-	-	-	-
4	Fine Silt	-	-	-	-
5	Clay	-	-	-	-
Total	-	100 %	100 %	100 %	100 %

Prepared by School of Civil Engineering - National Tech Univ. of Athens on behalf of ASPROFOS, 2022.

**Table D-32 Suspended Sediment Concentrations (mg/L) for Various Sediment Compositions**

x(m)	C1	C2	C3	C4
1.1	37.1	32.5	27.8	23.2
4.2	30.7	26.9	23.1	19.2
7.3	20.8	18.2	15.6	13.0
10.4	13.7	12.0	10.3	8.6
13.5	10.1	8.8	7.6	6.3
14.7	8.9	7.8	6.7	5.6
15.9	8.3	7.3	6.3	5.2
17.1	7.8	6.8	5.8	4.9
24.2	5.0	4.4	3.7	3.1
25.4	4.6	4.0	3.5	2.9
26.6	4.3	3.8	3.2	2.7
27.8	4.0	3.5	3.0	2.5
28.9	3.7	3.2	2.8	2.3
30.1	3.4	3.0	2.5	2.1
31.3	3.1	2.7	2.4	2.0
32.5	2.9	2.5	2.2	1.8
52.6	0.6	0.6	0.5	0.4

	<b>EASTMED PIPELINE PROJECT</b>		 
	EastMed Greek Section – Environmental and Social Impact Assessment		DOC No: PERM-GREE-ESIA-A09_0007_0_Annex9D
			REV. : 00
			PAGE : 154 OF 178

x(m)	C1	C2	C3	C4
62.1	0.3	0.3	0.2	0.2
78.7	0.1	0.1	0.1	0.1
127.3	0.0	0.0	0.0	0.0
128.5	0.0	0.0	0.0	0.0

Prepared by School of Civil Engineering - National Tech Univ. of Athens on behalf of ASPROFOS, 2022.

**Table D-33 Suspended Sediment Concentrations (mg/L) at x=50 m and x=100 m**

x(m)	C1	C2	C3	C4
50.0	0.8	0.7	0.6	0.5
100.0	0.0	0.0	0.0	0.0

Prepared by School of Civil Engineering - National Tech Univ. of Athens on behalf of ASPROFOS, 2022.

## 9 D.8. CONCLUSIONS AND PROPOSALS

### 9 D.8.1. Conclusions

The main conclusions are described in this chapter, based on the calculations with CORMIX for:

- the 8 scenarios considered for the minimum and maximum current velocities at the 4 sites LF2, LF3, LF4 and LF5; and
- the additional 32 scenarios considered in the sensitivity analysis.

#### 9 D.8.1.1 Flow Behaviour of the Sediment Plume

Table D-34 summarises the main flow characteristics that are as follows:

- Initially, the flow of the sediment plume is dominated by upward plume momentum (jet-like); the axis of the plume rises to a maximum height, being weakly deflected by the ambient current. The maximum height is approximately equal to 1.2 m and equal to 2.7 m for the maximum and minimum current velocity, respectively; the higher value for the minimum current velocity is due to the weaker effect of the current;
- Then, the plume is strongly affected by gravity, rapidly falls downward and impinges on the sea bottom; the impingement angle ranges from 20.2° to 32.5° for the maximum current velocity, while it is constant (approximately equal to 57°) for the minimum current velocity. The length of




the near field region ranges from 6.7 m to 13.5 m for the maximum current velocity and it is almost constant (175.0 m) for the minimum current velocity;

- After impingement, the flow laterally spreads across the ambient flow in the downstream direction, its half-width (BH) is steadily increasing and its thickness (BV) is decreasing. At the end of the near field region, BH ranges from 12.4 m to 26.0 m for the maximum current velocity, while for the minimum current velocity it is almost constant and approximately equal to 350.0 m; moreover, BV for the maximum current velocity ranges from 0.9 m to 1.4 m and for the minimum current velocity it is approximately equal to 0.28 m;
- The mixing rate is relatively small in all scenarios; thus, the dilution at 1,200 m downstream of the discharge location is also small, ranging from 3.3 to 3.9 for the maximum current velocity, while it is constant and equal to 4.7 for the minimum flow velocity. Thus, the worst conditions are those for the maximum current velocity; and
- Flow characteristics for the minimum current velocity (that is close to zero) are practically the same for all sites.

**Table D-34 Flow Characteristics of the Sediment Plume**

Site	LF2		LF3		LF4		LF5	
Current Velocity	Max	Min	Max	Min	Max	Min	Max	Min
Length of near field region (m)	6.69	174.87	13.46	175.29	11.63	175.64	11.23	175.71
BH at impingement (m)	9.68	292.99	20.27	293.69	17.43	294.29	16.79	294.41
BH at the end of near field region (m)	12.41	348.70	26.00	349.53	22.35	350.25	21.54	350.39
BH at x=1200 m	143.24	611.97	192.50	609.92	180.02	608.43	177.13	608.29
BV at impingement (m)	1.38	0.12	0.90	0.12	1.00	0.12	1.03	0.12
BV at the end of near field	1.38	0.28	0.87	0.28	0.94	0.28	0.96	0.28
BV at x=1200 m	0.18	0.21	0.15	0.21	0.16	0.21	0.16	0.21
Dilution at the end of near field	2.1	2.7	2.1	2.7	2.1	2.7	2.1	2.7
Dilution at x=1200 m	3.9	4.7	3.3	4.7	3.4	4.7	3.4	4.7

Prepared by School of Civil Engineering - National Tech Univ. of Athens on behalf of ASPROFOS, 2022.

	EASTMED PIPELINE PROJECT		 	
			DOC No: PERM-GREE-ESIA-A09_0007_0_Annex9D	
	EastMed Greek Section – Environmental and Social Impact Assessment		REV. :	00
			PAGE :	156 OF 178

### 9 D.8.1.2 Sediment Concentrations

Table D-35 summarises the values of sediment concentrations at various distances from the discharge location ( $x=0$  m) in the near field and the bottom layer.

**Table D-35 Sediment Concentrations (mg/L) in the Near Field and the Bottom Layer**

Site	LF2		LF3		LF4		LF5	
x(m)	Max	Min	Max	Min	Max	Min	Max	Min
50	108.8	173.7	110.0	173.7	111.5	173.7	111.8	173.7
100	106.0	115.3	107.3	115.3	108.8	115.3	109.0	115.3
400	91.0	69.8	96.3	69.8	96.8	69.8	96.8	69.8
600	81.3	64.0	89.3	64.0	89.3	64.0	89.0	64.0
1200	63.8	53.5	75.0	53.5	74.0	53.5	73.5	53.5

Prepared by School of Civil Engineering - National Tech Univ. of Athens on behalf of ASPROFOS, 2022.

From Table D-35, the following remarks can be made:

- The distribution of sediment concentrations for the minimum current velocity are practically the same for all sites;
- At distances shorter than  $x=100$  m from the discharge location, the sediment concentrations for the maximum current velocity range from 106.0 mg/L to 111.8 mg/L; these values are lower than the corresponding values for the minimum current velocity that range from 115.3 mg/L to 173.7 mg/L; and
- Far downstream from the discharge location, for example at a distance equal to  $x=1,200$  m from the discharge location, sediment concentrations for the maximum current velocity range from 63.8 mg/L to 75.0 mg/L; these values are higher than the corresponding value of 53.5 mg/L for the minimum current velocity at all of the sites.

### 9 D.8.1.3 Suspended Sediment Concentrations (SSC)

Table D-36 summarises the values of the suspended sediment concentrations in the water column at various distances from the discharge location ( $x=0$ ).

**Table D-36 Suspended Sediment Concentrations (mg/L) in the Water Column**

Site	LF2		LF3		LF4		LF5	
x(m)	Max	Min	Max	Min	Max	Min	Max	Min
10	6.8	21.6	14.6	115.1	38.8	147.0	35.0	153.1
20	4.7	2.5	6.2	13.2	27.7	23.3	23.7	36.7
30	3.1	0.0	3.4	0.0	23.1	8.2	18.2	7.4
40	1.9		1.7		19.9	7.9	15.0	6.7
50	1.2		0.8		18.2	7.6	13.1	5.4
75	0.3		0.1		16.2	6.9	11.1	4.4
100	0.1		0.0		15.2	5.4	10.4	3.9
150	0.0				13.9	4.4	9.6	3.1
200					12.7	2.3	8.9	2.7
300					10.7	2.0	7.8	2.3

Prepared by School of Civil Engineering - National Tech Univ. of Athens on behalf of ASPROFOS, 2022.

From Table D-36, the following remarks can be made:




- At distances shorter than 20 m from the discharge location, the suspended sediment concentrations for the maximum current velocity are lower than the threshold value of 35 mg/L for all sites. For the minimum current velocity, the corresponding concentrations are lower than the threshold value of 35 mg/L with the exception of site LF5 at which the suspended sediment concentration is slightly higher than the threshold value (36.7 mg/L); and
- At distances greater than 50 m from the dredging location, suspended sediment concentrations range from 0.8 to 18.2 mg/L for the maximum current velocity, while the corresponding concentrations for the minimum current velocity range from 0.0 mg/L (at sites LF2 and LF3) to 7.6 mg/L.

Moreover, it is noted that the duration of potential impacts lasts as long as dredging takes place and the increased suspended sediment concentrations do not persist in the water column after the dredging procedure.

#### **9 D.8.1.4 Sensitivity Analysis**

Sensitivity analysis calculations showed that when the current velocity increases the following are observed:



	EASTMED PIPELINE PROJECT		 
	EastMed Greek Section – Environmental and Social Impact Assessment		DOC No: PERM-GREE-ESIA-A09_0007_0_Annex9D
			REV. : 00
			PAGE : 158 OF 178




- The length of the near field region decreases;
- The initial thickness of the bottom layer increases and the initial half-width of the bottom layer decreases; and
- The suspended solid concentrations in the water column decrease; thus, the decrease of the current velocity results in more favourable conditions.

Moreover, it was verified that when the percentages of heavy material, such as chunks, increase, then suspended sediment concentrations and the area covered by relatively high suspended sediment concentrations decreases.

### 9 D.8.2. Proposed Measures during Dredging




It is proposed to adopt all available measures during dredging to reduce suspended sediment concentrations; some indicative measures are the following:

- Use auger dredgers that employ special equipment to move material towards the suction head and use pumping by piston action to enable transportation of high-density material;
- Use disc-cutter dredgers with a cutter head which rests horizontally and rotates its vertical blades slowly;
- Use scoop/sweep dredgers with special equipment to scrape the material towards the suction intake;
- When using a trailing suction hopper dredger: optimise trailing velocity, suction mouth and suction discharge and reduce or even eliminate overflow;
- When using a cutter suction dredger: optimises cutter speed, swing velocity and discharge and employ a special cutter-head design;
- When using a grab dredger: employ watertight grab/clamshell, use silt screen, limit grab time above water and limit grab dragging on bed; and
- When using a backhoe dredger: use a special bucket for reducing sediment losses and silt screen (applicable for current velocities less than 0.5 m/s).




	<p style="text-align: center;"><b>EASTMED PIPELINE PROJECT</b></p> <p style="text-align: center;">EastMed Greek Section – Environmental and Social Impact Assessment</p>	<div style="display: flex; justify-content: space-around; align-items: center;">   </div> <p>DOC No: PERM-GREE-ESIA-A09_0007_0_Annex9D</p> <p>REV. : 00</p> <p>PAGE : 159 OF 178</p>
---	--	---

## 9 D.9. REFERENCES




1. Akar P.J. and Jirka G.H. (1994). Buoyant spreading processes in pollutant transport and mixing. Part I: Lateral spreading in strong ambient current, *Journal of Hydraulic Research*, 32, pp. 815–831. <https://doi.org/10.1080/00221689409498692>.
2. Akar P.J. and Jirka G.H. (1995). Buoyant spreading processes in pollutant transport and mixing Part 2: Upstream spreading in weak ambient current, *Journal of Hydraulic Research*, 33, pp. 87–100. <https://doi.org/10.1080/00221689509498686>
3. Bernard W.D. (1978). Prediction and control of dredged material dispersion around dredging and open-water pipeline disposal operations. Technical Report DS-7-13, Dredged Material Research Program. USWES, Environmental Laboratory, Vicksburg, USA
4. Bray R. N., Bates A. D. and Land J. M. (1996). *Dredging: A Handbook for Engineers*, 2<sup>nd</sup> Ed., ISBN-13: 978-0340545249
5. Bridges T., Gustavson K., Schroeder P., Ells S., Hayes D., Nadeau S., Palermo M. and Patmont C. (2010). Dredging Processes and Remedy Effectiveness: Relationship to the 4 Rs of Environmental Dredging. *Integrated Environmental Assessment and Management*, 6(4), pp. 619-630. <https://doi.org/10.1002/ieam.71>
6. Burt N., Land J. and Otten H. (2007). Measurement of sediment release from a grab dredge in the River Tees, UK, for the calibration of turbidity prediction software. WODCON 2007 Conference Proceedings, Orlando (FL, USA), pp. 1173-1190
7. Chen C.J. and Rodi W. (1980). Vertical Buoyant Jets: A Review of Experimental Data, Pergamon Press, Oxford <https://ui.adsabs.harvard.edu/abs/1980STIA...8023073C/abstract>
8. Clarke D., Reine K., Dickerson C., Zappala, S., Pinzon R. and Gallo J. (2007). Suspended sediment plumes associated with navigation dredging in the Arthur Kill Waterway, New Jersey. WODCON XVIII, Orlando, USA.
9. Doneker R. L., Nash J. D. and Jirka G. H. (2004). Pollutant transport and mixing zone simulation of sediment density currents, *Journal of Hydraulic Engineering*, 130(4), pp. 349–359, [https://doi.org/10.1061/\(ASCE\)0733-9429\(2004\)130:4\(349\)](https://doi.org/10.1061/(ASCE)0733-9429(2004)130:4(349))
10. Doneker R.L. and Jirka G.H. (2007). CORMIX User Manual: A Hydrodynamic Mixing Zone Model and Decision Support System for Pollutant Discharges Into Surface Waters, MixZon, Portland, Ore, USA <http://www.cormix.info>
11. Erftemeijer P.L.A. and Lewis R.R.R. (2006). Environmental impacts of dredging on seagrasses: a review. *Marine Pollution Bulletin*, 52(12), pp. 1553–1572. <https://doi.org/10.1016/j.marpolbul.2006.09.006>
12. European Dredging Association, Types of Dredgers, (2018). Available online: [https://www.european-dredging.eu/Types\\_of\\_dredger](https://www.european-dredging.eu/Types_of_dredger).
13. Fischer H. B., List E. J., Koh. R. C. Y., Imberger J. and Brooks N. H. (1979). Mixing in Inland and Coastal Waters. Academic Press, New York, 483 pp.
14. Fissel D. B. and Lin Y. (2018). Modeling the Transport and Fate of Sediments Released from Marine Construction Projects in the Coastal Waters of British Columbia, Canada. *Journal of Marine Science and Engineering*. 6(3):103. <https://doi.org/10.3390/jmse6030103>

	<p style="text-align: center;"><b>EASTMED PIPELINE PROJECT</b></p> <p style="text-align: center;">EastMed Greek Section – Environmental and Social Impact Assessment</p>	<div style="display: flex; justify-content: space-around; align-items: center;">   </div> <div style="border: 1px solid black; padding: 2px;"> DOC No: PERM-GREE-ESIA- A09_0007_0_Annex9D REV. : 00 PAGE : 160 OF 178 </div>
---	--	---

15. Hayes D.F., Raymond G.L. and Mc Lellan T.N. (1984). Sediment resuspension from dredging activities, pp. 72-82. Dredging and dredged material disposal, Vol. I, ed. by R.L. Montgomery and J.W. Leach. Proc. Of Conf. Dredging, Florida, USA.
16. Herbich B. (1992). Handbook of Dredging Engineering, McGraw-Hill.
17. IMO (2006). International Regulations (MARPOL 73/78). "Revised Guidelines on Implementation of Effluent Standards and Performance Tests for Sewage Treatment Plants." Annex 26. Resolution MEPC.159(55). Adopted on 13 October 2006. MEPC 55/23.
18. Je C.H. and Hayes D.F. (2004). Development of a two-dimensional analytical model for predicting toxic sediment plumes due to environmental dredging operations. *Environ. Sci. Health Part A* 39, pp. 1935–1947. <https://doi.org/10.1081/ESE-120039366>
19. Je C.H., Hayes D.F. and Kim K. (2007). Simulation of resuspended sediments resulting from dredging operations by a numerical flocculent transport model. *Chemosphere*, 70, pp. 187-195. <https://doi.org/10.1016/j.chemosphere.2007.06.033>.
20. Jensen A. and Mogensen B. (2000). Effects, ecology and economy. Environmental aspects of dredging - Guide No. 6. International Association of Dredging Companies (IADC) and Central Dredging Association (CEDA), 119 pp.
21. Jirka G.H., Doneker R.L. and Hinton S.W. (1996). "User's Manual for CORMIX: A Hydrodynamic Mixing Zone Model and Decision Support System for Pollutant Discharges into Surface Waters", U.S. Environmental Protection Agency, Tech. Rep., Environmental Research Lab, Athens, Georgia, USA
22. Jones R., Wakeford M., Currey-Randall L., Miller K. and Tonin H. (2021). Drill cuttings and drilling fluids (muds) transport, fate and effects near a coral reef mesophotic zone, *Marine Pollution Bulletin*, 172 <https://doi.org/10.1016/j.marpolbul.2021.112717>
23. Intecsea / C&M Engineering Consortium (2020), PROJECT 416010-00225 - 00225-Cv10A-TDR-00024: Metocean Design Parameters Report – Offshore, Appendix D2: Extreme Current conditions, Dec. 2020.
24. Kuo A.Y. and Hayes D.F. (1991) Models for turbidity induced by bucket dredge. *Journal of Waterway, Port, Coastal, and Ocean Engineering*, ASCE 1991, 117 (6), pp. 610–623. [https://doi.org/10.1061/\(ASCE\)0733-950X\(1991\)117:6\(610\)](https://doi.org/10.1061/(ASCE)0733-950X(1991)117:6(610)).
25. Van Rijn, L. C. (2019). Turbidity due to dredging and dumping of sediments. [www.leovanrijn-sediment.com](http://www.leovanrijn-sediment.com) (last access 15<sup>th</sup> November 2021)
26. Lee H. W. J. and Jirka H.G. (1981). Vertical Round Buoyant Jet in Shallow Water, *Journal of the Hydraulics Division*, 107(12) <https://doi.org/10.1061/JYCEAJ.0005783>
27. Macinnis-Ng. C.M.O and Ralph P.J. (2003). In situ impact of petrochemicals on the photosynthesis of the seagrass *Zostera capricorni*. *Marine Pollution Bulletin*, 46(11), pp. 1395-1407.
28. Marine Strategy Framework (2008/56/EC). Directive 2008/56/EC of the European Parliament and of the Council of 17 June 2008 establishing a framework for community action in the field of marine environmental policy (Marine Strategy Framework Directive). Official Journal L 164 , 25/06/2008 P. 19 – 40. <http://data.europa.eu/eli/dir/2008/56/oj>

	<p style="text-align: center;"><b>EASTMED PIPELINE PROJECT</b></p> <p style="text-align: center;">EastMed Greek Section – Environmental and Social Impact Assessment</p>	<div style="display: flex; justify-content: space-between; align-items: center;">   </div> <div style="border: 1px solid black; padding: 2px;"> <p>DOC No: PERM-GREE-ESIA-A09_0007_0_Annex9D</p> <p>REV. : 00</p> <p>PAGE : 161 OF 178</p> </div>
---	--	---

29. Nash J.D., Jirka G.H. and Chen D. (1995). Large scale planar laser induced fluorescence in turbulent density-stratified flows. *Experiments in Fluids*, 19, pp. 297–304 .  
<https://doi.org/10.1007/BF00203413>
30. Newell R.C., Seiderer L.J. and Hitchcock D.R. (1998). The impact of dredging works in coastal waters: a review of the sensitivity to disturbance and subsequent recovery of biological resources on the seabed. *Oceanography and Marine Biology – an annual. Review* 36, pp. 127–178.
31. Orpin A.R., Ridd P.V., Thomas S., Anthony K.R.N., Marshall, P. and Oliver J. (2004). Natural turbidity variability and weather forecasts in risk management of anthropogenic sediment discharge near sensitive environments. *Marine Pollution Bulletin* 49(7-8), pp. 602–612.  
[doi:10.1016/j.marpolbul.2004.03.020](https://doi.org/10.1016/j.marpolbul.2004.03.020).
32. Pennekamp J.G.S., Epskamp R.J.C., Rosenbrand W.F., Mullie A., Wessel G.L., Arts T. and Deibel I.K. (1996). Turbidity caused by dredging: viewed in perspective. *Terra et Aqua* 64, pp. 10–17.  
<https://www.iadc-dredging.com/wp-content/uploads/2017/02/article-turbidity-caused-by-dredging-viewed-in-prespective-64-2.pdf>
33. Papakostantis I.G., Christodoulou G.C. and Papanicolaou P.N. (2011). Inclined negatively buoyant jets 1: Geometrical Characteristics. *Journal of Hydraulic Research* 49 (1), pp:3-12.  
<https://doi.org/10.1080/00221686.2010.537153>
34. Purnama A., Baawain M.S. and Shao D. (2016). Simulation of Sediment Discharges during an Outfall Dredging Operation, *International Journal of Oceanography*, 8097861,  
<http://dx.doi.org/10.1155/2016/8097861>.
35. Purnama A., Baawain M.S. and Shao D. (2015). CORMIX Simulations of Dredged Sediment Discharges in Coastal Waters, 5th International Conference on Estuaries and Coasts (ICEC2015) November 2-4, Muscat, Oman.
36. Schatzmann M. (1978). The integral equations for round buoyant jets in stratified flows. *Journal of Applied Mathematics and Physics (ZAMP)* 29, pp. 608–630 .  
<https://doi.org/10.1007/BF01601488>
37. Schroeder, P. and C.K. Ziegler, 2004. Understanding, predicting and monitoring contaminant releases during dredging. Paper presented at “Addressing Uncertainty and Managing Risk at Contaminated Sediment Sites”, USACE/USEPA/SMWG Joint Sediment Conference, US Army Corps of Engineers, October, 2004. Available at <http://el.erdc.usace.army.mil/workshops/04octccs/agenda.pdf>
38. Schroeder P. R., Palermo M. R., Myers T. E. and Lloyd C. M. (2004). The automated dredging and disposal alternatives modeling system (ADDAMS). ERDC TN EEDP-06-12. Vicksburg, MS: U.S. Army Engineer Research and Development Center. <http://el.erdc.usace.army.mil/eedp>.  
<https://erdc-library.erdc.dren.mil/jspui/bitstream/11681/8867/1/EEDP-06-12.pdf>
39. Stamou A.I., Matsoukis K., Douka Eis., Papagrigoriou S. and Bekiaris Y. (2009). Modeling the fate of sediment plumes during marine dredging operations, 11th International Conference on Environmental Science and Technology (CEST20 09 ), A-1410-1416, Sep 2009.
40. Shao D., Purnama A. and Sun T. (2015). Modelling the temporal evolution of dredging-induced turbidity in the far field. *Journal of Waterway, Port, Coastal and Ocean Engineering* 141(5) .  
[http://dx.doi.org/10.1061/\(ASCE\)WW.1943-5460.0000379](http://dx.doi.org/10.1061/(ASCE)WW.1943-5460.0000379).

	<p style="text-align: center;"><b>EASTMED PIPELINE PROJECT</b></p> <p style="text-align: center;">EastMed Greek Section – Environmental and Social Impact Assessment</p>	<div style="display: flex; justify-content: space-around; align-items: center;">   </div> <div style="border: 1px solid black; padding: 2px;"> DOC No: PERM-GREE-ESIA- A09_0007_0_Annex9D REV. : 00 PAGE : 162 OF 178 </div>
---	--	--

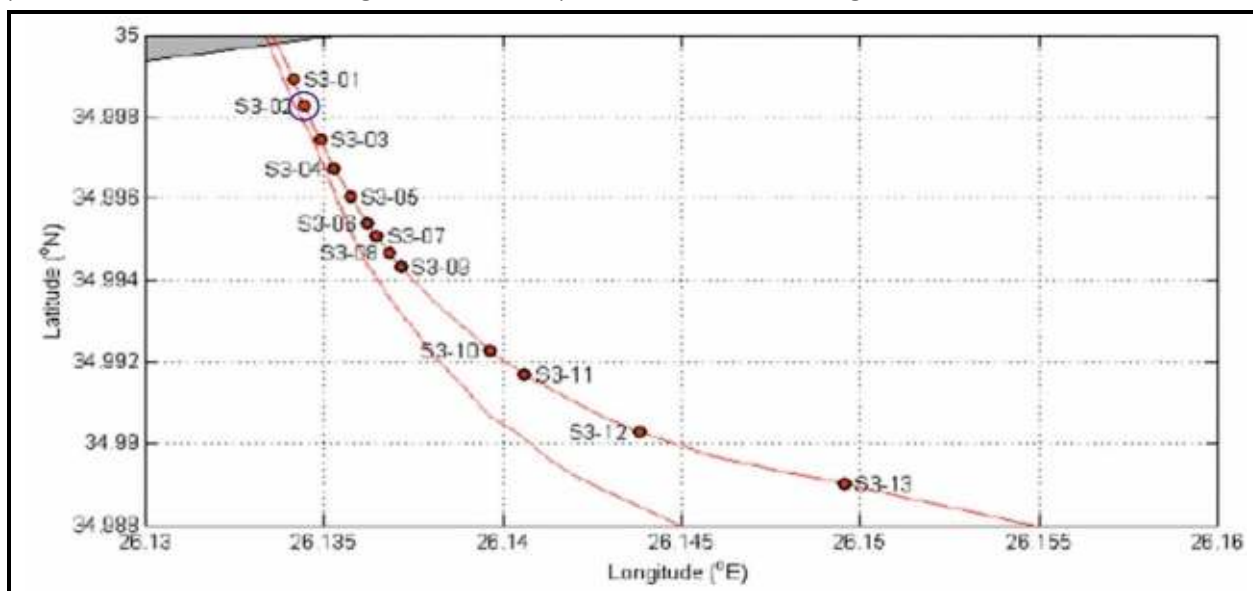
41. Stern E. M. and Stickley W. B. (1978). Effects of turbidity and suspended material in aquatic environments: literature review. U.S. Army Corps of Engineers, Waterways Experiment Station, Technical Report D-78-21, Vicksburg, Mississippi.  
<https://apps.dtic.mil/sti/citations/ADA056035>
42. Stuber L.M. (1976).Agitation dredging: Savannah Harbour, pp. 337-390. Dredging: Environmental effects and Technology. Proc. WODCON VII, San Francisco, USA
43. Sosnowski R.A. (1984). Sediment resuspension due to dredging and storms: an analogous pair. Dredging and dredged material disposal, Vol. I pp. 609-618, ed. by R.L. Montgomery and J.W. Leach. Proc. of Conf. Dredging, Florida, USA
44. USEPA, (1999). "Review of the D-CORMIX model". *Science Advisory Board Report EPA-SAB-EC-99-011, Washington DC, USA*.<http://www.epa.gov/science1/ec99011.pdf>
45. Water Framework (2000/60/EC). Directive 2000/60/EC of the European Parliament and of the Council of 23 October 2000 establishing a framework for Community action in the field of water policy. Official Journal L 327, 22/12/2000 P. 0001 – 0073.  
<http://data.europa.eu/eli/dir/2000/60/oj>
46. Wakeman T.H., Sustar J.F. and Dickson W.J. (1975). Impact of three dredge types compared in San Francisco District, pp. 9-14. World Dredging and Marine Construction
47. Willoughby M.A. and Crabb D.J. (1983). The behaviour of dredge generated sediment plumes in Moreton Bay, pp. 182-186. Sixth Australian Conference on Coastal and Ocean Engineering, Gold Coast, 13-15 July
48. World Bank Group (The World Bank, International Finance Corporation, and Multilateral Investment Guarantee Agency). 2015. "Environmental, Health, and Safety Guidelines Offshore Oil and Gas Development". June 5, 2015

## Appendix 1 Site Characteristics

### SITE CHARACTERISTICS OF LF2

The site characteristics were obtained from the Report: Intecsea / C&M Engineering Consortium (2020), PROJECT 416010-00225 - 00225-Cv10A-TDR-00024: Metocean Design Parameters Report – Offshore, Dec. 2020, p. 15 and p. 10.

These data are shown in Figures 1 and 2 and Table 1. Table 1 includes the coordinates of the EGSA system coordinates and in Figure 2 the Study Area is shown in Google Earth.






Prepared by School of Civil Engineering - National Tech Univ. of Athens on behalf of ASPROFOS, 2022.

Figure 1 Location of Output Points along the OSS4 Route (p.15)

Table 1 Bathymetry Data along OSS3 at the LF2 Area (p.10)

Name	KP (m)	Lon (deg)	Lat (deg)	EGSA (x)	EGSA (y)	Depth (m)
S3_01	160	26.13414	34.99892	694613.5939	3874715.3759	-10.0
S3_02	240	26.13446	34.99828	694644.3194	3874645.0095	-20.0
S3_03	340	26.13490	34.99744	694686.4727	3874552.6927	-30.4
S3_04	420	26.13530	34.99674	694724.6437	3874475.8273	-40.2
S3_05	510	26.13575	34.99603	694767.4028	3874397.9504	-50.4



	<b>EASTMED PIPELINE PROJECT</b>		 	
			DOC No: PERM-GREE-ESIA-A09_0007_0_Annex9D	
	EastMed Greek Section – Environmental and Social Impact Assessment		REV. :	00
			PAGE :	164 OF 178

Name	KP (m)	Lon (deg)	Lat (deg)	EGSA (x)	EGSA (y)	Depth (m)
S3_06	600	26.13620	34.99540	694809.9729	3874328.9474	-76.0
S3_07	640	26.13648	34.99508	694836.2904	3874293.9988	-97.9
S3_08	690	26.13683	34.99468	694869.1875	3874250.3132	-125.2
S3_09	740	26.13718	34.99432	694901.9899	3874211.0645	-150.7

Prepared by School of Civil Engineering - National Tech Univ. of Athens on behalf of ASPROFOS, 2022.



Prepared by School of Civil Engineering - National Tech Univ. of Athens on behalf of ASPROFOS, 2022.

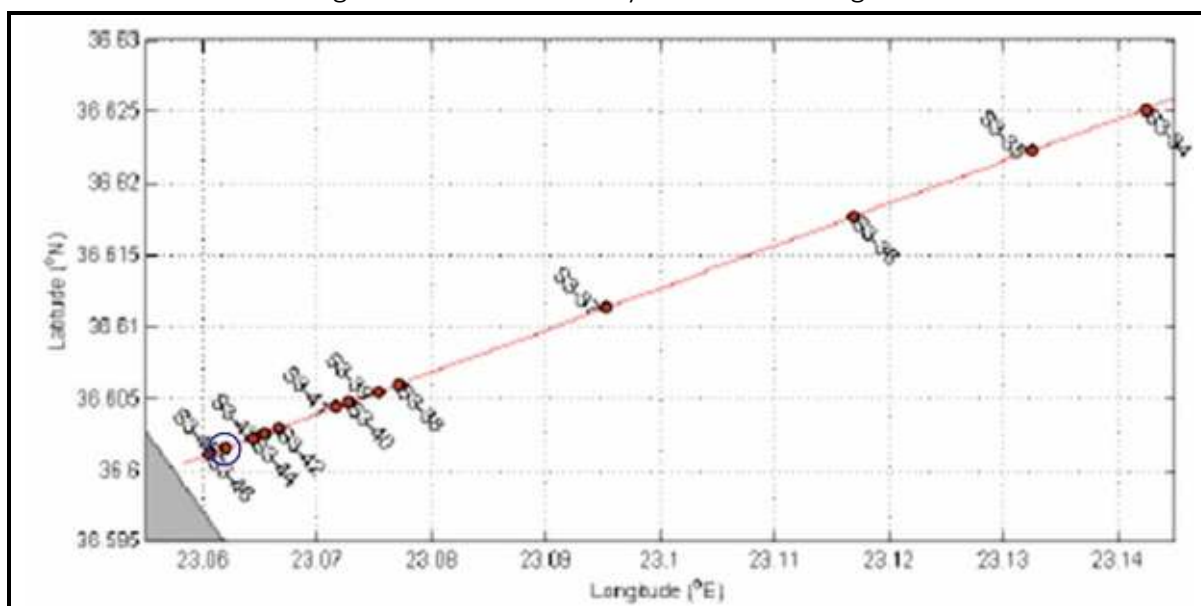
**Figure2** Location of Output Points along OSS3 Route at LF2 (in Google Earth



### SITE CHARACTERISTICS OF LF3

The site characteristics were obtained from the Report: Intecsea / C&M Engineering Consortium (2020), PROJECT 416010-00225 - 00225-Cv10A-TDR-00024: Metocean Design Parameters Report – Offshore, Dec. 2020, p. 15 and p. 10.

These data are shown in Figures 3 and 4 and Table 2; Table 2 includes the coordinates of the EGSA system coordinates and in Figure 4 the area of study is shown in Google Earth.






Prepared by School of Civil Engineering - National Tech Univ. of Athens on behalf of ASPROFOS, 2022.

**Figure 3** Location of Output Points along OSS3 Route (p.15)

**Table 2** Bathymetry Data along OSS3 at LF3 the Area (p.10)

Name	KP (m)	Lon (deg)	Lat (deg)	EGSA (x)	EGSA (y)	Depth (m)
S3_38	426730	23.07716	36.60601	417317.4586	4051275.3517	-150.3
S3_39	426900	23.07539	36.60550	417158.6111	4051220.2990	-124.5
S3_40	427150	23.07274	36.60475	416920.7991	4051139.3851	-100.1
S3_41	427250	23.07169	36.60445	416826.5674	4051107.0128	-73.8
S3_42	427730	23.06666	36.60301	416375.1395	4050951.6309	-50.1
S3_43	427850	23.06539	36.60260	416261.1080	4050907.2535	-40.0
S3_44	427950	23.06434	36.60225	416166.8171	4050869.3418	-29.7
S3_45	428170	23.06202	36.60159	415958.5988	4050798.1506	-20.3

	<b>EASTMED PIPELINE PROJECT</b>		 	
	EastMed Greek Section – Environmental and Social Impact Assessment		DOC No: PERM-GREE-ESIA-A09_0007_0_Annex9D	
			REV. :	00
			PAGE :	166 OF 178

Name	KP (m)	Lon (deg)	Lat (deg)	EGSA (x)	EGSA (y)	Depth (m)
S3_46	428310	23.06058	36.60117	415829.3469	4050752.8180	-10.0



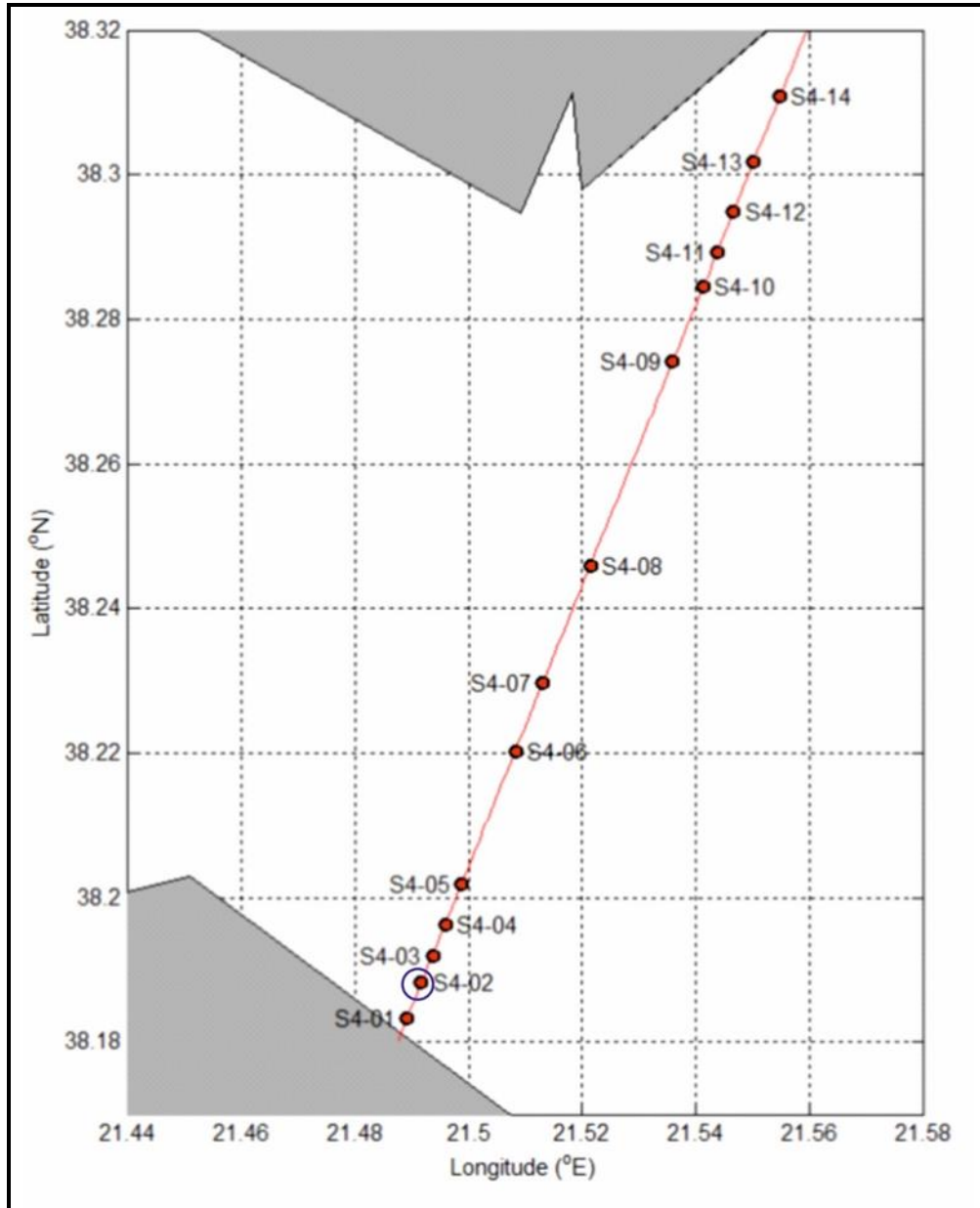
Prepared by School of Civil Engineering - National Tech Univ. of Athens on behalf of ASPROFOS, 2022.

**Figure 4** Location of Output Points along OSS3 Route at LF3 (in Google Earth)

#### *SITE CHARACTERISTICS OF LF4*

The site characteristics were obtained from the Report: Intecsea / C&M Engineering Consortium (2020), PROJECT 416010-00225 - 00225-Cv10A-TDR-00024: Metocean Design Parameters Report – Offshore, Dec. 2020, p. 16 and p. 11.

These data are shown in Figures 5 and 6 and Table 3; Table 3 includes the coordinates of the EGSA system coordinates and in Figure 6 the Study Area is shown in Google Earth.






Prepared by School of Civil Engineering - National Tech Univ. of Athens on behalf of ASPROFOS, 2022.

**Figure 5** Location of Output Points along OSS4 Route (p.16)

**Table 3** Bathymetry Data along OSS4 at the LF4 Area (p.11)

Name	KP (m)	Lon (deg)	Lat (deg)	EGSA (x)	EGSA (y)	Depth (m)
S4_01	360	21.48924	38.18334	279945.2383	4228849.2997	-10.0

	EASTMED PIPELINE PROJECT		 	
			DOC No: PERM-GREE-ESIA-A09_0007_0_Annex9D	
	EastMed Greek Section – Environmental and Social Impact Assessment		REV. :	00
			PAGE :	168 OF 178

Name	KP (m)	Lon (deg)	Lat (deg)	EGSA (x)	EGSA (y)	Depth (m)
S4_02	930	21.49172	38.18814	280176.9089	4229376.1251	-19.9
S4_03	1390	21.49366	38.19192	280285.4600	4229623.3496	-30.0
S4_04	1900	21.49590	38.19620	280358.1917	4229791.0350	-40.1
S4_05	2570	21.49875	38.20176	280567.2335	4230260.7285	-50.0

Prepared by School of Civil Engineering - National Tech Univ. of Athens on behalf of ASPROFOS, 2022.



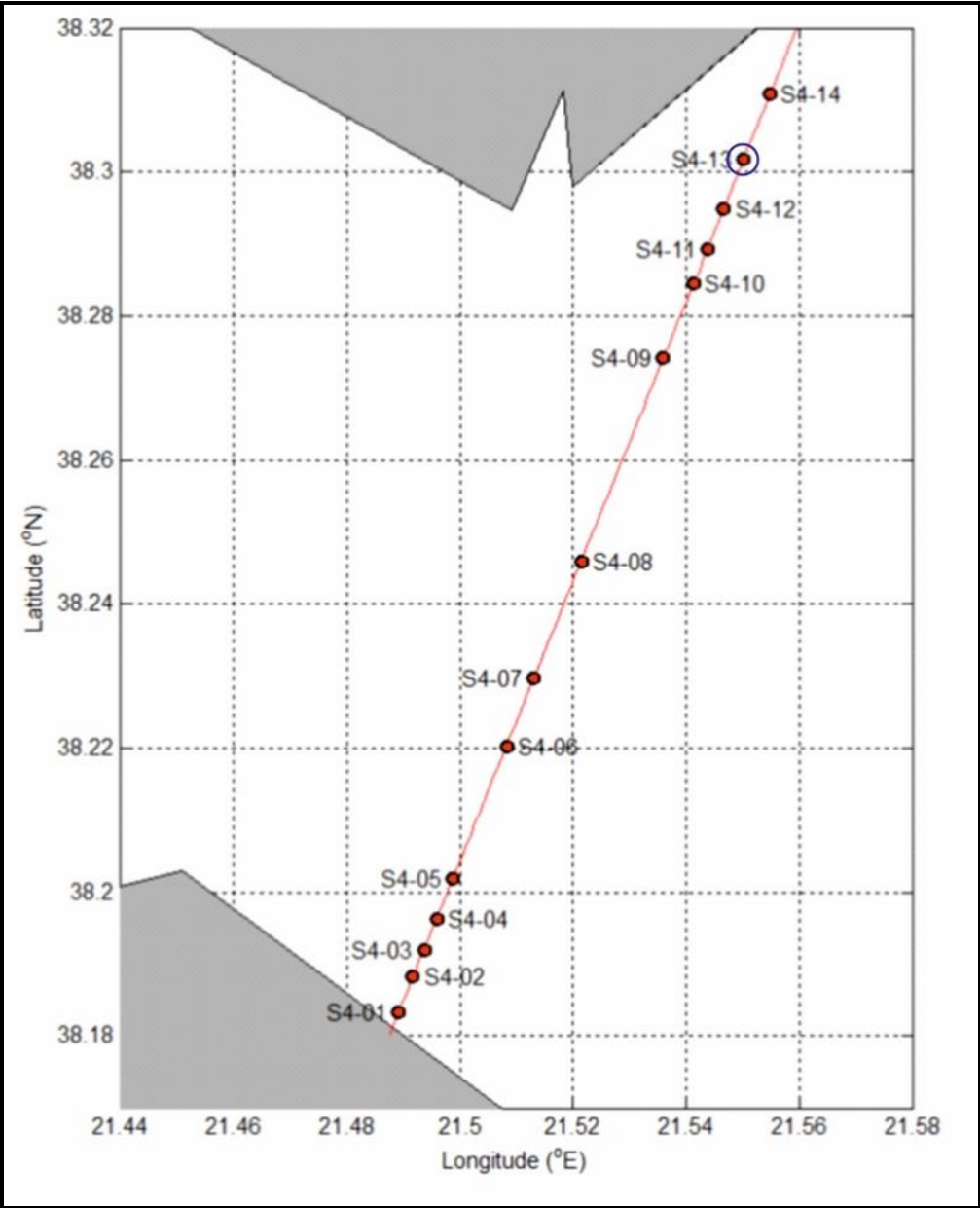
Prepared by School of Civil Engineering - National Tech Univ. of Athens on behalf of ASPROFOS, 2022.

**Figure 6** Location of Output Points along OSS4 Route (in Google Earth)

### *SITE CHARACTERISTICS OF LF5*

The site characteristics were obtained from the Report: Intecsea / C&M Engineering Consortium (2020), PROJECT 416010-00225 - 00225-Cv10A-TDR-00024: Metocean Design Parameters Report – Offshore, Dec. 2020, p. 16 and p. 11.

These data are shown in Figures 7 and 8 and Table 4; Table 4 includes the coordinates of the EGSA system coordinates and in Figure 8 the Study Area is shown in Google Earth.



Prepared by School of Civil Engineering - National Tech Univ. of Athens on behalf of ASPROFOS, 2022.

Figure 7                      Location of Output Points along OSS4 Route (p.16)



**Table 4 Bathymetry Data along OSS4 at the LF5 Area (p.11)**

Name	KP (m)	Lon (deg)	Lat (deg)	EGSA (x)	EGSA (y)	Depth (m)
S4_10	12470	21.54128	38.28443	284801.9748	4239946.1106	-50.0
S4_11	13050	21.54375	38.28930	285032.4060	4240480.8479	-39.9
S4_12	13710	21.54664	38.29478	285301.3423	4241082.3146	-30.0
S4_13	14550	21.55020	38.30180	285633.3705	4241853.1475	-20.0
S4_14	15620	21.55478	38.31076	286060.2368	4242836.9362	-10.0

Prepared by School of Civil Engineering - National Tech Univ. of Athens on behalf of ASPROFOS, 2022.



Prepared by School of Civil Engineering - National Tech Univ. of Athens on behalf of ASPROFOS, 2022.

**Figure 8 Location of Output Points along OSS4 Route (in Google Earth) από ΕΠ**

## Appendix 2 Ambient Physical Properties

The ambient physical properties were obtained from the Report: Intecsea / C&M Engineering Consortium (2020a), PROJECT 416010-00225 - 00225-Cv10A-TDR-00024: Metocean Design Parameters Report – Offshore; Appendix E: Air and seawater properties, Dec. 2020.

**Table 5 Water Properties at S3\_02; LF2**




	Bottom Temperature (°)			Bottom Salinity (psu)			Bottom Density (kg/m <sup>3</sup> )		
	Min	Avg	Max	Min	Avg	Max	Min	Avg	Max
January	15.29	16.90	19.16	38.79	38.98	39.18	1,028.07	1,028.64	1,029.04
February	14.87	16.06	17.42	38.82	38.99	39.21	1,028.52	1,028.85	1,029.12
March	14.78	15.88	16.87	38.85	38.98	39.11	1,028.64	1,028.89	1,029.11
April	15.04	16.37	18.82	38.73	38.99	39.13	1,028.24	1,028.78	1,029.07
May	16.20	18.59	21.68	38.83	39.02	39.14	1,027.44	1,028.24	1,028.92
June	18.19	21.70	25.76	38.81	39.06	39.18	1,026.28	1,027.43	1,028.41
July	21.65	24.54	26.70	39.0	39.15	39.40	1,026.04	1,026.67	1,027.51
August	23.28	25.72	27.75	39.02	39.21	39.48	1,025.70	1,026.34	1,026.96
September	22.42	25.14	27.16	39.0	39.22	39.46	1,025.91	1,026.53	1,027.22
October	19.78	23.53	26.38	38.99	39.16	39.32	1,026.18	1,026.97	1,028.05
November	18.63	20.91	23.68	38.87	39.06	39.23	1,026.86	1,027.65	1,028.22
December	16.55	18.37	21.18	38.85	38.99	39.22	1,027.58	1,028.28	1,028.73
All year	14.78	20.34	27.75	38.73	39.07	39.48	1,025.7	1,027.76	1,029.12

Prepared by School of Civil Engineering - National Tech Univ. of Athens on behalf of ASPROFOS, 2022.

**Table 6 Water properties at S3\_45; LF3**

	Bottom Temperature (°)			Bottom Salinity (psu)			Bottom Density (kg/m <sup>3</sup> )		
	Min	Avg	Max	Min	Avg	Max	Min	Avg	Max
January	13.79	16.12	18.42	38.25	38.60	39.01	1,028.02	1,028.58	1,029.24
February	13.33	14.97	16.74	38.34	38.57	38.72	1,028.42	1,028.82	1,029.23
March	13.29	15.01	17.61	38.28	38.57	38.69	1,028.24	1,028.82	1,029.25
April	14.26	16.19	19.89	38.35	38.58	38.67	1,027.61	1,028.55	1,028.97
May	15.32	18.55	23.34	38.28	38.57	38.67	1,026.60	1,027.95	1,028.76



	<b>EASTMED PIPELINE PROJECT</b>						 		
	EastMed Greek Section – Environmental and Social Impact Assessment						DOC No: PERM-GREE-ESIA-A09_0007_0_Annex9D		
							REV. :	00	
							PAGE :	172 OF 178	




	Bottom Temperature (°)			Bottom Salinity (psu)			Bottom Density (kg/m <sup>3</sup> )		
	Min	Avg	Max	Min	Avg	Max	Min	Avg	Max
June	17.75	21.00	25.24	38.35	38.58	38.66	1,026.01	1,027.30	1,028.13
July	20.77	23.18	27.81	38.50	38.61	38.75	1,025.32	1,026.70	1,027.43
August	22.14	24.83	28.13	38.53	38.65	38.82	1,025.19	1,026.23	1,026.96
September	23.19	25.00	27.62	38.28	38.68	38.84	1,025.39	1,026.20	1,026.73
October	21.13	23.61	26.14	38.12	38.70	38.84	1,025.91	1,026.64	1,027.38
November	18.73	21.29	24.18	38.36	38.74	38.91	1,026.51	1,027.34	1,028.16
December	15.83	18.48	21.27	38.18	38.68	39.00	1,027.31	1,028.05	1,028.96
All year	13.29	19.93	28.14	38.12	38.63	39.01	1,025.19	1,027.58	1029.25

Prepared by School of Civil Engineering - National Tech Univ. of Athens on behalf of ASPROFOS, 2022.

**Table 7 Water Properties at S4\_02; LF04**

	Bottom Temperature (°)			Bottom Salinity (psu)			Bottom Density (kg/m <sup>3</sup> )		
	Min	Avg	Max	Min	Avg	Max	Min	Avg	Max
January	13.64	16.06	18.35	38.32	38.61	39.01	1,028.00	1,028.59	1,029.28
February	13.25	14.86	16.53	38.36	38.57	38.76	1,028.45	1,028.84	1,029.26
March	12.97	14.84	17.34	38.35	38.57	38.70	1,028.30	1,028.85	1,029.32
April	13.57	15.98	19.11	38.40	38.58	38.69	1,027.82	1,028.59	1,029.15
May	14.61	18.34	22.42	38.35	38.57	38.67	1,026.89	1,028.00	1,028.89
June	17.07	21.10	24.87	38.40	38.57	38.68	1,026.15	1,027.27	1,028.30
July	21.18	23.42	27.33	38.50	38.61	38.74	1,025.50	1,026.64	1,027.31
August	22.47	25.08	27.79	38.53	38.64	38.82	1,025.33	1,026.16	1,026.86
September	23.27	25.19	27.49	38.41	38.67	38.82	1,025.43	1,026.15	1,026.75
October	21.25	23.71	26.14	38.29	38.70	38.83	1,025.88	1,026.61	1,027.36
November	18.41	21.34	24.22	38.44	38.74	38.91	1,026.49	1,027.33	1,028.18
December	15.63	18.48	21.31	38.33	38.68	39.01	1,027.30	1,028.05	1,028.99
All year	12.97	19.92	27.79	38.25	38.63	39.01	1025.33	1027.58	1029.32

Prepared by School of Civil Engineering - National Tech Univ. of Athens on behalf of ASPROFOS, 2022.

	EASTMED PIPELINE PROJECT			 	
	EastMed Greek Section – Environmental and Social Impact Assessment			DOC No: PERM-GREE-ESIA-A09_0007_0_Annex9D	
				REV. :	00
				PAGE :	173 OF 178

**Table 8 Water Properties at S4\_13; LF5**

	Bottom Temperature (°)			Bottom Salinity (psu)			Bottom Density (kg/m <sup>3</sup> )		
	Min	Avg	Max	Min	Avg	Max	Min	Avg	Max
January	13.68	16.05	18.41	38.28	38.60	39.01	1,028.00	1,028.59	1,029.28
February	13.22	14.85	16.52	38.30	38.56	38.76	1,028.45	1,028.84	1,029.26
March	13.16	14.87	17.44	38.35	38.57	38.70	1,028.28	1,028.84	1,029.28
April	14.03	16.05	19.13	38.39	38.58	38.69	1,027.81	1,028.58	1,029.05
May	14.86	18.37	22.23	38.35	38.57	38.68	1,026.92	1,027.99	1,028.84
June	16.92	21.10	25.03	38.40	38.57	38.67	1,026.09	1,027.27	1,028.34
July	21.21	23.50	27.69	38.50	38.61	38.74	1,025.37	1,026.61	1,027.28
August	22.62	25.23	27.96	38.53	38.64	38.81	1,025.27	1,026.11	1,026.83
September	23.46	25.35	27.60	38.40	38.67	38.82	1,025.39	1,026.10	1,026.65
October	21.25	23.80	26.29	38.30	38.70	38.83	1,025.83	1,026.59	1,027.36
November	18.25	21.35	24.35	38.40	38.74	38.92	1,026.45	1,027.33	1,028.20
December	15.44	18.49	21.33	38.32	38.68	39.01	1,027.30	1,028.05	1,028.98
All year	13.16	19.97	27.96	38.19	38.62	39.02	1025.27	1027.56	1029.28

Prepared by School of Civil Engineering - National Tech Univ. of Athens on behalf of ASPROFOS, 2022.

## Appendix 3 Ambient Current Velocities

### AMBIENT CURRENT VELOCITIES AT SITE LF2

The ambient extreme current velocities for the location S3\_02 are contained in the Report: Intecsea / C&M Engineering Consortium (2020), PROJECT 416010-00225 - 00225-Cv10A-TDR-00024: Metocean Design Parameters Report – Offshore, Appendix D2: Extreme Current conditions, Dec. 2020.




These data are shown in Table 9; Table 9 includes the coordinates of the EGSA system coordinates and in Figure 2 the Study Area is shown in Google Earth.

**Table 9 Extreme Current Conditions at S3\_02; LF2**

Extreme Surface Current, Usurface (m/s)									
RP	0	45	90	135	180	225	270	315	Omni-dir
(yr)	(°)	(°)	(°)	(°)	(°)	(°)	(°)	(°)	
1	0.31	0.54	0.94	0.52	0.45	0.74	0.62	0.33	0.94
5	0.39	0.61	1.09	0.62	0.50	0.80	0.68	0.41	1.09
10	0.42	0.63	1.15	0.66	0.52	0.83	0.71	0.44	1.15
50	0.49	0.69	1.29	0.75	0.57	0.88	0.76	0.52	1.29
100	0.53	0.72	1.35	0.79	0.59	0.90	0.78	0.55	1.35
Extreme Bottom Current, Ubottom (m/s)									
RP	0	45	90	135	180	225	270	315	Omni-dir
(yr)	(°)	(°)	(°)	(°)	(°)	(°)	(°)	(°)	
1	0.20	0.35	0.62	0.34	0.29	0.48	0.41	0.22	0.62
5	0.25	0.39	0.71	0.40	0.32	0.52	0.44	0.27	0.71
10	0.28	0.41	0.75	0.43	0.33	0.54	0.46	0.29	0.75
50	0.33	0.45	0.84	0.49	0.36	0.57	0.49	0.34	0.84
100	0.35	0.46	0.88	0.51	0.37	0.58	0.51	0.36	0.88

Prepared by School of Civil Engineering - National Tech Univ. of Athens on behalf of ASPROFOS, 2022.

Moreover, the data that are shown in Table 2 were provided by the research team of the NKUA that are based on the Copernicus Marine Environment Monitoring Service (CMEMS).

 <b>IGI Poseidon</b>	<b>EASTMED PIPELINE PROJECT</b>	 
	EastMed Greek Section – Environmental and Social Impact Assessment	DOCNo: PERM-GREE-ESIA- A09_0007_0_Annex9D
		REV. : 00 PAGE : 175 OF 178

**Table 10 Extreme Current Conditions at S3\_02; LF2 Based on CMEMS**

RP (yr)	Usurface (m/s)		Ubottom (m/s)	
	max	min	max	min
1	0.512	0.006	0.392	0.007
10	0.574	0.002	0.634	0.001
100	0.613	n/a	0.535	n/a

Prepared by School of Civil Engineering - National Tech Univ. of Athens on behalf of ASPROFOS, 2022.

### *AMBIENT CURRENT VELOCITIES AT SITE LF3*




The ambient extreme current velocities for the location S3\_45 are contained in the Report: Intecsea / C&M Engineering Consortium (2020), PROJECT 416010-00225 - 00225-Cv10A-TDR-00024: Metocean Design Parameters Report – Offshore, Appendix D2: Extreme Current conditions, Dec. 2020.

These data are shown in Table 11; Table 11 includes the coordinates of the EGSA system coordinates and in Figure 4 the Study Area is shown in Google Earth.

**Table 11 Extreme Current Conditions at S3\_45; LF3**

Extreme Surface Current, Usurface (m/s)									
RP	0	45	90	135	180	225	270	315	Omni-dir
(yr)	(°)	(°)	(°)	(°)	(°)	(°)	(°)	(°)	
1	0.40	0.35	0.22	0.26	0.75	0.39	0.15	0.17	0.75
5	0.47	0.41	0.24	0.30	0.83	0.46	0.17	0.19	0.83
10	0.51	0.43	0.26	0.32	0.86	0.49	0.18	0.20	0.86
50	0.58	0.49	0.28	0.36	0.93	0.55	0.21	0.22	0.93
100	0.61	0.51	0.30	0.37	0.95	0.58	0.22	0.23	0.95
Extreme Bottom Current, Ubottom (m/s)									
RP	0	45	90	135	180	225	270	315	Omni-dir
(yr)	(°)	(°)	(°)	(°)	(°)	(°)	(°)	(°)	
1	0.26	0.23	0.14	0.17	0.49	0.26	0.10	0.11	0.49
5	0.31	0.27	0.16	0.20	0.56	0.30	0.11	0.12	0.56
10	0.33	0.28	0.17	0.21	0.58	0.32	0.12	0.13	0.58
50	0.38	0.32	0.18	0.23	0.64	0.36	0.13	0.15	0.64
100	0.40	0.33	0.19	0.25	0.66	0.38	0.14	0.15	0.66

Prepared by School of Civil Engineering - National Tech Univ. of Athens on behalf of ASPROFOS, 2022.

	<b>EASTMED PIPELINE PROJECT</b>		 	
			DOC No: PERM-GREE-ESIA-A09_0007_0_Annex9D	
	EastMed Greek Section – Environmental and Social Impact Assessment		REV. :	00
			PAGE :	176 OF 178

Moreover, the data that are shown in Table 12 were provided by the research team of the NKUA that are based on the Copernicus Marine Environment Monitoring Service (CMEMS).

**Table 12 Extreme Current Conditions at S3\_45; LF3 Based on CMEMS**

RP (yr)	Usurface (m/s)		Ubottom (m/s)	
	max	min	max	min
1	0.175	0.003	0.392	0.007
10	0.229	0.001	0.534	0.001
100	0.263	n/a	0.535	n/a




Prepared by School of Civil Engineering - National Tech Univ. of Athens on behalf of ASPROFOS, 2022.

#### *AMBIENT CURRENT VELOCITIES AT SITE LF4*

The ambient extreme current velocities for location S4\_02 are contained in the Report: Intecsea / C&M Engineering Consortium (2020), PROJECT 416010-00225 - 00225-Cv10A-TDR-00024: Metocean Design Parameters Report – Offshore, Appendix D2: Extreme Current conditions, Dec. 2020. These data are shown in Table 13; Table 13 includes the coordinates of the EGSA system coordinates and in Figure 6 the Study Area is shown in Google Earth.

**Table13 Extreme Current Conditions at S4\_02**

Extreme Surface Current, Usurface (m/s)									
RP	0	45	90	135	180	225	270	315	Omni-dir
(yr)	(°)	(°)	(°)	(°)	(°)	(°)	(°)	(°)	
1	0.20	0.34	0.57	0.28	0.13	0.20	0.72	0.3	0.73
5	0.25	0.42	0.68	0.34	0.15	0.25	0.86	0.35	0.86
10	0.26	0.45	0.73	0.36	0.16	0.27	0.92	0.37	0.92
50	0.31	0.53	0.84	0.42	0.18	0.31	1.05	0.42	1.05
100	0.33	0.57	0.89	0.45	0.19	0.33	1.11	0.44	1.11

	<b>EASTMED PIPELINE PROJECT</b>		 
	EastMed Greek Section – Environmental and Social Impact Assessment		DOC No: PERM-GREE-ESIA-A09_0007_0_Annex9D
			REV. : 00 PAGE : 177 OF 178

Extreme Bottom Current, Ubottom (m/s)									
RP	0	45	90	135	180	225	270	315	Omni-dir
(yr)	(°)	(°)	(°)	(°)	(°)	(°)	(°)	(°)	
1	0.13	0.22	0.38	0.19	0.09	0.13	0.47	0.20	0.48
5	0.16	0.28	0.46	0.22	0.10	0.16	0.56	0.23	0.56
10	0.17	0.30	0.49	0.24	0.10	0.17	0.60	0.24	0.60
50	0.20	0.36	0.57	0.28	0.12	0.19	0.68	0.28	0.68
100	0.21	0.38	0.60	0.30	0.12	0.19	0.72	0.29	0.72

Prepared by School of Civil Engineering - National Tech Univ. of Athens on behalf of ASPROFOS, 2022.

Moreover, the data that are shown in Table 14 were provided by the research team of the NKUA that are based on the Copernicus Marine Environment Monitoring Service (CMEMS).

**Table 14** Extreme Current Conditions at S4\_02 Based on CMEMS

RP (yr)	Usurface (m/s)		Ubottom (m/s)	
	max	min	max	min
1	0.142	0.002	0.035	0.001
10	0.181	n/a	0.085	n/a
100	0.205	n/a	0.016	n/a




Prepared by School of Civil Engineering - National Tech Univ. of Athens on behalf of ASPROFOS, 2022.

### AMBIENT CURRENT VELOCITIES AT SITE LF5

The ambient extreme current velocities for the location S4\_13 are contained in the Report: Intecsea / C&M Engineering Consortium (2020), PROJECT 416010-00225 - 00225-Cv10A-TDR-00024: Metocean Design Parameters Report – Offshore, Appendix D2: Extreme Current conditions, Dec. 2020. These data are shown in Table 15; Table 15 includes the coordinates of the EGSA system coordinates and in Figure 8 the Study Area is shown in Google Earth.

**Table 15** Extreme Current Conditions at S4\_13; LF5

Extreme Surface Current, Usurface (m/s)									
RP	0	45	90	135	180	225	270	315	Omni-dir
(yr)	(°)	(°)	(°)	(°)	(°)	(°)	(°)	(°)	
1	0.20	0.34	0.57	0.28	0.14	0.20	0.72	0.29	0.73
5	0.25	0.42	0.68	0.34	0.16	0.25	0.86	0.33	0.86

	<p style="text-align: center;"><b>EASTMED PIPELINE PROJECT</b></p> <p style="text-align: center;">EastMed Greek Section – Environmental and Social Impact Assessment</p>	<div style="display: flex; justify-content: space-between; align-items: center;">   </div> <p>DOC No: PERM-GREE-ESIA- A09_0007_0_Annex9D</p> <p>REV. : 00</p> <p>PAGE : 178 OF 178</p>
---	--	--

10	0.27	0.45	0.73	0.36	0.17	0.27	0.92	0.35	0.92
50	0.31	0.53	0.84	0.42	0.19	0.31	1.05	0.40	1.05
100	0.33	0.56	0.89	0.44	0.20	0.33	1.10	0.42	1.10
<b>Extreme Bottom Current, Ubottom (m/s)</b>									
RP	0	45	90	135	180	225	270	315	Omni- dir
(yr)	(°)	(°)	(°)	(°)	(°)	(°)	(°)	(°)	
1	0.13	0.22	0.38	0.18	0.09	0.13	0.47	0.19	0.47
5	0.16	0.28	0.45	0.22	0.10	0.16	0.56	0.22	0.56
10	0.17	0.30	0.48	0.24	0.11	0.17	0.59	0.23	0.59
50	0.20	0.36	0.55	0.28	0.13	0.20	0.68	0.26	0.68
100	0.21	0.38	0.59	0.29	0.13	0.21	0.71	0.27	0.71

Prepared by School of Civil Engineering - National Tech Univ. of Athens on behalf of ASPROFOS, 2022.

Moreover, the data that are shown in Table 16 were provided by the research team of the NKUA that are based on the Copernicus Marine Environment Monitoring Service (CMEMS).

**Table 16 Extreme Current Conditions at S4\_13; LF5 Based on CMEMS**

RP (yr)	Usurface (m/s)		Ubottom (m/s)	
	max	min	max	min
1	0.113	0.004	0.067	0.002
10	0.243	n/a	0.116	n/a
100	0.324	n/a	0.146	n/a

Prepared by School of Civil Engineering - National Tech Univ. of Athens on behalf of ASPROFOS, 2022.